Optimization of Nanodisc Array Generation on Silicon Photonic Microring Resonators for Lipid-Protein and Membrane Protein-Protein Interaction Characterization

by

Sara Marie Medfisch

A dissertation submitted in partial fulfillment
of the requirements for the degree of
Doctor of Philosophy
(Chemistry)
in The University of Michigan
2021

Doctoral Committee:

Professor Ryan C. Bailey, Chair
Professor Sarah C. Keane
Professor James H. Morrissey
Professor Ayyalusamy Ramamoorthy

Sara Marie Medfisch

luttysar@umich.edu

ORCID iD: 0000-0002-6367-0031

DEDICATION

To my husband, Colin

ACKNOWLEDGEMENTS

TABLE OF CONTENTS

LIST OF TABLES

LIST OF ACRONYMS

18A	18 Amino Acid Long Peptide for Stabilizing Hydrophobic Molecules
14A	14 Amino Acid Long Peptide for Stabilizing Hydrophobic Molecules
22A	22 Amino Acid Long Peptide for Stabilizing Hydrophobic Molecules
37pA	Two 18A Peptides Linked with a Proline
4F	18A Peptide with 2 Phenylalanine Mutations
5A	37pA with 5 Alanine Mutations
Aβ	Amyloid β-Peptide
ABC	ATP Binding Cassette
ABC Hypothesis	"Anything But Choline" Hypothesis
AFM	Atomic Force Microscopy
AmtB	*E. coli* Ammonium Transporter
aPC	Activated Protein C
apoA-I	Apolipoprotein A-I
apoA-II	Apolipoprotein A-II
apoHDL-Gln	Apolipoprotein with a N-terminal Glutamine, Now Known as apo A-I
apoHDL-Thr	Apolipoprotein with a N-terminal Threonine, Now Known as apo A-II
Arg28	Human Factor X Arginine 28
ATP	Adenosine Triphosphate
BCA	Bicinchoninic Acid
bp	DNA Base Pairs
BSA	Bovine Serum Albumin
BSI	Backscattering Interferometry
CD	Circular Dichroism
CID	Collision Induced Dissociation
CIU	Collision Induced Unfolding
CMC	Critical Micelle Concentration
Cryo-EM	Cryogenic Electron Microscopy
DIBMA	Diisobutylene-Maleic Acid Copolymers
DLS	Dynamic Light Scattering
DNA	Deoxyribonucleic Acid
DSC	Differential Scanning Calorimetry
dsDNA	Double-stranded Deoxyribonucleic Acids
DTSSP	3'-dithiobis(sulfosuccinimydlpropionate)
E.coli	*Escherichia coli*
E7D	Human Factor X Glutamate 7 Mutated to Aspartate
E14D	Human Factor X Glutamate 14 Mutated to Aspartate
E19D	Human Factor X Glutamate 19 Mutated to Aspartate
E20D	Human Factor X Glutamate 20 Mutated to Aspartate
E25D	Human Factor X Glutamate 25 Mutated to Aspartate

E29D	Human Factor X Glutamate 29 Mutated to Aspartate
E32A	Human Factor X Glutamate 32 Mutated to Alanine
E32D	Human Factor X Glutamate 32 Mutated to Aspartate
EDTA	Ethylenediaminetetraacetic Acid
EDC	Ethyl-3-(3-dimethylaminopropyl))carbodiimide
EFC	Extended FC Binding Domain
EGF	Epidermal Growth Factor
ENTH	Epsin N-terminal Homology Lipid Binding Domain
ELISA	Enzyme-Linked Immunosorbent Assays
ELK	18 Amino Acid Long Peptide for Stabilizing Hydrophobic Molecules Composed of Mostly Glutamate, Leucine, and Lysine
EPR or ESR	Electron Paramagnetic Resonance or Electron Spin Resonance
FRET	Fluorescence Resonance Energy Transfer
FTIR	Fluorescence Transform Infrared
fIX	Factor IX
fIXa	Activated Factor IX
fVa	Activated Factor V
fVII	Factor VII
fVIIa	Activated Factor VII
fVIIIa	Activated Factor VIII
fX	Factor X
fX-GLA	Factor X GLA domain
fXa	Activated Factor X
FYVE	Zinc Finger Lipid Binding Domain
GFP	Green Fluorescent Protein
GLA	Lipid Binding Domain Rich in γ-Carboxyglutamate
Gla	γ-Carboxyglutamate
Gla14	Human Factor X γ-Carboxyglutamate 14
Gla19	Human Factor X γ-Carboxyglutamate 19
Gla29	Human Factor X γ-Carboxyglutamate 29
Gla32	Human Factor X γ-Carboxyglutamate 32
GPCR	G-Protein Coupled Receptor
GM	Ganglioside
GST	Glutathione S-Transferase
^{1}H-^{1}H NOESY	Nuclear Overhauser Effect Spectroscopy, Through-Space Correlation
^{1}H-^{1}H TOCSY	Total Correlated Spectroscopy, Through-Bond Correlation
HDL	High-Density Lipoprotein
HEPES	4-(2-hydroxyethyl)-1-piperazinetheanesulfonic Acid
HPC4	Calcium Dependent Antibody Invented Against Human Protein C
IPTG	Isopropyl β-D-1-thiogalacopyranoside
ITC	Isothermal Titration Calorimetry
K_a	Association Constant
K9Q	Human Factor X Lysine 9 Mutated to Glutamine
K10Q	Human Factor X Lysine 10 Mutated to Glutamine
K_d	Dissociation Constant
k_{off}	Kinetic Off Rate Constant

k_{on}	Kinetic On Rate Constant
LiMA	Liposome Microarray-Based Assay
LC	Liquid Chromatography
LCAT	Lectin:Cholesterol Acyltransferase
Lys10	Human Factor X Lysine 10
Lys165	Tissue Factor Lysine 165
Lys166	Tissue Factor Lysine 166
MALDI-TOF	Matrix Laser Desorption Ionization Time-of-Flight Mass Spectrometry
MAPK	Mitogen Activated Protein Kinase Pathway
MBP	Maltose-Binding Protein
MD	Molecular Dynamics
MES	2-(N-morpholino)ethanesulfonic Acid
MPA	3-Mercaptopropionic Acid
MRI	Magnetic Resonance Imaging
MS	Mass Spectrometry
MS/MS	Tandem Mass Spectrometry
MSP	Membrane Scaffold Protein
MSP1D1	Membrane Scaffold Protein Variant Generating 9.5 nm Diameter Nanodiscs
MSP1D1 D73C	Membrane Scaffold Protein Variant Generating 9.5 nm Diameter Nanodiscs With Aspartate 73 Mutated to Cysteine
MSP1E3D1	Membrane Scaffold Protein Variant Generating 13 nm Diameter Nanodiscs
Ni-NTA	Nickel Charged Nitrilotriacetic Acid Resin
NMR	Nuclear Magnetic Resonance Spectroscopy
Npu	Nostoc Punctiforme
NSP	18A Linked with Proline to 4F
NSP_r	Reverse NSP
PA	Phosphatidic Acid
PBS	Phosphate Buffered Saline
PC	Phosphatidylcholine
PDC-1009	Bovine Seminal Plasma Protein
PDMS	Polydimethylsiloxane
PE	Phosphatidylethanolamine
PG	Phosphatidylglycerol
PH	Pleckstrin Homology Lipid Binding Domain
PI(3)P	Phosphatidylinositol 3-monophosphate
$PI(3,4)P_2$	Phosphatidylinositol 3,4-bisphosphate
$PI(4,5)P_3$	Phosphatidylinositol 4,5-bisphosphate
$PI(3,4,5)P_3$	Phosphatidylinositol 3,4,5-triphosphate
PKC	Protein Kinase C
PLB	Phospholamban
PLC	Phospholipase C
PLM	Phospholemman
PMMA	Poly(methylmethacrylate) Copolymers
PS	Phosphatidylserine
PT	Prothrombin
PX	Human Phox Homology Lipid Binding Domain

R15Q	Human Factor X Arginine 15 Mutated to Glutamine
R28Q	Human Factor X Arginine 28 Mutated to Glutamine
RGS4	Regulator G-Protein Signaling 4
S. cervisiae	*Saccharomyces cerevisiae*
SAMDI-TOF	Self-Assembled Monolayers for Matrix Laser Desorption Ionization Time-of-Flight Mass Spectrometry
SANS	Small-Angle Neutron Scattering
SAXS	Small-Angle X-Ray Scattering
SDB	Standard Disc Buffer
SDS	Sodium Dodecyl Sulfate
SDS-PAGE	Sodium Dodecyl Sulfate Polyacrylamide Gel Electrophoresis
SEC	Size Exclusion Chromatography
SELDI-TOF	Surface Enhanced Laser Desorption Ionization Time-of-Flight Mass Spectrometry
SERCA	Sarco(endo)plasmic Reticulum Ca^{2+}-ATPase
SLS	Static Light Scattering
$SM(PEG)_6$	succinimydyl-[(N-maleimidopropionamido)-hexaethyleneglycol]ester
SMA	Styrene-Maleic Acid Copolymers
SMA-ED	Styrene-Maleic Acid-Ethylenediamine Copolymers
SMA-MA	Styrene-Maleic Acid-Methylamide Copolymers
SMA-QA	Styrene-Maleimide Quaternary Amine Copolymers
SMAd-A	Styrene-Maleimide Ethyleneamine Copolymers
SMI	Styrene-Maleimide Tertiary Amine Copolymers
SPR	Surface Plasmon Resonance
SPRi	Surface Plasmon Resonance Imaging
ssDNA	Single-stranded Deoxyribonucleic Acids
ssNMR	Solid State Nuclear Magnetic Resonance
T	Thrombin
TAAR13c	Trace-Amine Associated Receptor 13c
TAL	Thin Agarose Layers
TAMRA	5-Carboxamido-(6-Azidohexanyl) Tetramethylrhodamine
TBS	Tris Buffered Saline
TEM	Transmission Electron Microscopy
TF	Tissue Factor
TIRF	Total Internal Reflection Fourier-Transform
TIRFM	Total Internal Reflection Fluorescence Microscopy
Tris	Tris(hydroxymethyl)aminomethane
TSPO	Translocator Protein
UA	UniBlue A
UV	Ultraviolet
wtfX	Wildtype Human Factor X
zSMA	Styrene-Maleic Acid Anhydride Random Copolymer

ABSTRACT

Biological membranes are essential for all life. Membranes govern compartmentalization between cells and provide frameworks for processes such as cell growth and signaling. The interactions that occur at the membrane interface are driven by charge state interactions between lipid headgroups and/or membrane proteins at the surface and binding domains on soluble proteins. Sometimes these interactions are also regulated by second messengers such as calcium ions. Understanding the processes that occur at the membrane surface is pertinent for designing therapeutics that may be needed for intervention in the physiological process. One physiological process that depends on membrane surface interactions is the blood coagulation cascade.

The extrinsic pathway of blood coagulation relies on the membrane interface for initiation, propagation, and amplification. Upon tissue damage, phosphatidylserine (PS) and an integral membrane protein, tissue factor (TF), are exposed to the extracellular matrix. Together, PS and TF are essential for recruitment of blood coagulation factors for complex formation and proteolytic activation that initiates the cascade and continue downstream to form a blood clot. The principal interactions driving these membrane associations are from GLA domains which are regions rich in γ-carboxyglutamate that chelate calcium ions to the surface to bind with PS.

This doctoral dissertation presents the development and optimization of a high throughput technique for characterization of molecular interactions at the membrane interface using Nanodiscs which are high-density lipoprotein mimetics formed with membrane scaffold protein (MSP) and lipids. These Nanodiscs are arrayed on silicon photonic microring resonators for refractive index-based detection of molecular interactions at the membrane surface.

Nanodiscs were arrayed on silicon photonic microring resonators using physisorption between the lipid headgroups and silicon oxide coated surface. These arrays were generated using molecular printing or by pipette spotting under a microscope to produce 7 or 9 lipid environment arrays. These Nanodiscs were used to observe GLA domain enhanced binding affinity for environments with increasing PS or phosphatidic acid (PA). Of particular interest was the

increased binding affinity displayed by activated factor VII and activated protein C for PA over PS. These physisorption arrays also quantitated quantitate PS synergy with phosphatidylethanolamine (PE) for all GLA domain-containing blood coagulation factors. The most prominent synergistic behaviors were observed with factor X (fX) and prothrombin while the least synergy was seen with factor IX (fIX).

This physisorption technique is label-free and easy to use; however, the reliance on charge interactions limits the lipid environment and makes incorporation of membrane proteins difficult. Additionally, there is little to no control over the Nanodisc orientation on the surface. To overcome these challenges, DNA-tagged Nanodiscs were developed and optimized. Using DNA-tags, Nanodiscs are tethered above the surface which allows for more control over Nanodisc array loading with different lipid environments. Observation of Nanodisc loading overtime with DNA-tags provides quantitation of loading that was used for surface loading correction to calculate protein binding per leaflet. Using this technique, TF was incorporated into 7 different lipid environments of PC, PS, PA, and PE to observe differences in lipid binding preference of fIX and fX with and without TF. The multiplexity was then pushed to 26 for characterization the binding of fX-GLA domain mutants in 10 different lipid environments with 2-3 biological replicates. Through these studies, DNA-tagged Nanodiscs have demonstrated potential as a high throughput technology on silicon photonic microring resonators.

Keywords: microring resonators, blood coagulation, membrane characterization, lipid-protein interactions, membrane proteins, Nanodiscs

CHAPTER I

Introduction

Abstract

Biological membranes are responsible for compartmentalizing and supporting physiological processes. Analyzing the chemical interactions occurring at these interfaces is critical to understanding the driving forces for biological functions. Here, the first two sections provide background to biological membrane components and mimetics. These mimetics are used in each of the subsequent techniques discussed in the third section. Section four introduces blood coagulation as a model physiological process that utilizes membranes as a scaffold for initiation, propagation, and amplification. The final section is an overview of the work laid out in the following chapters.

1. Biological Membranes

Membranes and membrane proteins are essential to physiological processes such as cellular growth, metabolism, and homeostasis[1]; thus, there is a need to thoroughly understand physiological mechanisms and protein structure to improve development of therapeutics.[2] The main challenge in this field is stability of countless lipid and protein components.[3,4] The complex membrane environment encompasses over ten thousand different lipids[5] that are involved in formation of the nanodomains that have local enrichment of specific species[6,7] and protein interactions with lipid binding domains.[8–13]

Lipid binding domains belong in the top 15 most modular domains and are often connected to signal transduction and/or membrane trafficking.[14] The interactions between lipid binding domains

and lipids are mediated by charge or surface topography and may be associated with second messengers such as Ca^{2+}.[15] Binding domains containing essential histidine residues can be modulated with pH such as FYVE zinc finger (named after four cysteine-rich proteins),[16] pleckstrin homology (PH),[17] and epsin N-terminal homology (ENTH)[18] domains.

Phosphatidylserine (PS) is a common, targeted phospholipid that is enriched on the cytoplasmic side of the plasma membrane. One example of PS recognition is seen with apoptotic cells which expose PS to the extracellular domain to signal cell death.[19] One of the first PS binding domain studied was the C2 domain of protein kinase C (PKC).[20] The domain was discovered to be calcium dependent[21] and its X-ray crystal structure has been solved.[22] A few other example X-ray crystal structures are available for the C2 domain of synaptotagmin I,[23] PH domain of phospholipase C specific for phosphatidylinositol 3,4,5-triphosphate $(PI(3,4,5,)P_3)$,[24] and human phox homology (PX) domain of p47[phox] for interactions with phosphatidylinositol 3,4-bisphosphate $(PI(3,4)P_2)$ and phosphatidic acid (PA).[25] Computational models have also been used to understand lipid-protein interactions.[26–28]

2. Membrane Mimetics

Soluble membrane mimetics are essential for characterizing lipid-protein and membrane protein-protein interactions. The most common membrane mimetics (**Figure I.1**) are micelles, amphipols, bicelles, supported lipid bilayer, liposomes, and high-density lipoprotein (HDL)-like particles, also known as *nanodiscs*.[29,30]

Micelles utilize detergent to extract membrane proteins from their native environment (**Figure I.1A**). This is one of the most common ways to solubilize membrane proteins for downstream characterization or later processing into a different membrane mimetic. One downfall to micelles is that detergent has been shown to result in loss of protein function in some applications.[31,32] Amphipols are another class of surfactants used for membrane protein solubilization (**Figure I.1B**).[33] These surfactants are made of hydrophilic carbon backbones with hydrophobic chains to generate amphipathic polymers for membrane protein stabilization.[34] Even though amphipols are able to conserve protein function better than detergents, the mimetic does not correct for adoption of curvature which is common problem with surfactants that can result in the non-native protein folding.

Bilayer membrane mimetics overcome the issue of curvature by associating lipids in a more native-like environment around the membrane protein. Bicelles are generated by utilizing short chain phospholipids or detergents to stabilize lipids into a bilayer (**Figure I.1C**).[35,36] The size of these mimetics is easily controlled by adjusting the ratio of lipids to the short chain reagent; however, the choice of lipids and detergents is limited for ideal particle formation without disrupting the bilayer.[37] An alternative bilayer mimetic is supported lipid bilayers (**Figure I.1D**).[38,39] This surface based bilayer can be easily formed on substrates such as glass, silicon dioxide, gold, or nitrocellulose[29] for use with surface-sensitive characterization techniques.[40] These supported bilayers can display rigid behavior that can be overcome by tethering above the surface through surface functionalization and membrane additives.[41] However, this modification does not mitigate defects in bilayer formation.

Liposomes are soluble spherical bilayers[42] (**Figure I.1E**) that form by mechanical or chemical means such as sonication[43] or detergent removal.[44] This makes liposomes easy to assemble for various applications either in solution or by incorporation of a capture reagent for surface tethering.[45,46] Limitations to liposomes are compartmentalization due to access to only the outer portion of the bilayer, need for downstream purification for size specificity, and particle aggregation. Recent work using bolalipids, a lipid found in cell membranes of archaea bacteria, have been shown form liposomes that are more resistant to aggregation due to temperature fluctuations.[47]

Nanodiscs are a diverse bilayer system developed as copycat HDLs to be disc-like bilayers stabilized by various reagents (**Figure I.1F**). More detailed discussion about nanodiscs can be found in *Chapter 2*. Briefly, HDLs are crucial to physiological processes for cholesterol transport[48,49] and have been linked to coronary heart disease.[50] There are numerous reviews covering the topic of HDLs in physiology.[51–53] For generating mimics, stabilizing reagents have been designed similar to apolipoprotein A-I (apoA-I) which is a the main structural component in physiological HDLs.

The first examples were peptides designed to characterize apoA-I.[54–56] Studies were performed by adjusting the peptide sequence to determine the alpha helical structure of apoA-I provides the necessary amphipathic environment to stabilize the hydrophobic lipids.[57,58] This discovery has since led to the development of numerous peptides to further understand HDLs and to utilize their

properties. A few examples of these peptides are 18A,[54] 37pA,[56,59] 4F,[60] 5A,[61] NSP,[62,63] ELK,[64] multivalent-branched species,[65] and 22A.[66,67] Extensive work this area has resulted in the optimization for use as therapeutics for anti-inflammatory,[68–70] diabetes,[71] obesity,[72] amyloid beta aggregation,[73] chemotherapy,[74–76] and cancer vaccines.[77,78] A shortcoming of peptide nanodiscs is the lack of control over the number of peptides which can be a problem when adding functional groups for tagging or surface tethering.

Another stabilizing reagent was developed by the Sligar lab called membrane scaffold protein (MSP).[79] These nanodiscs have been shown to form with exactly two MSPs as the stabilizing belt.[80] Variants of MSPs have been designed to modify the diameter of the nanodisc.[81,82] There are many reviews covering the wide breadth of MSP nanodiscs applications to illustrate lipid-protein and membrane protein-protein interactions.[83–87] Circularization of MSP has been a recent development in the field to generate larger nanodiscs with enhanced thermal stability.[88] Two current methods involve use of split inteins[89] or sortase A.[90,91] An additional method for larger, circularized nanodiscs utilized DNA-origami barrels as corrals.[92] One drawback to protein and circularized nanodiscs is the need for detergent to stabilize reagents prior to stable bilayer formation of the nanodisc.

Polymer nanodiscs have displayed the advantage of forming discs without the need for prior detergent stabilization of lipids or membrane proteins.[93–96] The original polymer that was used to form these nanodiscs was a styrene-maleic acid copolymer (SMA).[97] These nanodiscs displayed pH and divalent cation instabilities[98–100] that led to experimentation with modifications to the SMA units[101–105] or use of other copolymer blends.[106,107] Disadvantages to using polymer nanodiscs are the need for harsh temperature fluctuations for formation and the lack of control over the number of polymers incorporated which can be a problem when adding functional groups for characterization or surface tethering.

Each of the membrane mimetics have their advantages and disadvantages. The important feature to consider in this field is reagent availability and protein stability. If the protein is stable and active, the micelles may be appropriate; however, a screening of the mimetics to preserve protein structure and function may be needed.

3. Lipid-Protein and Membrane Protein-Protein Characterization Techniques

There are many reviews of characterization techniques for lipid-protein and membrane protein-protein interactions *in vitro*,[108–111] in vivo,[112] and using molecular dynamics simulations.[113] Due to the focus of this dissertation, *in vitro* techniques will be briefly discussed separated into two classes—in solution or surface arrays.

3.1. In Solution

Liposome Sedimentation

Liposome sedimentation is performed through incubation of liposomes with proteins of interest before centrifugation at high speeds (> 20,000 xg). Due to the large size of liposomes, the membranes and any associated proteins are sedimented into the pellet while unbound species stay in the supernatant. Interactions are typically determined by sodium dodecyl sulfate polyacrylamide gel electrophoresis (SDS-PAGE) followed by Coomassie staining. Liposomes containing phosphatidylinositol 4,5-bisphosphate (PI(4,5)P$_2$) have been used to identify residues of interest for membrane binding with adaptor protein 180 and clathrin assembly lymphoid myeloid leukemia protein N-terminal domains that are similar to ENTH domains.[114] Another study compared the binding of an extended FC (EFC) lipid binding domain with phosphatidylethanolamine (PE), PIP(4,5)P$_2$, and brain lipids to determine the specificity for PIP(4,5)P$_2$.[115]

Use of Coomassie staining for quantification greatly limits the sensitivity of liposome sedimentation, so groups have modified the protocol to incorporate labels for improvement. Regulator G-protein signaling 4 (RGS4) was modified as a glutathione s-transferase (GST) fusion construct to observe binding with PI(3,4,5)P$_3$ using immunoblotting.[116] Other modifications used are maltose-binding protein (MBP) fusion[117] and radiolabeling with ^{35}S-methionine and cysteine[118] or iondination.[119] To eliminate the need for SDS-PAGE analysis, crosslinking with lipids using UV activation or click chemistry can be combined with mass spectrometry for protein identification.[120,121]

Isothermal Titration Calorimetry

Isothermal titration calorimetry (ITC) measures heat generated or absorbed during formation of complexes in a label-free environment.[122] The enthalpy of lipid-protein binding can be measured

by filling the sample cell with lipid vesicles and injecting protein or peptide to measure the heat given off by the injection.[123] Binding constants can be also be calculated by doing the inverse of filling the sample cell with the protein or peptide and injecting lipid vesicles. Proteins can be screened for lipid specificity using ITC. For example, bovine seminal plasma protein (PDC-1009), preferentially binds phosphatidylcholine (PC) over phosphatidylglycerol (PG) or PE by calculating binding affinity in addition to enthalpy.[124] ITC can also be used to screen the concentration of secondary ions required for stable binding.[125]

Electron Spin Resonance

Electron spin resonance (ESR) can utilize spin labels near the end of fatty acid acyl chains of lipids to determine lipid-protein interactions.[126] The most common spin label utilizes a ^{14}N-nitroxyl group that becomes restricted in movement upon interaction with the protein of interest. This technique can be used to determine stoichiometry and selectivity of proteins for a specific lipid species.[127] An ADT-ATP carrier protein was determined to have 50 lipid binding sites along its transmembrane dimer domain and show selectivity for anionic phospholipids such as cardiolipin.[128]

Fluorescence Methods

Fluorescence utilizing methods rely on the sensitivity of the chosen fluorophore. One method, fluorescence resonance energy transfer (FRET) also relies on the close proximity of donor and acceptor species. FRET utilizes the transfer of energy from the donor molecule to increase the signal of the acceptor for detection. Depending on the molecules and length of linker regions, the proximity may need to be between 1-100 Å. For example, the pairing of phospholipase C (PLC) labelled with fluorescein and rhodamine-labelled PE is limited to a maximum distance of 80 Å. This pairing was been used to determine that PLC lipid binding domain preferentially binds PI(4,5)P$_2$.[129] FRET can be used to determine ionic strength effects on interactions[130] or to look at lipid cooperativity to enhance interactions.[125] A similar strategy has been used with polymer nanodiscs to characterize the polymer to lipid distance by labelling the polymer belt with biotin for binding an avidin labelled donor to interact with an acceptor modified lipid. Differences in signal were noted based on changing the length of the avidin donor linkage.[131] In contrast to using labelled lipids, MSP has been modified with 5-carboxamido-(6-azidohexanyl)

tetramethylrhodamine (TAMRA) to observe interactions with UniBlue A (UA) labeled talin head domain.[132] This allowed for screening of interaction proximity without adding any bias from potentially interfering fluorophore modified lipids.

Unlike FRET, fluorescence polarization (or fluorescence anisotropy) relies on a single fluorophore to observe emission intensities parallel and perpendicular to an excitation plane. The intensity of the fluorescence changes based on the molecular weight of the tumbling species; thus, lipid-protein and membrane protein-protein interactions can be observed. Titration of nanodiscs with various lipid concentrations have been used to identify interactions with labelled FYVE and PX domains to prefer phosphatidylinositol 3-monophosphate (PI(3)P) and PI(3,4)P$_2$, respectively.[133] Alternatively, the fluorophore can label lipids,[134] nanodisc belt,[135] or not be present at all to rely on intrinsic tryptophan fluorescence.[136]

Nuclear Magnetic Resonance

Nuclear magnetic resonance (NMR) spectroscopy is used to observe changes in a resonance frequency to identify lipid-protein and membrane protein-protein interactions. A recent review has been published outlining solution NMR used with various membrane reconstitution methods.[137] Resonances of liposomes observed using wide line ^{2}H NMR were shifted when incubated with sarco(endo)plasmic reticulum Ca^{2+}-ATPase (SERCA) and SERCA with phospholamban (PLB).[138] By switching the observed resonance for ^{13}P NMR, broad peaks observed with SERCA and PG indicate lipid specific binding. Alternatively, two-dimensional (2D) NMR techniques such as ^{1}H-^{1}H TOCSY and NOESY can be used to identify resonances that are spatially close.[139] NMR has also been shown as a promising technique with protein[140] and polymer[141] nanodiscs.

Fourier Transform Infrared

Fourier transform infrared (FTIR) spectroscopy can be used to observe differences in infrared intensity and wavenumber between various samples. Incubation of liposomes with mutants of protein can be used to identify the residues that are involved in lipid binding.[142] Peptides have been used to mimic the hydrophobic core of membrane proteins to observe binding changes based on liquid or gel phase.[143] The gel phase state showed more dependence on lipid chain length.

Circular Dichroism

Protein secondary structures can be characterized using circular dichroism (CD) based on differential absorption of left and right circularly polarized light. Peptides of phospholemman (PLM) were compared in their phosphorylated and not phosphorylated states for affinity with lipids using CD.[144] The not phosphorylated form was observed to be less likely to form an α-helical structure in the presence of lipids which results in less ordered structure when near the membrane. Additionally, a mitogen activated protein kinase (MAPK) pathway recruit scaffold protein Ste5 has been shown to stabilize in an α-helical structure in the presence of SDS micelles.[139]

Mass Spectrometry

Mass spectrometry is a newly evolving field for studying lipid-protein and membrane protein-protein interactions. Nano-electrospray mass spectrometry has been performed in detergent micelles to observe oligomeric structure of ATP binding cassette (ABC) transporters as long as the detergent concentration was above the critical micelle concentration (CMC).[145] More recent work has involved MSP nanodiscs due to their stable and uniform structures.[146–148] Recent studies have looked at lipid recruiting of membrane proteins to identify substrates or key lipids for structure. Collision induced unfolding (CIU) has been used to screen substrates for translocator protein (TSPO) for enhanced stability of the protein.[149] In tandem, chloroform extractions can be performed for tandem mass spectrometry (MS/MS) for copurifying lipid identification. In another recent study, membrane lipid distribution biases were identified when incorporating a membrane protein of interest.[150] *E. coli* ammonium transporter AmtB was shown to enhance the lipid exchange between nanodiscs to enrich for PG and PC. Collision induced dissociation (CID) was also used to identify lipids that had a higher energy of dissociation from AmtB.

3.2. Surface Array

Generating Surface Arrays

Surface arrays can be formed using surface substrates such as glass, silicon dioxide, gold, or nitrocellulose.[29] Modifications to these supports can generate more consistent and stable arrays. One of the earliest surface modifications was alkylation of glass.[151] The alkylation provides hydrophobic support for monolayers of lipids to be stabilized via a pseudo-bilayer with the surface.

Using a similar scheme, free standing arrays can utilize alkylated gold platforms adjacent a silicon dioxide well to form free standing bilayers over the well.[152] Unmodified gold, photoresist, or aluminum oxide can be used as barrier for increasing multiplexity in an array.[153] This can be coupled with etched glass to reduce background and enhance detection.[154] Various methods have also been optimized for control of lipid array formation such as high-volume, low-pressure (HVLP) gun polyelectrolyte deposition on top of gold.[155] Tethered lipid arrays can also be formed using biotinylated species for support on materials such as polydimethylsiloxane (PDMS).[156]

Lipid arrays can be used as a detection or pull-down method for lipid-protein interactions.[46,157] Two of the most common methods of detection with lipid arrays are immunoblotting with epitope tags[158] and fluorescence imaging.[159] Commercially available multiplexed lipid arrays have been used for screening interactions with phosphatidylinositol phosphates such as PLC. One array, PIP Strips[TM], can be used to screen all eight different phosphate modifications of phosphatidylinositol in addition to seven other phospholipids and a blank for reference.[130] Using PIP Array[TM], interactions can be observed against multiple concentrations of all eight phosphate modified phosphatidylinositols at the same time.[160] There is also a commercially available array for screening of interactions for sphingolipids utilizing SphingoStrips[TM].

A simple variation to lipid arrays is the liposome microarray-based assay (LiMA).[161] Here, liposomes are spatially spotted on thin agarose layers (TAL) using a microfluidic PDMS channels to prevent cross-contamination. Binding intensity is normalized by comparing the fluorescence of labelled lipids incorporated into the liposomes and green fluorescent protein (GFP) labelled proteins of interest. Though this technique is easily multiplexed, alternative methods have been utilized to generate liposome arrays above the surface using biotin-streptavidin[162] or epitope tag[163] functionalization.

Protein arrays can also be generated on solid supports to determine interactions with liposomes or other proteins.[164] The microarray can be printed using a quill-pin printer onto a γ-aminopropylsilane modified glass surface.[159] This technique has been used for monitoring interactions with G-protein coupled receptors (GPCR) and lipids. Currently, the full proteome microarray is available for yeast, *S. cervisiae*. This array is generated by either using aldehyde treated chips for N-terminal attachment of the proteins of interest or nickel coated slides for histidine tag (His-tag) binding.[165,166]

Label-based Methods

Labels can be incorporated as fluorophores or fusion tags for various detection methods. Total internal reflection fluorescence microscopy (TIRFM) requires fluorescence labeling of either the surface substrate or the analyte of interest. The penetration depth of the laser determines the sensitivity of the measurement. Lipid arrays doped with fluorescein modified PE have been utilized to calculate binding constants for toxin fragments.[167] Conversely, unmodified lipid arrays can be used to monitor lipid fusion with fluorescently tagged viral particles based on transfer to the array.[168] Methods have been developed similar to enzyme-linked immunosorbent assays (ELISA) by utilizing either lipid or protein arrays as the analyte capture system. The captured species can then be recognized by primary antibody recognition either to a fusion or affinity tag or intrinsic properties followed by secondary antibody imaging by fluorescence.[169] Other recognition methods utilize primary antibody-enzyme conjugates for colorimetric,[170,171] chemiluminescence detection,[172] or functionalized quantum dots.[173]

Atomic Force Microscopy

Surface analysis using atomic force microscopy (AFM) has been used to observe changes on the surface of the array. Lipid monolayers exposed to bovine serum albumin, melitin, and wild type or mutant α-synuclein to observe disruptions in the membrane with using tapping mode.[174] Other studies using AFM involve functionalization of the cantilever with full length or truncated lipid binding proteins. Interactions have been observed with PS and gangliosides (GM) using either C2 domain[175] or cholera toxin[176] cantilever modification, respectively.

Mass Spectrometry

Affinity matrices have been used with a multitude of mass spectrometry techniques to identify interacting species. Matrix laser desorption ionization time-of-flight (MALDI-TOF) mass spectrometry was used to identify cholera toxin absorption to lipid matrices containing GM.[177] In this technique, the cholera toxin was incubated with the lipids before being dried down and applied to a metal plate for laser desorption. Surface enhanced laser desorption ionization time-of-flight (SELDI-TOF) is different in sample preparation due to the proteins actively interacting with the surface substrate prior to laser irradiation. Using this method, wildtype and mutant α-synuclein binding was characterized to a mixture of PC and PS before liquid chromatography (LC) MS/MS

was then used to identify oligomeric states.[174] Protein arrays generated with His-tag immobilization were recently used for self-assembled monolayers for MALDI-TOF (SAMDI-TOF) to observe binding of rhodopsin to transducin.[178]

Surface Plasmon Resonance

Surface plasmon resonance (SPR) uses light deflection through plasmsons from thin layers of certain metals, typically gold to measure changes proportional to the refractive index at the surface. Depending on the SPR sensor, the angle, wavelength, or intensity of the light can be detected with variations based on refractive index changes on the surface.[179,180] SPR has been adapted to measure lipid-protein and membrane protein-protein interactions using many different surface functionalization techniques.[181] Silicate modified gold surface has been used for deposition of lipids for binding interactions between $PI(4,5)P_2$ and $PI(4,5)P_2$ binding protein[155] as well as GM and cholera toxin.[182] The interaction between GM and cholera toxin have been the standard assay for development of other SPR techniques utilizing nanodisc immobilization by His-tag affinity[163] and amplification with anti-cholera toxin biotin conjugates for enhanced sensitivity.[183] Another immobilization technique covalently bound nanodiscs to the surface using PE and 1-ethyl-3-(3-dimethylaminopropyl)carbodiimide (EDC) chemistry to monitor KRas lipid association.[184] These methods utilized SPR by monitoring the change in angle over time are limited in multiplexity due to the need for separate flow channels for each interaction. In comparison, surface plasmon resonance imaging (SPRi) measures the intensity or percent reflectivity of light at a fixed angle over an arrays separated by photoresist.[185] Cholera toxin interactions have been observed using 3-mercaptopropionic acid (MPA) stabilized arrays of various lipid environments,[186] etched glass arrays for enhanced spatial control and sensitivity,[154,187] and PDMS guided flow channels with various concentrations of cholera toxin.[156]

Silicon Photonic Microring Resonators

Silicon photonic microring resonators are refractive index-based sensors similar to SPR.[188–190] The Bailey lab has pioneered silicon photonic microring resonators as a detection method for proteins[191–195] and nucleic acids[196–198] as biomarkers as well as separations coupled with liquid chromatography[199–201] and capillary electrophoresis.[202] Silicon photonic microring resonators utilize refractive index-based sensing of 128 individually addressable rings with a diameter of 30

µm (**Figure I.2A**). Light travels down a linear waveguide adjacent to the rings through total internal reflection. When the resonant condition is met, light couples into the ring cavity (**Figure I.2B**). The resonant condition is governed by the equation:

$$\lambda_r = \frac{2\pi r n_{eff}}{m} \qquad \textbf{(I.1)}$$

where λ_r is the resonant wavelength, $2\pi r$ is the circumference of the microring, n_{eff} is the effective refractive index, and m is a nonzero integer representing the number of optical wavelengths around the perimeter of the ring.[188,189] The change in resonant wavelength is monitored as a dip in transmission overtime as refractive index changes at the sensor surface (**Figure I.2C-D**). Nanodiscs have been interfaced to silicon photonic microring resonators utilizing flow cells to direct functionalization to the surface via electrostatic physisorption between the lipid headgroups and the silicon oxide surface.[203] This shows the potential for characterization of lipid-protein interactions using this technique but does not utilize the full multiplexing capability of the sensor surface.

4. Blood Coagulation

4.1. Extrinsic Pathway Background

The blood coagulation cascade relies on lipid-protein and membrane protein-protein interactions for initiation, propagation, and amplification.[204–207] There are two pathways that make up the blood coagulation cascade, the intrinsic and extrinsic pathway, which are connected through the common pathway. The extrinsic pathway is triggered by tissue damage by exposing PS and tissue factor (TF) which acts as the initiator for subsequent clotting events (**Figure I.3A**). TF is commonly expressed in perivascular and epithelial cells,[208] but events such as inflammation and thrombosis can induce production in other cell types.[209] Blood-borne TF has been found in plasma[210] with an encryption and decryption mechanism for activation.[211]

TF recruits activated factor VII (fVIIa) for proteolytic cleavage of inactive, zymogen factor VII (fVII) bound to neighboring TF.[212,213] The TF-fVIIa complex is known as the extrinsic tenase complex that is responsible for proteolytic activation of factors IX (fIX) and X (fX) (**Figure I.3B**).[214] Activated fIX (fIXa) forms a protease complex with activated factor VIII (fVIIIa) to generate more activated factor X (fXa). The amplification of fXa feeds into the common pathway

to generate the prothrombinase complex with fXa and activated factor V (fVa) to cleave prothrombin (PT) to thrombin. Thrombin is responsible for amplification through positive feedback into the extrinsic pathway by activation of factor V and factor VIII, downstream processing to generate fibrin for blood clot formation, and anti-coagulation through activation of the protein C pathway.[206]

Pro-coagulation factors (fVII, fIX, fX, and PT) and anti-coagulation factors (protein C, protein S, and protein Z) contain N-terminal regions rich in γ-carboxyglutamate (GLA domain) that use Ca^{2+} to interact with PS headgroups.[204] The GLA domains are typically 47 amino acids in length with 9 to 12 glutamates, three of which are conserved among all seven factors. Adjacent to the GLA domain, clotting factors have two domains homologous to epidermal growth factor (EGF) and trypsin-like serine protease domain for cleavage of arginine containing substrates.[215] The GLA domain on the clotting factors is responsible for membrane association for physiological function. Crystal structures are available for the GLA domains of PT,[216] fX,[217] and fIX.[218]

4.2. Blood Coagulation Characterization

Characterization of the interactions at the lipid-protein and membrane protein-protein interface for the blood coagulation cascade is critical for physiological understanding. The following is a brief overview of activity assays specific for blood coagulation and studies that have been done to characterize TF and GLA domains.

Activity Assays

Measurements for activity can be tailored for the physiological system of interest and work well alongside biochemical methods mentioned earlier. The two most common techniques for blood coagulation cascade interactions characterization are clotting and colorimetric assays. Clotting assays are more reliable and reproducible for longer clot times, so optimization may be needed. Typical readouts for clotting assays use either electromechanical recognition for fibrin strands wrapping around a steel ball or turbidity detection by light scattering.[219] Colorimetric assays utilize substrates designed to mimic physiological substrates for proteolytic cleavage of p-nitroanilide which absorbs light at 405 nm.[220,221] The combination of activity assays and biochemical methods can be used to fully understand the physiological interactions of the extrinsic pathway.

Tissue Factor Characterization

Characterization of the membrane interface with TF has been critical to understanding formation of the extrinsic tenase complex. Soluble TF, TF that has had the transmembrane portion removed, was compared to a membrane bound version using a colorimetric substrate for fXa as an indirect detection method of the TF-fVIIa complex formation.[222] The activities and binding were determined to be the indistinguishable when an epitope tag is incorporated. TF has also been modified with chimeras for displacement above the membrane.[223] This study showed similar activity colorimetrically with decreasing binding with increasing distance from the membrane as expected. Clot time was also observed to increase with increasing membrane proximity; thus, showing that the membrane interaction with fVIIa is crucial for complex formation with TF.

The membrane-TF interface has been probed to characterize lipid interactions by using liposome and nanodiscs with varying PS content to show rate of activity was shown to increase with increasing PS.[224] To understand potential membrane-TF interactions, single amino acid mutants of TF were generated with mutations near the membrane interface.[225] Activity assays with fIX, fX, and fVIIa specific substrates were performed to identify interesting residues in the serine loop (residues 160-163) and the exocite (Lys165 and Lys166); however, increase in PS and/or PE content of the membrane overcame any loss in activity. Further investigation into Lys165 by SPR showed similar on rate to wild type but a slower off rate. Therefore, showing interest into continued characterization of the membrane-TF interface.

GLA Domain Characterization

GLA domain characterization is essential to uncovering interactions in the formation of the extrinsic tenase complex and many other interactions downstream in the cascade. PS clustering has been observed in the presence of calcium ions using solid state NMR which can be used to explain part of the GLA domain PS binding interaction.[226] Using SPR, nanodiscs were immobilized on the surface using His-tag affinity to a Ni-NTA functionalized chip. [224] Higher affinity for fX was observed with increasing PS content. By continuing to probe these interactions by doping other phospholipids into the environment, the "Anything But Choline" hypothesis was born.[227] This hypothesis states that a single PS binding site works cooperatively with phosphate groups from lipids other than PC. In a native membrane environment, the cooperativity is likely

seen between PS and PE due to the 12% and 25% physiological abundance respectively.[8] PA has been shown to enhance the binding of fVIIa and aPC.[228] This difference in GLA domain interaction could be potentially due to the unhindered access to the phosphate or negative curvature.[229] Recently, molecular dynamics simulations have been used to predict specific lipid chemical group association with the GLA domain of factor X.[226]

5. Thesis Overview

To better understand nanodiscs, *Chapter 2* is a review about high-density lipoprotein mimetic technology. It is meant to provide unbiased overviews of each stabilization reagent used for nanodisc formation since most reviews focus on one type. *Chapter 3* begins to push the multiplex technology of silicon photonic microring resonators with nanodiscs by comparing seven different environments of PS, PA, and PC binding with blood coagulation clotting factors containing a GLA domain.[230] This provides a proof of concept to show the multiplexed capability with nanodiscs and match the trends observed with increasing PS content with GLA domain-containing proteins and preferred PA specific binding with fVIIa and activated protein C (aPC). *Chapter 4* focuses on continuing to leverage the multiplexing capability of silicon photonic microring resonators with nanodiscs by calculating PS-PE synergistic binding for all seven GLA domain-containing clotting factors.[231]

Chapter 5 is a continued optimization of the nanodisc interface on the microring resonators by modifying the nanodisc preparation to incorporate DNA tags. This optimization allows for the nanodiscs to be tethered above the surface for monitoring of nanodisc loading over time to correct for loading differences, prevent loading bias based on the local nanodisc environment, and characterize TF mutants in various lipid environments. *Chapters 6* utilizes this new technology to characterize GLA domain binding of fX mutants for amino acid requirement for membrane binding. *Chapter 7* is a summary of the work laid out in this thesis and outlines future directions using DNA tethered nanodisc arrays on silicon photonic microring resonators.
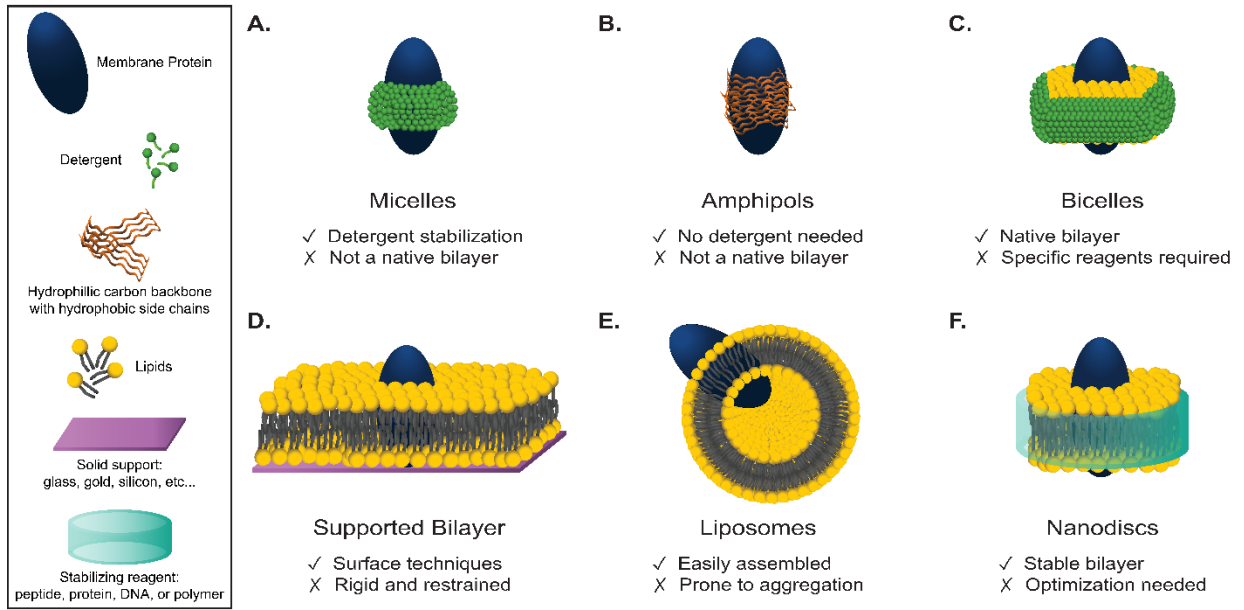
Figure I.1. Schematic of Membrane Mimetics with Advantages and Disadvantages.
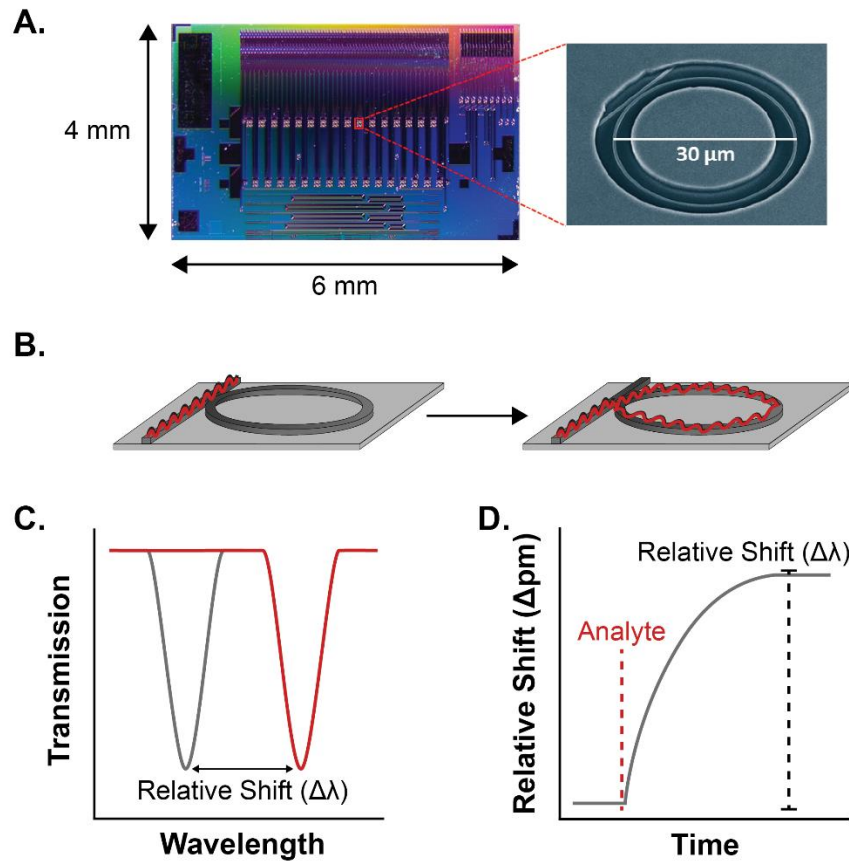
Figure I.2. Silicon Photonic Microring Resonators. (**A**) Silicon on insulator chip with array of 32 clusters of 4 microrings with 30 µm diameter arranged on 4 x 6 mm chips. (**B**) Adjacent linear waveguide utilizes total internal reflection to carry light from the laser source centered at 1550 nm to the detector. (**C**) When the resonance condition is met, light is coupled into the microring and the dip in transmittance is measured. (**D**) The change in the transmittance over time is proportional to the refractive index change at the microring surface.
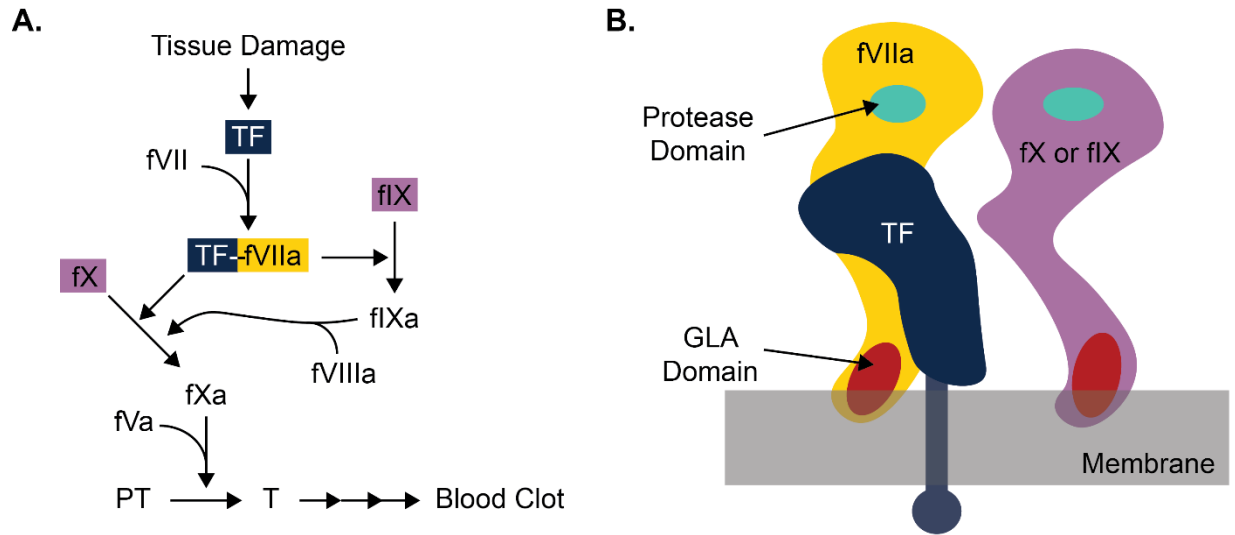
Figure I.3. Extrinsic Blood Coagulation Cascade. (**A**) The extrinsic pathway initiation and propagation to a blood clot. (**B**) The extrinsic tenase complex binding to either fX or fIX. Abbreviations: tissue factor (TF); factor VII (fVII); activated factor VII (fVIIa); factor IX (IX); activated factor IX (fIXa); factor X (fX); activated factor X (Xa); activated factor V (fVa); activated factor VIII (fVIIIa); prothrombin (PT); thrombin (T).

REFERENCES

(1)   Wymann, M. P.; Schneiter, R. Lipid Signalling in Disease. *Nat. Rev. Mol. Cell Biol.* **2008**, *9* (2), 162–176.

(2)   Sudhahar, C. G.; Haney, R. M.; Xue, Y.; Stahelin, R. V. Cellular Membranes and Lipid-Binding Domains as Attractive Targets for Drug Development. *Curr. Drug Targets* **2008**, *9* (8), 603–613.

(3)   van Meer, G.; Voelker, D. R.; Feigenson, G. W. Membrane Lipids: Where They Are and How They Behave. *Nat. Rev. Mol. Cell Biol.* **2008**, *9* (2), 112–124.

(4)   van Meer, G.; de Kroon, A. I. P. M. Lipid Map of the Mammalian Cell. *J. Cell Sci.* **2011**, *124* (1), 5–8.

(5)   Fahy, E.; Subramaniam, S.; Murphy, R. C.; Nishijima, M.; Raetz, C. R. H.; Shimizu, T.; Spener, F.; Van Meer, G.; Wakelam, M. J. O.; Dennis, E. A. Update of the LIPID MAPS Comprehensive Classification System for Lipids. *J. Lipid Res.* **2009**, *50* (SUPPL.), 9–14.

(6)   Cebecauer, M.; Amaro, M.; Jurkiewicz, P.; Sarmento, M. J.; Šachl, R.; Cwiklik, L.; Hof, M. Membrane Lipid Nanodomains. *Chem. Rev.* **2018**, *118* (23), 11259–11297.

(7)   Sezgin, E.; Levental, I.; Mayor, S.; Eggeling, C. The Mystery of Membrane Organization: Composition, Regulation and Roles of Lipid Rafts. *Nat. Rev. Mol. Cell Biol.* **2017**, *18* (6), 361–374.

(8)   Leventis, P. A.; Grinstein, S. The Distribution and Function of Phosphatidylserine in Cellular Membranes. *Annu. Rev. Biophys.* **2010**, *39*, 407–427.

(9)   Narayan, K.; Lemmon, M. A. Determining Selectivity of Phosphoinositide-Binding Domains. *Methods* **2006**, *39* (2), 122–133.

(10)   Lemmon, M. A. Membrane Recognition by Phospholipid-Binding Domains. *Nat. Rev. Mol. Cell Biol.* **2008**, *9* (2), 99–111.

(11)   McLaughlin, S.; Murray, D. Plasma Membrane Phosphoinositide Organization by Protein Electrostatics. *Nature* **2005**, *438* (7068), 605–611.

(12)   Stace, C. L.; Ktistakis, N. T. Phosphatidic Acid- and Phosphatidylserine-Binding Proteins. *Biochim. Biophys. Acta - Mol. Cell Biol. Lipids* **2006**, *1761* (8), 913–926.

(13)   Stahelin, R. V. Lipid Binding Domains: More than Simple Lipid Effectors. *J. Lipid Res.* **2009**, *50* (Suppl), 299–304.

(14)   Cho, W.; Stahelin, R. V. Membrane-Protein Interactions in Cell Signaling and Membrane Trafficking. *Annu. Rev. Biophys. Biomol. Struct.* **2005**, *34*, 119–151.

(15)   DiNitto, J. P.; Cronin, T. C.; Lambright, D. G. Membrane Recognition and Targeting by Lipid-Binding Domains. *Sci. STKE* **2003**, *2003* (213), 1–16.

(16)   Lee, S. A.; Eyeson, R.; Cheever, M. L.; Geng, J.; Verkhusha, V. V.; Burd, C.; Overduin, M.; Kutateladze, T. G. Targeting of the FYVE Domain to Endosomal Membranes Is Regulated by a Histidine Switch. *Proc. Natl. Acad. Sci. U. S. A.* **2005**, *102* (37), 13052–13057.

(17)   He, J.; Haney, R. M.; Vora, M.; Verkhusha, V. V.; Stahelin, R. V.; Kutateladze, T. G. Molecular Mechanism of Membrane Targeting by the GRP1 PH Domain. *J. Lipid Res.* **2008**, *49* (8), 1807–1815.

(18)   Hom, R. A.; Vora, M.; Regner, M.; Subach, O. M.; Cho, W.; Verkhusha, V. V.; Stahelin, R. V.; Kutateladze, T. G. PH-Dependent Binding of the Epsin ENTH Domain and the AP180 ANTH Domain to PI(4,5)P2-Containing Bilayers. *J. Mol. Biol.* **2007**, *373* (2), 412–423.

(19)   Fadok, V. A.; Bratton, D. L.; Frasch, S. C.; Warner, M. L.; Henson, P. M. The Role of Phosphatidylserine in Recognition of Apoptotic Cells by Phagocytes. *Cell Death Differ.* **1998**, *5* (7), 551–562.

(20)   Newton, A. C.; Johnson, J. E. Protein Kinase C: A Paradigm for Regulation of Protein Function by Two Membrane-Targeting Modules. *Biochim. Biophys. Acta - Rev. Biomembr.* **1998**, *1376* (2), 155–172.

(21)   Takai, Y.; Kishimoto, A.; Iwasa, Y.; Kawahara, Y.; Mori, T.; Nishizuka, Y. Calcium-Dependent Activation of a Multifunctional Protein Kinase by Membrane Phospholipids. *J. Biol. Chem.* **1979**, *254* (10), 3692–3695.

(22)   Zhang, G.; Kazanietz, M. G.; Blumberg, P. M.; Hurley, J. H. Crystal Structure of the Cys2 Activator-Binding Domain of Protein Kinase Cδ in Complex with Phorbol Ester. *Cell* **1995**, *81* (6), 917–924.

(23)   Sutton, R. B.; Davletov, B. A.; Berghuis, A. M.; Sudhof, T. C.; Sprang, S. R. Structure of the First C2 Domain of Synaptotagmin I: A Novel Ca2+/Phospholipid-Binding Fold. *Cell* **1995**, *80* (6), 929–938.

(24)   Ferguson, K. M.; Lemmon, M. A.; Schlessinger, J.; Sigler, P. B. Structure of the High

Affinity Complex of Inositol Trisphosphate with a Phospholipase C Pleckstrin Homology Domain. *Cell* **1995**, *83* (6), 1037–1046.

(25)   Karathanassis, D.; Stahelin, R. V.; Bravo, J.; Perisic, O.; Pacold, C. M.; Cho, W.; Williams, R. L. Binding of the PX Domain of P47phox to Phosphatidylinositol 3, 4-Bisphosphate and Phosphatidic Acid Is Masked by an Intramolecular Interaction. *EMBO J.* **2002**, *21* (19), 5057–5068.

(26)   Brown, M. F. Soft Matter in Lipid – Protein Interactions. *Annu. Rev. Biophys.* **2017**, *46*, 379–410.

(27)   Ingolfsson, H. I.; Arnarez, C.; Periole, X.; Marrink, S. J. Computational 'microscopy of Cellular Membranes. *J. Cell Sci.* **2016**, *129* (2), 257–268.

(28)   Newport, T. D.; Sansom, M. S. P.; Stansfeld, P. J. The MemProtMD Database: A Resource for Membrane-Embedded Protein Structures and Their Lipid Interactions. *Nucleic Acids Res.* **2019**, *47*, D390–D397.

(29)   Loose, M.; Schwille, P. Biomimetic Membrane Systems to Study Cellular Organization. *J. Struct. Biol.* **2009**, *168* (1), 143–151.

(30)   *Biomimetic Lipid Membranes: Fundamentals, Applications, and Commercialization*; Kök, F. N., Yildiz, A. A., Inci, F., Eds.; Springer Nature Switzerland: Cham, Switzerland, 2019.

(31)   Brotherus, J. R.; Jost, P. C.; Griffith, O. H.; Hokin, L. E. Detergent Inactivation of Sodium- and Potassium-Activated Adenosinetriphosphatase of the Electric Eel. *Biochemistry* **1979**, *18* (23), 5043–5050.

(32)   Breyton, C.; Tribet, C.; Olive, J.; Dubacq, J.-P.; Popot, J.-L. Dimer to Monomer Conversion of Cytochrome B6f Complex. *J. Biol. Chem.* **1997**, *272* (35), 21892–21900.

(33)   Zoonens, M.; Popot, J. L. Amphipols for Each Season. *J. Membr. Biol.* **2014**, *247* (9–10), 759–796.

(34)   Tribet, C.; Audebert, R.; Popot, J. L. Amphipols: Polymers That Keep Membrane Proteins Soluble in Aqueous Solutions. *Proc. Natl. Acad. Sci. U. S. A.* **1996**, *93* (26), 15047–15050.

(35)   Whiles, J. A.; Deems, R.; Vold, R. R.; Dennis, E. A. Bicelles in Structure-Function Studies of Membrane-Associated Proteins. *Bioorg. Chem.* **2002**, *30* (6), 431–442.

(36)   Dürr, U. H. N.; Gildenberg, M.; Ramamoorthy, A. The Magic of Bicelles Lights up Membrane Protein Structure. *Chem. Rev.* **2012**, *112* (11), 6054–6074.

(37)   Mäler, L.; Gräslund, A. Artificial Membrane Models for the Study of Macromolecular

Delivery. In *Macromolecular Drug Delivery: Methods and Protocols*; Belting, M., Ed.; Humana Press: New York, 2009; Vol. 480, pp 129–138.

(38) Mingeot-Leclercq, M.-P.; Deleu, M.; Brasseur, R.; Dufrêne, Y. F. Atomic Force Microscopy of Supported Lipid Bilayers. *Nat. Protoc.* **2008**, *3* (10), 1654–1659.

(39) Penkauskas, T.; Preta, G. Biological Applications of Tethered Bilayer Lipid Membranes. *Biochimie* **2019**, *157*, 131–141.

(40) Junghans, A.; Köper, I. Structural Analysis of Tethered Bilayer Lipid Membranes. *Langmuir* **2010**, *26* (13), 11035–11040.

(41) Rossi, C.; Briand, E.; Parot, P.; Odorico, M.; Chopineau, J. Surface Response Methodology for the Study of Supported Membrane Formation. *J. Phys. Chem. B* **2007**, *111* (26), 7567–7576.

(42) Akbarzadeh, A.; Rezaei-sadabady, R.; Davaran, S.; Joo, S. W.; Zarghami, N.; Hanifehpour, Y.; Samiei, M.; Kouhi, M.; Nejati-Koshki, K. Liposome: Classification, Preparation, and Applications. *Nanoscale Res. Lett.* **2013**, *8* (1), 102–110.

(43) Patil, Y. P.; Jadhav, S. Novel Methods for Liposome Preparation. *Chem. Phys. Lipids* **2014**, *177*, 8–18.

(44) Wagner, A.; Vorauer-Uhl, K. Liposome Technology for Industrial Purposes. *J. Drug Deliv.* **2011**, *2011*, 1–9.

(45) Christensen, S. M.; Stamou, D. Vesicle Arrays as Model-Membranes and Biochemical Reactor Systems. In *Biomimetic Membranes for Sensor and Separation Applications*; Hélix-Nielsen, C., Ed.; Springer: New York, 2011; pp 87–112.

(46) Bally, M.; Bailey, K.; Sugihara, K.; Grieshaber, D.; Vörös, J.; Stäler, B. Liposome and Lipid Bilayer Arrays towards Biosensing Applications. *Small* **2010**, *6* (22), 2481–2497.

(47) Müller, S.; Kind, M.; Gruhle, K.; Hause, G.; Meister, A.; Drescher, S. Mixing Behaviour of Bilayer-Forming Phosphatidylcholines with Single-Chain Alkyl-Branched Bolalipids: Effect of Lateral Chain Length. *Biophys. Chem.* **2019**, *244*, 1–10.

(48) Orth, M.; Bellosta, S. Cholesterol: Its Regulation and Role in Central Nervous System Disorders. *Cholesterol* **2012**, *2012*, 1–19.

(49) Lund-Katz, S.; Phillips, M. C. High Density Lipoprotein Structure-Function and Role in Reverse Cholesterol Transport. In *Cholesterol Binding and Cholesterol Transport: Structure and Function in Health and Disease*; Harris, J. R., Ed.; Springer: New York, 2010;

pp 183–227.

(50) Gordon, T.; Castelli, W. P.; Hjortland, M. C.; Kannel, W. B.; Dawber, T. R. High Density Lipoprotein as a Protective Factor against Coronary Heart Disease. The Framingham Study. *Am. J. Med.* **1977**, *62* (5), 707–714.

(51) Segrest, J. P.; De Loof, H.; Dohlman, J. G.; Brouillette, C. G.; Anantharamaiah, G. M. Amphipathic Helix Motif: Classes and Properties. *Proteins* **1990**, *8* (2), 103–117.

(52) Vickers, K. C.; Remaley, A. T. HDL and Cholesterol: Life after the Divorce? 1. *J. Lipid Res.* **2014**, *55* (1), 4–12.

(53) Mulder, W. J. M.; Van Leent, M. M. T.; Lameijer, M.; Fisher, E. A.; Fayad, Z. A.; Pérez-Medina, C. High-Density Lipoprotein Nanobiologics for Precision Medicine. *Acc. Chem. Res.* **2018**, *51* (1), 127–137.

(54) Kanellis, P.; Romans, A. Y.; Johnson, B. J.; Kercretg, H.; Chiovetti, R.; Allen, T. M.; Segrest, J. P. Studies of Synthetic Peptide Analogs of the Amphiphatic Helix: Effect of Charged Amino Acid Residue Topography on Lipid Affinity. *J. Biol. Chem.* **1980**, *255* (23), 11464–11472.

(55) Anantharamaiah, G. M.; Jones, J. L.; Brouillette, C. G.; Schmidt, C. F.; Chung, B. H.; Hughes, T. A.; Bhown, A. S.; Segrest, J. P. Studies of Synthetic Peptide Analogs of the Amphiphatic Helix: Structure of Complexes with Dimyrstoyl Phosphatidylcholine. *J. Biol. Chem.* **1985**, *260* (18), 10256–10262.

(56) Chung, B. H.; Anantharamaiah, G. M.; Brouillette, C. G.; Nishida, T.; Segrest, J. P. Studies of Synthetic Peptide Analogs of the Amphiphatic Helix. Correlation of Structure with Function. *J. Biol. Chem.* **1985**, *260* (18), 10256–10262.

(57) Segrest, J. P.; Jackson, R. L.; Morrisett, J. D.; Gotto, A. M. A Molecular Theory of Lipid-Protein Interactions in the Plasma Lipoproteins. *FEBS Lett.* **1974**, *38* (3), 247–253.

(58) Segrest, J. P. Amphipathic Helixes and Plasma Lipoproteins: Thermodynamic and Geometric Considerations. *Chem. Phys. Lipids* **1977**, *18* (1), 7–22.

(59) Larsen, A. N.; Sørensen, K. K.; Johansen, N. T.; Martel, A.; Kirkensgaard, J. J. K.; Jensen, K. J.; Arleth, L.; Midtgaard, S. R. Dimeric Peptides with Three Different Linkers Self-Assemble with Phospholipids to Form Peptide Nanodiscs That Stabilize Membrane Proteins. *Soft Matter* **2016**, *12* (27), 5937–5949.

(60) Datta, G.; Chaddha, M.; Hama, S.; Navab, M.; Fogelman, A. M.; Garber, D. W.; Mishra,

V. K.; Epand, R. M.; Epand, R. F.; Lund-Katz, S.; Phillips, M. C.; Segrest, J. P.; Anantharamaiah, G. M. Effects of Increasing Hydrophobicity on the Physical-Chemical and Biological Properties of a Class A Amphipathic Helical Peptide. *J. Lipid Res.* **2001**, *42* (7), 1096–1104.

(61)   Sethi, A. A.; Stonik, J. A.; Thomas, F.; Demosky, S. J.; Amar, M.; Neufeld, E.; Brewer, H. B.; Davidson, W. S.; D'Souza, W.; Sviridov, D.; Remaley, A. T. Asymmetry in the Lipid Affinity of Bihelical Amphipathic Peptides: A Structural Determinant for the Specificity of ABCA1-Dependent Cholesterol Efflux by Peptides. *J. Biol. Chem.* **2008**, *283* (47), 32273–32282.

(62)   Carlson, M. L.; Young, J. W.; Zhao, Z.; Fabre, L.; Jun, D.; Li, J.; Li, J.; Dhupar, H. S.; Wason, I.; Mills, A. T.; Beatty, J. T.; Klassen, J. S.; Rouiller, I.; Duong, F. The Peptidisc, a Simple Method for Stabilizing Membrane Proteins in Detergent-Free Solution. *Elife* **2018**, *7* (e34085), 1–23.

(63)   Kariyazono, H.; Nadai, R.; Miyajima, R.; Takechi-Haraya, Y.; Baba, T.; Shigenaga, A.; Okuhira, K.; Otaka, A.; Saito, H. Formation of Stable Nanodiscs by Bihelical Apolipoprotein A-I Mimetic Peptide. *J. Pept. Sci.* **2015**, *22* (2), 116–122.

(64)   Islam, R. M.; Pourmousa, M.; Sviridov, D.; Gordon, S. M.; Neufeld, E. B.; Freeman, L. A.; Perrin, B. S.; Pastor, R. W.; Remaley, A. T. Structural Properties of Apolipoprotein A-I Mimetic Peptides That Promote ABCA1-Dependent Cholesterol Efflux. *Sci. Rep.* **2018**, *8* (1), 1–15.

(65)   Zhao, Y.; Imura, T.; Leman, L. J.; Curtiss, L. K.; Maryanoff, B. E.; Ghadiri, M. R. Mimicry of High-Density Lipoprotein: Functional Peptide-Lipid Nanoparticles Based on Multivalent Peptide Constructs. *J. Am. Chem. Soc.* **2013**, *135* (36), 13414–13424.

(66)   Dassaux, J.-L. Peptide/Lipid Complex Formation by Co-Lyophilization. 10/252,940, 2007.

(67)   Dassaux, J.-L.; Sekul, R.; Büttner, K.; Cornut, I.; Metz, G.; Dufourcq, J. Apolipoprotein A-I Agonists and Their Use to Treat Dyslipidemic Disorders. 08/940,095, 1999.

(68)   Anantharamaiah, G. M.; Mishra, V. K.; Garber, D. W.; Datta, G.; Handattu, S. P.; Palgunachari, M. N.; Chaddha, M.; Navab, M.; Reddy, S. T.; Segrest, J. P.; Fogelman, A. M. Structural Requirements for Antioxidative and Anti-Inflammatory Properties of Apolipoprotein A-I Mimetic Peptides. *J. Lipid Res.* **2007**, *48* (9), 1915–1923.

(69)   Watson, C. E.; Weissbach, N.; Kjems, L.; Ayalasomayajula, S.; Zhang, Y.; Chang, I.;

Navab, M.; Hama, S.; Hough, G.; Reddy, S. T.; Soffer, D.; Rader, D. J.; Fogelman, A. M.; Schecter, A. Treatment of Patients with Cardiovascular Disease with L-4F, an Apo-A1 Mimetic, Did Not Improve Select Biomarkers of HDL Function. *J. Lipid Res.* **2011**, *52* (2), 361–373.

(70) Bloedon, L. A. T.; Dunbar, R.; Duffy, D.; Pinell-Salles, P.; Norris, R.; DeGroot, B. J.; Movva, R.; Navab, M.; Fogelman, A. M.; Rader, D. J. Safety, Pharmacokinetics, and Pharmacodynamics of Oral ApoA-I Mimetic Peptide D-4F in High-Risk Cardiovascular Patients. *J. Lipid Res.* **2008**, *49* (6), 1344–1352.

(71) Sherman, C. B.; Peterson, S. J.; Frishman, W. H. Apolipoprotein A-I Mimetic Peptides: A Potential New Therapy for the Prevention of Atherosclerosis. *Cardiol. Rev.* **2010**, *18* (3), 141–147.

(72) *Apolipoprotein Mimetic Peptides for Stimulating Cholesterol Efflux*; Anantharamaiah, G. M., Goldberg, D., Eds.; Adis: Switzerland, 2015.

(73) Sahoo, B. R.; Genjo, T.; Cox, S. J.; Stoddard, A. K.; Anantharamaiah, G. M.; Fierke, C.; Ramamoorthy, A. Nanodisc-Forming Scaffold Protein Promoted Retardation of Amyloid-Beta Aggregation. *J. Mol. Biol.* **2018**, *430* (21), 4230–4244.

(74) Kuai, R.; Yuan, W.; Son, S.; Nam, J.; Xu, Y.; Fan, Y.; Schwendeman, A.; Moon, J. J. Elimination of Established Tumors with Nanodisc-Based Combination Chemoimmunotherapy. *Sci. Adv.* **2018**, *4* (4), 1–14.

(75) Kadiyala, P.; Li, D.; Nunez, F. M.; Altshuler, D.; Doherty, R.; Kuai, R.; Yu, M.; Kamran, N.; Edwards, M.; Moon, J. J.; Lowenstein, P. R.; Castro, M. G.; Schwendeman, A. High-Density Lipoprotein-Mimicking Nanodiscs for Chemo-Immunotherapy against Glioblastoma Multiforme. *ACS Nano* **2019**, *13* (2), 1365–1384.

(76) Scheetz, L.; Park, K. S.; Li, Q.; Lowenstein, P. R.; Castro, M. G.; Schwendeman, A.; Moon, J. J. Engineering Patient-Specific Cancer Immunotherapies. *Nat. Biomed. Eng.* **2019**, *3* (10), 768–782.

(77) Kuai, R.; Ochyl, L. J.; Bahjat, K. S.; Schwendeman, A.; Moon, J. J. Designer Vaccine Nanodiscs for Personalized Cancer Immunotherapy. *Nat. Mater.* **2017**, *16* (4), 489–498.

(78) Kuai, R.; Sun, X.; Yuan, W.; Xu, Y.; Schwendeman, A.; Moon, J. J. Subcutaneous Nanodisc Vaccination with Neoantigens for Combination Cancer Immunotherapy. *Bioconjug. Chem.* **2018**, *29* (3), 771–775.

(79) Bayburt, T. H.; Grinkova, Y. V.; Sligar, S. G. Self-Assembly of Discoidal Phospholipid Bilayer Nanoparticles with Membrane Scaffold Proteins. *Nano Lett.* **2002**, *2* (8), 853–856.

(80) Denisov, I. G.; Grinkova, Y. V.; Lazarides, A. A.; Sligar, S. G. Directed Self-Assembly of Monodisperse Phospholipid Bilayer Nanodiscs with Controlled Size Directed Self-Assembly of Monodisperse Phospholipid Bilayer Nanodiscs with Controlled Size. *Nano Lett.* **2004**, *126* (11), 3477–3487.

(81) Hagn, F.; Nasr, M. L.; Wagner, G. Assembly of Phospholipid Nanodiscs of Controlled Size for Structural Studies of Membrane Proteins by NMR. *Nat. Protoc.* **2018**, *13* (1), 79–98.

(82) Grinkova, Y. V.; Denisov, I. G.; Sligar, S. G. Engineering Extended Membrane Scaffold Proteins for Self-Assembly of Soluble Nanoscale Lipid Bilayers. *Protein Eng. Des. Sel.* **2010**, *23* (11), 843–848.

(83) Schuler, M. A.; Denisov, I. G.; Sligar, S. G. Nanodiscs as a New Tool to Examine Lipid-Protein Interactions. In *Methods in Molecular Biology*; Kleinschmidt, J., Ed.; Springer Science: New York, 2013; Vol. 974, pp 415–433.

(84) Denisov, I. G.; Sligar, S. G. Nanodiscs in Membrane Biochemistry and Biophysics. *Chem. Rev.* **2017**, *117* (6), 4669–4713.

(85) McLean, M. A.; Gregory, M. C.; Sligar, S. G. Nanodiscs: A Controlled Bilayer Surface for the Study of Membrane Proteins. *Annu. Rev. Biophys.* **2018**, *47* (1), 107–124.

(86) Nath, A.; Atkins, W. M.; Sligar, S. G. Applications of Phospholipid Bilayer Nanodiscs in the Study of Membranes and Membrane Proteins Current Topics Applications of Phospholipid Bilayer Nanodiscs in the Study of Membranes And. *Biochemistry* **2007**, *46* (8), 2059–2069.

(87) Bayburt, T. H.; Sligar, S. G. Membrane Protein Assembly into Nanodiscs. *FEBS Lett.* **2010**, *584* (9), 1721–1727.

(88) Nasr, M. L. Large Nanodiscs Going Viral. *Curr. Opin. Struct. Biol.* **2020**, *60*, 150–156.

(89) Miehling, J.; Goricanec, D.; Hagn, F. A Split-Intein-Based Method for the Efficient Production of Circularized Nanodiscs for Structural Studies of Membrane Proteins. *ChemBioChem* **2018**, *19* (18), 1927–1933.

(90) Nasr, M. L.; Baptista, D.; Strauss, M.; Sun, Z. Y. J.; Grigoriu, S.; Huser, S.; Plückthun, A.; Hagn, F.; Walz, T.; Hogle, J. M.; Wagner, G. Covalently Circularized Nanodiscs for Studying Membrane Proteins and Viral Entry. *Nat. Methods* **2017**, *14* (1), 49–52.

(91) Johansen, N. T.; Tidemand, F. G.; Nguyen, T. T. T. N.; Rand, K. D.; Pedersen, M. C.; Arleth, L. Circularized and Solubility-Enhanced MSPs Facilitate Simple and High-Yield Production of Stable Nanodiscs for Studies of Membrane Proteins in Solution. *FEBS J.* **2019**, *286* (9), 1734–1751.

(92) Zhao, Z.; Zhang, M.; Hogle, J. M.; Shih, W. M.; Wagner, G.; Nasr, M. L. DNA-Corralled Nanodiscs for the Structural and Functional Characterization of Membrane Proteins and Viral Entry. *J. Am. Chem. Soc.* **2018**, *140* (34), 10639–10643.

(93) Dörr, J. M.; Scheidelaar, S.; Koorengevel, M. C.; Dominguez, J. J.; Schäfer, M.; van Walree, C. A.; Killian, J. A. The Styrene–Maleic Acid Copolymer: A Versatile Tool in Membrane Research. *Eur. Biophys. J.* **2016**, *45* (1), 3–21.

(94) Stroud, Z.; Hall, S. C. L.; Dafforn, T. R. Purification of Membrane Proteins Free from Conventional Detergents: SMA, New Polymers, New Opportunities and New Insights. *Methods* **2018**, *147*, 106–117.

(95) Ravula, T.; Hardin, N. Z.; Ramamoorthy, A. Polymer Nanodiscs: Advantages and Limitations. *Chem. Phys. Lipids* **2019**, *219*, 45–49.

(96) Overduin, M.; Klumperman, B. Advancing Membrane Biology with Poly(Styrene-Co-Maleic Acid)-Based Native Nanodiscs. *Eur. Polym. J.* **2019**, *110*, 63–68.

(97) Knowles, T. J.; Finka, R.; Smith, C.; Lin, Y. P.; Dafforn, T.; Overduin, M. Membrane Proteins Solubilized Intact in Lipid Containing Nanoparticles Bounded by Styrene Maleic Acid Copolymer. *J. Am. Chem. Soc.* **2009**, *131* (22), 7484–7485.

(98) Morrison, K. A.; Akram, A.; Mathews, A.; Khan, Z. A.; Patel, J. H.; Zhou, C.; Hardy, D. J.; Moore-Kelly, C.; Patel, R.; Odiba, V.; Knowles, T. J.; Javed, M. U. H.; Chmel, N. P.; Dafforn, T. R.; Rothnie, A. J. Membrane Protein Extraction and Purification Using Styrene-Maleic Acid (SMA) Copolymer: Effect of Variations in Polymer Structure. *Biochem. J.* **2016**, *473* (23), 4349–4360.

(99) Tanaka, M.; Hosotani, A.; Tachibana, Y.; Nakano, M.; Iwasaki, K.; Kawakami, T.; Mukai, T. Preparation and Characterization of Reconstituted Lipid-Synthetic Polymer Discoidal Particles. *Langmuir* **2015**, *31* (46), 12719–12726.

(100) Scheidelaar, S.; Koorengevel, M. C.; van Walree, C. A.; Dominguez, J. J.; Dörr, J. M.; Killian, J. A. Effect of Polymer Composition and PH on Membrane Solubilization by Styrene-Maleic Acid Copolymers. *Biophys. J.* **2016**, *111* (9), 1974–1986.

(101) Ravula, T.; Hardin, N. Z.; Ramadugu, S. K.; Ramamoorthy, A. PH Tunable and Divalent Metal Ion Tolerant Polymer Lipid Nanodiscs. *Langmuir* **2017**, *33* (40), 10655–10662.

(102) Ravula, T.; Hardin, N. Z.; Ramadugu, S. K.; Cox, S. J.; Ramamoorthy, A. Formation of PH-Resistant Monodispersed Polymer–Lipid Nanodiscs. *Angew. Chemie - Int. Ed.* **2018**, *57* (5), 1342–1345.

(103) Ravula, T.; Hardin, N. Z.; Bai, J.; Im, S. C.; Waskell, L.; Ramamoorthy, A. Effect of Polymer Charge on Functional Reconstitution of Membrane Proteins in Polymer Nanodiscs. *Chem. Commun.* **2018**, *54* (69), 9615–9618.

(104) Hall, S. C. L.; Tognoloni, C.; Charlton, J.; Bragginton, É. C.; Rothnie, A. J.; Sridhar, P.; Wheatley, M.; Knowles, T. J.; Arnold, T.; Edler, K. J.; Dafforn, T. R. An Acid-Compatible Co-Polymer for the Solubilization of Membranes and Proteins into Lipid Bilayer-Containing Nanoparticles. *Nanoscale* **2018**, *10* (22), 10609–10619.

(105) Fiori, M. C.; Zheng, W.; Kamilar, E.; Simiyu, G.; Guillermo, A. A. Extraction and Reconstitution of Membrane Proteins into Lipid Nanodiscs Encased by Zwitterionic Styrene-Maleic Amide Copolymers. *Sci. Rep.* **2020**, *10* (1), 1–13.

(106) Yasuhara, K.; Arakida, J.; Ravula, T.; Ramadugu, S. K.; Sahoo, B.; Kikuchi, J. I.; Ramamoorthy, A. Spontaneous Lipid Nanodisc Fomation by Amphiphilic Polymethacrylate Copolymers. *J. Am. Chem. Soc.* **2017**, *139* (51), 18657–18663.

(107) Oluwole, A. O.; Danielczak, B.; Meister, A.; Babalola, J. O.; Vargas, C.; Keller, S. Solubilization of Membrane Proteins into Functional Lipid-Bilayer Nanodiscs Using a Diisobutylene/Maleic Acid Copolymer. *Angew. Chemie - Int. Ed.* **2017**, *56* (7), 1919–1924.

(108) Hsia, C.-Y.; Richards, M. J.; Daniel, S. A Review of Traditional and Emerging Methods to Characterize Lipid-Protein Interactions in Biological Membranes. *Anal. Methods* **2015**, *7* (17), 7076–7094.

(109) Zhao, H.; Lappalainen, P. A Simple Guide to Biochemical Approaches for Analyzing Protein-Lipid Interactions. *Mol. Biol. Cell* **2012**, *23* (15), 2823–2830.

(110) Yin, H.; Flynn, A. D. Drugging Membrane Protein Interactions. *Annu. Rev. Biomed. Eng.* **2016**, *18* (1), 51–76.

(111) Smith, A. W. Lipid-Protein Interactions in Biological Membranes: A Dynamic Perspective. *Biochim. Biophys. Acta - Biomembr.* **2012**, *1818* (2), 172–177.

(112) Saliba, A.-E.; Vonkova, I.; Gavin, A.-C. The Systematic Analysis of Protein–Lipid

Interactions Comes of Age. *Nat. Rev. Mol. Cell Biol.* **2015**, *16* (12), 753–761.

(113) Cho, H.; Wu, M.; Bilgin, B.; Walton, S. P.; Chan, C. Latest Developments in Experimental and Computational Approaches to Characterize Protein-Lipid Interactions. *Proteomics* **2012**, *12* (22), 3273–3285.

(114) Ford, M. G. J.; Pearse, B. M. F.; Higgins, M. K.; Vallis, Y.; Owen, D. J.; Gibson, A.; Hopkins, C. R.; Evans, P. R.; McMahon, H. T. Simultaneous Binding of PtdIns (4,5) P2 and Clathrin by AP180 in the Nucleation of Clathrin Lattices on Membranes. *Science (80-.).* **2001**, *291* (5506), 1051–1055.

(115) Tsujita, K.; Suetsugu, S.; Sasaki, N.; Furutani, M.; Oikawa, T.; Takenawa, T. Coordination between the Actin Cytoskeleton and Membrane Deformation by a Novel Membrane Tubulation Domain of PCH Proteins Is Involved in Endocytosis. *J. Cell Biol.* **2006**, *172* (2), 269–279.

(116) Ishii, M.; Fujita, S.; Yamada, M.; Hosaka, Y.; Kurachi, Y. Phosphatidylinositol 3,4,5-Trisphosphate and Ca2+/Calmodulin Competitively Bind to the Regulators of G-Protein-Signalling (RGS) Domain of RGS4 and Reciprocally Regulate Its Action. *Biochem. J.* **2005**, *385* (1), 65–73.

(117) Lee, S. H.; Jin, J. B.; Song, J.; Min, M. K.; Park, D. S.; Kim, Y. W.; Hwang, I. The Intermolecular Interaction between the PH Domain and the C-Terminal Domain of Arabidopsis Dynamin-like 6 Determines Lipid Binding Specificity. *J. Biol. Chem.* **2002**, *277* (35), 31842–31849.

(118) Dalton, A. K.; Murray, P. S.; Murray, D.; Vogt, V. M. Biochemical Characterization of Rous Sarcoma Virus MA Protein Interaction with Membranes. *J. Virol.* **2005**, *79* (10), 6227–6238.

(119) Benfenati, F.; Greengard, P.; Brunner, J.; Bähler, M. Electrostatic and Hydrophobic Interactions of Synapsin I and Synapsin I Fragments with Phospholipid Bilayers. *J. Cell Biol.* **1989**, *108* (5), 1851–1862.

(120) Haberkant, P.; Van Meer, G. Protein-Lipid Interactions: Paparazzi Hunting for Snap-Shots. *Biol. Chem.* **2009**, *390* (8), 795–803.

(121) Gubbens, J.; De Kroon, A. I. P. M. Proteome-Wide Detection of Phospholipid-Protein Interactions in Mitochondria by Photocrosslinking and Click Chemistry. *Mol. Biosyst.* **2010**, *6* (10), 1751–1759.

(122) Wiseman, T.; Williston, S.; Brandts, J. F.; Lin, L. N. Rapid Measurement of Binding Constants and Heats of Binding Using a New Titration Calorimeter. *Anal. Biochem.* **1989**, *179* (1), 131–137.

(123) Seelig, J. Titration Calorimetry of Lipid-Peptide Interactions. *Biochim. Biophys. Acta - Rev. Biomembr.* **1997**, *1331* (1), 103–116.

(124) Anbazhagan, V.; Sankhala, R. S.; Singh, B. P.; Swamy, M. J. Isothermal Titration Calorimetric Studies on the Interaction of the Major Bovine Seminal Plasma Protein, PDC-109 with Phospholipid Membranes. *PLoS One* **2011**, *6* (10).

(125) Radhakrishnan, A.; Stein, A.; Jahn, R.; Fasshauer, D. The Ca2+ Affinity of Synaptotagmin 1 Is Markedly Increased by a Specific Interaction of Its C2B Domain with Phosphatidylinositol 4,5-Bisphosphate. *J. Biol. Chem.* **2009**, *284* (38), 25749–25760.

(126) Marsh, D.; Horváth, L. I. Structure, Dynamics and Composition of the Lipid-Protein Interface. Perspectives from Spin-Labelling. *Biochim. Biophys. Acta - Rev. Biomembr.* **1998**, *1376* (3), 267–296.

(127) Marsh, D. Electron Spin Resonance in Membrane Research: Protein-Lipid Interactions from Challenging Beginnings to State of the Art. *Eur. Biophys. J.* **2010**, *39* (4), 513–525.

(128) Horváth, L. I.; Marsh, D.; Drees, M.; Beyer, K.; Klingenberg, M.; Horváth, L. I. Lipid-Protein Interactions in ADP-ATP Carrier/Egg Phosphatidylcholine Recombinants Studied by Spin-Label ESR Spectroscopy. *Biochemistry* **1990**, *29* (47), 10664–10669.

(129) Romoser, V.; Ball, R.; Smrcka, A. V. Phospholipase C B2 Association with Phospholipid Interfaces Assessed by Fluorescence Resonance Energy Transfer. *J. Biol. Chem.* **1996**, *271* (41), 25071–25078.

(130) Nomikos, M.; Mulgrew-Nesbitt, A.; Pallavi, P.; Mihalyne, G.; Zaitseva, I.; Swann, K.; Lai, F. A.; Murray, D.; McLaughlin, S. Binding of Phosphoinositide-Specific Phospholipase C-ζ (PLC-ζ) to Phospholipid Membranes: Potential Role of an Unstructured Cluster of Basic Residues. *J. Biol. Chem.* **2007**, *282* (22), 16644–16653.

(131) Lindhoud, S.; Carvalho, V.; Pronk, J. W.; Aubin-Tam, M. E. SMA-SH: Modified Styrene-Maleic Acid Copolymer for Functionalization of Lipid Nanodiscs. *Biomacromolecules* **2016**, *17* (4), 1516–1522.

(132) Ye, X.; McLean, M. A.; Sligar, S. G. Conformational Equilibrium of Talin Is Regulated by Anionic Lipids. *Biochim. Biophys. Acta - Biomembr.* **2016**, *1858* (8), 1833–1840.

(133) Kobashigawa, Y.; Harada, K.; Yoshida, N.; Ogura, K.; Inagaki, F. Phosphoinositide-Incorporated Lipid-Protein Nanodiscs: A Tool for Studying Protein-Lipid Interactions. *Anal. Biochem.* **2011**, *410* (1), 77–83.

(134) Mustafa, A. K.; Van Rossum, D. B.; Patterson, R. L.; Maag, D.; Ehmsen, J. T.; Gazi, S. K.; Chakraborty, A.; Barrow, R. K.; Amzel, L. M.; Snyder, S. H. Glutamatergic Regulation of Serine Racemase via Reversal of PIP2 Inhibition. *Proc. Natl. Acad. Sci. U. S. A.* **2009**, *106* (8), 2921–2926.

(135) Gregory, M. C.; McLean, M. A.; Sligar, S. G. Interaction of KRas4b with Anionic Membranes: A Special Role for PIP 2. *Biochem. Biophys. Res. Commun.* **2017**, *487* (2), 351–355.

(136) Guillén, J.; González-Álvarez, A.; Villalaín, J. A Membranotropic Region in the C-Terminal Domain of Hepatitis C Virus Protein NS4B. Interaction with Membranes. *Biochim. Biophys. Acta - Biomembr.* **2010**, *1798* (3), 327–337.

(137) Puthenveetil, R.; Vinogradova, O. Solution NMR: A Powerful Tool for Structural and Functional Studies of Membrane Proteins in Reconstituted Environments. *J. Biol. Chem.* **2019**, *294* (44), 15914–15931.

(138) Hughes, E.; Clayton, J. C.; Middleton, D. A. Cytoplasmic Residues of Phospholamban Interact with Membrane Surfaces in the Presence of SERCA: A New Role for Phospholipids in the Regulation of Cardiac Calcium Cycling? *Biochim. Biophys. Acta - Biomembr.* **2009**, *1788* (2), 559–566.

(139) Bhunia, A.; Mohanram, H.; Bhattacharjya, S. Structural Determinants of the Specificity of a Membrane Binding Domain of the Scaffold Protein Ste5 of Budding Yeast: Implications in Signaling by the Scaffold Protein in MAPK Pathway. *Biochim. Biophys. Acta - Biomembr.* **2012**, *1818* (5), 1250–1260.

(140) Viegas, A.; Viennet, T.; Etzkorn, M. The Power, Pitfalls and Potential of the Nanodisc System for NMR-Based Studies. *Biol. Chem.* **2016**, *397* (12), 1335–1354.

(141) Ravula, T.; Kim, J.; Lee, D. K.; Ramamoorthy, A. Magnetic Alignment of Polymer Nanodiscs Probed by Solid-State NMR Spectroscopy. *Langmuir* **2020**, *36* (5), 1258–1265.

(142) Alegre-Cebollada, J.; Cunietti, M.; Herrero-Galán, E.; Gavilanes, J. G.; Martínez-del-Pozo, Á. Calorimetric Scrutiny of Lipid Binding by Sticholysin II Toxin Mutants. *J. Mol. Biol.* **2008**, *382* (4), 920–930.

(143) Hoernke, M.; Schwieger, C.; Kerth, A.; Blume, A. Binding of Cationic Pentapeptides with Modified Side Chain Lengths to Negatively Charged Lipid Membranes: Complex Interplay of Electrostatic and Hydrophobic Interactions. *Biochim. Biophys. Acta - Biomembr.* **2012**, *1818* (7), 1663–1672.

(144) Hughes, E.; Whittaker, C. A. P.; Barsukov, I. L.; Esmann, M.; Middleton, D. A. A Study of the Membrane Association and Regulatory Effect of the Phospholemman Cytoplasmic Domain. *Biochim. Biophys. Acta - Biomembr.* **2011**, *1808* (4), 1021–1031.

(145) Barrera, N. P.; Isaacson, S. C.; Zhou, M.; Bavro, V. N.; Welch, A.; Schaedler, T. A.; Seeger, M. A.; Miguel, R. N.; Korkhov, V. M.; van Veen, H. W.; Venter, H.; Walmsley, A. R.; Tate, C. G.; Robinson, C. V. Mass Spectrometry of Membrane Transporters Reveals Subunit Stoichiometry and Interactions. *Nat. Methods* **2009**, *6* (8), 585–587.

(146) Redhair, M.; Clouser, A. F.; Atkins, W. M. Hydrogen-Deuterium Exchange Mass Spectrometry of Membrane Proteins in Lipid Nanodiscs. *Chem. Phys. Lipids* **2019**, *220*, 14–22.

(147) Keener, J. E.; Zambrano, D. E.; Zhang, G.; Zak, C. K.; Reid, D. J.; Deodhar, B. S.; Pemberton, J. E.; Prell, J. S.; Marty, M. T. Chemical Additives Enable Native Mass Spectrometry Measurement of Membrane Protein Oligomeric State within Intact Nanodiscs. *J. Am. Chem. Soc.* **2019**, *141* (2), 1054–1061.

(148) Marty, M. T.; Hoi, K. K.; Gault, J.; Robinson, C. V. Probing the Lipid Annular Belt by Gas-Phase Dissociation of Membrane Proteins in Nanodiscs. *Angew. Chemie - Int. Ed.* **2016**, *55* (2), 550–554.

(149) Fantin, S. M.; Parson, K. F.; Niu, S.; Liu, J.; Polasky, D. A.; Dixit, S. M.; Ferguson-Miller, S. M.; Ruotolo, B. T. Collision Induced Unfolding Classifies Ligands Bound to the Integral Membrane Translocator Protein. *Anal. Chem.* **2019**, *91* (24), 15469–15476.

(150) Zhang, G.; Keener, J. E.; Marty, M. T. Measuring Remodeling of the Lipid Environment Surrounding Membrane Proteins with Lipid Exchange and Native Mass Spectrometry. *Anal. Chem.* **2020**, *92* (8), 5666–5669.

(151) von Tscharner, V.; McConnell, H. M. Physical Properties of Lipid Monolayers on Alkylated Planar Glass Surfaces. *Biophys. J.* **1981**, *36* (2), 421–427.

(152) Ganesan, P. V.; Boxer, S. G. A Membrane Interferometer. *Proc. Natl. Acad. Sci. U. S. A.* **2009**, *106* (14), 5627–5632.

(153) Ulman, N.; Groves, J. T.; Boxer, S. G. Micropatterning Fluid Membranes. *Adv. Mater.* **1997**, *9* (14), 1121–1123.

(154) Linman, M. J.; Abbas, A.; Roberts, C. C.; Cheng, Q. Etched Glass Microarrays with Differential Resonance for Enhanced Contrast and Sensitivity of Surface Plasmon Resonance Imaging Analysis. *Anal. Chem.* **2011**, *83* (15), 5936–5943.

(155) Linman, M. J.; Culver, S. P.; Cheng, Q. Fabrication of Fracture-Free Nanoglassified Substrates by Layer-by-Layer Deposition with a Paint Gun Technique for Real-Time Monitoring of Protein - Lipid Interactions. *Langmuir* **2009**, *25* (5), 3075–3082.

(156) Taylor, J. D.; Linman, M. J.; Wilkop, T.; Cheng, Q. Regenerable Tethered Bilayer Lipid Membrane Arrays for Multiplexed Label-Free Analysis of Lipid-Protein Interactions on Poly(Dimethylsiloxane) Microchips Using SPR Imaging. *Anal. Chem.* **2009**, *81* (3), 1146–1153.

(157) Boisselier, É.; Demers, É.; Cantin, L.; Salesse, C. How to Gather Useful and Valuable Information from Protein Binding Measurements Using Langmuir Lipid Monolayers. *Adv. Colloid Interface Sci.* **2017**, *243*, 60–76.

(158) Dowler, S.; Kular, G.; Alessi, D. R. Protein Lipid Overlay Assay. *Sci. STKE* **2002**, *2002* (129), 1–11.

(159) Fang, Y.; Frutos, A. G.; Lahiri, J. Membrane Protein Microarrays. *J. Am. Chem. Soc.* **2002**, *124* (11), 2394–2395.

(160) Guittard, G.; Gérard, A.; Dupuis-Coronas, S.; Tronchère, H.; Mortier, E.; Favre, C.; Olive, D.; Zimmermann, P.; Payrastre, B.; Nunès, J. A. Cutting Edge: Dok-1 and Dok-2 Adaptor Molecules Are Regulated by Phosphatidylinositol 5-Phosphate Production in T Cells. *J. Immunol.* **2009**, *182* (7), 3974–3978.

(161) Saliba, A. E.; Vonkova, I.; Ceschia, S.; Findlay, G. M.; Maeda, K.; Tischer, C.; Deghou, S.; Van Noort, V.; Bork, P.; Pawson, T.; Ellenberg, J.; Gavin, A. C. A Quantitative Liposome Microarray to Systematically Characterize Protein-Lipid Interactions. *Nat. Methods* **2014**, *11* (1), 47–50.

(162) Losey, E. A.; Smith, M. D.; Meng, M.; Best, M. D. Microplate-Based Analysis of Protein-Membrane Binding Interactions via Immobilization of Whole Liposomes Containing a Biotinylated Anchor. *Bioconjug. Chem.* **2009**, *20* (2), 375–383.

(163) Borch, J.; Torta, F.; Sligar, S. G.; Roepstorff, P. Nanodiscs for Immobilization of Lipid

Bilayers and Membrane Receptors: Kinetic Analysis of Cholera Toxin Binding to a Glycolipid Receptor. *Anal. Chem.* **2008**, *80* (16), 6245–6252.

(164) Yamazaki, V.; Sirenko, O.; Shafer, R. J.; Nguyen, L.; Gutsmann, T.; Brade, L.; Groves, J. T. Cell Membrane Array Fabrication and Assay Technology. *BMC Biotechnol.* **2005**, *5* (18), 1–11.

(165) Zhu, H.; Bilgin, M.; Bangham, R.; Hall, D.; Casamayor, A.; Bertone, P.; Lan, N.; Jansen, R.; Bidlingmaier, S.; Houfek, T.; Mitchell, T.; Miller, P.; Dean, R. A.; Gerstein, M.; Snyder, M. Global Analysis of Protein Activities Using Proteome Chips. *Science (80-.).* **2001**, *293* (5537), 2101–2105.

(166) Lu, K. Y.; Tao, S. C.; Yang, T. C.; Ho, Y. H.; Lee, C. H.; Lin, C. C.; Juan, H. F.; Huang, H. C.; Yang, C. Y.; Chen, M. S.; Lin, Y. Y.; Lu, J. Y.; Zhu, H.; Chen, C. S. Profiling Lipid-Protein Interactions Using Nonquenched Fluorescent Liposomal Nanovesicles and Proteome Microarrays. *Mol. Cell. Proteomics* **2012**, *11* (11), 1177–1190.

(167) Moran-Mirabal, J. M.; Edel, J. B.; Meyer, G. D.; Throckmorton, D.; Singh, A. K.; Craighead, H. G. Micrometer-Sized Supported Lipid Bilayer Arrays for Bacterial Toxin Binding Studies through Total Internal Reflection Fluorescence Microscopy. *Biophys. J.* **2005**, *89* (1), 296–305.

(168) Rawle, R. J.; Villamil Giraldo, A. M.; Boxer, S. G.; Kasson, P. M. Detecting and Controlling Dye Effects in Single-Virus Fusion Experiments. *Biophys. J.* **2019**, *117* (3), 445–452.

(169) Phillips, K. S.; Cheng, Q. Microfluidic Immunoassay for Bacterial Toxins with Supported Phospholipid Bilayer Membranes on Poly(Dimethylsiloxane). *Anal. Chem.* **2005**, *77* (1), 327–334.

(170) Rowland, M. M.; Gong, D.; Bostic, H. E.; Lucas, N.; Cho, W.; Best, M. D. Microarray Analysis of Akt PH Domain Binding Employing Synthetic Biotinylated Analogs of All Seven Phosphoinositide Headgroup Isomers. *Chem. Phys. Lipids* **2012**, *165* (2), 207–215.

(171) Gallego, O.; Betts, M. J.; Gvozdenovic-Jeremic, J.; Maeda, K.; Matetzki, C.; Aguilar-Gurrieri, C.; Beltran-Alvarez, P.; Bonn, S.; Fernández-Tornero, C.; Jensen, L. J.; Kuhn, M.; Trott, J.; Rybin, V.; Müller, C. W.; Bork, P.; Kaksonen, M.; Russell, R. B.; Gavin, A. C. A Systematic Screen for Proteing-Lipid Interactions in Saccharomyces Cerevisiae. *Mol. Syst. Biol.* **2010**, *6* (430), 1–15.

(172) Gong, D.; Smith, M. D.; Manna, D.; Bostic, H. E.; Cho, W.; Best, M. D. Microplate-Based

Characterization of Protein-Phosphoinositide Binding Interactions Using a Synthetic Biotinylated Headgroup Analogue. *Bioconjug. Chem.* **2009**, *20* (2), 310–316.

(173) Goluch, E. D.; Shaw, A. W.; Sligar, S. G.; Liu, C. Microfluidic Patterning of Nanodisc Lipid Bilayers and Multiplexed Analysis of Protein Interaction. *Lab Chip* **2008**, *8* (10), 1723–1728.

(174) Giannakis, E.; Pacífico, J.; Smith, D. P.; Hung, L. W.; Masters, C. L.; Cappai, R.; Wade, J. D.; Barnham, K. J. Dimeric Structures of α-Synuclein Bind Preferentially to Lipid Membranes. *Biochim. Biophys. Acta - Biomembr.* **2008**, *1778* (4), 1112–1119.

(175) Park, J. H.; Kwon, E. Y.; Jung, H. Il; Kim, D. E. Direct Force Measurement of the Interaction between Liposome and the C2A Domain of Synaptotagmin I Using Atomic Force Microscopy. *Biotechnol. Lett.* **2006**, *28* (7), 505–509.

(176) Tark, S.-H.; Das, A.; Sligar, S. G.; Dravid, V. P. Nanomechanical Detection of Cholera Toxin Using Microcantilevers Functionalized with Ganglioside Nanodiscs. *Nanotechnology* **2010**, *21* (43), 435502.

(177) Joubert, J. R.; Smith, K. A.; Johnson, E.; Keogh, J. P.; Wysocki, V. H.; Gale, B. K.; Conboy, J. C.; Saavedra, S. S. Stable, Ligand-Doped, Poly(Bis-SorbPC) Lipid Bilayer Arrays for Protein Binding and Detection. *ACS Appl. Mater. Interfaces* **2009**, *1* (6), 1310–1315.

(178) Marin, V. L.; Bayburt, T. H.; Sligar, S. G.; Mrksich, M. Functional Assays of Membrane-Bound Proteins with SAMDI-TOF Mass Spectrometry. *Angew. Chemie - Int. Ed.* **2007**, *46* (46), 8796–8798.

(179) Homola, J. Surface Plasmon Resonance Sensors for Detection of Chemical and Biological Species. *Chem. Rev.* **2008**, *108* (2), 462–493.

(180) Helmerhorst, E.; Chandler, D. J.; Nussio, M.; Mamotte, C. D. Real-Time and Label-Free Bio-Sensing of Molecular Interactions by Surface Plasmon Resonance: A Laboratory Medicine Perspective. *Clin. Biochem. Rev.* **2012**, *33* (4), 161–173.

(181) Beseničar, M.; Maček, P.; Lakey, J. H.; Anderluh, G. Surface Plasmon Resonance in Protein-Membrane Interactions. *Chem. Phys. Lipids* **2006**, *141* (1–2), 169–178.

(182) Phillips, K. S.; Han, J. H.; Martinez, M.; Wang, Z.; Carter, D.; Cheng, Q. Nanoscale Classification of Gold Substrates for Surface Plasmon Resonance Analysis of Protein Toxins with Supported Lipid Membranes. *Anal. Chem.* **2006**, *78* (2), 596–603.

(183) Liu, Y.; Cheng, Q. Detection of Membrane-Binding Proteins by Surface Plasmon

Resonance with an All-Aqueous Amplification Scheme. *Anal. Chem.* **2012**, *84* (7), 3179–3186.

(184) Jang, H.; Abraham, S. J.; Chavan, T. S.; Hitchinson, B.; Khavrutskii, L.; Tarasova, N. I.; Nussinov, R.; Gaponenko, V. Mechanisms of Membrane Binding of Small GTPase K-Ras4B Farnesylated Hypervariable Region. *J. Biol. Chem.* **2015**, *290* (15), 9465–9477.

(185) Brockman, J. M.; Nelson, B. P.; Corn, R. M. Surface Plasmon Resonance Imaging Measurements of Ultrathin Organic Films. *Annu. Rev. Phys. Chem.* **2000**, *51*, 41–63.

(186) Wang, Z.; Wilkop, T.; Jong, H. H.; Dong, Y.; Linman, M. J.; Cheng, Q. Development of Air-Stable, Supported Membrane Arrays with Photolithography for Study of Phosphoinositide-Protein Interactions Using Surface Plasmon Resonance Imaging. *Anal. Chem.* **2008**, *80* (16), 6397–6404.

(187) Phillips, K. S.; Wilkop, T.; Wu, J. J.; Al-Kaysi, R. O.; Cheng, Q. Surface Plasmon Resonance Imaging Analysis of Protein-Receptor Binding in Supported Membrane Arrays on Gold Substrates with Calcinated Silicate Films. *J. Am. Chem. Soc.* **2006**, *128* (30), 9590–9591.

(188) Iqbal, M.; Gleeson, M. a; Spaugh, B.; Tybor, F.; Gunn, W. G.; Hochberg, M.; Baehr-jones, T.; Bailey, R. C.; Gunn, L. C.; Resonators, R.; Optical, H.; Iqbal, M.; Gleeson, M. a; Spaugh, B.; Tybor, F.; Gunn, W. G.; Hochberg, M.; Baehr-jones, T.; Bailey, R. C.; Gunn, L. C. Label-Free Biosensor Arrays Based on Silicon Scanning Instrumentation. *IEEE J. Sel. Top. Quantum Electron.* **2010**, *16* (3), 654–661.

(189) Luchansky, M. S.; Washburn, A. L.; Martin, T. A.; Iqbal, M.; Gunn, L. C.; Bailey, R. C. Characterization of the Evanescent Field Profile and Bound Mass Sensitivity of a Label-Free Silicon Photonic Microring Resonator Biosensing Platform. *Biosens. Bioelectron.* **2010**, *26* (4), 1283–1291.

(190) Wade, J. H.; Bailey, R. C. Applications of Optical Microcavity Resonators in Analytical Chemistry. *Annu. Rev. Anal. Chem.* **2016**, *9* (1), 1–25.

(191) Washburn, A.; Gunn, L.; Bailey, R. Label-Free Quantitation of a Cancer Biomarker in Complex Media Using Silicon Photonic Microring Resonators. *Anal. Chem.* **2009**, *81* (22), 9499–9506.

(192) Luchansky, M. S.; Bailey, R. C. Rapid, Multiparameter Profiling of Cellular Secretion Using Silicon Photonic Microring Resonator Arrays. *J. Am. Chem. Soc.* **2011**, *133* (50),

20500–20506.

(193) Kindt, J. T.; Luchansky, M. S.; Qavi, A. J.; Lee, S. H.; Bailey, R. C. Subpicogram per Milliliter Detection of Interleukins Using Silicon Photonic Microring Resonators and an Enzymatic Signal Enhancement Strategy. *Anal. Chem.* **2013**, *85* (22), 10653–10657.

(194) Robison, H. M.; Escalante, P.; Valera, E.; Erskine, C. L.; Auvil, L.; Sasieta, H. C.; Bushell, C.; Welge, M.; Bailey, R. C. Precision Immunoprofiling to Reveal Diagnostic Signatures for Latent Tuberculosis Infection and Reactivation Risk Stratification. *Integr. Biol.* **2019**, *11* (1), 16–25.

(195) Wade, J. H.; Alsop, A. T.; Vertin, N. R.; Yang, H.; Johnson, M. D.; Bailey, R. C. Rapid, Multiplexed Phosphoprotein Profiling Using Silicon Photonic Sensor Arrays. *ACS Cent. Sci.* **2015**, *1* (7), 374–382.

(196) Qavi, A. J.; Bailey, R. C. Multiplexed Detection and Label-Free Quantitation of MicroRNAs Using Arrays of Silicon Photonic Microring Resonators. *Angew. Chemie - Int. Ed.* **2010**, *49* (27), 4608–4611.

(197) Graybill, R. M.; Para, C. S.; Bailey, R. C. PCR-Free, Multiplexed Expression Profiling of MicroRNAs Using Silicon Photonic Microring Resonators. *Anal. Chem.* **2016**, *88* (21), 10347–10351.

(198) Cardenosa-Rubio, M. C.; Graybill, R. M.; Bailey, R. C. Combining Asymmetric PCR-Based Enzymatic Amplification with Silicon Photonic Microring Resonators for the Detection of LncRNAs from Low Input Human RNA Samples. *Analyst* **2018**, *143* (5), 1210–1216.

(199) Wade, J. H.; Bailey, R. C. Refractive Index-Based Detection of Gradient Elution Liquid Chromatography Using Chip- Integrated Microring Resonator Arrays. *Anal. Chem.* **2014**, *86* (1), 913–919.

(200) Mordan, E. H.; Wade, J. H.; Wiersma, Z. S. B.; Pearce, E.; Pangburn, T. O.; Degroot, A. W.; Meunier, D. M.; Bailey, R. C. Silicon Photonic Microring Resonator Arrays for Mass Concentration Detection of Polymers in Isocratic Separations. *Anal. Chem.* **2019**, *91* (1), 1011–1018.

(201) Mordan, E. H.; Wade, J. H.; Pearce, E.; Meunier, D. M.; Bailey, R. C. A Linear Mass Concentration Detector for Solvent Gradient Polymer Separations. *Analyst* **2020**, *Advance Ar*.

(202) Orlet, J. D.; Bailey, R. C. Silicon Photonic Microring Resonator Arrays as a Universal Detector for Capillary Electrophoresis. *Anal. Chem.* **2020**, *92*, 2331–2338.

(203) Sloan, C. D. K.; Marty, M. T.; Sligar, S. G.; Bailey, R. C. Interfacing Lipid Bilayer Nanodiscs and Silicon Photonic Sensor Arrays for Multiplexed Protein − Lipid and Protein − Membrane Protein Interaction Screening. *Anal. Chem.* **2013**, *85* (5), 2970–2976.

(204) Davie, E. W.; Fujikawa, K.; Kisiel, W. The Coagulation Cascade: Initiation, Maintenance, and Regulation. *Perspect. Biochem.* **1991**, *30* (42), 10363–10370.

(205) Zwaal, R. F. A.; Comfurius, P.; Bevers, E. M. Lipid–Protein Interactions in Blood Coagulation. *Biochim. Biophys. Acta (BBA)-Reviews Biomembr.* **1998**, *1376* (3), 433–453.

(206) Yau, J. W.; Teoh, H.; Verma, S. Endothelial Cell Control of Thrombosis. *BMC Cardiovasc. Disord.* **2015**, *15* (1), 1–11.

(207) Mackman, N. Role of Tissue Factor in Hemostasis and Thrombosis. *Blood Cells, Mol. Dis.* **2006**, *36* (2), 104–107.

(208) Fleck, R. A.; Rao, L. V. M.; Rapaport, S. I.; Varki, N. Localization of Human Tissue Factor Antigen by Immunostaining with Monospecific, Polyclonal Anti-Human Tissue Factor Antibody. *Thromb. Res.* **1990**, *57* (2), 287.

(209) Drake, T. A.; Morissey, J. H.; Edgington, T. S. Selective Cellular Expression of Tissue Factor in Human Tissues. Implications for Disorders of Hemostasis and Thrombosis. *Am. J. Pathol.* **1989**, *134* (5), 1087–1097.

(210) Giesen, P. L. A.; Rauch, U.; Bohrmann, B.; Kling, D.; Roqué, M.; Fallon, J. T.; Badimon, J. J.; Himber, J.; Riederer, M. A.; Nemerson, Y. Blood-Borne Tissue Factor: Another View of Thrombosis. *Proc. Natl. Acad. Sci. U. S. A.* **1999**, *96* (5), 2311–2315.

(211) Ansari, S. A.; Pendurthi, U. R.; Rao, L. V. M. Role of Cell Surface Lipids and Thiol-Disulphide Exchange Pathways in Regulating the Encryption and Decryption of Tissue Factor. *Thromb. Haemost.* **2019**, *119* (6), 860–870.

(212) Yamamoto, M.; Nakagaki, T.; Kisiel, W. Tissue Factor-Dependent Autoactivation of Human Blood Coagulation Factor VII. *J. Biol. Chem.* **1992**, *267* (27), 19089–19094.

(213) Neuenschwander, P. F.; Fiore, M. M.; Morrissey, J. H. Factor VII Autoactivation Proceeds via Interaction of Distinct Protease- Cofactor and Zymogen-Cofactor Complexes. Implications of a Two-Dimensional Enzyme Kinetic Mechanism. *J. Biol. Chem.* **1993**, *268* (29), 21489–21492.

(214) Zelaya, H.; Rothmeier, A. S.; Ruf, W. Tissue Factor at the Crossroad of Coagulation and Cell Signaling. *J. Thromb. Haemost.* **2018**, *16* (10), 1941–1952.

(215) Stenflo, J. Contributions of Gla and EGF-like Domains to the Function of Vitamin K-Dependent Coagulation Factors. *Crit. Rev. Eukaryot. Gene Expr.* **1999**, *9* (1), 59–88.

(216) Huang, M.; Rigby, A. C.; Morelli, X.; Grant, M. A.; Huang, G.; Furie, B.; Seaton, B.; Furie, B. C. Structural Basis of Membrane Binding by Gla Domains of Vitamin K-Dependent Proteins. *Nat. Struct. Biol.* **2003**, *10* (9), 751–756.

(217) Mizuno, H.; Fujimoto, Z.; Atoda, H.; Morita, T. Crystal Structure of an Anticoagulant Protein in Complex with the Gla Domain of Factor X. *Proc Natl Acad Sci U S A* **2001**, *98* (13), 7230–7234.

(218) Huang, M.; Furie, B. C.; Furie, B. Crystal Structure of the Calcium-Stabilized Human Factor IX Gla Domain Bound to A Conformation-Specific Anti-Factor IX Antibody. *J. Biol. Chem.* **2004**, *279* (14), 14338–14346.

(219) Laffin, M. A.; Manning, R. A. Investigation of Haemostasis. In *Dacie and Lewish Practical Haematology*; Bain, B. J., Bates, I., Laffan, M. A., Eds.; Elsevier, Limited, 2017; pp 366–409.

(220) Griffith, M. J.; Breitkreutz, L.; Trapp, H.; Briet, E.; Noyes, C. M.; Lundblad, R. L.; Roberts, H. R. Characterization of the Clotting Activities of Structurally Different Forms of Activated Factor IX. *J. Clin. Invest.* **1985**, *75* (January), 4–10.

(221) Aurell, L.; Friberger, P.; Karlsson, G.; Claeson, G. A New Sensitive and Highly Specific Chromogenic Peptide Substrate for Factor Xa. *Thromb. Res.* **1977**, *11* (5), 595–609.

(222) Waters, E. K.; Morrissey, J. H. Restoring Full Biological Activity to the Isolated Ectodomain of an Integral Membrane Protein. *Biochemistry* **2006**, *45* (11), 3769–3774.

(223) Waters, E. K.; Yegneswaran, S.; Morrissey, J. H. Raising the Active Site of Factor VIIa above the Membrane Surface Reduces Its Procoagulant Activity but Not Factor VII Autoactivation. *J. Biol. Chem.* **2006**, *281* (36), 26062–26068.

(224) Shaw, A. W.; Pureza, V. S.; Sligar, S. G.; Morrissey, J. H. The Local Phospholipid Environment Modulates the Activation of Blood Clotting. *J. Biol. Chem.* **2007**, *282* (9), 6556–6563.

(225) Ke, K.; Yuan, J.; Morrissey, J. H. Tissue Factor Residues That Putatively Interact with Membrane Phospholipids. *PLoS One* **2014**, *9* (2), 1–8.

(226) Muller, M. P.; Wang, Y.; Morrissey, J. H.; Tajkhorshid, E. Lipid Specificity of the Membrane Binding Domain of Coagulation Factor X. *J. Thromb. Haemost.* **2017**, *15* (10), 2005–2016.

(227) Tavoosi, N.; Davis-Harrison, R. L.; Pogorelov, T. V.; Ohkubo, Y. Z.; Arcario, M. J.; Clay, M. C.; Rienstra, C. M.; Tajkhorshid, E.; Morrissey, J. H. Molecular Determinants of Phospholipid Synergy in Blood Clotting. *J. Biol. Chem.* **2011**, *286* (26), 23247–23253.

(228) Tavoosi, N.; Smith, S. A.; Davis-Harrison, R. L.; Morrissey, J. H. Factor VII and Protein C Are Phosphatidic Acid-Binding Proteins. *Biochemistry* **2013**, *52* (33), 5545–5552.

(229) McMahon, H. T.; Boucrot, E. Membrane Curvature at a Glance. *J. Cell Sci.* **2015**, *128* (6), 1065–1070.

(230) Muehl, E. M.; Gajsiewicz, J. M.; Medfisch, S. M.; Wiersma, Z. S. B.; Morrissey, J. H.; Bailey, R. C. Multiplexed Silicon Photonic Sensor Arrays Enable Facile Characterization of Coagulation Protein Binding to Nanodiscs with Variable Lipid Content. *J. Biol. Chem.* **2017**, jbc.M117.800938.

(231) Medfisch, S. M.; Muehl, E. M.; Morrissey, J. H.; Bailey, R. C. Phosphatidylethanolamine-Phosphatidylserine Binding Synergy of Seven Coagulation Factors Revealed Using Nanodisc Arrays on Silicon Photonic Sensors. *Sci. Rep.* **2020**, *10* (17407), 1–7.

CHAPTER II

A "Buyer's Guide" to High-Density Lipoprotein Mimetics: Pros, Cons, and How to Choose the Best Membrane Mimetic for Your Biochemical Application

Abstract

High-density lipoproteins generate disc-like bilayers or spheres with apolipoprotein stabilization of lipids and other hydrophobic molecules for lipid transport. This physiological stability sparked engineering of mimetics to study lipid-protein and membrane protein-protein interactions. The mimetics have been termed "nanodiscs." These nanodiscs can be stabilized by peptides, proteins, DNA, or polymers that are designed to mimic the amphipathic chemical environment of apolipoproteins. Current work with these nanodiscs is biased due to the application "need" or available resources; however, these nanodiscs can be used interchangeably in most cases. Each mimetic needs optimization and each have advantages whether it be for size or resistance to conditions. Researchers who are new or have only used a subset of these nanodisc types may not fully understand the wide breadth or the origins of the field of nanodiscs. In this review, we discuss the origins of high-density lipoproteins and nanodiscs. We highlight the advantages and disadvantages of each type that should be considered for choosing the nanodisc to best fit applications for groups that are new to this field or who have been using one type of nanodisc exclusively.

---

1. Introduction

Biological membranes play a crucial role in processes such as cell signaling and membrane trafficking events. Due to this, approximately 60% of current pharmaceuticals target membrane proteins[1] with a wide range of efficacy due to lack of structural and functional information for majority of membrane proteins. The challenge to studying membrane proteins is due to the complex membrane environment. There are many informative reviews that outline membrane components,[2,3] membrane nanodomains,[4,5] lipid binding domains,[6–11] and computational modeling[12–14] to understand the complex environment. Accurately mimicking the membrane environment is required for stable protein incorporation and function with the necessary membrane components. Therefore, the field of membrane mimetics has been of large interest.[15,16]

Membrane proteins can be solubilized from their native membrane environments using surfactants. Detergents are one type that generates micelles for membrane protein stabilization. This is one of the easiest and most accessible reagents to use for extraction from the native membrane; however, there have been studies showing interactions with detergent can result in protein function loss.[17,18] Similar reagents have been developed to model detergent behavior that are termed amphipols.[19] These species utilize hydrophilic carbon backbones with hydrophobic chains for protein stabilization.[20] Alternatively, peptergents[21,22] have been designed to model peptide and detergent behavior while lipopeptides[23–25] exploit peptide and lipid motifs for membrane protein stabilization. Salipros undergo a similar stabilization of solubilizing membrane proteins from their native environment using saposin A as a stabilizing agent but exhibit pH effects on lipid preference.[26] These models are all easy to use, but do not represent the native membrane bilayer which can lead to adopting non-native structures.

To mimic the native membrane bilayer, bicelles, liposomes, and supported bilayers were developed. Bicelles utilize short chain molecules similar to lipids or detergents to stabilize lipids with or without an incorporated membrane protein into a disc-like shape.[27,28] The downfall is the limited species of lipids and detergents that can be used to form these bilayers.[29] Liposomes are lipid vesicles generated by mechanical or chemical means such as sonication or detergent removal in the presence of excess lipid.[30,31] Limitations arise from the lack of size control and tendency to aggregate.[32] Recent work has utilized bolalipids, which resemble a dimer of lipids connected by an extended alkyl tail group.[33] This class of lipids was discovered in archaea, thermoacidophiles;

thus, there is promise to generation of bolasomes that are more resistant to pH and temperature aggregation. Supported bilayers form stable surface coatings of lipids on surfaces such as glass, gold, or silicon.[15,34,35] The surface interaction can lead to a rigid, restrained surface that can be overcome by tethering[36]; however, defects can still be present in the surface.[34,37]

Another membrane bilayer mimetic has been designed after high-density lipoproteins (HDLs) by mimicking characteristics of apolipoprotein A-I (apoA-I) in the form of a stabilizing reagent. The stabilizing reagent can be peptides[38], proteins[39–45], DNA[46], or polymers[47–52] which act as a belt around lipid tails to stabilize a disc-shaped bilayer (**Figure II.1**). These have been termed "nanodiscs" and can range in size from 4 nm to 70 nm in diameter (**Table II.1**).

Most HDL mimetic reviews focus on advantages of one technique and disadvantages of others. The aim of this review is to tell the unbiased story on the development of HDL mimetics as a stable bilayer technique for characterizing membrane proteins. The lack of bias will give context to groups that are new to this technology to make an informed decision for the best mimetic for their application and/or educate groups who work with a select few of the mimics. The Bailey lab has worked closely with the Sligar and Ramamoorthy groups on protein and peptide/polymer nanodiscs respectively, while the Morrissey lab has worked with the Arleth group on circularized nanodiscs in addition to the Sligar group. This gives us the ability to show the true advantages and disadvantages to each technique. We have worked to tell a neutral story for incoming researchers to make the best decision on the ideal technique their application. In this review, we start by explaining HDL presence in physiology before exploring nanodiscs stabilized with peptides, proteins, DNA, or polymers.

2. High-Density Lipoproteins

There are many reviews covering the topic of high-density lipoproteins (HDLs).[53–57] Here, we will give a brief overview of HDL characterization to lead into the development of HDL mimetics.

HDLs are comprised of lipids, other partially hydrophobic molecules, and stabilizing proteins called apolipoproteins. There are two subclasses of apolipoproteins: those that move from lipoprotein to another (A-I, A-II, A-IV, C-I, C-II, C-III, and E) and those that remain on the same lipoprotein from biosynthesis to catabolism (B-100 and B-48).[53] Studies have shown there are connections between HDL levels and coronary heart disease.[58] Low levels of HDLs lead to a higher

likelihood of coronary heart disease due to their in cholesterol transport.[54,55,58] Recently, the cholesterol transport interactions have been identified between HDLs and lecithin:cholesterol acyltransferase (LCAT) using crosslinking and hydrogen-deuterium exchange mass spectrometry[59]

Early work on HDLs focused on understanding the peptide sequence[60] which ultimately led to the identification of multiple different apolipoproteins on a single HDL.[61,62] Through rigorous purification and characterization, the two apolipoproteins were named after their N-terminal residue—apoHDL-Gln (now known as apoA-I) and apoHDL-Thr (now known as apoA-II).[63,64] The percentage of α-helical structure for the apolipoproteins were determined to be 40-50% for apoA-I and 90% for apoA-II with the former occurring at naturally higher abundance in physiology. The α-helical secondary structure of apoA-I was found to be the source of lipid binding[65] with amphipathic character contributing to structural stability in solution.[66,67]

Multiple structures for HDLs exist that resemble a disc or sphere-like structure. The disc model was hypothesized when apoA-I was observed to have lateral packing via NMR.[68] This led to a belt model to describe apoA-I stabilization of lipids from crystal structures[69] and polarized attenuated total internal reflection Fourier-transform (TIRF).[70] The discs can then undergo remodeling[54] to sphere structures whose stability is explained by the trefoil model.[71] The spherical structure of HDLs are not the focus of this review, but this structure has been leveraged for precision medicine.[57] The disc structure has been inspiration for nanodiscs by modeling peptides, proteins, DNA, and polymers to have a similar amphipathic character to apoA-I.

3. Peptide Nanodiscs

Peptide nanodiscs have been mostly used for antioxidative and anti-inflammatory properties *in vivo*[38] and have shown promise in generating treatments for numerous diseases.[72] The development of the peptide nanodisc field surfaced through truncated apoA-I sequences that were originally used to understand HDL properties in physiology.[73–75]

To confirm α-helical structure is important for apoA-I association with lipids, peptides were designed with various charged amphipathic sequences.[73] The peptide with ideal lipid binding characteristics became known as *18A* (18 amino acids long) or *2F* (for having 2 phenylalanines) (**Table II.2**). A hybrid chain of 18A, known as *37pA*, was tested to look at peptide chain length[74]

and showed the same lipid affinity and LCAT activation as 18A.[75] Further comparisons of 18A and 37pA were done by modifying the proline linker by deletion, double glycine replacement,[76] or alanine replacement.[77,78] The linker changes showed the more flexible sequence created more adaptable sizes of HDLs,[76] but a proline linker displayed better *in vivo* HDL association.[78] The downfall to the sequence of 18A and 37pA was the preferred peptide-peptide interactions over peptide-lipid which can generate aggregates instead of discs.[79]

The 18A peptide itself has been modified in a few different ways. One group used a truncated version called *14A* for NMR structure analysis of disc formation.[80] Another group screened a panel of peptides that varied in hydrophobic phenylalanine residue content.[81] The peptide with four phenylalanines, *4F*, showed the most stable lipid interactions, second highest solubility in water, and most effective in clarifying lipid vesicles along with mimicking apoA-I activity *in vivo*. These lipid interactions are from orthogonal peptide orientation compared to lipid tail groups observed with NMR.[82] Additional research has been performed using 4F to retard amyloid β-peptide (Aβ) 40 aggregation[83] and treat diseases such as cardiovascular disease[84,85] along with obesity and diabetes.[86]

Another mutation test of the original peptides was been to mutate various residues across both helices of to 37pA to alanine.[87] The mutant with 5 alanines, also known as *5A*, experiences less of a hydrophobic moment than 37pA. This allows for easier solubility in water which ultimately resulted in better synthetic vesicle and comparable natural vesicle solubility to 37pA. The lipid composition used to form HDLs with 5A was screened to show that lipid composition effects which cholesterol efflux pathway is targeted.[88]

A combination of 18A and 4F with a proline linker was developed as a nanodisc scaffold peptide (NSP).[89] The NSP showed better thermal stability and comparable solubilization of natural vesicles to 4F. To improve the solubility of NSP in water, the sequence was reverse to make NSP$_r$.[90] The reversal of the sequence generated a peptide that acted more like an amphipol than a HDL since no additional lipids are needed to be added when incorporating membrane proteins.

A recent study leveraged the instability of 18A peptide nanodiscs overtime[76,91] to form supported lipid bilayers.[92] A membrane protein of interest, either bacterial magnesium transporter (CorA) or blood coagulation tissue factor, were stabilized in nanodiscs with 18A. The nanodiscs

were deposited onto silicon oxide, mica, and gold surfaces using electrostatic interaction between lipids and the surface followed by extraneous washing to remove the peptides to allow formation of supported lipid bilayers with incorporated membrane proteins. The surface was characterized using surface sensitive techniques such as atomic force microscopy and utilized to observe of binding of tissue factor and one of its binding partners, activated factor VII.[92]

A few unique peptides have been designed separately from those previously discussed. One of type called *ELKs* are comprised of mostly glutamate, leucine, and lysine with varying amounts of alanine.[93] Similar amino acid sequences were used to create peptides with various charge states to understand charge effects on cholesterol efflux. The ELKs showed lesser or similar cholesterol efflux to apoA-I and evidence that the peptide belt may be at a 140° angle to bilayer plane.[93] Another peptide was designed to generate multivalent branched helices at 21 and 16 amino acids long with N-terminal cysteines.[94] The monomer species was shown to generate HDLs better using less peptide than 4F, while the multivalent species were shown to promote more cholesterol efflux and HDL remodeling.

The peptide that has shown the greatest interest for developing nanodisc therapeutics has been 22A. This peptide was modeled after apoA-I.[95,96] The nanodiscs formed with 22A have been shown to withstand several freeze thaw cycles.[97] This stability makes them a promising candidate for therapeutics. Recent studies have shown the incorporation of lipid modified reagents to perform certain physiological functions. One study delivered antigen-lipid conjugates using an incorporated modified cholesterol for targeted delivery.[98] This antigen was successful at generating an immune response and eliminating melanoma tumors in >85% of mice. This was then used as a combination therapy to show the use in precision medicine.[99] Similar work has been performed to incorporate chemotherapy drug-lipid conjugates. The design can be programmed to release in the acidic environment of the tumor to eliminate ~80% of colon carcinoma in mice.[100] Additional chemotherapy delivery has been performed for glioblastoma[101] and colon adenocarcinoma[102] in mice.

Peptide nanodiscs have the application advantage due to their current use *in vivo* for various therapeutics and ease of assembly that does not always require detergent. The size of peptide nanodiscs is easily adjusted for applications by modifying the peptide to lipid ratio during formation but this ease of adjustment can come at the cost of time screening ratios. These nanodiscs

also have a variable stability based on pH and salt that can be problematic for some assays but can also be leveraged for use such as therapeutic release. Other disadvantages are the need for synthetic routes to create the peptides and the potential need for temperature fluctuations for solubility. Inability to control the number of peptides used to form the nanodisc can also pose a problem when incorporating functionalization for applications such as fluorophore tagging or surface tethering.

4. Protein Nanodiscs

Proteins have also been designed after apoA-I for generating HDL mimics named membrane scaffold proteins (MSP).[103] The main modification to the apoA-I sequence was the elimination of the globular N-terminal domain. Unlike the peptides, the size variation of nanodiscs using MSP is achieved by changing the number of α-helices instead of adjusting the ratio of peptides to lipids.[104–106] There are numerous articles that compare the sequences for developed MSPs.[41,106,107]

Extensive characterization has been performed on nanodiscs with MSP (also called *Nanodiscs*) to confirm that two MSPs are incorporated into every nanodisc and show the ease of control over the lipid and protein stoichiometric environment.[108–111] The stability and homogeneity of MSP nanodiscs has been shown using native mass spectrometry.[112] Initial studies looking at membrane protein incorporation determined the oligomeric control over bacteriorhodopsin[113,114] and fully functional G-protein coupled receptor incorporation.[115]

Many traditional biochemical assays have been performed on MSP nanodiscs using techniques such as activity assays,[116–118] resonance raman,[119] and solution NMR[120–122] or solid state NMR (ssNMR).[123–125] Each of these studies utilizes the stoichiometric control of lipid and protein incorporation into the nanodiscs. One key example focusing on the specific lipid environment is shown using phosphatidylinositol pulldowns.[126] This study compared binding domains bound to nanodiscs with various phosphate modified phosphatidylinositol nanodiscs. In addition to these traditional assays, unique mass spectrometry dissociation methods are being developed to identify lipids that tightly bind to specific membrane proteins.[127–129]

Surface functionalization with MSP nanodiscs has been achieved with and without modifications to the assembled nanodisc. The electrostatic interactions between lipid headgroups and a silicon oxide surface have been utilized to observe lipid specific binding over time with silicon photonic microring resonators.[130,131] Other studies have utilized a histidine tag (his-tag) on

MSP to generate nanodisc arrays for self-assembled monolayers for matrix maser desorption ionization time-of-flight mass spectrometry (SAMDI-TOF)[127] and surface plasmon resonance (SPR).[118,132–137] These arrays have been used to observe binding over time and, in some cases, as a support system for cell lysate pull downs.[134] A similar capture design has utilized antibodies specific for an incorporated membrane protein.[138] One particular study incorporated trace-amine-associated receptor 13c (TAAR13c) to use as a bioelectric response for cadaverine which is an odor associated with food spoilage.[139] Additionally, incorporation of modified lipids can be utilized for surface specific interactions.[140]

Chemical modifications to the nanodisc have also been used to generate functionalized surfaces. Nanodiscs can be easily covalently bound by free amines from phosphatidylethanolamine using 1-ethyl-3-(3-dimethylaminopropyl)carbodiimide (EDC) chemistry for SPR.[141] Another example utilized ,3'-dithiobis(sulfosuccinimydlpropionate) (DTSSP) to covalently attach lysine residues on MSP to a gold cantilever for cholera toxin detection with gangliosides.[142] These techniques utilize the native state of the nanodisc for surface modification without a change to the nanodisc assembly itself; however, other studies have selectively modified MSP for controlled incorporation of functional groups to the nanodisc.

The ease of assembly with the strict two MSPs per nanodisc provides control over functional group addition. One example labeled the N-terminus of MSP to observe fluorescence polarization with KRas4b.[143] This study determined that KRas4b shows a lipid headgroup specific preference when it was originally thought to have a charge lipid preference. Another method for controlled labeling utilizes a single cysteine mutant of MSP. This species has been used for labeling with a fluorescent dye for nanodisc tracking with and without incorporated MRI contrast agent *in vivo*.[144] This system was used to determine direct targeting of cell membranes and show that MRI contrast agent incorporation into nanodiscs gives increased sensitivity and ability to perform cell tracking studies. Additionally, the cysteine mutant can be labeled for fluorescence resonance energy transfer (FRET).[145] Using this technique, the anionic lipid requirement for membrane binding and calculated distance to hypothesis conformational change in the binding domain of talin was determined.

MSP nanodiscs offer the advantage of high controllability over lipid and protein stoichiometric incorporation with exactly two MSP molecules for functionalization. Another key characteristic

of using MSP is the ease of expression in *E. coli*. However, MSP nanodiscs do need detergent to form properly and the ratio of MSP to lipids may need to be optimized for monodisperse formation.

5. Circularized Nanodiscs

The main goal for nanodisc circularization was to generate more homogenous and larger membrane bilayers for structural studies.[45] Nanodiscs using peptides and MSP had been observed to be no larger than 20 nm in diameter,[89,106] which is problematic when studying membrane interactions with large protein complexes or viruses. This spun a new type of nanodiscs generated with circularized stabilizing reagents made of modified MSPs and DNA.

One modification of MSP was made to utilize the split-intein-based method.[146] In particular, the study utilized fusion of *Nostoc punctiforme* (*Npu*) DnaE split-intein divided into two pieces at the termini for MSP (**Figure II.2A**).[147] Upon protein expression, the intein fragments combine to be functional for splicing MSP together. The end result was a circularized MSP generated *in vivo* that formed nanodiscs that had increased thermal stability. The downside to this reaction is the low yield, about ¼, of circularized MSP per culture compared to normal MSP and the formation of dimer side products.

Another modification of MSP was generated to utilize sortase A[148] as a method for circularization (**Figure II.2B**). The original study reported a Cu^{2+} chip, Ni-NTA, and in solution method to scale the circularization method.[149] Extensive characterization was performed to show kinks between helices when the nanodisc was under-lipidated. Nanodiscs were assembled to be up to 50 nm in diameter to observe interactions with poliovirus that showed the formation of a pore in the bilayer followed by excretion of the poliovirus RNA. A troubleshooting guide is available for this process[150] and has been to study bacteriorhodopsin compared with a not circularized MSP of the same size.[151] The yield using the sortase A method with these MSP constructs is comparable to the split-intein method.[152] To improve the yield of circularized MSP, modifications to the sequence were made to enhance solubility by adding a solubility enhancing tag[152] or modifying the MSP sequence.[153] The mutations allowed for a similar yield to regular MSP.

DNA-corralled nanodiscs is the term used to describe DNA-origami barrel stabilized nanodiscs.[46] The mechanism for stabilization uses a triple cysteine mutant of MSP, called NW11, that has been conjugated with 21 bp DNA (**Figure II.2C**). Nanodiscs are formed with conjugated

NW11 before being mixed with a large DNA-origami barrel that has been designed to have complementary DNA strands inside. This directs the MSP to the inside edge of the DNA barrel and aggregates multiple smaller nanodiscs to form larger ones upon dialysis. Interactions with a 70 nm in diameter nanodisc were observed with poliovirus to show bending of the NW11 nanodisc away from the DNA-origami barrel.[46]

Circularized nanodiscs using either circularized MSP or DNA-corrals can form larger nanodiscs with improved stability and proteolytic resistance. The disadvantages to using these stabilization reagents is that detergent is still needed to form and the ratios of stabilizing reagent to lipid may need optimization. Also, circularized MSP suffers from variable yield during the circularization reaction. There is also no direct interaction between the DNA-corral and lipids which can be useful to not affect the lipid environment, but also a drawback for stabilizing the bilayer when looking at interactions that may result in curvature.

6. Polymer Nanodiscs

To mimic a similar structure to apoA-I, hydrophobic structure properties of polymers were utilized to eliminate the need for detergents when solubilizing membrane proteins.[154,155] Polymer nanodiscs began with the use of styrene maleic acid (SMA) copolymers and have evolved into a field with limitless possibilities (**Table II.3**).

One of the main draws to using SMA to assemble nanodiscs was the ability to use circular dichroism (CD) for biochemical characterization.[156] The negligible CD absorbance by SMA makes this a promising lipid bilayer stabilization reagent. Further characterization using ^{1}H ssNMR showed close proximity of styrene to the lipid acyl chains as the mechanism for stabilization of the nanodisc.[157] The outer edge lipids displayed the most interactions with SMA, while the central lipids were unaffected. SMA nanodiscs have been shown to incorporate membrane proteins from their native environment. The incorporated proteins can be analyzed using techniques such as lipidomics to identify associating lipids[158] or used for antigens in flow cytometry.[159]

The mechanism for the formation of nanodiscs with SMA is predicted to be styrene intercalation into the membrane to generate an initial surface interaction.[160,161] The styrene is then able to insert further to destabilize the membrane. The resulting circularization of SMA polymers around the lipids stabilizes the hydrophobic interactions and results in a "cookie cutter" like action

of the membrane. A recent study has been performed on *E. coli* membranes to observe the effects of SMA concentration, temperature, incubation time, and salt dependence on this mechanism.[162] SMA was comparted to sodium dodecyl cholate (SDS) due to its pH and salt dependences.

The size of these polymer nanodiscs can be adjusted similarly to peptide nanodiscs due to the dependence on the ratio of lipid to polymer. The initial SMA copolymer suffered from aggregation below pH 6.6.[163] This was able to be tuned by adjusting the ratio of styrene to maleic acid and molecular weight.[164–167] The result showed that lower styrene content was more stable at lower pH values while molecular weight contributed to little to no change. Another simple modification to the SMA copolymer was the addition of cysteamine to maleic acid for conjugation of functional groups.[168] Avidin functionalization to the polymer has been used to show changes in FRET with variable length biotinylated donors to acceptor-lipid conjugates.

Optimization of the copolymer structure has been an attractive direction to overcome the SMA pH and divalent cation instability.[163,164,169] Most of the modifications were performed on the maleic acid component due to its charge state changes with pH contributing to aggregation and its intrinsic metal chelating behavior with divalent cations (**Table II.3**). Maleic acid modification to maleimide with an ethyleneamine (SMAd-A) made the copolymer stable below pH 6 and tolerant to divalent cations.[170] Comparatively, the open-ring structure with the addition of ethylenediamine (SMA-ED) directly to the maleic acid presented stability below pH 5 and above pH 7; however, divalent cations destabilized the accessible carboxylic acid at basic pH.[170]

Using the characterization from these species, the copolymer structure was modified based on SMAd-A with modification to the amine to with methyl groups to form a quaternary ammonium (SMA-QA).[171] The resulting copolymer was tolerant in the pH range from 2-10 and of divalent cations at 100x the concentration of SMA. The basic pI of SMA-QA has been utilized to reconstitute a net positively charged membrane protein due to the repulsion from the polymer belt preventing aggregation between the polymer and protein.[172] Similarly, a variant of SMA-ED with an alcohol in place of the amine (SMA-EA) has been shown to reconstitute a net negatively charged membrane protein.[172] Another modification close to the open-ring structure of SMA-ED utilized a methylamide addition (SMA-MA) which showed a slightly increased tolerance of divalent cations at near physiological concentrations.[173]

Using a similar copolymer made of a styrene maleimide with a tertiary amine (SMI), researchers found the same trends in divalent cation stability, but preference for pH below 7.8.[174] Due to physiological conditions staying around pH 7.4, SMI is a good candidate for native membranes. The drawback for SMI is the small size of nanodiscs that are formed, 5-10 nm, and potential for acting more like an amphipol than a nanodisc polymer. New work into zwitterionic SMA copolymers (zSMA) have modified the maleic acid to resemble the head group of PC that has enabled an increased pH stability range and a range of nanodisc sizes.[175]

Polymers without styrene have also been developed for nanodisc formation to eliminate background in UV and fluorescence spectra and the direct lipid interactions with styrene. The design utilized poly(methyl methacrylate) copolymers (PMMAs, **Table II.3**).[176] Optimization screened the moderate hydrophobicity fraction needed to dissolute lipid vesicles to be between 0.4 and 0.6 with a molecular weight ranging between 3 to 9 kg per mole. A similar design has been utilized by continuing to utilize the maleic acid for formation of diisobutylene-maleic acid (DIBMA) copolymers. DIBMA was shown to be unaffected by a calcium dependent activity assay[177] and intercalate less into the lipid bilayer.[178] Recent studies have also shown that physiological concentrations of divalent cations improve the efficiency of membrane protein extraction with DIBMA.[179]

A few studies have further investigated the extraction differences between SMA of various styrene to maleic acid ratios and DIBMA from native membranes. One study found that both polymers were able to extract rhomboid proteases.[180] One particular protease, *Vibrio cholerea* rhomboid protease (VcROM), is prone to self-processing during purification; however, use of DIBMA for extraction minimized this self-processing. Lipid preferences have been observed between SMA, SMA-QA, and DIBMA for *E. coli* and mammalian Jurkat cells.[181] This can be useful in solubilizing a specific membrane protein of interest if there are known lipids needed for activity or stabilization.

Polymer nanodiscs have the true advantage of being able to natively extract lipids and proteins from their environment without the use of detergent. Depending on the polymer in use, pH and salt conditions can destabilize the bilayer, but this could potentially be leveraged in the same way that it has for peptide nanodiscs. The polymerization synthesis process can result in polydisperse species that results in the need for optimization of the polymer to lipid ratio for a specific

application. There is also the potential need for temperature fluctuations for lipid solubility and an inability to control the number of polymers forming the disc like the peptide nanodiscs.

7. What is the Best Nanodisc?

When weighing the choices of what nanodisc stabilization agent to choose, the availability and application are the main deciding factors. Availability is the easiest way to try something new but can also be a double-edged sword. If both sides are not completely informed on the application or the technique, then there are potential variables that can go unnoticed and end in wasting time and resources.

Each apoA-I mimetic has their advantages and disadvantages in making nanodiscs (**Table II.4**). Key application features can be used to determine which nanodisc is best (**Figure II.3**). For example, if a protein is prone to self-processing when it encounters detergent, then polymer should be used to extract it directly from the native membrane into a nanodisc. The size of the membrane needed to study a particular membrane protein can easily narrow down the stabilization agent of choice. This field is continuously growing to minimize the disadvantages and utilize the advantages. The most important thing is realizing that each reagent does have its advantages and disadvantages and that there are many cases when more than one can be used to achieve at the same result.

In addition to key application features, available characterization techniques for the intended outcome may need to be considered. Since 2015, each nanodisc type has been used for numerous biochemical studies to obtain structural and functional information (**Table II.5**).

Peptide nanodiscs have been used for many techniques except cryogenic electron microscopy (Cryo-EM) and x-ray crystallography. This could be potentially due to the chemical stability due to the temperature change or the conditions needed for crystallization resulting in breakdown of the nanodisc. Use of peptide nanodiscs for mass spectrometry has been performed with NSP_r, which acts more like an amphipol. This amphipol-like character may also be useful for Cryo-EM or x-ray crystallography. No recent studies have been performed using peptide nanodiscs utilizing ultracentrifugation due to this technique being used for testing of peptide-lipid interactions when screening peptides for nanodisc formation and purifying nanodiscs away from free peptides. Other

techniques that have not utilized peptide nanodiscs are electron spin resonance spectroscopy (EPR), FRET, and electrochemical detection.

MSP nanodiscs have the widest breadth of utilized techniques of the HDL mimetics. These nanodiscs have been utilized in all the common techniques in Table 5, some of which have dedicated reviews such as ultracentrifugation,[182] NMR,[183,184] Cryo-EM,[185] mass spectrometry,[186] and molecular dynamics simulations.[187]

Circularized nanodiscs stabilized with protein and DNA are very new techniques, so not many studies have been performed with them. Circularized protein nanodiscs have similar properties with increased thermal and proteolytic stability compared to MSP nanodiscs; therefore, common characterization techniques should be easily translated to circularized MSP including *in vivo* techniques. DNA-corralled nanodiscs have the potential to be easily translated as well, but the bending of the lipid bilayer away from the DNA may need to be taken into considering depending on the strength of the interactions being characterized.

Polymer nanodiscs have undergone extensive structural characterization techniques during polymer modification optimization. Techniques such as isothermal titration calorimetry (ITC), fluorescence polarization, electrochemical detection, and SPR could be within reach of polymer nanodiscs if the chosen polymer is tolerant of the temperature, pH, and salt conditions necessary. No studies have tested the polymer nanodiscs *in vivo* to know of any potential

In conclusion, there are many metrics to consider when choosing the ideal HDL mimetic for an application. All nanodiscs are stable bilayers that can be utilized as an empty mimetic to look at lipid-protein interactions or to incorporate a membrane protein of interest for analysis. The characterization technique and reaction conditions are key to considering which mimetic or mimetics can be ideal for a given application.
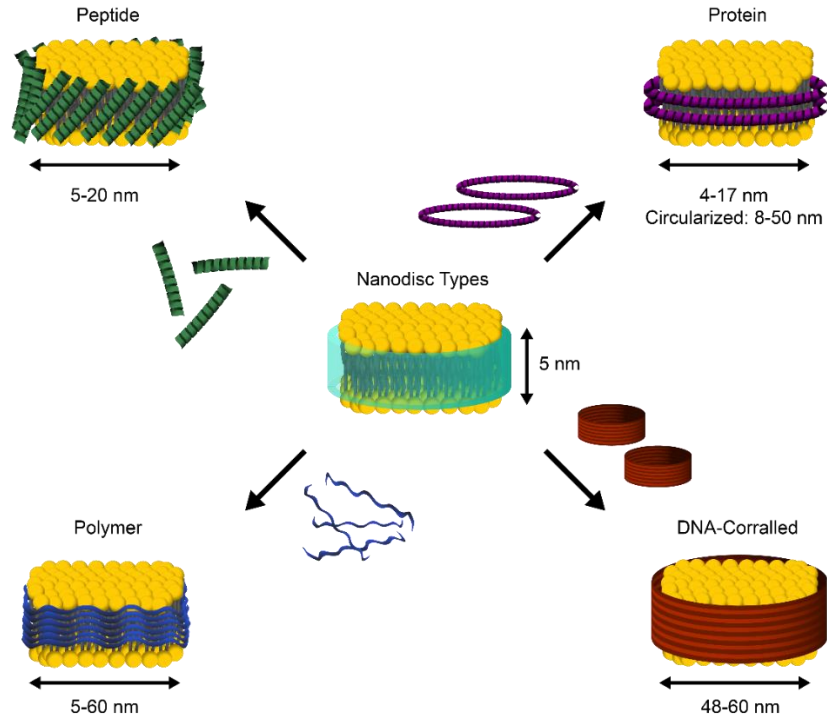
Figure II.1. Diagram of Nanodisc Types. Nanodiscs are stable disc shaped bilayers stabilized by reagents modeled after the amphipathic structure of apoA-I. The thickness of the bilayer is dictated by the lipid tail groups, with an average of about 5 nm. The diameter of the nanodisc is determined by the stabilizing reagent such as peptides (green), protein (purple), DNA (red/orange), or polymer (blue).
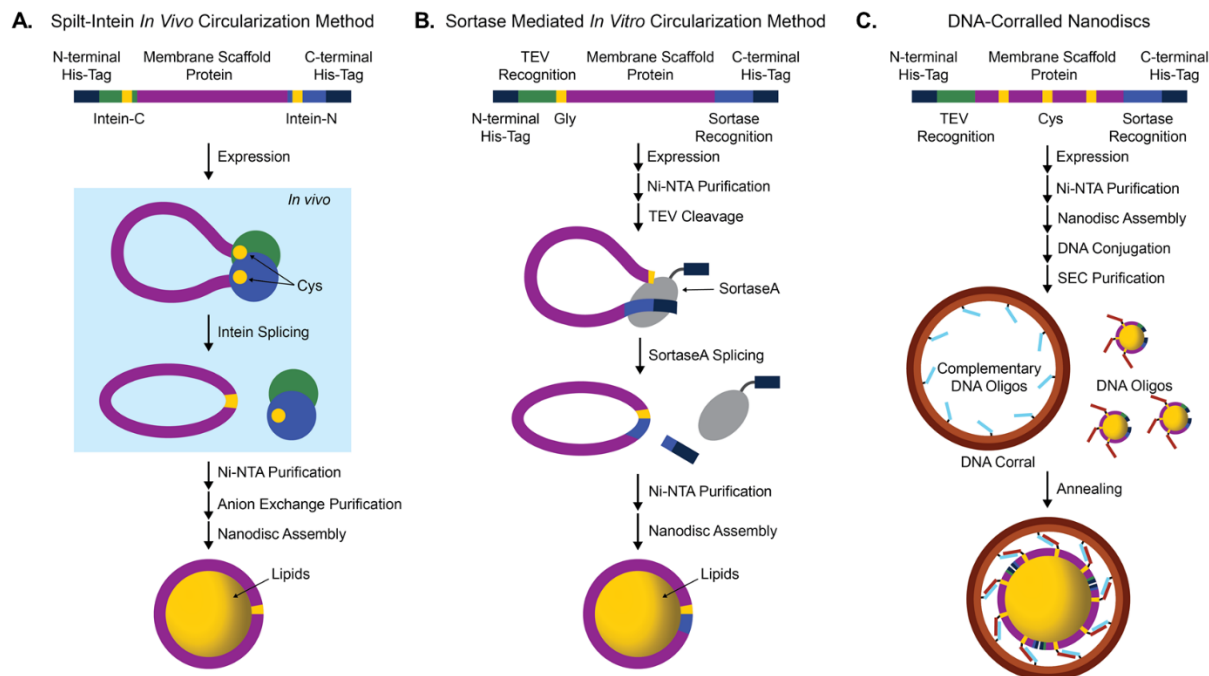
Figure II.2. Schematics for Generating Circularized Nanodiscs. A. The split-intein method for circularization of MSP utilizes *in vivo* processing. The intein is expressed in split on either end of the MSP. When successfully expressed, the intein is assembled and localized for the circularization reaction. Due to the reaction cleavage of the affinity tags, the Ni-NTA purification separates the intein from the MSP before secondary anion exchange purification. **B.** The sortase method for circularization of MSP occurs *in vitro* after cleavage of one of the purification tags. The purification steps need to be repeated to clean-up the reaction. **C.** DNA-corralled nanodiscs are another method for generating circularized nanodiscs. This method starts similar with making MSP nanodiscs, but utilizes complementary DNA and annealing procedures for incorporation into DNA barrels, referred to here as *corrals*.

Figure II.3. Nanodisc Decision Tree. This decision tree proposes key membrane and membrane protein characteristics that should be taken into consideration when determining the best stabilizing agent for an application. The stabilizing agents are represented in green (peptides), purple (protein), orange/purple (circularized protein), red/orange (DNA), and blue (polymer).
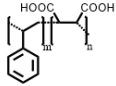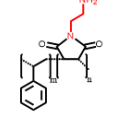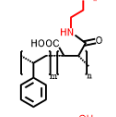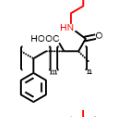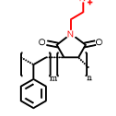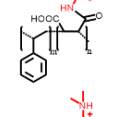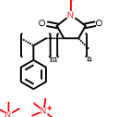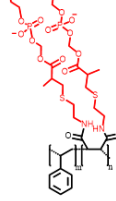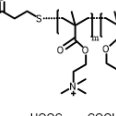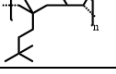
Table II.1. List of Stabilizing Agents for Generating Nanodiscs

Category	Size dependence	Key Characteristic	Reference
Peptide	Peptide to lipid ratio	Adaptability, monodisperse discs regardless of the amount of peptide added	(36, 89)
Protein	Size of protein	Control over lipid and protein stoichiometry	(106, 107)
Circularized Protein	Size of protein	Large size range, enhanced thermal stability	(150)
DNA-Corralled	Size of DNA	Large size	(46)
Polymer	Polymer to lipid ratio	No detergent needed	(171)

Table II.2. List of Peptide Sequences for Assembling Nanodiscs

Peptide	Brief Description	Sequence	Reference
18A or 2F	18 amino acids long	DWLKAFWDKVAEKLKEAF	(73)
37pA	2 linked 18A chains with a Pro	DWFKAFYDKVAEKFKEAF-P- DWFKAFYDKVAEKFKEAF	(74)
14A	Shortened 18A	DYLKAFYDKLKEAF	(80)
4F	18A with 2 Phe mutations	DWFKAFYDKVAEKFKEAF	(81)
5A	37pA + 5 Ala mutations	DWFKAFYDKVAEKFKEAF-P-DWAKAAYDKAAEKAKEAA	(87)
Multivalent$_{23}$	Modified apoA-I helix 10	CGVKESFJASFKSAKEEWTKKLN	(94)
NSP	18A -P-4F	DWLKAFYDKVAEKLKEAA-P-DWFKAFYDKVAEKFKEAF	(89)
NSP$_r$	Reverse NSP	FAEKFKEAVKDYFAKFWD-P-AAEKLKEAVKDYFAKLWD	(90)
22A	22 amino acids long	PVLDLFRELLNELLEALKQKLK	(97)
ELK (neutral)	Mostly Glu, Leu, Lys	EELKEKLEELKEKLEEKL	(93)

Table II.3. List of Copolymers for Assembling Nanodiscs

Polymer	Description	Monomers	Key Characteristic	Reference
SMA	Styrene-maleic acid copolymer		No detergent needed, adjusting the styrene-maleic acid ratio can tune pH and divalent cation stability	(156)
SMAd-A	Styrene-maleimide ehtyleneamine		Stable pH < 6 Tolerant to divalent cations	(176)
SMA-ED	Styrene-maleic acid-ethylenediamine		Stable at pH < 5 and pH >7 Tolerant to divalent cations at acidic pH	(170)
SMA-EA	Styrene-maleic acid-ethanol amine		Stabilize proteins with pI < 7	(172)
SMA-QA	Styrene-maleimide quaternary amine		Stabilize proteins with pI > 7	(171)
SMA-MA	Styrene-maleic acid- methylamide		Slight tolerance to divalent cations at physiological concentration	(173)
SMI	Styrene-maleimide tertiary amine		Commercially available polymer, stabilize proteins below pH 7.8	(174)
zSMA	Styrene-maleic anhydride random copolymers		Increased pH stability in acidic and alkaline conditions	(175)
PMMA	Poly(methylmethacrylate) copolymers		Does not intercalate with lipid tails	(176)
DIBMA	Diisobutylene-maleic acid copolymer		Divalent cation resistant, does not intercalate with lipid tails	(177)

m and *n* denote monomers in the copolymer blends

Table II.4. Advantages and Disadvantages of Stabilizing Agents

Category	Advantages	Disadvantages
Peptide	1. Stability is variable with pH and salt that can be leveraged for various uses 2. Some peptides do not require the use of detergent	1. Stability is variable with pH and salt which can be problematic for assays 2. Unable to control the number of peptides incorporated which limits control of functionalization 3. Synthetic route for generating peptides 4. May need to do temperature fluctuations or use detergent 5. Conditions need to be optimized to form well
Protein	1. Highly controllable lipid and protein stoichiometry 2. Exactly 2 MSPs per Nanodisc gives control over functionalization 3. Protein is easily expressed in *E. coli*	1. Detergent is needed to form 2. Size range is limited 3. Conditions need to be optimized to form well
Circularized Protein	1. Generate larger nanodiscs 2. Improved thermal stability and proteolytic resistance	1. Detergent is needed to form 2. Yield for circularization can be variable 3. Conditions need to be optimized to form well
DNA-Corralled	1. Generate larger nanodiscs 2. There is no direct interaction between the DNA and the lipids, so there is no effect on the lipid environment	1. Detergent is needed to form 2. There is no direct interaction between the DNA and the lipids, so there is not a strong force stabilizing the lipid bilayer 3. Conditions need to be optimized to form well
Polymer	1. There is no detergent or extra lipids needed when working with cell lysate 2. Can remove proteins directly from their native environment	1. Stability is variable with pH and salt conditions for some of the polymers 2. Polymerization methods can be polydisperse 3. Unable to control the number of polymers incorporated which limits control of functionalization 4. May need to do temperature fluctuations 5. Direct interaction between the lipids and polymer 6. Conditions need to be optimized to form well

Table II.5. Summary of Biochemical Techniques Utilized with Nanodiscs

Common Biochemical Techniques	Peptide	Protein	Circularized		Polymer
			Protein	DNA-Corralled	
Structural					
Circular Dichroism (CD)	(188)	(189)	(190)		(191)
Differential Scanning Calorimetry (DSC)	(192)	(193)			(194)
Light Scattering [Right Angle, Static (SLS), Dynamic (DLS)]	(76)	(195)	(153)		(174)
Small-Angle X-Ray (SAXS) and Neutron Scattering (SANS)	(196)	(197)	(198)		(178)
Transmission Electron Microscopy (TEM)	(199)	(200)	(147)	(46)	(201)
Atomic Force Microscopy (AFM)	(202)	(203)			(204)
Nuclear Magnetic Resonance Microscopy (NMR)	(205)	(107)	(149)		(172)
Cryogenic Electron Microscopy (Cryo-EM)	(206)	(207)	(208)	(46)	(176)
X-ray Crystallography		(209)			(210)
Mass Spectrometry	(90)	(129)	(152)		(211)
Molecular Dynamic (MD) Simulations	(93)	(212)			(161)
Functional					
Ultracentrifugation		(111)			(213)
Activity Assays	(214)	(215)			(177)
In Vivo Techniques	(100)	(216)			
In Vitro Cell Techniques	(98)	(144)			(181)
NMR	(97)	(217)	(218)		(219)
Electron Spin Resonance Spectroscopy (EPR)		(220)			(221)
Isothermal Titration Calorimetry (ITC)	(214)	(222)			
Fluorescence Quenching	(83)	(223)			(169)
Fluorescence Polarization	(224)	(143)			
Fluorescence Resonance Energy Transfer (FRET)		(145)			(168)
Mass Spectrometry		(225)	(151)		
Surface Plasmon Resonance (SPR)	(92)	(141)	(198)		
Electrochemical Detection		(138)			
MD Simulations	(83)	(226)			(204)

REFERENCES

(1)   Overington, J. P.; Al-Lazikani, B.; Hopkins, A. L. How Many Drug Targets Are There ? PubMed Commons. *Nat. Rev. Drug Discov.* **2006**, *5* (12), 993–996.

(2)   van Meer, G.; Voelker, D. R.; Feigenson, G. W. Membrane Lipids: Where They Are and How They Behave. *Nat. Rev. Mol. Cell Biol.* **2008**, *9* (2), 112–124.

(3)   van Meer, G.; de Kroon, A. I. P. M. Lipid Map of the Mammalian Cell. *J. Cell Sci.* **2011**, *124* (1), 5–8.

(4)   Cebecauer, M.; Amaro, M.; Jurkiewicz, P.; Sarmento, M. J.; Šachl, R.; Cwiklik, L.; Hof, M. Membrane Lipid Nanodomains. *Chem. Rev.* **2018**, *118* (23), 11259–11297.

(5)   Sezgin, E.; Levental, I.; Mayor, S.; Eggeling, C. The Mystery of Membrane Organization: Composition, Regulation and Roles of Lipid Rafts. *Nat. Rev. Mol. Cell Biol.* **2017**, *18* (6), 361–374.

(6)   Leventis, P. A.; Grinstein, S. The Distribution and Function of Phosphatidylserine in Cellular Membranes. *Annu. Rev. Biophys.* **2010**, *39*, 407–427.

(7)   Narayan, K.; Lemmon, M. A. Determining Selectivity of Phosphoinositide-Binding Domains. *Methods* **2006**, *39* (2), 122–133.

(8)   Lemmon, M. A. Membrane Recognition by Phospholipid-Binding Domains. *Nat. Rev. Mol. Cell Biol.* **2008**, *9* (2), 99–111.

(9)   McLaughlin, S.; Murray, D. Plasma Membrane Phosphoinositide Organization by Protein Electrostatics. *Nature* **2005**, *438* (7068), 605–611.

(10)   Stace, C. L.; Ktistakis, N. T. Phosphatidic Acid- and Phosphatidylserine-Binding Proteins. *Biochim. Biophys. Acta - Mol. Cell Biol. Lipids* **2006**, *1761* (8), 913–926.

(11)   Stahelin, R. V. Lipid Binding Domains: More than Simple Lipid Effectors. *J. Lipid Res.* **2009**, *50* (Suppl), 299–304.

(12)   Brown, M. F. Soft Matter in Lipid – Protein Interactions. *Annu. Rev. Biophys.* **2017**, *46*, 379–410.

(13)   Ingolfsson, H. I.; Arnarez, C.; Periole, X.; Marrink, S. J. Computational 'microscopy of Cellular Membranes. *J. Cell Sci.* **2016**, *129* (2), 257–268.

(14)   Newport, T. D.; Sansom, M. S. P.; Stansfeld, P. J. The MemProtMD Database: A Resource for Membrane-Embedded Protein Structures and Their Lipid Interactions. *Nucleic Acids*

Res. **2019**, *47*, D390–D397.

(15)   Loose, M.; Schwille, P. Biomimetic Membrane Systems to Study Cellular Organization. *J. Struct. Biol.* **2009**, *168* (1), 143–151.

(16)   *Biomimetic Lipid Membranes: Fundamentals, Applications, and Commercialization*; Kök, F. N., Yildiz, A. A., Inci, F., Eds.; Springer Nature Switzerland: Cham, Switzerland, 2019.

(17)   Brotherus, J. R.; Jost, P. C.; Griffith, O. H.; Hokin, L. E. Detergent Inactivation of Sodium- and Potassium-Activated Adenosinetriphosphatase of the Electric Eel. *Biochemistry* **1979**, *18* (23), 5043–5050.

(18)   Breyton, C.; Tribet, C.; Olive, J.; Dubacq, J.-P.; Popot, J.-L. Dimer to Monomer Conversion of Cytochrome B6f Complex. *J. Biol. Chem.* **1997**, *272* (35), 21892–21900.

(19)   Zoonens, M.; Popot, J. L. Amphipols for Each Season. *J. Membr. Biol.* **2014**, *247* (9–10), 759–796.

(20)   Tribet, C.; Audebert, R.; Popot, J. L. Amphipols: Polymers That Keep Membrane Proteins Soluble in Aqueous Solutions. *Proc. Natl. Acad. Sci. U. S. A.* **1996**, *93* (26), 15047–15050.

(21)   Corin, K.; Baaske, P.; Ravel, D. B.; Song, J.; Brown, E.; Wang, X.; Wienken, C. J.; Jerabek-Willemsen, M.; Duhr, S.; Luo, Y.; Braun, D.; Zhang, S. Designer Lipid-like Peptides: A Class of Detergents for Studying Functional Olfactory Receptors Using Commercial Cell-Free Systems. *PLoS One* **2011**, *6* (11), 1–9.

(22)   Khoe, U.; Yang, Y.; Zhang, S. Self-Assembly of Nanodonut Structure from a Cone-Shaped Designer Lipid-like Peptide Surfactant. *Langmuir* **2009**, *25* (7), 4111–4114.

(23)   Tao, H.; Lee, S. C.; Moeller, A.; Roy, R. S.; Siu, F. Y.; Zimmermann, J.; Stevens, R. C.; Potter, C. S.; Carragher, B.; Zhang, Q. Engineered Nanostructured β-Sheet Peptides Protect Membrane Proteins. *Nat. Methods* **2013**, *10* (8), 759–761.

(24)   Privé, G. G. Lipopeptide Detergents for Membrane Protein Studies. *Curr. Opin. Struct. Biol.* **2009**, *19* (4), 379–385.

(25)   McGregor, C. L.; Chen, L.; Pomroy, N. C.; Hwang, P.; Go, S.; Chakrabartty, A.; Privé, G. G. Lipopeptide Detergents Designed for the Structural Study of Membrane Proteins. *Nat. Biotechnol.* **2003**, *21* (2), 171–176.

(26)   Frauenfeld, J.; Löving, R.; Armache, J. P.; Sonnen, A. F. P.; Guettou, F.; Moberg, P.; Zhu, L.; Jegerschöld, C.; Flayhan, A.; Briggs, J. A. G.; Garoff, H.; Löw, C.; Cheng, Y.; Nordlund, P. A Saposin-Lipoprotein Nanoparticle System for Membrane Proteins. *Nat. Methods* **2016**,

13 (4), 345–351.

(27) Whiles, J. A.; Deems, R.; Vold, R. R.; Dennis, E. A. Bicelles in Structure-Function Studies of Membrane-Associated Proteins. *Bioorg. Chem.* **2002**, *30* (6), 431–442.

(28) Dürr, U. H. N.; Gildenberg, M.; Ramamoorthy, A. The Magic of Bicelles Lights up Membrane Protein Structure. *Chem. Rev.* **2012**, *112* (11), 6054–6074.

(29) Mäler, L.; Gräslund, A. Artificial Membrane Models for the Study of Macromolecular Delivery. In *Macromolecular Drug Delivery: Methods and Protocols*; Belting, M., Ed.; Humana Press: New York, 2009; Vol. 480, pp 129–138.

(30) Patil, Y. P.; Jadhav, S. Novel Methods for Liposome Preparation. *Chem. Phys. Lipids* **2014**, *177*, 8–18.

(31) Wagner, A.; Vorauer-Uhl, K. Liposome Technology for Industrial Purposes. *J. Drug Deliv.* **2011**, *2011*, 1–9.

(32) Akbarzadeh, A.; Rezaei-sadabady, R.; Davaran, S.; Joo, S. W.; Zarghami, N.; Hanifehpour, Y.; Samiei, M.; Kouhi, M.; Nejati-Koshki, K. Liposome: Classification, Preparation, and Applications. *Nanoscale Res. Lett.* **2013**, *8* (1), 102–110.

(33) Müller, S.; Kind, M.; Gruhle, K.; Hause, G.; Meister, A.; Drescher, S. Mixing Behaviour of Bilayer-Forming Phosphatidylcholines with Single-Chain Alkyl-Branched Bolalipids: Effect of Lateral Chain Length. *Biophys. Chem.* **2019**, *244*, 1–10.

(34) Mingeot-Leclercq, M.-P.; Deleu, M.; Brasseur, R.; Dufrêne, Y. F. Atomic Force Microscopy of Supported Lipid Bilayers. *Nat. Protoc.* **2008**, *3* (10), 1654–1659.

(35) Penkauskas, T.; Preta, G. Biological Applications of Tethered Bilayer Lipid Membranes. *Biochimie* **2019**, *157*, 131–141.

(36) Rossi, C.; Briand, E.; Parot, P.; Odorico, M.; Chopineau, J. Surface Response Methodology for the Study of Supported Membrane Formation. *J. Phys. Chem. B* **2007**, *111* (26), 7567–7576.

(37) Junghans, A.; Köper, I. Structural Analysis of Tethered Bilayer Lipid Membranes. *Langmuir* **2010**, *26* (13), 11035–11040.

(38) Anantharamaiah, G. M.; Mishra, V. K.; Garber, D. W.; Datta, G.; Handattu, S. P.; Palgunachari, M. N.; Chaddha, M.; Navab, M.; Reddy, S. T.; Segrest, J. P.; Fogelman, A. M. Structural Requirements for Antioxidative and Anti-Inflammatory Properties of Apolipoprotein A-I Mimetic Peptides. *J. Lipid Res.* **2007**, *48* (9), 1915–1923.

(39) Ritchie, T. K.; Grinkova, Y. V.; Bayburt, T. H.; Denisov, I. G.; Zolnerciks, J.; Atkins, W. M.; Sligar, S. G. Reconstitution of Membrane Proteins in Phospholipid Bilayer Nanodiscs. In *Methods in Enzymology*; Duzgunes, N., Ed.; Elsevier Masson SAS: San Diego, CA, 2009; Vol. 464, pp 211–231.

(40) Schuler, M. A.; Denisov, I. G.; Sligar, S. G. Nanodiscs as a New Tool to Examine Lipid-Protein Interactions. In *Methods in Molecular Biology*; Kleinschmidt, J., Ed.; Springer Science: New York, 2013; Vol. 974, pp 415–433.

(41) Denisov, I. G.; Sligar, S. G. Nanodiscs in Membrane Biochemistry and Biophysics. *Chem. Rev.* **2017**, *117* (6), 4669–4713.

(42) McLean, M. A.; Gregory, M. C.; Sligar, S. G. Nanodiscs: A Controlled Bilayer Surface for the Study of Membrane Proteins. *Annu. Rev. Biophys.* **2018**, *47* (1), 107–124.

(43) Nath, A.; Atkins, W. M.; Sligar, S. G. Applications of Phospholipid Bilayer Nanodiscs in the Study of Membranes and Membrane Proteins Current Topics Applications of Phospholipid Bilayer Nanodiscs in the Study of Membranes And. *Biochemistry* **2007**, *46* (8), 2059–2069.

(44) Bayburt, T. H.; Sligar, S. G. Membrane Protein Assembly into Nanodiscs. *FEBS Lett.* **2010**, *584* (9), 1721–1727.

(45) Nasr, M. L. Large Nanodiscs Going Viral. *Curr. Opin. Struct. Biol.* **2020**, *60*, 150–156.

(46) Zhao, Z.; Zhang, M.; Hogle, J. M.; Shih, W. M.; Wagner, G.; Nasr, M. L. DNA-Corralled Nanodiscs for the Structural and Functional Characterization of Membrane Proteins and Viral Entry. *J. Am. Chem. Soc.* **2018**, *140* (34), 10639–10643.

(47) Dörr, J. M.; Scheidelaar, S.; Koorengevel, M. C.; Dominguez, J. J.; Schäfer, M.; van Walree, C. A.; Killian, J. A. The Styrene–Maleic Acid Copolymer: A Versatile Tool in Membrane Research. *Eur. Biophys. J.* **2016**, *45* (1), 3–21.

(48) Lee, S. C.; Knowles, T. J.; Postis, V. L. G.; Jamshad, M.; Parslow, R. A.; Lin, Y. P.; Goldman, A.; Sridhar, P.; Overduin, M.; Muench, S. P.; Dafforn, T. R. A Method for Detergent-Free Isolation of Membrane Proteins in Their Local Lipid Environment. *Nat. Protoc.* **2016**, *11* (7), 1149–1162.

(49) Stroud, Z.; Hall, S. C. L.; Dafforn, T. R. Purification of Membrane Proteins Free from Conventional Detergents: SMA, New Polymers, New Opportunities and New Insights. *Methods* **2018**, *147*, 106–117.

(50) Ravula, T.; Hardin, N. Z.; Ramamoorthy, A. Polymer Nanodiscs: Advantages and Limitations. *Chem. Phys. Lipids* **2019**, *219*, 45–49.

(51) Overduin, M.; Klumperman, B. Advancing Membrane Biology with Poly(Styrene-Co-Maleic Acid)-Based Native Nanodiscs. *Eur. Polym. J.* **2019**, *110*, 63–68.

(52) Esmaili, M.; Overduin, M. Membrane Biology Visualized in Nanometer-Sized Discs Formed by Styrene Maleic Acid Polymers. *Biochim. Biophys. Acta - Biomembr.* **2018**, *1860* (2), 257–263.

(53) Segrest, J. P.; De Loof, H.; Dohlman, J. G.; Brouillette, C. G.; Anantharamaiah, G. M. Amphipathic Helix Motif: Classes and Properties. *Proteins* **1990**, *8* (2), 103–117.

(54) Lund-Katz, S.; Phillips, M. C. High Density Lipoprotein Structure-Function and Role in Reverse Cholesterol Transport. In *Cholesterol Binding and Cholesterol Transport: Structure and Function in Health and Disease*; Harris, J. R., Ed.; Springer: New York, 2010; pp 183–227.

(55) Orth, M.; Bellosta, S. Cholesterol: Its Regulation and Role in Central Nervous System Disorders. *Cholesterol* **2012**, *2012*, 1–19.

(56) Vickers, K. C.; Remaley, A. T. HDL and Cholesterol: Life after the Divorce? 1. *J. Lipid Res.* **2014**, *55* (1), 4–12.

(57) Mulder, W. J. M.; Van Leent, M. M. T.; Lameijer, M.; Fisher, E. A.; Fayad, Z. A.; Pérez-Medina, C. High-Density Lipoprotein Nanobiologics for Precision Medicine. *Acc. Chem. Res.* **2018**, *51* (1), 127–137.

(58) Gordon, T.; Castelli, W. P.; Hjortland, M. C.; Kannel, W. B.; Dawber, T. R. High Density Lipoprotein as a Protective Factor against Coronary Heart Disease. The Framingham Study. *Am. J. Med.* **1977**, *62* (5), 707–714.

(59) Manthei, K. A.; Patra, D.; Wilson, C. J.; Fawaz, M. V.; Piersimoni, L.; Shenkar, J. C.; Yuan, W.; Andrews, P. C.; Engen, J. R.; Schwendeman, A.; Ohi, M. D.; Tesmer, J. J. G. Structural Analysis of Lecithin:Cholesterol Acyltransferase Bound to High Density Lipoprotein Particles. *Commun. Biol.* **2020**, *3* (1), 1–11.

(60) Shore, B. C- and N-Terminal Amino Acids of Human Serum Lipoproteins. *Arch. Biochem. Biophys.* **1957**, *71*, 1–10.

(61) Shore, B.; Shore, V. Heterogeneity in Protein Subunits of Human Serum High-Density Lipoproteins. *Biochemistry* **1968**, *7* (8), 2773–2777.

(62)   Shore, V.; Shore, B. Some Physical and Chemical Studies on Two Polypeptide Components of High-Density Lipoproteins of Human Serum. *Biochemistry* **1968**, *7* (10), 3396–3403.

(63)   Gotto, A. M.; Shore, B. Conformation of Human Serum High Density Lipoprotein and Its Peptide Components. *Nature* **1969**, *224* (5214), 69–70.

(64)   Kostner, G.; Alaupovic, P. Isolation of Human Plasma HDL. *FEBS Lett.* **1971**, *15* (4), 320–324.

(65)   Jackson, R. L.; Baker, H. N.; David, J. S. K.; Gotto, A. M. Isolation of a Helical, Lipid-Binding Fragment from the Human Plasma High Density Lipoprotein, ApoLP-Gln-I. *Biochem. Biophys. Res. Commun.* **1972**, *49* (6), 1444–1451.

(66)   Segrest, J. P.; Jackson, R. L.; Morrisett, J. D.; Gotto, A. M. A Molecular Theory of Lipid-Protein Interactions in the Plasma Lipoproteins. *FEBS Lett.* **1974**, *38* (3), 247–253.

(67)   Segrest, J. P. Amphipathic Helixes and Plasma Lipoproteins: Thermodynamic and Geometric Considerations. *Chem. Phys. Lipids* **1977**, *18* (1), 7–22.

(68)   Brouillette, C. G.; Jones, J. L.; Ng, T. C.; Kercret, H.; Chung, B. H.; Segrest, J. P. Structural Studies of Apolipoprotein A-I/Phosphatidylcholine Recombinants by High-Field Proton NMR, Nondenaturing Gradient Gel Electrophoresis, and Electron Microscopy. *Biochemistry* **1984**, *23* (2), 359–367.

(69)   Borhani, D. W.; Rogers, D. P.; Engler, J. A.; Brouillette, C. G. Crystal Structure of Truncated Human Apolipoprotein A-I Suggests a Lipid-Bound Conformation. *Proc. Natl. Acad. Sci. U. S. A.* **1997**, *94* (23), 12291–12296.

(70)   Koppaka, V.; Silvestro, L.; Engler, J. A.; Brouillette, C. G.; Axelsen, P. H. The Structure of Human Lipoprotein A-I: Evidence for the "Belt" Model. *J. Biol. Chem.* **1999**, *274* (21), 14541–14544.

(71)   Huang, R.; Silva, R. A. G. D.; Jerome, W. G.; Kontush, A.; Chapman, M. J.; Curtiss, L. K.; Hodges, T. J.; Davidson, W. S. Apolipoprotein A-I Structural Organization in High-Density Lipoproteins Isolated from Human Plasma. *Nat. Struct. Mol. Biol.* **2011**, *18* (4), 416–423.

(72)   *Apolipoprotein Mimetic Peptides for Stimulating Cholesterol Efflux*; Anantharamaiah, G. M., Goldberg, D., Eds.; Adis: Switzerland, 2015.

(73)   Kanellis, P.; Romans, A. Y.; Johnson, B. J.; Kercretg, H.; Chiovetti, R.; Allen, T. M.; Segrest, J. P. Studies of Synthetic Peptide Analogs of the Amphiphatic Helix: Effect of Charged Amino Acid Residue Topography on Lipid Affinity. *J. Biol. Chem.* **1980**, *255* (23),

11464–11472.

(74)   Anantharamaiah, G. M.; Jones, J. L.; Brouillette, C. G.; Schmidt, C. F.; Chung, B. H.; Hughes, T. A.; Bhown, A. S.; Segrest, J. P. Studies of Synthetic Peptide Analogs of the Amphiphatic Helix: Structure of Complexes with Dimyrstoyl Phosphatidylcholine. *J. Biol. Chem.* **1985**, *260* (18), 10256–10262.

(75)   Chung, B. H.; Anantharamaiah, G. M.; Brouillette, C. G.; Nishida, T.; Segrest, J. P. Studies of Synthetic Peptide Analogs of the Amphiphatic Helix. Correlation of Structure with Function. *J. Biol. Chem.* **1985**, *260* (18), 10256–10262.

(76)   Larsen, A. N.; Sørensen, K. K.; Johansen, N. T.; Martel, A.; Kirkensgaard, J. J. K.; Jensen, K. J.; Arleth, L.; Midtgaard, S. R. Dimeric Peptides with Three Different Linkers Self-Assemble with Phospholipids to Form Peptide Nanodiscs That Stabilize Membrane Proteins. *Soft Matter* **2016**, *12* (27), 5937–5949.

(77)   Wool, G. D.; Reardon, C. A.; Getz, G. S. Apolipoprotein A-I Mimetic Peptide Helix Number and Helix Linker Influence Potentially Anti-Atherogenic Properties. *J. Lipid Res.* **2008**, *49* (6), 1268–1283.

(78)   Wool, G. D.; Vaisar, T.; Reardon, C. A.; Getz, G. S. An ApoA-I Mimetic Peptide Containing a Proline Residue Has Greater in Vivo HDL Binding and Anti-Inflammatory Ability than the 4F Peptide. *J. Lipid Res.* **2009**, *50* (9), 1889–1900.

(79)   Mishra, V. K.; Palgunachari, M. N.; Lund-Katz, S.; Phillips, M. C.; Segrest, J. P.; Anantharamaiah, G. M. Effect of the Arrangement of Tandem Repeating Units of Class A Amphipathic α-Helixes on Lipid Interactions. *J. Biol. Chem.* **1995**, *270* (4), 1602–1611.

(80)   Salnikov, E. S.; Anantharamaiah, G. M.; Bechinger, B. Supramolecular Organization of Apolipoprotein-A-I-Derived Peptides within Disc-like Arrangements. *Biophys. J.* **2018**, *115* (3), 467–477.

(81)   Datta, G.; Chaddha, M.; Hama, S.; Navab, M.; Fogelman, A. M.; Garber, D. W.; Mishra, V. K.; Epand, R. M.; Epand, R. F.; Lund-Katz, S.; Phillips, M. C.; Segrest, J. P.; Anantharamaiah, G. M. Effects of Increasing Hydrophobicity on the Physical-Chemical and Biological Properties of a Class A Amphipathic Helical Peptide. *J. Lipid Res.* **2001**, *42* (7), 1096–1104.

(82)   Mishra, V. K.; Palgunachari, M. N.; Krishna, N. R.; Glushka, J.; Segrest, J. P.; Anantharamaiah, G. M. Effect of Leucine to Phenylalanine Substitution on the Nonpolar

Face of a Class A Amphipathic Helical Peptide on Its Interaction with Lipid: High Resolution Solution NMR Studies of 4F-Dimyristoylphosphatidylcholine Discoidal Complex. *J. Biol. Chem.* **2008**, *283* (49), 34393–34402.

(83)   Sahoo, B. R.; Genjo, T.; Cox, S. J.; Stoddard, A. K.; Anantharamaiah, G. M.; Fierke, C.; Ramamoorthy, A. Nanodisc-Forming Scaffold Protein Promoted Retardation of Amyloid-Beta Aggregation. *J. Mol. Biol.* **2018**, *430* (21), 4230–4244.

(84)   Watson, C. E.; Weissbach, N.; Kjems, L.; Ayalasomayajula, S.; Zhang, Y.; Chang, I.; Navab, M.; Hama, S.; Hough, G.; Reddy, S. T.; Soffer, D.; Rader, D. J.; Fogelman, A. M.; Schecter, A. Treatment of Patients with Cardiovascular Disease with L-4F, an Apo-A1 Mimetic, Did Not Improve Select Biomarkers of HDL Function. *J. Lipid Res.* **2011**, *52* (2), 361–373.

(85)   Bloedon, L. A. T.; Dunbar, R.; Duffy, D.; Pinell-Salles, P.; Norris, R.; DeGroot, B. J.; Movva, R.; Navab, M.; Fogelman, A. M.; Rader, D. J. Safety, Pharmacokinetics, and Pharmacodynamics of Oral ApoA-I Mimetic Peptide D-4F in High-Risk Cardiovascular Patients. *J. Lipid Res.* **2008**, *49* (6), 1344–1352.

(86)   Sherman, C. B.; Peterson, S. J.; Frishman, W. H. Apolipoprotein A-I Mimetic Peptides: A Potential New Therapy for the Prevention of Atherosclerosis. *Cardiol. Rev.* **2010**, *18* (3), 141–147.

(87)   Sethi, A. A.; Stonik, J. A.; Thomas, F.; Demosky, S. J.; Amar, M.; Neufeld, E.; Brewer, H. B.; Davidson, W. S.; D'Souza, W.; Sviridov, D.; Remaley, A. T. Asymmetry in the Lipid Affinity of Bihelical Amphipathic Peptides: A Structural Determinant for the Specificity of ABCA1-Dependent Cholesterol Efflux by Peptides. *J. Biol. Chem.* **2008**, *283* (47), 32273–32282.

(88)   Schwendeman, A.; Sviridov, D. O.; Yuan, W.; Guo, Y.; Morin, E. E.; Yuan, Y.; Stonik, J.; Freeman, L.; Ossoli, A.; Thacker, S.; Killion, S.; Pryor, M.; Chen, Y. E.; Turner, S.; Remaley, A. T. The Effect of Phospholipid Composition of Reconstituted HDL on Its Cholesterol Efflux and Anti-Inflammatory Properties. *J. Lipid Res.* **2015**, *56* (9), 1727–1737.

(89)   Kariyazono, H.; Nadai, R.; Miyajima, R.; Takechi-Haraya, Y.; Baba, T.; Shigenaga, A.; Okuhira, K.; Otaka, A.; Saito, H. Formation of Stable Nanodiscs by Bihelical Apolipoprotein A-I Mimetic Peptide. *J. Pept. Sci.* **2015**, *22* (2), 116–122.

(90)   Carlson, M. L.; Young, J. W.; Zhao, Z.; Fabre, L.; Jun, D.; Li, J.; Li, J.; Dhupar, H. S.; Wason, I.; Mills, A. T.; Beatty, J. T.; Klassen, J. S.; Rouiller, I.; Duong, F. The Peptidisc, a Simple Method for Stabilizing Membrane Proteins in Detergent-Free Solution. *Elife* **2018**, *7* (e34085), 1–23.

(91)   Midtgaard, S. R.; Pedersen, M. C.; Kirkensgaard, J. J. K.; Sørensen, K. K.; Mortensen, K.; Jensen, K. J.; Arleth, L. Self-Assembling Peptides Form Nanodiscs That Stabilize Membrane Proteins. *Soft Matter* **2014**, *10* (5), 738–752.

(92)   Luchini, A.; Tidemand, F. G.; Johansen, N. T.; Campana, M.; Sotres, J.; Ploug, M.; Cárdenas, M.; Arleth, L. Peptide Disc Mediated Control of Membrane Protein Orientation in Supported Lipid Bilayers for Surface-Sensitive Investigations. *Anal. Chem.* **2020**, *92* (1), 1081–1088.

(93)   Islam, R. M.; Pourmousa, M.; Sviridov, D.; Gordon, S. M.; Neufeld, E. B.; Freeman, L. A.; Perrin, B. S.; Pastor, R. W.; Remaley, A. T. Structural Properties of Apolipoprotein A-I Mimetic Peptides That Promote ABCA1-Dependent Cholesterol Efflux. *Sci. Rep.* **2018**, *8* (1), 1–15.

(94)   Zhao, Y.; Imura, T.; Leman, L. J.; Curtiss, L. K.; Maryanoff, B. E.; Ghadiri, M. R. Mimicry of High-Density Lipoprotein: Functional Peptide-Lipid Nanoparticles Based on Multivalent Peptide Constructs. *J. Am. Chem. Soc.* **2013**, *135* (36), 13414–13424.

(95)   Dassaux, J.-L. Peptide/Lipid Complex Formation by Co-Lyophilization. 10/252,940, 2007.

(96)   Dassaux, J.-L.; Sekul, R.; Büttner, K.; Cornut, I.; Metz, G.; Dufourcq, J. Apolipoprotein A-I Agonists and Their Use to Treat Dyslipidemic Disorders. 08/940,095, 1999.

(97)   Zhang, M.; Huang, R.; Ackermann, R.; Im, S. C.; Waskell, L.; Schwendeman, A.; Ramamoorthy, A. Reconstitution of the Cytb5-CytP450 Complex in Nanodiscs for Structural Studies Using NMR Spectroscopy. *Angew. Chemie - Int. Ed.* **2016**, *55* (14), 4497–4499.

(98)   Kuai, R.; Ochyl, L. J.; Bahjat, K. S.; Schwendeman, A.; Moon, J. J. Designer Vaccine Nanodiscs for Personalized Cancer Immunotherapy. *Nat. Mater.* **2017**, *16* (4), 489–498.

(99)   Kuai, R.; Sun, X.; Yuan, W.; Xu, Y.; Schwendeman, A.; Moon, J. J. Subcutaneous Nanodisc Vaccination with Neoantigens for Combination Cancer Immunotherapy. *Bioconjug. Chem.* **2018**, *29* (3), 771–775.

(100)   Kuai, R.; Yuan, W.; Son, S.; Nam, J.; Xu, Y.; Fan, Y.; Schwendeman, A.; Moon, J. J.

Elimination of Established Tumors with Nanodisc-Based Combination Chemoimmunotherapy. *Sci. Adv.* **2018**, *4* (4), 1–14.

(101) Kadiyala, P.; Li, D.; Nunez, F. M.; Altshuler, D.; Doherty, R.; Kuai, R.; Yu, M.; Kamran, N.; Edwards, M.; Moon, J. J.; Lowenstein, P. R.; Castro, M. G.; Schwendeman, A. High-Density Lipoprotein-Mimicking Nanodiscs for Chemo-Immunotherapy against Glioblastoma Multiforme. *ACS Nano* **2019**, *13* (2), 1365–1384.

(102) Scheetz, L.; Park, K. S.; Li, Q.; Lowenstein, P. R.; Castro, M. G.; Schwendeman, A.; Moon, J. J. Engineering Patient-Specific Cancer Immunotherapies. *Nat. Biomed. Eng.* **2019**, *3* (10), 768–782.

(103) Bayburt, T. H.; Grinkova, Y. V.; Sligar, S. G. Self-Assembly of Discoidal Phospholipid Bilayer Nanoparticles with Membrane Scaffold Proteins. *Nano Lett.* **2002**, *2* (8), 853–856.

(104) Denisov, I. G.; Grinkova, Y. V.; Lazarides, A. A.; Sligar, S. G. Directed Self-Assembly of Monodisperse Phospholipid Bilayer Nanodiscs with Controlled Size Directed Self-Assembly of Monodisperse Phospholipid Bilayer Nanodiscs with Controlled Size. *Nano Lett.* **2004**, *126* (11), 3477–3487.

(105) Hagn, F.; Etzkorn, M.; Raschle, T.; Wagner, G. Optimized Phospholipid Bilayer Nanodiscs Facilitate High-Resolution Structure Determination of Membrane Proteins. *J. Am. Chem. Soc.* **2013**, *135* (5), 1919–1925.

(106) Grinkova, Y. V.; Denisov, I. G.; Sligar, S. G. Engineering Extended Membrane Scaffold Proteins for Self-Assembly of Soluble Nanoscale Lipid Bilayers. *Protein Eng. Des. Sel.* **2010**, *23* (11), 843–848.

(107) Hagn, F.; Nasr, M. L.; Wagner, G. Assembly of Phospholipid Nanodiscs of Controlled Size for Structural Studies of Membrane Proteins by NMR. *Nat. Protoc.* **2018**, *13* (1), 79–98.

(108) Skar-Gislinge, N.; Johansen, N. T.; Høiberg-Nielsen, R.; Arleth, L. Comprehensive Study of the Self-Assembly of Phospholipid Nanodiscs: What Determines Their Shape and Stoichiometry? *Langmuir* **2018**, *34* (42), 12569–12582.

(109) Camp, T.; McLean, M.; Kato, M.; Cheruzel, L.; Sligar, S. The Hydrodynamic Motion of Nanodiscs. *Chem. Phys. Lipids* **2019**, *220*, 28–35.

(110) Camp, T.; Mehta, K.; Sligar, S. G.; Zhang, K. Molecular Orientation Determination in Nanodiscs at the Single-Molecule Level. *Anal. Chem.* **2020**, *92* (2), 2229–2236.

(111) Her, C.; Filoti, D. I.; McLean, M. A.; Sligar, S. G.; Alexander Ross, J. B.; Steele, H.; Laue,

T. M. The Charge Properties of Phospholipid Nanodiscs. *Biophys. J.* **2016**, *111* (5), 989–998.

(112) Marty, M. T.; Sloan, C. D. K.; Bailey, R. C.; Sligar, S. G. Nonlinear Analyte Concentration Gradients for One-Step Kinetic Analysis Employing Optical Microring Resonators. *Anal. Chem.* **2012**, *84* (13), 5556–5564.

(113) Bayburt, T. H.; Grinkova, Y. V.; Sligar, S. G. Assembly of Single Bacteriorhodopsin Trimers in Bilayer Nanodiscs. *Arch. Biochem. Biophys.* **2006**, *450* (2), 215–222.

(114) Bayburt, T. H.; Leitz, A. J.; Xie, G.; Oprian, D. D.; Sligar, S. G. Transducin Activation by Nanoscale Lipid Bilayers Containing One and Two Rhodopsins. *J. Biol. Chem.* **2007**, *282* (20), 14875–14881.

(115) Leitz, A. J.; Bayburt, T. H.; Barnakov, A. N.; Springer, B. A.; Sligar, S. G. Functional Reconstitution of B2-Adrenergic Receptors Utilizing Self-Assembling Nanodisc Technology. *Biotechniques* **2006**, *40* (5), 601–612.

(116) Finkenwirth, F.; Sippach, M.; Landmesser, H.; Kirsch, F.; Ogienko, A.; Grunzel, M.; Kiesler, C.; Steinhoff, H. J.; Schneider, E.; Eitinger, T. ATP-Dependent Conformational Changes Trigger Substrate Capture and Release by an ECF-Type Biotin Transporter. *J. Biol. Chem.* **2015**, *290* (27), 16929–16942.

(117) Heuveling, J.; Frochaux, V.; Ziomkowska, J.; Wawrzinek, R.; Wessig, P.; Herrmann, A.; Schneider, E. Conformational Changes of the Bacterial Type i ATP-Binding Cassette Importer HisQMP2 at Distinct Steps of the Catalytic Cycle. *Biochim. Biophys. Acta - Biomembr.* **2014**, *1838* (1 Pt B), 106–116.

(118) Shaw, A. W.; Pureza, V. S.; Sligar, S. G.; Morrissey, J. H. The Local Phospholipid Environment Modulates the Activation of Blood Clotting. *J. Biol. Chem.* **2007**, *282* (9), 6556–6563.

(119) Mak, P. J.; Denisov, I. G.; Grinkova, Y. V.; Sligar, S. G.; Kincaid, J. R. Defining CYP3A4 Structural Responses to Substrate Binding. Raman Spectroscopic Studies of a Nanodisc-Incorporated Mammalian Cytochrome P450. *J. Am. Chem. Soc.* **2011**, *133* (5), 1357–1366.

(120) Wan, C.; Wu, B.; Song, Z.; Zhang, J.; Chu, H.; Wang, A.; Liu, Q.; Shi, Y.; Li, G.; Wang, J. Insights into the Molecular Recognition of the Granuphilin C2A Domain with PI(4,5)P2. *Chem. Phys. Lipids* **2015**, *186*, 61–67.

(121) Yokogawa, M.; Kobashigawa, Y.; Yoshida, N.; Ogura, K.; Harada, K.; Inagaki, F. NMR

Analyses of the Interaction between the FYVE Domain of Early Endosome Antigen 1 (EEA1) and Phosphoinositide Embedded in a Lipid Bilayer. *J. Biol. Chem.* **2012**, *287* (42), 34936–34945.

(122) Inagaki, S.; Ghirlando, R.; White, J. F.; Gvozdenovic-Jeremic, J.; Northup, J. K.; Grisshammer, R. Modulation of the Interaction between Neurotensin Receptor NTS1 and Gq Protein by Lipid. *J. Mol. Biol.* **2012**, *417* (1–2), 95–111.

(123) Kijac, A. Z.; Li, Y.; Sligar, S. G.; Rienstra, C. M. Magic-Angle Spinning Solid-State NMR Spectroscopy of Nanodisc-Embedded Human CYP3A4. *Biochemistry* **2007**, *46* (48), 13696–13703.

(124) Mörs, K.; Roos, C.; Scholz, F.; Wachtveitl, J.; Dötsch, V.; Bernhard, F.; Glaubitz, C. Modified Lipid and Protein Dynamics in Nanodiscs. *Biochim. Biophys. Acta - Biomembr.* **2013**, *1828* (4), 1222–1229.

(125) Ding, Y.; Fujimoto, L. M.; Yao, Y.; Marassi, F. M. Solid-State NMR of the Yersinia Pestis Outer Membrane Protein Ail in Lipid Bilayer Nanodiscs Sedimented by Ultracentrifugation. *J. Biomol. NMR* **2015**, *61* (3–4), 275–286.

(126) Kobashigawa, Y.; Harada, K.; Yoshida, N.; Ogura, K.; Inagaki, F. Phosphoinositide-Incorporated Lipid-Protein Nanodiscs: A Tool for Studying Protein-Lipid Interactions. *Anal. Biochem.* **2011**, *410* (1), 77–83.

(127) Marin, V. L.; Bayburt, T. H.; Sligar, S. G.; Mrksich, M. Functional Assays of Membrane-Bound Proteins with SAMDI-TOF Mass Spectrometry. *Angew. Chemie - Int. Ed.* **2007**, *46* (46), 8796–8798.

(128) Marty, M. T.; Hoi, K. K.; Gault, J.; Robinson, C. V. Probing the Lipid Annular Belt by Gas-Phase Dissociation of Membrane Proteins in Nanodiscs. *Angew. Chemie - Int. Ed.* **2016**, *55* (2), 550–554.

(129) Keener, J. E.; Zambrano, D. E.; Zhang, G.; Zak, C. K.; Reid, D. J.; Deodhar, B. S.; Pemberton, J. E.; Prell, J. S.; Marty, M. T. Chemical Additives Enable Native Mass Spectrometry Measurement of Membrane Protein Oligomeric State within Intact Nanodiscs. *J. Am. Chem. Soc.* **2019**, *141* (2), 1054–1061.

(130) Sloan, C. D. K.; Marty, M. T.; Sligar, S. G.; Bailey, R. C. Interfacing Lipid Bilayer Nanodiscs and Silicon Photonic Sensor Arrays for Multiplexed Protein − Lipid and Protein − Membrane Protein Interaction Screening. *Anal. Chem.* **2013**, *85* (5), 2970–2976.

(131) Muehl, E. M.; Gajsiewicz, J. M.; Medfisch, S. M.; Wiersma, Z. S. B.; Morrissey, J. H.; Bailey, R. C. Multiplexed Silicon Photonic Sensor Arrays Enable Facile Characterization of Coagulation Protein Binding to Nanodiscs with Variable Lipid Content. *J. Biol. Chem.* **2017**, jbc.M117.800938.

(132) Trahey, M.; Li, M. J.; Kwon, H.; Woodahl, E. L.; McClary, W. D.; Atkins, W. M. Applications of Lipid Nanodiscs for the Study of Membrane Proteins by Surface Plasmon Resonance. *Curr. Protoc. Protein Sci.* **2015**, *81*, 29.13.1-29.13.16.

(133) Tavoosi, N.; Smith, S. A.; Davis-Harrison, R. L.; Morrissey, J. H. Factor VII and Protein C Are Phosphatidic Acid-Binding Proteins. *Biochemistry* **2013**, *52* (33), 5545–5552.

(134) Borch, J.; Roepstorff, P.; Møller-Jensen, J. Nanodisc-Based Co-Immunoprecipitation for Mass Spectrometric Identification of Membrane-Interacting Proteins. *Mol. Cell. Proteomics* **2011**, *10* (7), 1–9.

(135) Das, A.; Zhao, J.; Schatz, G. C.; Sligar, S. G.; Van Duyne, R. P. Screening of Type I and II Drug Binding to Human Cytochrome P450-3A4 in Nanodiscs by Localized Surface Plasmon Resonance Spectroscopy. *Anal. Chem.* **2009**, *81* (10), 3754–3759.

(136) Borch, J.; Torta, F.; Sligar, S. G.; Roepstorff, P. Nanodiscs for Immobilization of Lipid Bilayers and Membrane Receptors: Kinetic Analysis of Cholera Toxin Binding to a Glycolipid Receptor. *Anal. Chem.* **2008**, *80* (16), 6245–6252.

(137) Bocquet, N.; Kohler, J.; Hug, M. N.; Kusznir, E. A.; Rufer, A. C.; Dawson, R. J.; Hennig, M.; Ruf, A.; Huber, W.; Huber, S. Real-Time Monitoring of Binding Events on a Thermostabilized Human A2A Receptor Embedded in a Lipid Bilayer by Surface Plasmon Resonance. *Biochim. Biophys. Acta - Biomembr.* **2015**, *1848* (5), 1224–1233.

(138) Lee, M.; Yang, H.; Kim, D.; Yang, M.; Park, T. H.; Hong, S. Human-like Smelling of a Rose Scent Using an Olfactory Receptor Nanodisc-Based Bioelectronic Nose. *Sci. Rep.* **2018**, *8* (1), 1–12.

(139) Yang, H.; Kim, D.; Kim, J.; Moon, D.; Song, H. S.; Lee, M.; Hong, S.; Park, T. H. Nanodisc-Based Bioelectronic Nose Using Olfactory Receptor Produced in Escherichia Coli for the Assessment of the Death-Associated Odor Cadaverine. *ACS Nano* **2017**, *11* (12), 11847–11855.

(140) Goluch, E. D.; Shaw, A. W.; Sligar, S. G.; Liu, C. Microfluidic Patterning of Nanodisc Lipid Bilayers and Multiplexed Analysis of Protein Interaction. *Lab Chip* **2008**, *8* (10), 1723–

1728.

(141) Jang, H.; Abraham, S. J.; Chavan, T. S.; Hitchinson, B.; Khavrutskii, L.; Tarasova, N. I.; Nussinov, R.; Gaponenko, V. Mechanisms of Membrane Binding of Small GTPase K-Ras4B Farnesylated Hypervariable Region. *J. Biol. Chem.* **2015**, *290* (15), 9465–9477.

(142) Tark, S.-H.; Das, A.; Sligar, S. G.; Dravid, V. P. Nanomechanical Detection of Cholera Toxin Using Microcantilevers Functionalized with Ganglioside Nanodiscs. *Nanotechnology* **2010**, *21* (43), 435502.

(143) Gregory, M. C.; McLean, M. A.; Sligar, S. G. Interaction of KRas4b with Anionic Membranes: A Special Role for PIP 2. *Biochem. Biophys. Res. Commun.* **2017**, *487* (2), 351–355.

(144) Carney, C. E.; Lenov, I. L.; Baker, C. J.; Macrenaris, K. W.; Eckermann, A. L.; Sligar, S. G.; Meade, T. J. Nanodiscs as a Modular Platform for Multimodal MR-Optical Imaging. *Bioconjug. Chem.* **2015**, *26* (5), 899–905.

(145) Ye, X.; McLean, M. A.; Sligar, S. G. Conformational Equilibrium of Talin Is Regulated by Anionic Lipids. *Biochim. Biophys. Acta - Biomembr.* **2016**, *1858* (8), 1833–1840.

(146) Iwai, H.; Züger, S.; Jin, J.; Tam, P. H. Highly Efficient Protein Trans-Splicing by a Naturally Split DnaE Intein from Nostoc Punctiforme. *FEBS Lett.* **2006**, *580* (7), 1853–1858.

(147) Miehling, J.; Goricanec, D.; Hagn, F. A Split-Intein-Based Method for the Efficient Production of Circularized Nanodiscs for Structural Studies of Membrane Proteins. *ChemBioChem* **2018**, *19* (18), 1927–1933.

(148) Pishesha, N.; Ingram, J. R.; Ploegh, H. L. Sortase A: A Model for Transpeptidation and Its Biological Applications. *Annu. Rev. Cell Dev. Biol.* **2018**, *34* (1), 163–188.

(149) Nasr, M. L.; Baptista, D.; Strauss, M.; Sun, Z. Y. J.; Grigoriu, S.; Huser, S.; Plückthun, A.; Hagn, F.; Walz, T.; Hogle, J. M.; Wagner, G. Covalently Circularized Nanodiscs for Studying Membrane Proteins and Viral Entry. *Nat. Methods* **2017**, *14* (1), 49–52.

(150) Nasr, M. L.; Wagner, G. Covalently Circularized Nanodiscs; Challenges and Applications. *Curr. Opin. Struct. Biol.* **2018**, *51*, 129–134.

(151) Yeh, V.; Lee, T. Y.; Chen, C. W.; Kuo, P. C.; Shiue, J.; Chu, L. K.; Yu, T. Y. Highly Efficient Transfer of 7TM Membrane Protein from Native Membrane to Covalently Circularized Nanodisc. *Sci. Rep.* **2018**, *8* (1), 1–11.

(152) Yusuf, Y.; Massiot, J.; Chang, Y. T.; Wu, P. H.; Yeh, V.; Kuo, P. C.; Shiue, J.; Yu, T. Y. Optimization of the Production of Covalently Circularized Nanodiscs and Their Characterization in Physiological Conditions. *Langmuir* **2018**, *34* (11), 3525–3532.

(153) Johansen, N. T.; Tidemand, F. G.; Nguyen, T. T. T. N.; Rand, K. D.; Pedersen, M. C.; Arleth, L. Circularized and Solubility-Enhanced MSPs Facilitate Simple and High-Yield Production of Stable Nanodiscs for Studies of Membrane Proteins in Solution. *FEBS J.* **2019**, *286* (9), 1734–1751.

(154) Tonge, S. R.; Tighe, B. J. Responsive Hydrophobically Associating Polymers: A Review of Structure and Properties. *Adv. Drug Deliv. Rev.* **2001**, *53* (1), 109–122.

(155) Tonge, S. R. Composition for Use in the Solubilisation of Hydrophobic Active Agents. GB2426703, 2006.

(156) Knowles, T. J.; Finka, R.; Smith, C.; Lin, Y. P.; Dafforn, T.; Overduin, M. Membrane Proteins Solubilized Intact in Lipid Containing Nanoparticles Bounded by Styrene Maleic Acid Copolymer. *J. Am. Chem. Soc.* **2009**, *131* (22), 7484–7485.

(157) Orwick, M. C.; Judge, P. J.; Procek, J.; Lindholm, L.; Graziadei, A.; Engel, A.; Gröbner, G.; Watts, A. Detergent-Free Formation and Physicochemical Characterization of Nanosized Lipid-Polymer Complexes: Lipodisq. *Angew. Chemie - Int. Ed.* **2012**, *51* (19), 4653–4657.

(158) Swainsbury, D. J. K.; Scheidelaar, S.; Van Grondelle, R.; Killian, J. A.; Jones, M. R. Bacterial Reaction Centers Purified with Styrene Maleic Acid Copolymer Retain Native Membrane Functional Properties and Display Enhanced Stability. *Angew. Chemie - Int. Ed.* **2014**, *53* (44), 11803–11807.

(159) Luna, V. M.; Vazir, M.; Vaish, A.; Chong, S.; Chen, I.; Yamane, H. K. Generation of Membrane Proteins in Polymer-Based Lipoparticles as Flow Cytometry Antigens. *Eur. Polym. J.* **2018**, *109* (June), 483–488.

(160) Scheidelaar, S.; Koorengevel, M. C.; Pardo, J. D.; Meeldijk, J. D.; Breukink, E.; Killian, J. A. Molecular Model for the Solubilization of Membranes into Nanodisks by Styrene Maleic Acid Copolymers. *Biophys. J.* **2015**, *108* (2), 279–290.

(161) Orekhov, P. S.; Bozdaganyan, M. E.; Voskoboynikova, N.; Mulkidjanian, A. Y.; Steinhoff, H. J.; Shaitan, K. V. Styrene/Maleic Acid Copolymers Form SMALPs by Pulling Lipid Patches out of the Lipid Bilayer. *Langmuir* **2019**, *35* (10), 3748–3758.

(162) Kopf, A. H.; Dörr, J. M.; Koorengevel, M. C.; Antoniciello, F.; Jahn, H.; Killian, J. A. Factors Influencing the Solubilization of Membrane Proteins from Escherichia Coli Membranes by Styrene–Maleic Acid Copolymers. *Biochim. Biophys. Acta - Biomembr.* **2020**, *1862* (2), 183125.

(163) Tanaka, M.; Hosotani, A.; Tachibana, Y.; Nakano, M.; Iwasaki, K.; Kawakami, T.; Mukai, T. Preparation and Characterization of Reconstituted Lipid-Synthetic Polymer Discoidal Particles. *Langmuir* **2015**, *31* (46), 12719–12726.

(164) Scheidelaar, S.; Koorengevel, M. C.; van Walree, C. A.; Dominguez, J. J.; Dörr, J. M.; Killian, J. A. Effect of Polymer Composition and PH on Membrane Solubilization by Styrene-Maleic Acid Copolymers. *Biophys. J.* **2016**, *111* (9), 1974–1986.

(165) Smith, A. A. A.; Autzen, H. E.; Laursen, T.; Wu, V.; Yen, M.; Hall, A.; Hansen, S. D.; Cheng, Y.; Xu, T. Controlling Styrene Maleic Acid Lipid Particles through RAFT. *Biomacromolecules* **2017**, *18* (11), 3706–3713.

(166) Hall, S. C. L.; Tognoloni, C.; Price, G. J.; Klumperman, B.; Edler, K. J.; Dafforn, T. R.; Arnold, T. Influence of Poly(Styrene- Co -Maleic Acid) Copolymer Structure on the Properties and Self-Assembly of SMALP Nanodiscs. *Biomacromolecules* **2018**, *19* (3), 761–772.

(167) Craig, A. F.; Clark, E. E.; Sahu, I. D.; Zhang, R.; Frantz, N. D.; Al-Abdul-Wahid, M. S.; Dabney-Smith, C.; Konkolewicz, D.; Lorigan, G. A. Tuning the Size of Styrene-Maleic Acid Copolymer-Lipid Nanoparticles (SMALPs) Using RAFT Polymerization for Biophysical Studies. *Biochim. Biophys. Acta - Biomembr.* **2016**, *1858* (11), 2931–2939.

(168) Lindhoud, S.; Carvalho, V.; Pronk, J. W.; Aubin-Tam, M. E. SMA-SH: Modified Styrene-Maleic Acid Copolymer for Functionalization of Lipid Nanodiscs. *Biomacromolecules* **2016**, *17* (4), 1516–1522.

(169) Morrison, K. A.; Akram, A.; Mathews, A.; Khan, Z. A.; Patel, J. H.; Zhou, C.; Hardy, D. J.; Moore-Kelly, C.; Patel, R.; Odiba, V.; Knowles, T. J.; Javed, M. U. H.; Chmel, N. P.; Dafforn, T. R.; Rothnie, A. J. Membrane Protein Extraction and Purification Using Styrene-Maleic Acid (SMA) Copolymer: Effect of Variations in Polymer Structure. *Biochem. J.* **2016**, *473* (23), 4349–4360.

(170) Ravula, T.; Hardin, N. Z.; Ramadugu, S. K.; Ramamoorthy, A. PH Tunable and Divalent Metal Ion Tolerant Polymer Lipid Nanodiscs. *Langmuir* **2017**, *33* (40), 10655–10662.

(171) Ravula, T.; Hardin, N. Z.; Ramadugu, S. K.; Cox, S. J.; Ramamoorthy, A. Formation of PH-Resistant Monodispersed Polymer–Lipid Nanodiscs. *Angew. Chemie - Int. Ed.* **2018**, *57* (5), 1342–1345.

(172) Ravula, T.; Hardin, N. Z.; Bai, J.; Im, S. C.; Waskell, L.; Ramamoorthy, A. Effect of Polymer Charge on Functional Reconstitution of Membrane Proteins in Polymer Nanodiscs. *Chem. Commun.* **2018**, *54* (69), 9615–9618.

(173) Beriashvili, D.; Spencer, N. R.; Dieckmann, T.; Overduin, M.; Palmer, M. Characterization of Multimeric Daptomycin Bound to Lipid Nanodiscs Formed by Calcium-Tolerant Styrene-Maleic Acid Copolymer. *Biochim. Biophys. Acta - Biomembr.* **2020**, *1862* (6), 183234.

(174) Hall, S. C. L.; Tognoloni, C.; Charlton, J.; Bragginton, É. C.; Rothnie, A. J.; Sridhar, P.; Wheatley, M.; Knowles, T. J.; Arnold, T.; Edler, K. J.; Dafforn, T. R. An Acid-Compatible Co-Polymer for the Solubilization of Membranes and Proteins into Lipid Bilayer-Containing Nanoparticles. *Nanoscale* **2018**, *10* (22), 10609–10619.

(175) Fiori, M. C.; Zheng, W.; Kamilar, E.; Simiyu, G.; Guillermo, A. A. Extraction and Reconstitution of Membrane Proteins into Lipid Nanodiscs Encased by Zwitterionic Styrene-Maleic Amide Copolymers. *Sci. Rep.* **2020**, *10* (1), 1–13.

(176) Yasuhara, K.; Arakida, J.; Ravula, T.; Ramadugu, S. K.; Sahoo, B.; Kikuchi, J. I.; Ramamoorthy, A. Spontaneous Lipid Nanodisc Fomation by Amphiphilic Polymethacrylate Copolymers. *J. Am. Chem. Soc.* **2017**, *139* (51), 18657–18663.

(177) Oluwole, A. O.; Danielczak, B.; Meister, A.; Babalola, J. O.; Vargas, C.; Keller, S. Solubilization of Membrane Proteins into Functional Lipid-Bilayer Nanodiscs Using a Diisobutylene/Maleic Acid Copolymer. *Angew. Chemie - Int. Ed.* **2017**, *56* (7), 1919–1924.

(178) Oluwole, A. O.; Klingler, J.; Danielczak, B.; Babalola, J. O.; Vargas, C.; Pabst, G.; Keller, S. Formation of Lipid-Bilayer Nanodiscs by Diisobutylene/Maleic Acid (DIBMA) Copolymer. *Langmuir* **2017**, *33* (50), 14378–14388.

(179) Danielczak, B.; Meister, A.; Keller, S. Influence of Mg 2+ and Ca 2+ on Nanodisc Formation by Diisobutylene/Maleic Acid (DIBMA) Copolymer. *Chem. Phys. Lipids* **2019**, *221*, 30–38.

(180) Barniol-Xicota, M.; Verhelst, S. H. L. Stable and Functional Rhomboid Proteases in Lipid Nanodiscs by Using Diisobutylene/Maleic Acid Copolymers. *J. Am. Chem. Soc.* **2018**, *140*

(44), 14557–14561.

(181) Barniol-Xicota, M.; Verhelst, S. H. L. Comparative Analysis of Maleic Acid Copolymer-Based Lipid Nanodiscs Reveals Preferential Lipid and Protein Solubilization. *ChemRxiv* **2020**, 1–25.

(182) Inagaki, S.; Ghirlando, R. Nanodisc Characterization by Analytical Ultracentrifugation. *Nanotechnol. Rev.* **2017**, *6* (1), 3–14.

(183) Viegas, A.; Viennet, T.; Etzkorn, M. The Power, Pitfalls and Potential of the Nanodisc System for NMR-Based Studies. *Biol. Chem.* **2016**, *397* (12), 1335–1354.

(184) Puthenveetil, R.; Vinogradova, O. Solution NMR: A Powerful Tool for Structural and Functional Studies of Membrane Proteins in Reconstituted Environments. *J. Biol. Chem.* **2019**, *294* (44), 15914–15931.

(185) Efremov, R. G.; Gatsogiannis, C.; Raunser, S. Lipid Nanodiscs as a Tool for High-Resolution Structure Determination of Membrane Proteins by Single-Particle Cryo-EM. In *Methods in Enzymology*; Ziegler, C., Ed.; Elsevier Inc., 2017; Vol. 594, pp 1–30.

(186) Redhair, M.; Clouser, A. F.; Atkins, W. M. Hydrogen-Deuterium Exchange Mass Spectrometry of Membrane Proteins in Lipid Nanodiscs. *Chem. Phys. Lipids* **2019**, *220*, 14–22.

(187) Pourmousa, M.; Pastor, R. W. Molecular Dynamics Simulations of Lipid Nanodiscs. *Biochim. Biophys. Acta - Biomembr.* **2018**, *1860* (10), 2094–2107.

188. Ikeda, K., Horiuchi, A., Egawa, A., Tamaki, H., Fujiwara, T., and Nakano, M. (2017) Nanodisc-to-Nanofiber Transition of Noncovalent Peptide-Phospholipid Assemblies. ACS Omega. 2, 2935–2944

189. Son, M., Pinnola, A., Gordon, S. C., Bassi, R., and Schlau-Cohen, G. S. (2020) Observation of dissipative chlorophyll-to-carotenoid energy transfer in light-harvesting complex II in membrane nanodiscs. Nat. Commun. 11, 1–8

190. Huang, H. Y., Syue, M. L., Chen, I. C., Yu, T. Y., and Chu, L. K. (2019) Influence of Lipid Compositions in the Events of Retinal Schiff Base of Bacteriorhodopsin Embedded in Covalently Circularized Nanodiscs: Thermal Isomerization, Photoisomerization, and Deprotonation. J. Phys. Chem. B. 123, 9123–9133

191. Sahoo, B. R., Genjo, T., Nakayama, T. W., Stoddard, A. K., Ando, T., Yasuhara, K., Fierke, C. A., and Ramamoorthy, A. (2019) A cationic polymethacrylate-

copolymer acts as an agonist for β-amyloid and an antagonist for amylin fibrillation. Chem. Sci. 10, 3976–3986

192. Barnaba, C., Sahoo, B. R., Ravula, T., Medina-Meza, I. G., Im, S. C., Anantharamaiah, G. M., Waskell, L., and Ramamoorthy, A. (2018) Cytochrome-P450-Induced Ordering of Microsomal Membranes Modulates Affinity for Drugs. Angew. Chemie - Int. Ed. 57, 3391–3395

193. Yahalom, A., Davidov, G., Kolusheva, S., Shaked, H., Barber-Zucker, S., Zarivach, R., and Chill, J. H. (2019) Structure and membrane-targeting of a Bordetella pertussis effector N-terminal domain. Biochim. Biophys. Acta - Biomembr. 1861, 183054

194. Dominguez Pardo, J. J., Dörr, J. M., Iyer, A., Cox, R. C., Scheidelaar, S., Koorengevel, M. C., Subramaniam, V., and Killian, J. A. (2017) Solubilization of lipids and lipid phases by the styrene–maleic acid copolymer. Eur. Biophys. J. 46, 91–101

195. Damiati, S., Scheberl, A., Zayni, S., Damiati, S. A., Schuster, B., and Kompella, U. B. (2019) Albumin-bound nanodiscs as delivery vehicle candidates: Development and characterization. Biophys. Chem. 251, 1–8

196. Prade, E., Mahajan, M., Im, S. C., Zhang, M., Gentry, K. A., Anantharamaiah, G. M., Waskell, L., and Ramamoorthy, A. (2018) A Minimal Functional Complex of Cytochrome P450 and FBD of Cytochrome P450 Reductase in Nanodiscs. Angew. Chemie - Int. Ed. 57, 8458–8462

197. Shih, O., Yeh, Y. Q., Liao, K. F., Su, C. J., Wu, P. H., Heenan, R. K., Yu, T. Y., and Jeng, U. S. (2018) Membrane Charging and Swelling upon Calcium Adsorption as Revealed by Phospholipid Nanodiscs. J. Phys. Chem. Lett. 9, 4287–4293

198. Tidemand, F. G., Østergaard, H., Ploug, M., Kragelund, B. B., and Arleth, L. (2020) Efficient refolding and reconstitution of tissue factor into nanodiscs facilitates structural investigation of a multicomponent system on a lipid bilayer. Biochim. Biophys. Acta - Biomembr. 1862, 183214

199. Scheetz, L. M., Yu, M., Li, D., Castro, M. G., Moon, J. J., and Schwendeman, A. (2020) Synthetic HDL nanoparticles delivering docetaxel and cpg for chemoimmunotherapy of colon adenocarcinoma. Int. J. Mol. Sci. 21, 1–11

200. Shenkarev, Z. O., Karlova, M. G., Kulbatskii, D. S., Kirpichnikov, M. P., Lyukmanova, E. N., and Sokolova, O. S. (2018) Recombinant Production, Reconstruction in Lipid–Protein Nanodiscs, and Electron Microscopy of Full-Length α-Subunit of Human Potassium Channel Kv7.1. Biochem. 83, 562–573

201. Postis, V., Rawson, S., Mitchell, J. K., Lee, S. C., Parslow, R. A., Dafforn, T. R., Baldwin, S. A., and Muench, S. P. (2015) The use of SMALPs as a novel membrane protein scaffold for structure study by negative stain electron microscopy. Biochim. Biophys. Acta - Biomembr. 1848, 496–501

202. Ravula, T., Ishikuro, D., Kodera, N., Ando, T., Anantharamaiah, G. M., and Ramamoorthy, A. (2018) Real-Time Monitoring of Lipid Exchange via Fusion of Peptide Based Lipid-Nanodiscs. Chem. Mater. 30, 3204–3207

203. Haruyama, T., Sugano, Y., Kodera, N., Uchihashi, T., Ando, T., Tanaka, Y., Konno, H., and Tsukazaki, T. (2019) Single-Unit Imaging of Membrane Protein-Embedded Nanodiscs from Two Oriented Sides by High-Speed Atomic Force Microscopy. Structure. 27, 152-160.e3

204. Sahoo, B. R., Genjo, T., Moharana, K. C., and Ramamoorthy, A. (2019) Self-Assembly of Polymer-Encased Lipid Nanodiscs and Membrane Protein Reconstitution. J. Phys. Chem. B. 123, 4562–4570

205. Salnikov, E. S., Aisenbrey, C., Anantharamaiah, G. M., and Bechinger, B. (2019) Solid-state NMR structural investigations of peptide-based nanodiscs and of transmembrane helices in bicellar arrangements. Chem. Phys. Lipids. 219, 58–71

206. Liu, J., Wan, F., Jin, Q., Li, X., Bhat, E. A., Guo, J., Lei, M., Guan, F., Wu, J., and Ye, S. (2020) Cryo-EM structures of human calcium homeostasis modulator 5. Cell Discov. 6, 4–7

207. Zhao, D. Y., Pöge, M., Morizumi, T., Gulati, S., Van Eps, N., Zhang, J., Miszta, P., Filipek, S., Mahamid, J., Plitzko, J. M., Baumeister, W., Ernst, O. P., and Palczewski, K. (2019) Cryo-EM structure of the native rhodopsin dimer in nanodiscs. J. Biol. Chem. 294, 14215–14230

208. Kuo, Y. C., Chen, H., Shang, G., Uchikawa, E., Tian, H., Bai, X. C., and Zhang, X. (2020) Cryo-EM structure of the PlexinC1/A39R complex reveals inter-domain interactions critical for ligand-induced activation. Nat. Commun. 11, 1–12

209. Nikolaev, M., Round, E., Gushchin, I., Polovinkin, V., Balandin, T., Kuzmichev, P., Shevchenko, V., Borshchevskiy, V., Kuklin, A., Round, A., Bernhard, F., Willbold, D., Büldt, G., and Gordeliy, V. (2017) Integral Membrane Proteins Can Be Crystallized Directly from Nanodiscs. Cryst. Growth Des. 17, 945–948

210. Broecker, J., Eger, B. T., and Ernst, O. P. (2017) Crystallogenesis of Membrane Proteins Mediated by Polymer-Bounded Lipid Nanodiscs. Structure. 25, 384–392

211. Hellwig, N., Peetz, O., Ahdash, Z., Tascón, I., Booth, P. J., Mikusevic, V., Diskowski, M., Politis, A., Hellmich, Y., Hänelt, I., Reading, E., and Morgner, N. (2018) Native mass spectrometry goes more native: Investigation of membrane protein complexes directly from SMALPs. Chem. Commun. 54, 13702–13705

212. López, C. A., Swift, M. F., Xu, X. P., Hanein, D., Volkmann, N., and Gnanakaran, S. (2019) Biophysical Characterization of a Nanodisc with and without BAX: An Integrative Study Using Molecular Dynamics Simulations and Cryo-EM. Structure. 27, 988-999.e4

213. Swainsbury, D. J. K., Proctor, M. S., Hitchcock, A., Cartron, M. L., Qian, P., Martin, E. C., Jackson, P. J., Madsen, J., Armes, S. P., and Hunter, C. N. (2018) Probing the local lipid environment of the Rhodobacter sphaeroides cytochrome bc1 and Synechocystis sp. PCC 6803 cytochrome b6f complexes with styrene maleic acid. Biochim. Biophys. Acta - Bioenerg. 1859, 215–225

214. Liu, J., Zhu, L., Zhang, X., Wu, B., Zhu, P., Zhao, H., and Wang, J. (2019) Peptide-based NTA(Ni)-nanodiscs for studying membrane enhanced FGFR1 kinase activities. PeerJ. 7, 1–13

215. Li, M. J., Nath, A., and Atkins, W. M. (2017) Differential Coupling of Binding, ATP Hydrolysis, and Transport of Fluorescent Probes with P-Glycoprotein in Lipid Nanodiscs. Biochemistry. 56, 2506–2517

216. Huda, P., Binderup, T., Pedersen, M. C., Midtgaard, S. R., Elema, D. R., Kjær, A., Jensen, M., and Arleth, L. (2015) PET/CT based in vivo evaluation of 64Cu labelled nanodiscs in tumor bearing mice. PLoS One. 10, 1–14

217. Fang, Z., Marshall, C. B., Nishikawa, T., Gossert, A. D., Jansen, J. M., Jahnke, W., and Ikura, M. (2018) Inhibition of K-RAS4B by a Unique Mechanism of Action: Stabilizing Membrane-Dependent Occlusion of the Effector-Binding Site. Cell

Chem. Biol. 25, 1327–1336

218. Chien, C.-T. H., Helfinger, L. R., Bostock, M. J., Solt, A., Tan, Y. L., and Nietlispach, D. (2017) An Adaptable Phospholipid Membrane Mimetic System for Solution NMR Studies of Membrane Proteins. J. Am. Chem. Soc. 139, 14829–14832

219. Ravula, T., Kim, J., Lee, D. K., and Ramamoorthy, A. (2020) Magnetic Alignment of Polymer Nanodiscs Probed by Solid-State NMR Spectroscopy. Langmuir. 36, 1258–1265

220. Qasim, A., Sher, I., Hirschhorn, O., Shaked, H., Qasem, Z., Ruthstein, S., and Chill, J. H. (2019) Investigation of a KcsA Cytoplasmic pH Gate in Lipoprotein Nanodiscs. ChemBioChem. 20, 813–821

221. Colbasevici, A., Voskoboynikova, N., Orekhov, P. S., Bozdaganyan, M. E., Karlova, M. G., Sokolova, O. S., Klare, J. P., Mulkidjanian, A. Y., Shaitan, K. V., and Steinhoff, H. J. (2020) Lipid dynamics in nanoparticles formed by maleic acid-containing copolymers: EPR spectroscopy and molecular dynamics simulations. Biochim. Biophys. Acta - Biomembr. 10.1016/j.bbamem.2020.183207

222. Elliot Murphy, R., Samal, A. B., Vlach, J., Mas, V., Prevelige, P. E., and Saad, J. S. (2019) Structural and biophysical characterizations of HIV-1 matrix trimer binding to lipid nanodiscs shed light on virus assembly. J. Biol. Chem. 294, 18600–18612

223. Crisafi, E., and Pandit, A. (2017) Disentangling protein and lipid interactions that control a molecular switch in photosynthetic light harvesting. Biochim. Biophys. Acta - Biomembr. 1859, 40–47

224. Barnaba, C., Ravula, T., Medina-Meza, I. G., Im, S. C., Anantharamaiah, G. M., Waskell, L., and Ramamoorthy, A. (2018) Lipid-exchange in nanodiscs discloses membrane boundaries of cytochrome-P450 reductase. Chem. Commun. 54, 6336–6339

225. Walker, L. R., and Marty, M. T. (2020) Revealing the Specificity of a Range of Antimicrobial Peptides in Lipid Nanodiscs by Native Mass Spectrometry. Biochemistry. 59, 2135–42

226. Travers, T., López, C. A., Van, Q. N., Neale, C., Tonelli, M., Stephen, A. G., and Gnanakaran, S. (2018) Molecular recognition of RAS/RAF complex at the membrane: Role of RAF cysteine-rich domain. Sci. Rep. 8, 1–15

Multiplexed Silicon Photonic Sensor Arrays Enable Facile Characterization of Coagulation Protein Binding to Nanodiscs with Variable Lipid Content

Abstract

Interactions of soluble proteins with the cell membrane are critical within the blood coagulation cascade. Of particular interest are the interactions of γ-carboxyglutamic acid–rich (GLA) domain–containing clotting proteins with lipids. Variability among conventional analytical methods presents challenges for comparing clotting protein–lipid interactions. Most previous studies have investigated only a single clotting protein and lipid composition and have yielded widely different binding constants. Herein, we demonstrate that a combination of lipid bilayer Nanodiscs and a multiplexed silicon photonic analysis technology enables high-throughput probing of many protein–lipid interactions among blood-clotting proteins. This approach allowed direct comparison of the binding constants of prothrombin, factor X, activated factor VII, and activated protein C to seven different binary lipid compositions. In a single experiment, the binding constants of one protein interacting with all lipid compositions were simultaneously determined. A simple surface regeneration then facilitated similar binding measurements for three other coagulation proteins. As expected, our results indicated that all proteins exhibit tighter binding (lower K_d) as the proportion of anionic lipid increases. Interestingly, at high proportions of phosphatidylserine, the K_d values of all four proteins began to converge. We also found that although k_{off} values for all four proteins followed trends similar to those observed for the K_d values, the variation among the proteins was much lower, indicating that much of the variation came from the kinetic binding (k_{on})

of the proteins. These findings indicate that the combination of silicon photonic microring resonator arrays and Nanodiscs enables rapid interrogation.

1. Introduction

The study of complex, multifactorial biomolecular binding interactions using direct physical methods, such as surface plasmon resonance, can be a time consuming and complicated process that often requires large quantities of expensive reagents. This holds especially true for monitoring interactions at the cell membrane surface, which plays a critical role in the regulation of important biological processes such as cell-signaling and blood coagulation, the latter of which involves protein-protein and protein-lipid interactions and is of particular relevance to this study.

Protein-membrane interactions governing processes such as blood coagulation are difficult to study due to their multimodal nature, but also because of the complicated environment of the cell membrane. The many varieties of lipids, including phospholipids, sphingolipids, and glycolipids, as well as small molecules such as sterols and polyketides[1] can influence direct binding of proteins to the cell membrane or membrane proteins. Therefore, the use of a model membrane system is an attractive approach to probing the biophysics of interactions in a more well-defined and simplified environment. Among several different model lipid bilayer systems,[2–4] Nanodiscs offer many advantages for probing biomolecular interactions at membrane surfaces. Nanodiscs are discoidal lipid bilayers approximately 10 nm in diameter, held together by 2 membrane scaffold proteins (MSPs).[3] Their small size and ease of assembly give a high degree of control over lipid composition.[5–7] Previous work has also shown that MSP offers a handle-like structure to which tags can be attached,[8] thereby not interfering with the lipid bilayer. Unlike liposomes, the small size of Nanodiscs allows for a wider range of lipid compositions to be probed without complications from aggregation.[9] The unique versatility of Nanodiscs has been proven through a variety of studies, including determination of membrane protein orientation,[10] dimer vs. monomer activity of rhodopsin,[6] and solid state NMR experiments.[11] A recent review describes the versatility and stability of Nanodiscs across an array of biochemical and biophysical characterization applications.[12]

Silicon photonic microring resonators have emerged as a promising, array-based detection technology that has been applied to a number of bioanalytical applications, including the

quantitation of protein[13–16] and nucleic acid[17,18] biomarkers. Notably, the technology has also been applied to the determination of kinetic and thermodynamic binding constants.[19–21] Microring resonators are chip-integrated waveguide structures that support optical resonances, and the wavelength of these resonances is sensitive to the local refractive index environment.[22] Previous proof-of-concept experiments demonstrated that binding interactions between solution phase proteins and Nanodiscs immobilized onto a microring array could be probed; however, the nature of these interactions was extremely simple.[23]

For this study we combined the versatility of Nanodiscs with highly-multiplexible silicon photonic microring resonators to study protein-lipid interactions involved in the blood coagulation cascade. Many of the key regulatory processes of both thrombosis and hemostasis are initiated through the successive action of a series of serine proteases that ultimately leads to the formation of a blood clot. Most of these enzymatic cleavage events occur at the membrane surface and are strongly influenced by the underlying lipid composition.[9,24,25] Of particular interest are the 7 GLA domain-containing coagulation proteins, which include prothrombin (PT), factor VII (fVII), factor X (fX), and activated protein C (aPC). These proteins reversibly bind membrane surfaces through their GLA domains, each rich in post translationally-modified γ-carboxyglutamate (GLA) residues and containing 7-9 divalent metal binding sites.[26–30] Ca^{2+} is absolutely required for proper folding and binding of the GLA domain to membrane surfaces.[27] Furthermore, it is well established that GLA domains bind anionic phosphatidylserine (PS) lipids but, despite structural similarities, the GLA domains of coagulation proteins have affinities for PS spanning three orders of magnitude.[31,32] Both aPC and fVIIa bind poorly to PS-containing membranes; however, these proteins have been shown to bind the lipid phosphatidic acid (PA) with much higher affinity.[33] This higher affinity also affects enzyme activity, with aPC and fVIIa having greater activity when interacting with membranes containing specific mixtures of PA and PS compared to membranes with PS alone.[33] It has also been demonstrated that other lipids, including phosphatidylethanolamine, phosphatidylglycerol, and phosphatidylinositol are able to effectively reduce the concentration of PS required to achieve maximal activity. This "Anything But Choline" (ABC) hypothesis postulates that any lipids not containing the bulky choline headgroup found on PC will synergize with PS and dramatically reduce the PS content required for maximal enzymatic activity.[24]

Past studies of coagulation protein-lipid binding using techniques like surface plasmon resonance (SPR)[9,24,33] have yielded important insights into the mechanisms of interaction; however, the relatively low throughput nature of the most common configuration of this technology (Biacore) presents practical limitations in terms of the number of both proteins and lipid compositions that can be evaluated in a reasonable amount of time. Additionally, in order to assess numerous conditions using SPR, multiple experimental runs – each consisting of the adsorption of lipids, experimentation, and regeneration of the surface – are required, increasing experimental variability and reagents used.

Herein, we demonstrate the utility of Nanodiscs and silicon photonic microring resonator technologies as a platform for the facile and thorough interrogation of protein-membrane interactions through the investigation of 28 different clotting protein-lipid interactions—4 clotting proteins, each at 7 different binary lipid combinations. Both the absolute values and relative trends of equilibrium binding constants were determined. We also find that the coagulation proteins investigated—fX, PT, fVIIa, and aPC—not only exhibit varying binding affinities for PS and PA, but also require differing proportions of these lipids to achieve maximal membrane binding. In addition to determining the dissociation equilibrium constant, K_d, we report the off-rate constants (k_{off}) for each of the 28 interactions probed. These studies demonstrate the powerful biochemical analysis combination of the silicon photonic microring detector platform coupled with Nanodiscs to rapidly interrogate binding interactions at model cell membrane interfaces.

2. Materials and Methods

Chemicals and reagents

Phosphatidylcholine (PC; 1-palmitoyl-2-oleoyl-sn-glycero-3-phosphocholine), phosphatidylserine (PS; 1-palmitoyl-2-oleoyl-sn-glycero-2-phosphoserine), and phosphatidic acid (PA; 1-palmitoyl-2-oleoyl-sn-glycero-3-phosphatidic acid) were purchased from Avanti Polar lipids (Alabaster, AL). MSP1D1 was expressed in *E. coli* and purified as described previously.[3] fX, PT, and aPC were purchased from Enzyme Research Laboratories (South Bend, IN). A non-clinical, recombinant human fVIIa produced in mammalian milk was generously provided by rEVO Biologics (Framingham, MA). Amberlite XAD-2 hydrophobic beads and all other chemicals were purchased from Sigma Aldrich (St. Louis, MO) and used as received, unless

otherwise noted. Buffers were prepared with 18.2 MΩ deionized water and sterile filtered prior to use.

Solution preparation

Nanodisc solutions were prepared in a TBS buffer (20 mM Tris-HCl, 100 mM NaCl, and 0.01% (w/v) NaN3, pH 7.4). Clotting protein solutions were made in TBS buffer with 2.5 mM CaCl2 added. All clotting protein solutions were prepared in a HEPES buffer (10 mM HEPES, 150 mM NaCl, 50 μM EDTA, 2.5 mM CaCl2, 0.1% (w/v) PEG 8000). Solutions of fVIIa and aPC also contained 0.2% (w/v) BSA, pH 7.4. The HEPES rinse buffer (HEPES(-)) for surface regeneration was made without CaCl2.

Nanodisc preparation and purification

Nanodisc preparation and purification has been described in detail previously.[3–5] Briefly, lipids solubilized in chloroform were measured into test tubes and dried under nitrogen. For Nanodiscs containing mixtures of POPS and POPC, or POPA and POPC, the lipids were mixed at appropriate ratios prior to drying. After drying, lipids were placed in a lyophilizer, under vacuum for 60-90 mins. Once completely dry, lipids were dissolved in TBS buffer with 100 mM deoxycholate to give a final ratio of 2:1 dexoycholate:phospholipids. Dissolved lipids were then combined with MSP1D1 in TBS to give a final ratio of 70:1 phospholipid:MSP. The solution of MSP and lipids was actively mixed at room temperature for approximately 1 hr. Half the volume of the MSP/lipid solution of Amberlite XAD-2 hydrophobic beads was added and then left to mix at room temperature for approximately 1.5 hr. Bio-beads were then removed by filtering through a 0.22 μm syringe filter. Nanodiscs were then purified using size exclusion chromatography. For studies of regeneration stability, Nanodiscs were made in an identical fashion but using the larger MSP1E3D1 construct.

Silicon photonic microring resonators

The Maverick M1 optical scanning instrumentation and microring resonator sensor chips were purchased from Genalyte, Inc. (San Diego, CA). The operation of the instrumentation has been previously described.[22] The sensor chips were each 4 mm X 6 mm sensor chips and contained 128, 30 μm diameter active sensor microrings grouped into sets of four, plus four temperature control

microrings and two dedicated to detecting leaks from the microfluidic gasket positioned atop the sensor chip during microring detection experiments.

Sensor chip array functionalization

Prior to use, sensor chips were cleaned with a freshly made piranha solution (3:1 H_2SO_4:30% HOOH) for 30 sec then rinsed with water and dried with N_2 (Caution! Piranha solution must be handled with extreme care and will react explosively with organics). The Bioforce Nano eNabler™ was then used to spot Nanodisc solutions onto individual clusters of 4 microrings. A spotting map showing the arrangement of the Nanodisc solutions on the sensor substrate is shown in **Figure III.1**. Nanodisc solutions containing unique lipid compositions and ranging in concentration from 0.5 to 10 µM. Nanodiscs containing greater percentages of negative charge were spotted at higher concentrations since their physisorption was less efficient due to electrostatic repulsion,[23] as the bare silicon microring surface also bears a negative charge. After spotting, chips were stored in a humidity chamber at 4°C for at least 4 hours before use. For array studies, Nanodiscs were spotted in buffer lacking Ca^{2+}; however, titrations were also performed using 50% PS and 50% PA Nanodiscs spotted in the presence of 2.5 mM Ca^{2+}. For unknown reasons, prothrombin was found to exhibit slightly higher K_d values for Nanodiscs spotted with Ca^{2+} (**Table III.1**), though similar differences in equilibrium dissociation constant were observed for PS- and PA-containing Nanodiscs.

Protein binding titrations

Laser cut Mylar gaskets that directed fluid flow across the chip were aligned onto the functionalized sensor chips, assembled into a Teflon cartridge, and loaded into the sensor scanner instrument. A 2% BSA in TBS buffer was first flowed across the chip surface at 10 µL/min to prevent nonspecific binding of proteins. For the PT and fX titrations in the K_d determination titrations, the proteins were flowed across the chip in increasing concentrations at 10 µL/min and the response allowed to equilibrate before the next solution injection. The same was done for fVIIa and aPC, but at a 5 µL/min flow rate. Following the series of increasing concentrations, all of the proteins were released from the surface by flowing HEPES(-) buffer solution. The titration was then repeated with the next protein. For the PT and fX titrations used to determine k_{off} rates, a given concentration of protein was flowed across the chip for 5 minutes at 10 µL/minute followed by a

10-minute rinse with HEPES buffer to observe dissociation, and then a 5 minute rinse in HEPES(-) to regenerate the surface. The next concentration of protein was then introduced, and the process repeated throughout the concentration series. All protein solutions were made in HEPES buffer. This protocol was subsequently repeated for the other three proteins. The same procedure was used for fVIIa and aPC k_{off} titrations, except with a flow rate of 5 μL/min and each rinse step was 15 min.

Data Analysis

Data analysis was performed using software provided by Genalyte, Inc. as well as custom scripts written in Origin 9.1. Sensor traces were corrected for temperature fluctuations and any residual non-specific binding by subtraction of response of 100% POPC Nanodiscs. Data fits for determining K_d were performed in Prism and fitting for k_{off} in Origin 9.1.

3. Results

In previous work,[23] a 4-channel microfluidic chamber was used to direct solutions of four Nanodiscs, each having different lipid composition, across different regions of a microring resonator substrate to create a 4-component sensing array. That method demonstrated that unique binding to each of the four distinct types of Nanodiscs could be monitored without cross reactivity, but fluidic immobilization did not facilitate higher throughput studies. In this study we used a microarrayer to create higher density arrays and use these arrays to probe biophysical interactions between blood coagulation proteins and Nanodiscs of variable lipid composition. Using physisorption as an immobilization method, seven different compositions of Nanodiscs were deposited onto clusters of four microrings using a Bioforce Nano eNabler™. The lipid compositions investigated included 100% PC, as well as binary combinations of PC and PS (10, 30, 50, and 70% PS, with the balance being PC) or PC and PA (30 and 50% PA, with the balance being PC). It is important to note that anionic lipid percentages higher than those naturally occurring are required because of the discrete size of Nanodiscs, which limit the spatial area over which lipids can be recruited into clusters by divalent cations and/or GLA domains. Because the Nanodiscs naturally physisorb to the silicon oxide surface, neither the surface nor the Nanodiscs were modified for attachment.

Arrays of these Nanodiscs with seven different lipid compositions were used to determine both the equilibrium dissociation constant, K_d, and kinetic dissociation rate, k_{off}, for interactions with four different proteins involved in the blood coagulation pathway: PT, fX, fVIIa, and aPC. **Figure III.2A** shows a representative K_d determination titration for PT. PT was flowed across the Nanodisc array at increasing concentrations and the shift in microring resonance wavelength monitored in real time. At each step, the binding response was allowed to equilibrate before introducing the next concentration. As PT does not specifically bind to PC lipids, the small response measured from the 100% PC Nanodisc-functionalized rings was subtracted to correct for non-specific protein adsorption. The real time resonance shift data, replotted as a function of PT concentration, is presented in **Figure III.2B**. Since all of the coagulation proteins studied bind in a Ca^{2+}-dependent manner, the Nanodisc array could be completely regenerated by simply flowing a Ca^{2+}-free buffer, followed by interrogation of subsequent coagulation protein/lipid interactions. In this way, identical titrations for fX, fVIIa, and aPC were performed and can be found in **Figure III.3-6**. To verify the ability to regenerate nanodiscs arrays for subsequent titrations and also to investigate the role of Ca^{2+} in the spotting buffer, an additional set of PT titrations was performed, as described under "Experimental procedures." The determined K_d values are shown in **Table III.2**. The regeneration studies verified consistent K_d values across multiple surface regenerations; however, the determined values from these measurements are slightly different from those measured for the multiplexed array. This discrepancy is attributed to completely different lots of reagents. The studies of Ca^{2+}-containing spotting buffers did reveal that PT had higher K_d values to nanodiscs spotted with Ca^{2+}. The reason for this difference is unknown and will be the subject of future studies.

To determine K_d values for each coagulation protein at each lipid composition, the concentration-dependent shifts in resonance wavelength were fit according to a single-site binding model using the following equation:

$$\Delta pm = B_{max}\left(\frac{[protein]}{K_d + [protein]}\right) \qquad \text{(III.1)}$$

where B_{max} is the maximum shift the protein is approaching and K_d is the equilibrium dissociation constant. **Figure III.7** shows K_d values determined for the binding of PT, fX, fVIIa, and aPC to the different Nanodisc compositions. These values are also tabulated in **Table III.2**. Overall,

binding increased (K_d decreased) as the %PS composition of the Nanodisc increased. At 10% PS, fX exhibited the lowest K_d, followed by PT, aPC, and fVIIa; these relative binding affinities are consistent with those observed previously.[24] At 30% PS, PT and fX (**Figure III.7A-B**, red bars) bound to the membrane surface with Kd values approximately an order of magnitude smaller than fVIIa or aPC (**Figure III.7C-D**, red bars); however, when the PS content was increased to 70%, all four proteins bound with similar K_d values of 140 – 440 nM (**Table III.2**). To investigate how the PS content affected the K_d, we evaluated the percentage change in K_d as a function of %PS. For both PT and fX, the largest percent change in K_d occurred between 10 – 30% PS (84% decrease). Conversely, fVIIa and aPC binding to Nanodiscs increased most significantly when the PS content was increased from 30% to 50% (80% and 75% decrease, respectively). fVIIa and aPC were previously demonstrated to be PA-binding proteins.[24] To confirm, we next evaluated the binding of PT, fX, fVIIa, and aPC to 30 and 50% PA-containing Nanodiscs (**Figure III.7**, green bars); as expected, fVIIa and aPC bound more tightly to PA than PS Nanodiscs exhibiting K_d values for binding to 50% PA Nanodiscs of 125 nM for fVIIa and 90 nM for aPC, compared to 600 and 1200 nM, respectively, to 50% PS.

In addition to determining equilibrium binding constants, the real-time analysis capabilities also permit interrogation of binding kinetics. Interactions between anionic lipids and the GLA domain are multivalent, making extraction of binding rate (k_{on}) difficult; however, an apparent unbinding rate (k_{off}) can be determined through a kinetic titration. To achieve this, a given concentration of a coagulation protein was flowed across the surface, and after reaching steady stage, a Ca^{2+}-containing buffer is flowed to watch the dissociation of the protein from the immobilized Nanodiscs. An entire representative titration for PT binding to variable lipid content Nanodiscs is shown in **Figure III.8-9**. For clarity, the overlaid binding and unbinding curves for PT interacting with 50% PS-containing Nanodiscs is shown in **Figure III.10**. The real-time dissociation was fit for each titration according to:

$$\Delta pm = A + Ae^{-k_{off}(t-t_0)} \tag{III.2}$$

where Δpm is the resonance shift as a function of time, A is a constant, t is time, and k_{off} is the dissociation off rate. This process was repeated for the other coagulation proteins again using a multiplexed Nanodisc composition array to simultaneously allow determination of multiple k_{off}

values for a particular coagulation protein. Full titrations for fX, fVIIa, and aPC, as well as overlaid binding and unbinding curves for each are presented in **Figures III.11-16**.

The resulting k_{off} values for each coagulation protein and lipid composition are shown graphically in **Figure III.17** and numerically in **Table III.3**. Like K_d, the overall trend showed a decrease in k_{off} as %PS increased, but the overall changes were much smaller (**Figure III.17**, red bars). As the %PS was increased from 10-70%, fVIIa saw the largest decrease (55%) and aPC saw the lowest (10%). PT and fX decreased 45 and 52% respectively. The k_{off} values of each protein were much closer than was seen for K_d values. At 50% PS the range of k_{off} values was 0.66—0.87 min-1 (**Table III.3**). Another interesting difference was that aPC had the lowest k_{off} at 10% PS while PT had the highest (0.64 and 1.36 min^{-1}, respectively). When analyzing the k_{off} values for PA containing Nanodiscs there was a decrease in k_{off} as %PA increased. Both fVIIa and aPC had the lower k_{off} values when comparing PA to PS containing Nanodiscs with k_{off} values of 50% PA Nanodiscs of 0.344 and 0.293 min-1 compared to 0.51 and 0.67 min-1 for 50% PS respectively (**Table III.3**).

4. Discussion

PT, fX, fVIIa, and aPC bind to the membrane surface through their GLA domains.[24,25] Each of the proteins' GLA domains are homologous and have multiple, specific binding sites for PS head groups; however, PS is not the only lipid that can affect clotting protein binding and activation. Other lipids have been shown to synergize with PS to reduce the amount of PS lipids needed for full activation of fVIIa and fX.[24] One such lipid is PA and its effects on fVIIa and aPC binding are especially clear from the presented microring resonator array results. Both of these coagulation proteins bind with lower K_d to PA lipid-presenting Nanodiscs, compared to those with equivalent amounts of PS. They also show tighter binding as the amount of PA is increased.

Examining K_d values reveals several interesting trends in protein binding as a function of lipid composition. As expected from previous studies,[9,33] the K_d had an inverse relationship with PS and PA concentration. That is, coagulation protein binding was generally tighter (smaller K_d) with greater amounts of anionic lipid in the Nanodiscs. The fact that all of the proteins bound more tightly as PS content increased is consistent with the literature.[9]

A considerable advantage to using microring resonator technology is the direct comparison of different proteins binding to the same Nanodisc-modified sensor array. This unprecedented continuity across multiple experiments allows for a more confident analysis of results. Though our results largely support those found previously, the ability to directly compare across proteins allows for a deeper interpretation. One such insight comes from the finding that at high %PS, binding affinities for the coagulation proteins tested converge, with fVIIa and aPC binding significantly better than at high percent PS. Interestingly, PS has been shown to undergo calcium-induced clustering in vitro,[11] and thus the presence of PS-rich nanodomains within the lipid bilayer may act to recruit fVIIa and aPC to PA-deficient membrane surfaces under certain conditions.

PT, fX, fVIIa, and aPC bind to the membrane surface through their GLA domains.[24,25] Each of the proteins' GLA domains are homologous and have multiple, specific binding sites for PS head groups, but PS is not the only lipid that can affect clotting protein binding and activation. Other lipids have been shown to synergize with PS to reduce the amount of PS lipids needed for full activation of fVIIa and fX.[24] One such lipid is PA and its effects on fVIIa and aPC binding are especially clear from the presented microring resonator array results. Both of these coagulation proteins bind with lower K_ds to PA lipid-presenting Nanodiscs, compared to those with equivalent amounts of PS. They also show tighter binding as the amount of PA is increased.

It is worth pointing out that the increased binding affinity does not strictly lead to a larger magnitude of observed resonance shift due to variable amount of specific Nanodisc loaded onto the surface. As we showed previously,[23] the charge of lipids within Nanodiscs plays a large role in determining the relative amount of physisorption, with Nanodiscs with higher percentages of negatively charged lipids (PS and PA) having reduced loading due to electrostatic repulsion with the natively negatively charges SiO_x surface of the microring . This accounts for a reduced magnitude of resonance shift. However, K_d values mathematically-determined from fitting of the data to the single-site binding model do reflect the expected trends as a function of lipid composition. In general, K_d values obtained using the silicon photonic microring resonator platform are lower than those generally obtained using SPR;[33] however, the trends as a function of lipid composition are identical. Furthermore, the internal consistency of these simultaneously performed measurements provides further confidence in the resulting trends.

Importantly, by using the Nanodisc-functionalized microring sensor array, a single experiment yielded internally consistent K_d values for six distinct interactions per coagulation protein. This is in contrast to lower throughput methods that would require many more measurements across multiple sensor substrates and multiple days of experimentation to obtain this amount of binding interaction data, a laborious process that introduces experimental uncertainties and is prone to run-to-run variation.

Similar to K_d values, k_{off} values also show trends related to the anionic lipid content in Nanodiscs. Specifically, the rate of unbinding is lower as the amount of PS or PA is increased, which is consistent with the measured lower K_d values (tighter binding). For fVIIa and aPC the k_{off} values are also proportionally lower for PA-containing discs, compared to equivalent amounts of PC. Notably, the variation within k_{off} alone is not enough to fully explain differences in K_d, suggesting that there must also be corresponding differences in the kinetic rate of binding, k_{on} (K_d =k_{on}/ k_{off}) for different protein-lipid combinations. However, as mentioned earlier, direct measurement of k_{on} is difficult due to the multivalent nature of the GLA domain interaction (6-8 lipids bound/GLA domain[24]), and likely need for lipid rearrangement during binding of GLA domains (leading to complicated binding kinetics). However, the coupled K_d and k_{off} values obtained using this technology platform provide confidence in inferring variations in k_{on}.

5. Conclusion

The interactions of clotting proteins with cell membrane lipids are critical to the blood coagulation cascade as well as many other biological processes. Previous work studying protein-lipid interactions has been relatively low throughput, so only a limited number of proteins or lipid compositions are examined. This paper introduces a multiplexed technique where interactions with many different lipid compositions can be monitored simultaneously in real time. Because Nanodiscs were spotted and allowed to physisorb to the surface of the chip, no tags were required to monitor binding. Here, the binding constants of four coagulation proteins (PT, fX, fVIIa, and aPC) binding to Nanodiscs of six different lipid compositions were determined. While absolute K_d values were lower than those reported by SPR, qualitative trends in terms of binding as a function of anionic lipid content was consistent. The benefits of utilizing both Nanodiscs and microring resonator technologies for probing protein-membrane interactions are numerous. Unlike

liposomes, the local (nanoscale) lipid composition of Nanodiscs can be precisely controlled due to their small size, making them an ideal substrate on which to study these interactions. The simultaneous interrogation of numerous binding interactions from a single measurement using the photonic microring resonators increases intra-assay precision and eliminates experimental variability. Additionally, due to its multiplexed nature, utilization of microring resonators decreases the consumption of precious reagents and reduces instrument time compared to traditional techniques such as Biacore. Finally, the ability to evaluate the binding of numerous proteins to the same lipid surface eliminates inherent differences in substrate (i.e., Nanodisc) loading and the associated run-to-run variability.

In the future, this technique can be applied to further examine the effect of different lipids on the binding of clotting proteins to membranes, as well as ternary and quaternary lipid mixtures. Previous work has shown that combinations of lipids with PS have led to synergistic binding and activation for fVIIa and aPC.[9,33] Similar binding studies of other clotting proteins containing GLA domains could be obtained in a high throughput manner using the silicon photonic microring resonator platform in combination with multiplex Nanodiscs.

6. Acknowledgements

Dr. Ellen Muehl and Dr. Josh Gajsiewicz conceived the experimental design and ran most of the experiments. My contribution in the research corresponds to studies relating to the concentration of ions for stable array formation. I also contributed to minor changes from observations of reviewers.
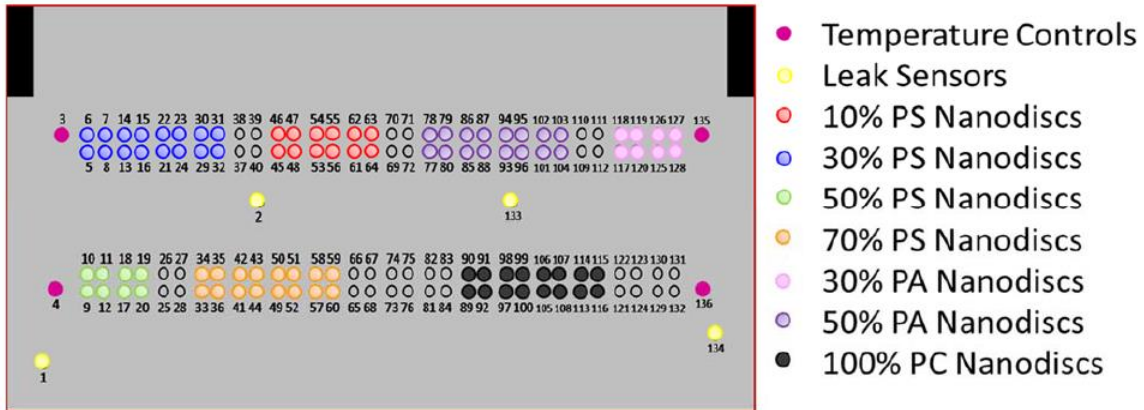
Figure III.1. Sensor Chip Layout. The layout of the sensor chip used to run the protein titrations. The bright pink rings are the temperature control rings, yellow rings are the leak sensors, red rings are spotted with 10% PS Nanodiscs, blue rings are spotted with 30% PS Nanodiscs, green rings are spotted with 50% PS rings, orange rings are spotted with 70% PS Nanodiscs, light pink rings are spotted with 30% PA Nanodiscs, purple rings are spotted with 50% PA Nanodiscs, and black rings are spotted with 100% PC Nanodiscs.
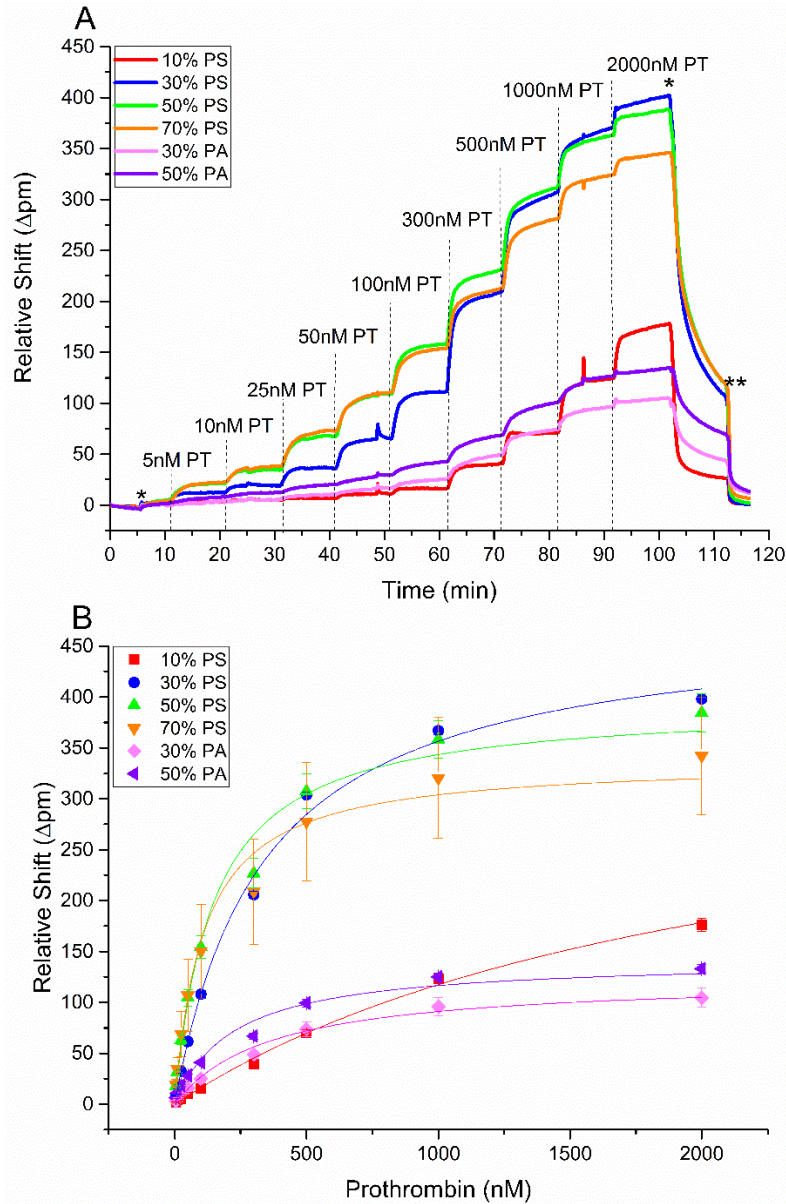
Figure III.2. Prothrombin Titration. (**A**) Real time shifts in resonance wavelength during PT K_d titration at different Nanodisc compositions. The dashed lines indicate the addition of a new concentration of protein of interest, the *marks the transition to HEPES buffer, and ** marks the transition to HEPES(-). Minimal binding to the 100% PC microrings were subtracted from the other responses to account for non-specific binding. The different concentrations of PT (ranging from 50-2000 nM) flowed across the sensor array ad different times is indicated. (**B**) Plots of relative wavelength shift as a function of PT concentration. In each panel, error bars represent the standard deviation from at least n = 8 microrings in a single detection experiment.

99
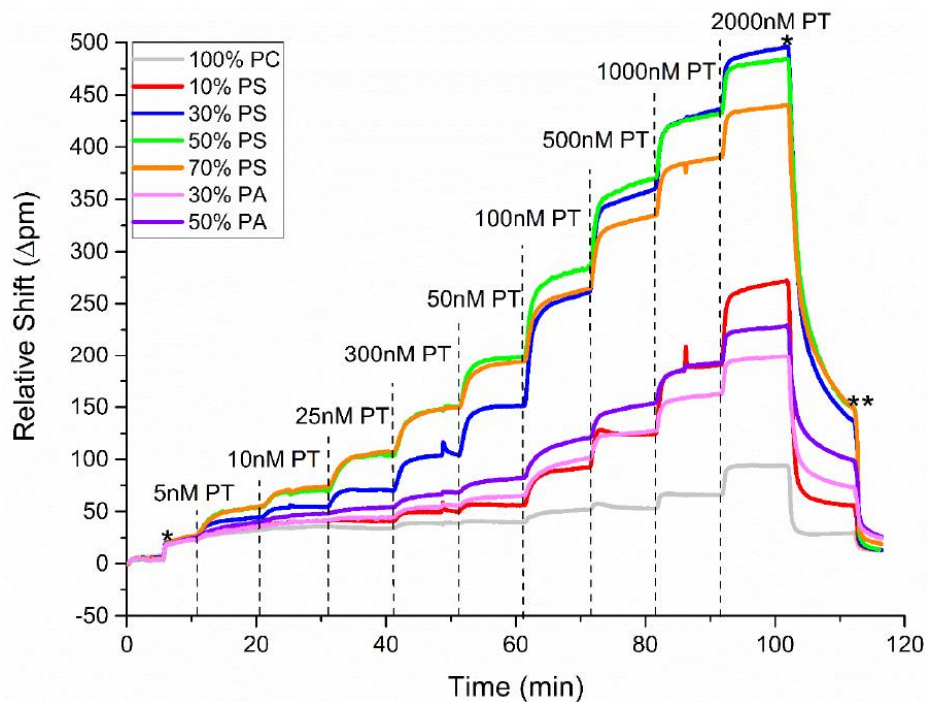
Figure III.3. Concentration-dependent prothrombin (PT) binding as a function of lipid proportions. The PT binding response during a typical titration, flowed at 10 μL/min. PT concentrations at each step are indicated, as are Nanodisc compositions. At each step, the binding is allowed to reach steady state.
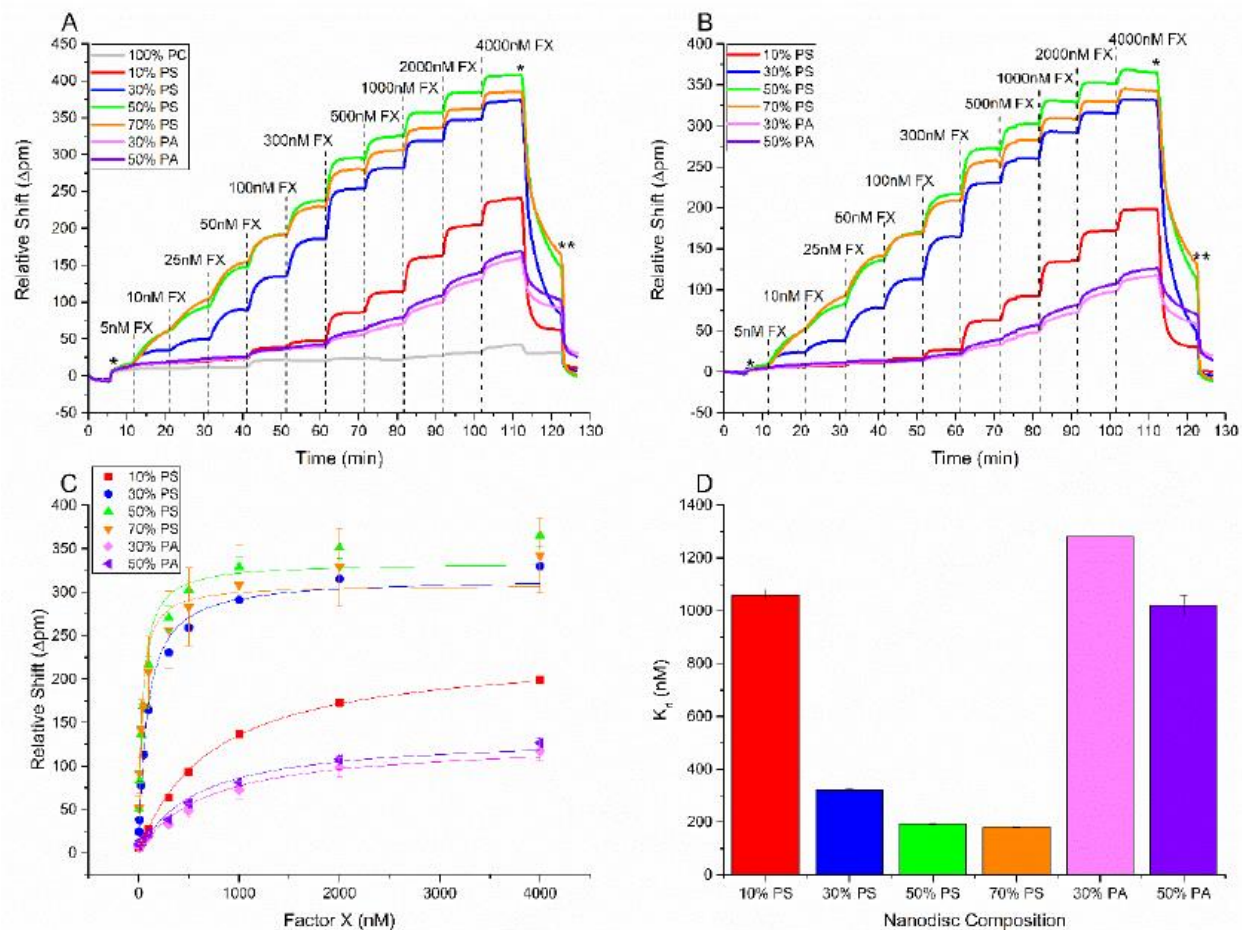
Figure III.4. K_d determination for factor X (fX). To determine the K_d of factor X (fX) binding to Nanodiscs of various lipid composition, a single chip was spotted with the Nanodiscs with lipids 10% PS, 30% PS, 50% PS, 70% PS, 30% PA, 50%PA, and as a control 100% PC (the balance of PS and PA lipid Nanodiscs was made up of PC lipids). In (**A**) and (**B**) the dashed lines indicate the addition of a new concentration of protein of interest, the *marks the transition to HEPES buffer, and ** marks the transition to HEPES(-). (**A**) The fX binding response during a typical titration, flowed at 10 μL/min. At each step, the binding is allowed to reach steady state. (**B**) The fX titration controlled for the 100% PC control rings. (**C**) Plot of the max pm shift of fX binding at each of the concentration steps. The plots of fX-Nanodisc binding were fit according to **Equation III.1**. (**D**) The K_d values determined for fX binding to each type of Nanodiscs. K_d of fX binding to PS-containing Nanodiscs are shown in red and PA-containing Nanodiscs in green.

101
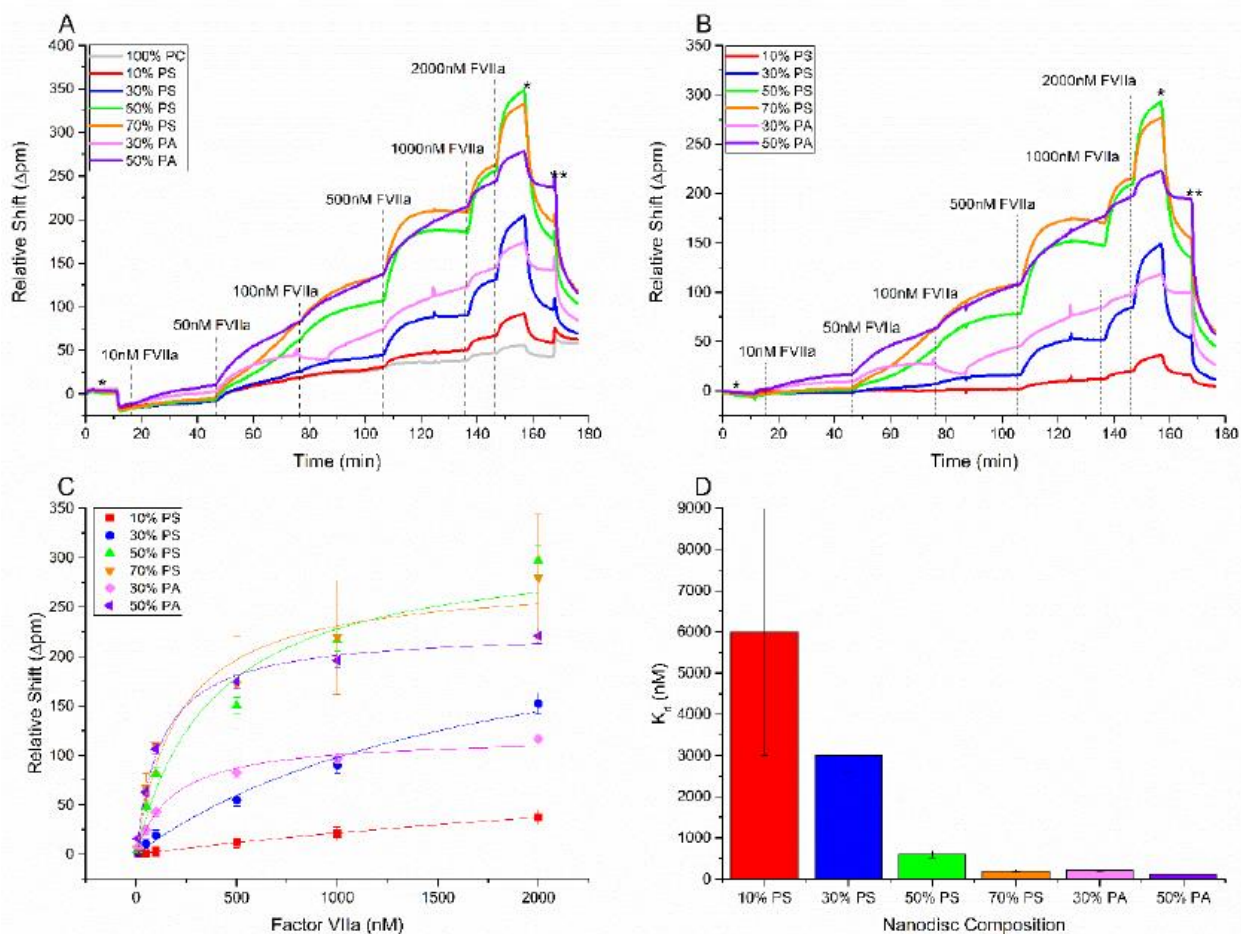
Figure III.5. K_d determination for factor VIIa (fVIIa). To determine the K_d of factor VIIa (fVIIa) binding to Nanodiscs of various lipid composition, a single chip was spotted with the Nanodiscs with lipids 10% PS, 30% PS, 50% PS, 70% PS, 30% PA, 50%PA, and as a control 100% PC (the balance of PS and PA lipid Nanodiscs was made up of PC lipids). In (**A**) and (**B**) the dashed lines indicate the addition of a new concentration of protein of interest, the *marks the transition to HEPES buffer, and ** marks the transition to HEPES(-). (**A**) The fVIIa binding response during a typical titration, flowed at 5 μL/min. At each step, the binding is allowed to reach steady state. (**B**) The fVIIa titration controlled for the 100% PC control rings. (**C**) Plot of the max pm shift of fVIIa binding at each of the concentration steps. The plots of fVIIa-Nanodisc binding were fit according to **Equation III.1**. (**D**) The K_d values determined for fVIIa binding to each type of Nanodiscs. K_d of fVIIa binding to PS-containing Nanodiscs are shown in red and PA-containing Nanodiscs in green.
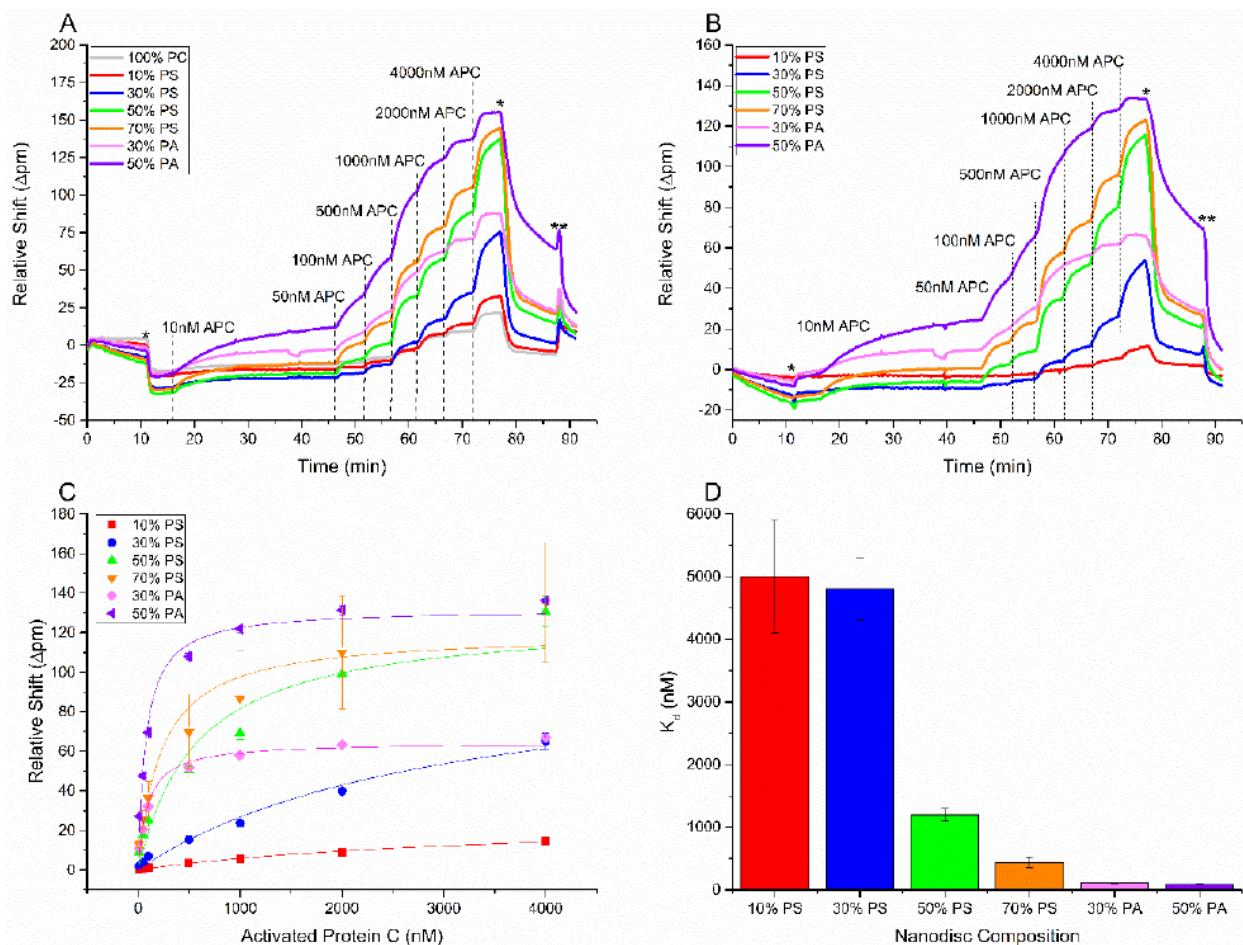
Figure III.6. *K_d* determination for activated protein C (aPC). To determine the K_d of activated protein C (aPC) binding to Nanodiscs of various lipid composition, a single chip was spotted with the Nanodiscs with lipids 10% PS, 30% PS, 50% PS, 70% PS, 30% PA, 50%PA, and as a control 100% PC (the balance of PS and PA lipid Nanodiscs was made up of PC lipids). In (**A**) and (**B**) the dashed lines indicate the addition of a new concentration of protein of interest, the *marks the transition to HEPES buffer, and ** marks the transition to HEPES(-). (**A**) The aPC binding response during a typical titration, flowed at 5 μL/min. At each step, the binding is allowed to reach steady state. (**B**) The aPC titration controlled for the 100% PC control rings. (**C**) Plot of the max pm shift of aPC binding at each of the concentration steps. The plots of aPC-Nanodisc binding were fit according to **Equation III.1**. (**D**) The K_d values determined for aPC binding to each type of Nanodiscs. K_d of aPC binding to PS-containing Nanodiscs are shown in red and PA-containing Nanodiscs in green.

103
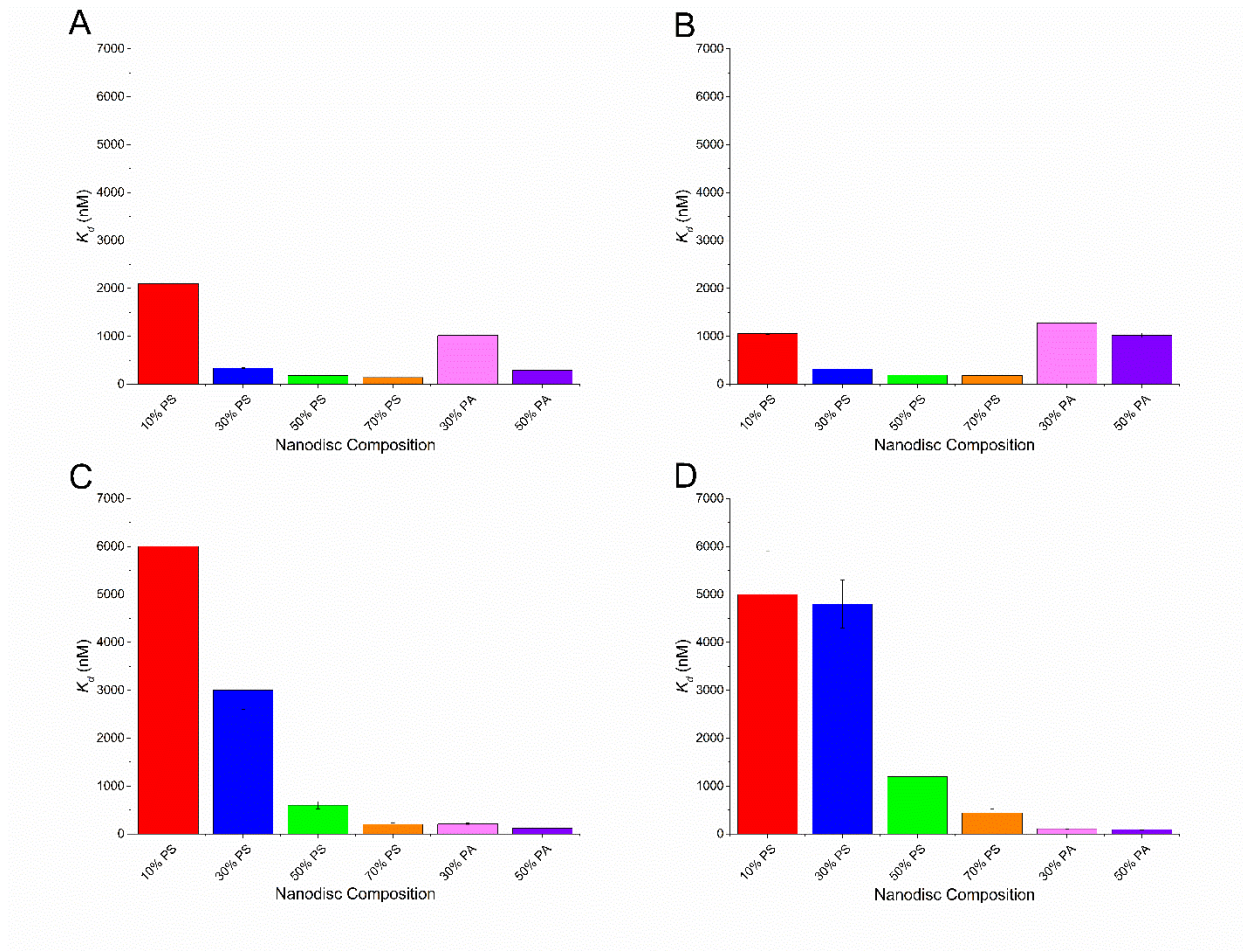
Figure III.7. K_d values in nM of (**A**) PT (**B**) fX (**C**) fVIIa (**D**) aPC binding to variable lipid content Nanodiscs, as indicated. Each was determined by plotting relative shift of binding vs. concentration of protein and fitting to **Equation III.1**. Error bars represent the standard deviation from at least n = 8 microrings in a single detection experiment.

104
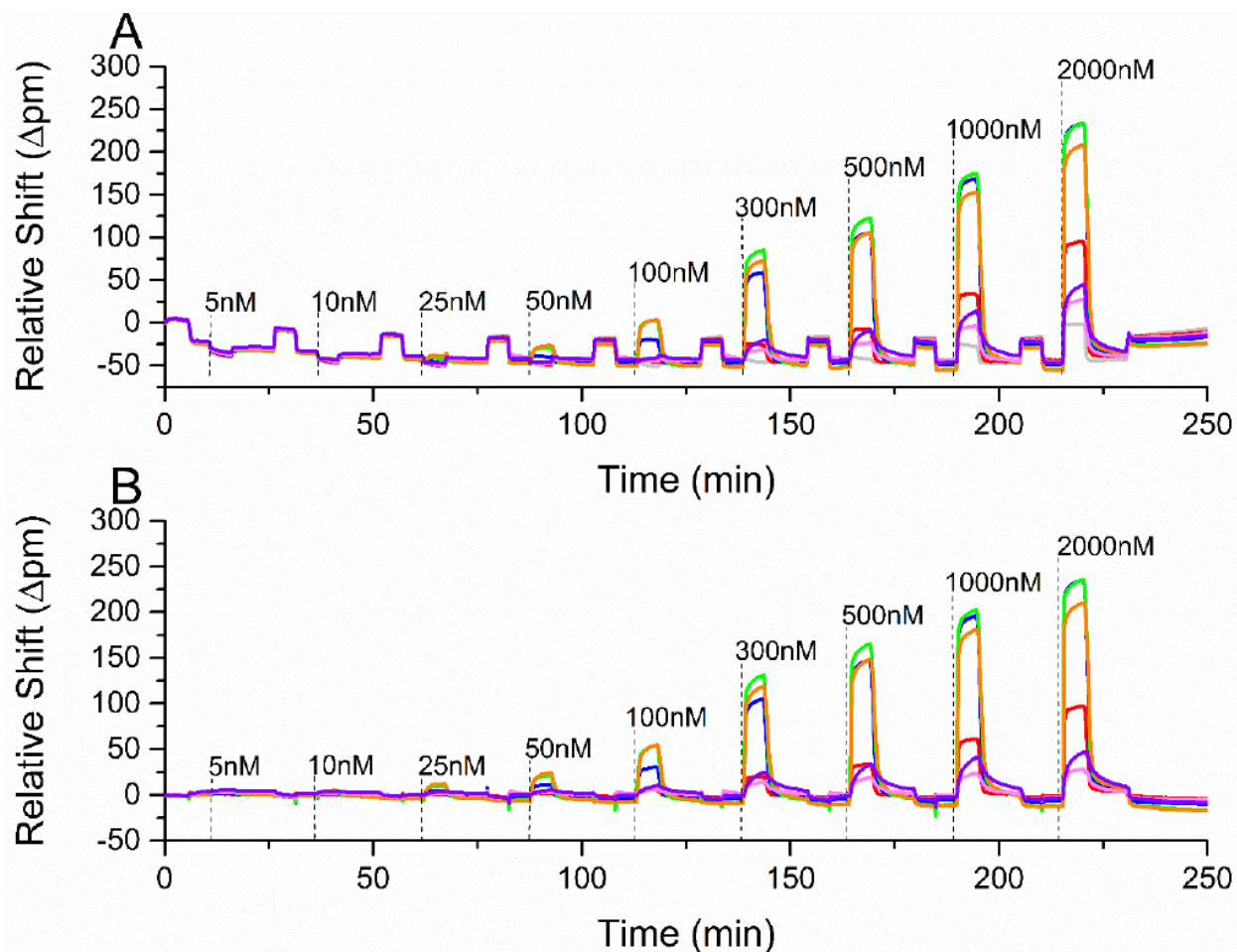
Figure III.8. Association and dissociation responses for PT as a function of lipid proportions. (**A**) PT binding and falloff titration, flowed at 10 µL/min. Each dashed line indicated when PT was flowed across the surface. Each binding step was run for 5 min and after, the HEPES buffer was flowed across the chip surface for 10 min and was then followed by a 5 min HEPES(-) rinse to remove any excess protein bound. The grey line represents PT binding to 100% PC Nanodisc, orange is PT binding to 70% PS Nanodiscs, green is PT binding to 50% PS Nanodiscs, blue is PT binding to 30% PS Nanodiscs, red is PT binding to 10% PS Nanodiscs, pink is PT binding to 30% PA Nanodiscs, and violet is PT binding to 50% PA Nanodiscs. (**B**) PT binding and falloff titration controlled for non-specific binding by subtraction of 100% PC Nanodisc binding curves.
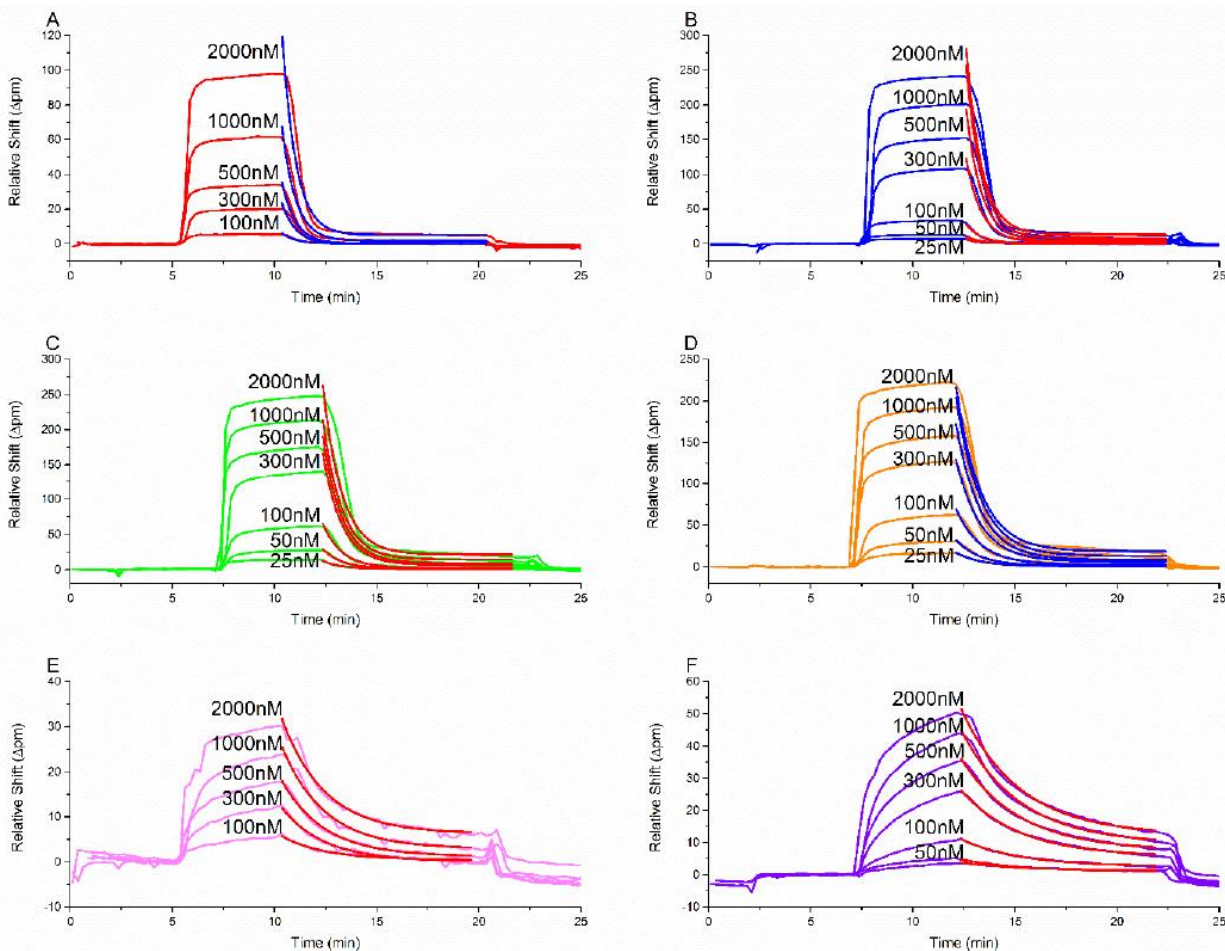
Figure III.9. k_{off} determination for PT. After collecting the results from the binding and falloff titrations, the binding and falloff curves for each type of Nanodisc were stacked. The falloff curves were then globally fit using **Equation III.2**, the red curves are the fits (except for PT-10% PS binding where the fit is shown in blue) (**A**) PT-10% PS Nanodisc binding and falloff (**B**) PT-30% PS Nanodisc binding and falloff (**C**) PT-50% PS Nanodisc binding and falloff (**D**) PT-70% PS Nanodisc binding and falloff (**E**) PT-30% PA Nanodisc binding and falloff (**F**) PT-50% PA Nanodisc binding and falloff.
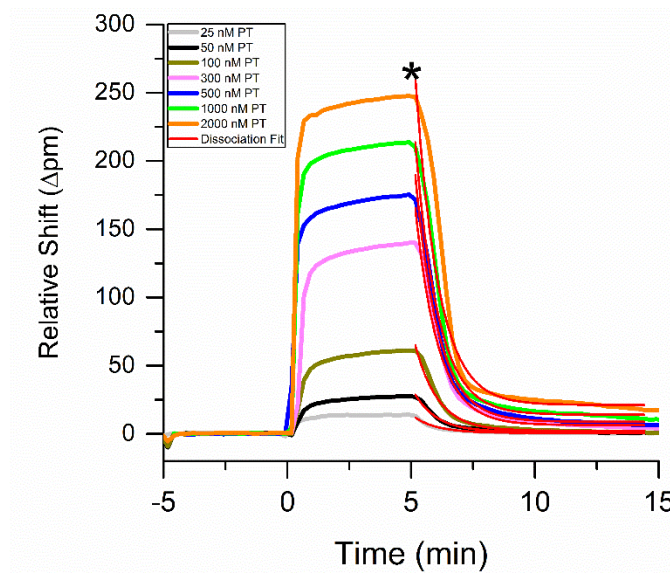
Figure III.10. Real-time resonance shifts measured during the binding and unbinding of PT to Nanodiscs with a lipid composition of 50% PS 50% PC. After achieving a stable baseline in buffer, PT was introduced at varying conditions at t = 0. After 5 min, the solution was changed to HEPES buffer (*) and dissociation was observed. The red traces are fits to the dissociation phase obtained by globally fitting all concentrations using **Equation III.2**.
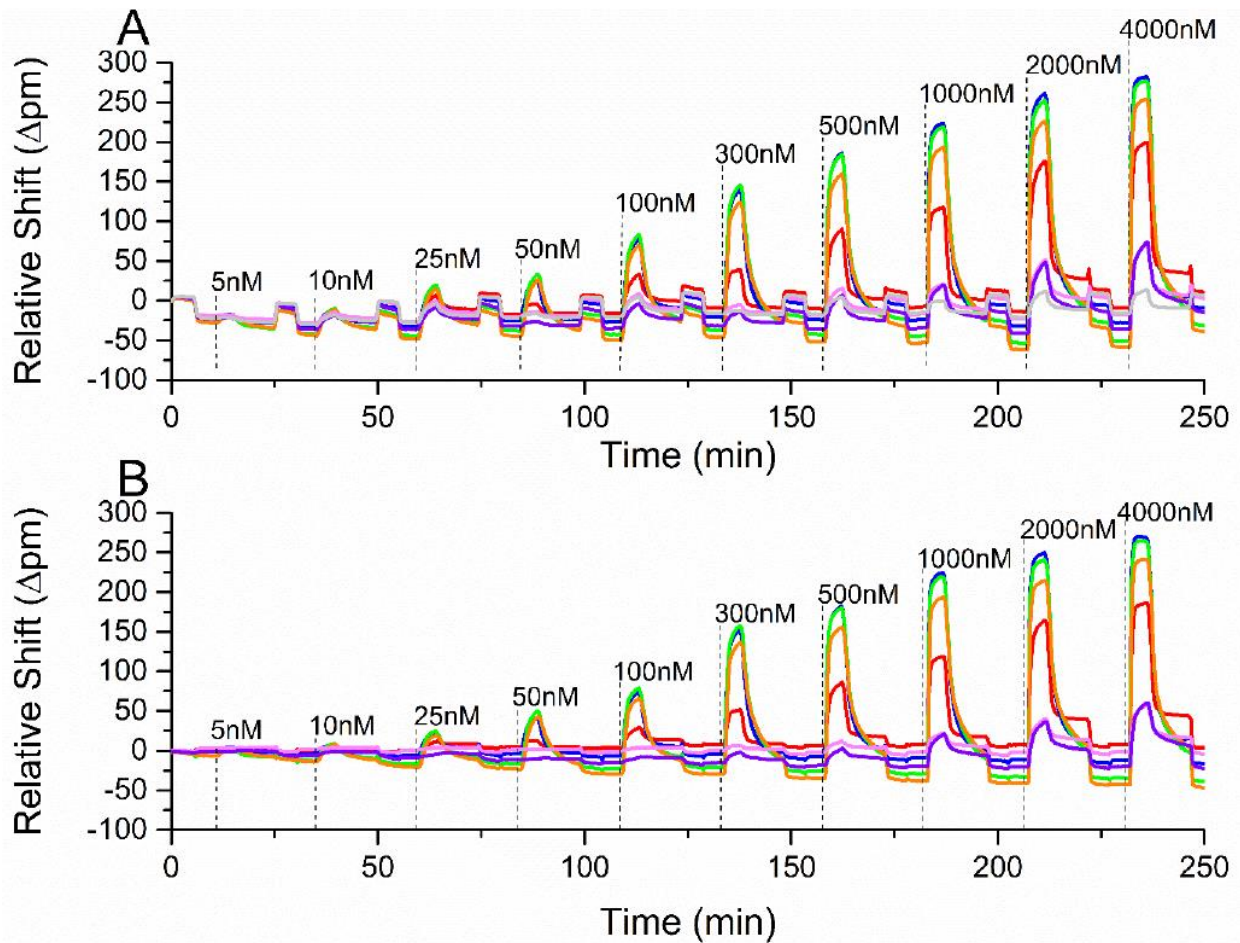
Figure III.11 Association and dissociation responses for fX as a function of lipid proportions.
(**A**) fX binding and falloff titration, flowed at 10 μL/min. Each dashed line indicated when fX was flowed across the surface. Each binding step was run for 5 min and after, the HEPES buffer was flowed across the chip surface for 10 min and was then followed by a 5 min HEPES(-) rinse to remove any excess protein bound. The grey line represents fX binding to 100% PC Nanodisc, orange is fX binding to 70% PS Nanodiscs, green is fX binding to 50% PS Nanodiscs, blue is fX binding to 30% PS Nanodiscs, red is fX binding to 10% PS Nanodiscs, pink is fX binding to 30% PA Nanodiscs, and violet is fX binding to 50% PA Nanodiscs. (**B**) fX binding and falloff titration controlled for non-specific binding by subtraction of 100% PC Nanodisc binding curves.
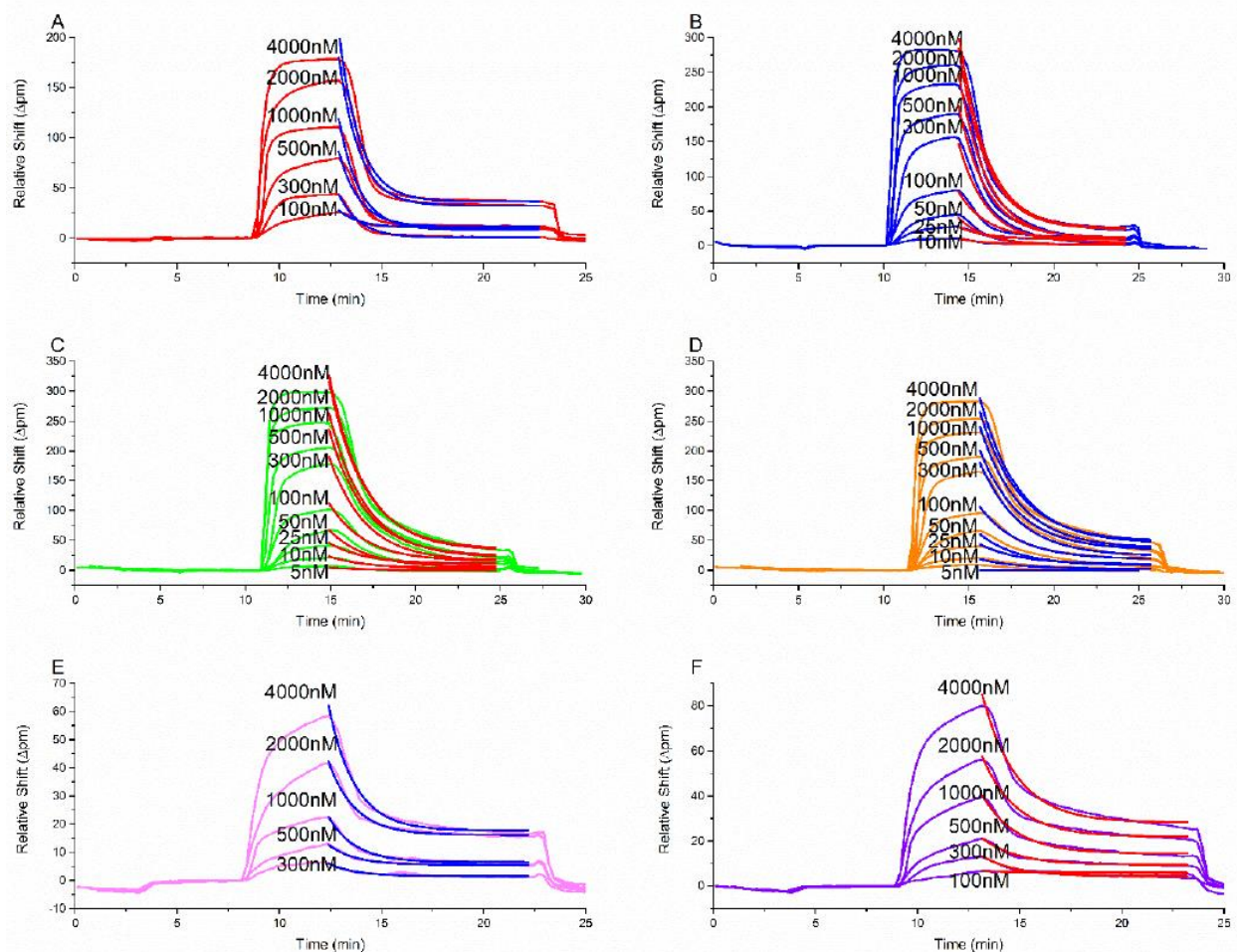
Figure III.12. *k_{off}* **determination for fX.** After collecting the results from the binding and falloff titrations, the binding and falloff curves for each type of Nanodisc were stacked. The falloff curves were then globally fit using **Equation III.2**, the red curves are the fits (except for fX-10% PS binding where the fit is shown in blue) (**A**) fX-10% PS Nanodisc binding and falloff (**B**) fX-30% PS Nanodisc binding and falloff (**C**) fX-50% PS Nanodisc binding and falloff (**D**) fX-70% PS Nanodisc binding and falloff (**E**) fX-30% PA Nanodisc binding and falloff (**F**) fX-50% PA Nanodisc binding and falloff.
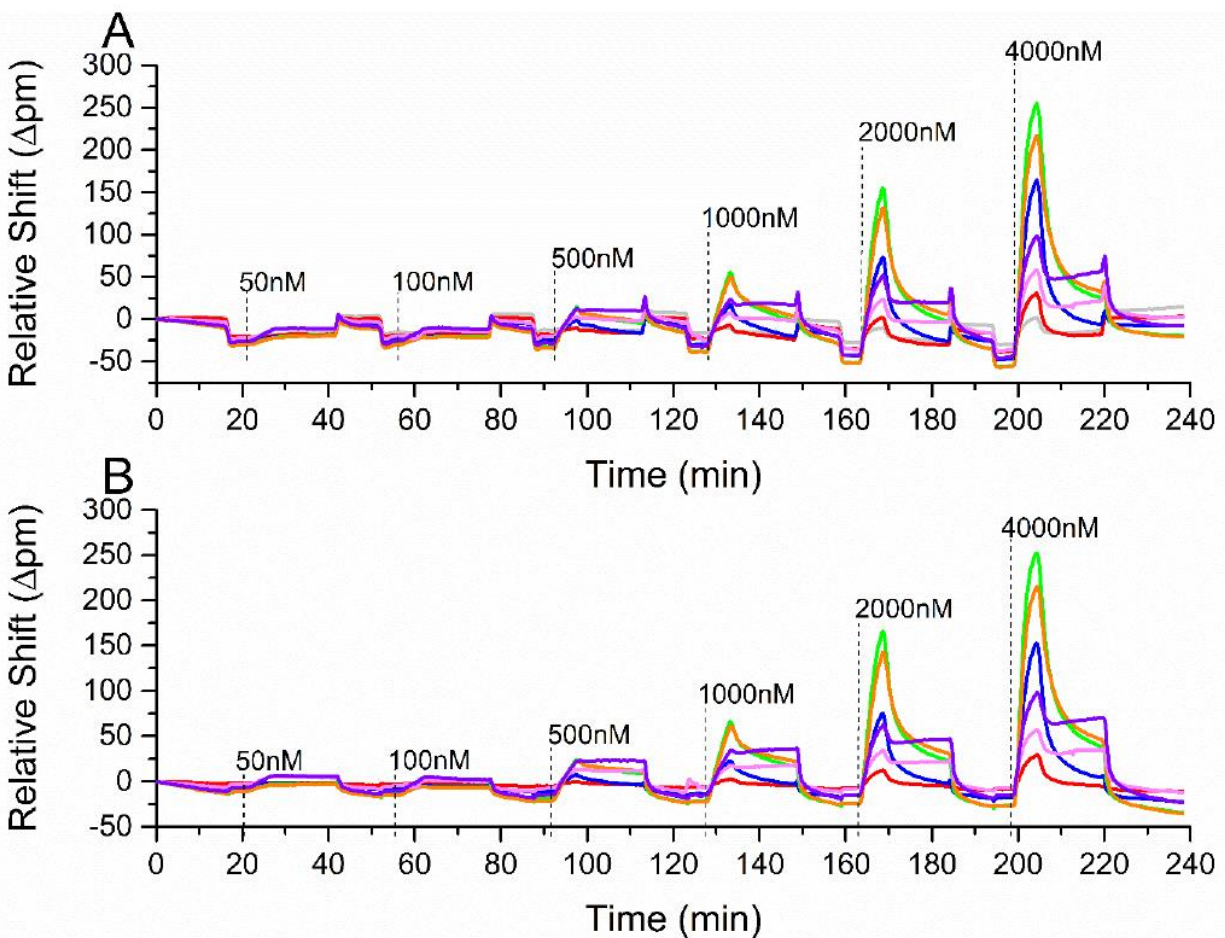
Figure III.13. Association and dissociation responses for fVIIa as a function of lipid proportions. (**A**) fVIIa binding and falloff titration, flowed at 5 μL/min. Each dashed line indicated when fVIIa was flowed across the surface. Each binding step was run for 5 min and after, the HEPES buffer was flowed across the chip surface for 15 min and was then followed by a 5 min HEPES(-) rinse to remove any excess protein bound. The grey line represents fVIIa binding to 100% PC Nanodisc, orange is fVIIa binding to 70% PS Nanodiscs, green is fVIIa binding to 50% PS Nanodiscs, blue is fVIIa binding to 30% PS Nanodiscs, red is fVIIa binding to 10% PS Nanodiscs, pink is fVIIa binding to 30% PA Nanodiscs, and violet is fVIIa binding to 50% PA Nanodiscs. (**B**) fVIIa binding and falloff titration controlled for nonspecific binding by subtraction of 100% PC Nanodisc binding curves.
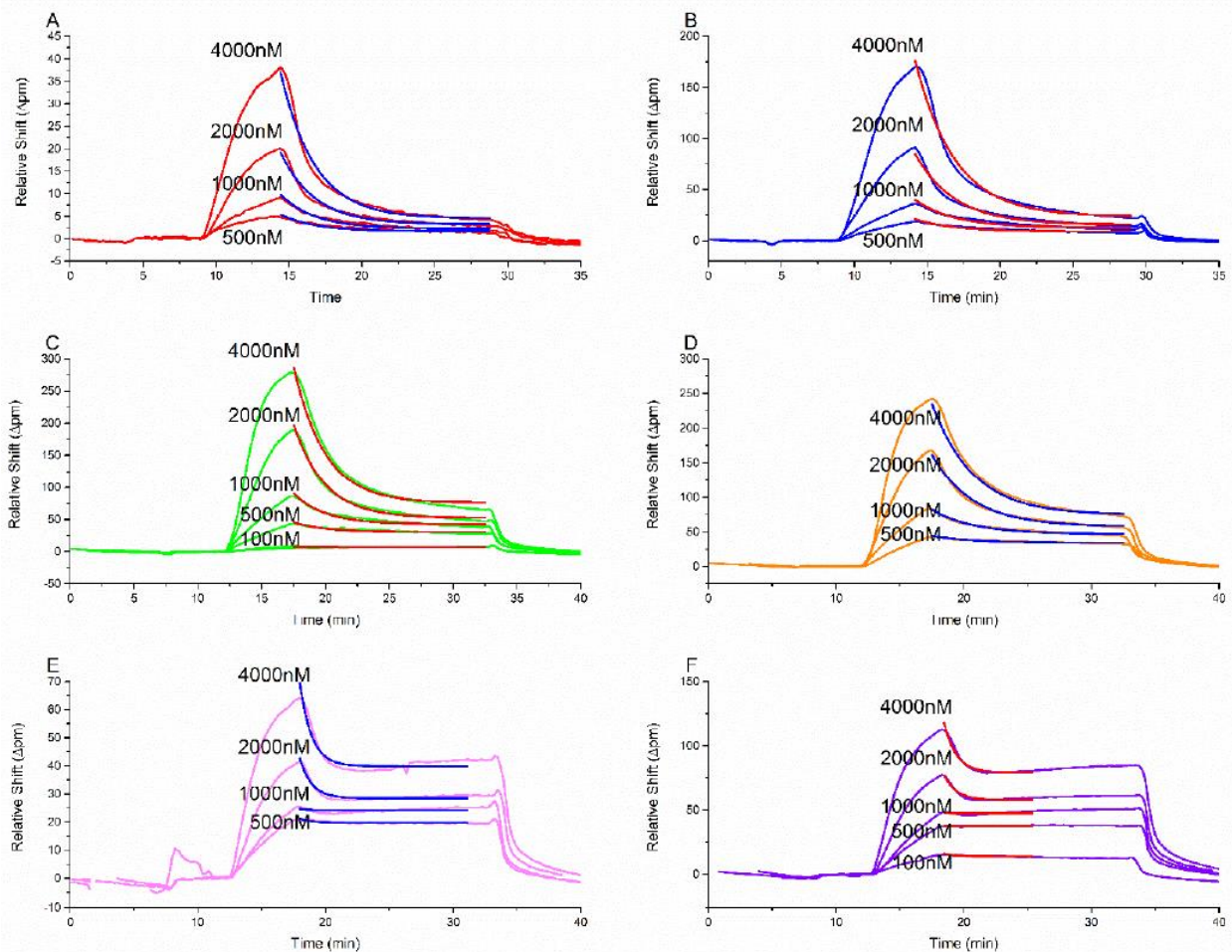
Figure III.14. k_{off} **determination for fVIIa.** After collecting the results from the binding and falloff titrations, the binding and falloff curves for each type of Nanodisc were stacked. The falloff curves were then globally fit using **Equation III.2**, the red curves are the fits (except for fVIIa-10% PS binding where the fit is shown in blue) (**A**) fVIIa-10% PS Nanodisc binding and falloff (**B**) fVIIa-30% PS Nanodisc binding and falloff (**C**) fVIIa-50% PS Nanodisc binding and falloff (**D**) fVIIa-70% PS Nanodisc binding and falloff (**E**) fVIIa-30% PA Nanodisc binding and falloff (**F**) fVIIa-50% PA Nanodisc binding and falloff.
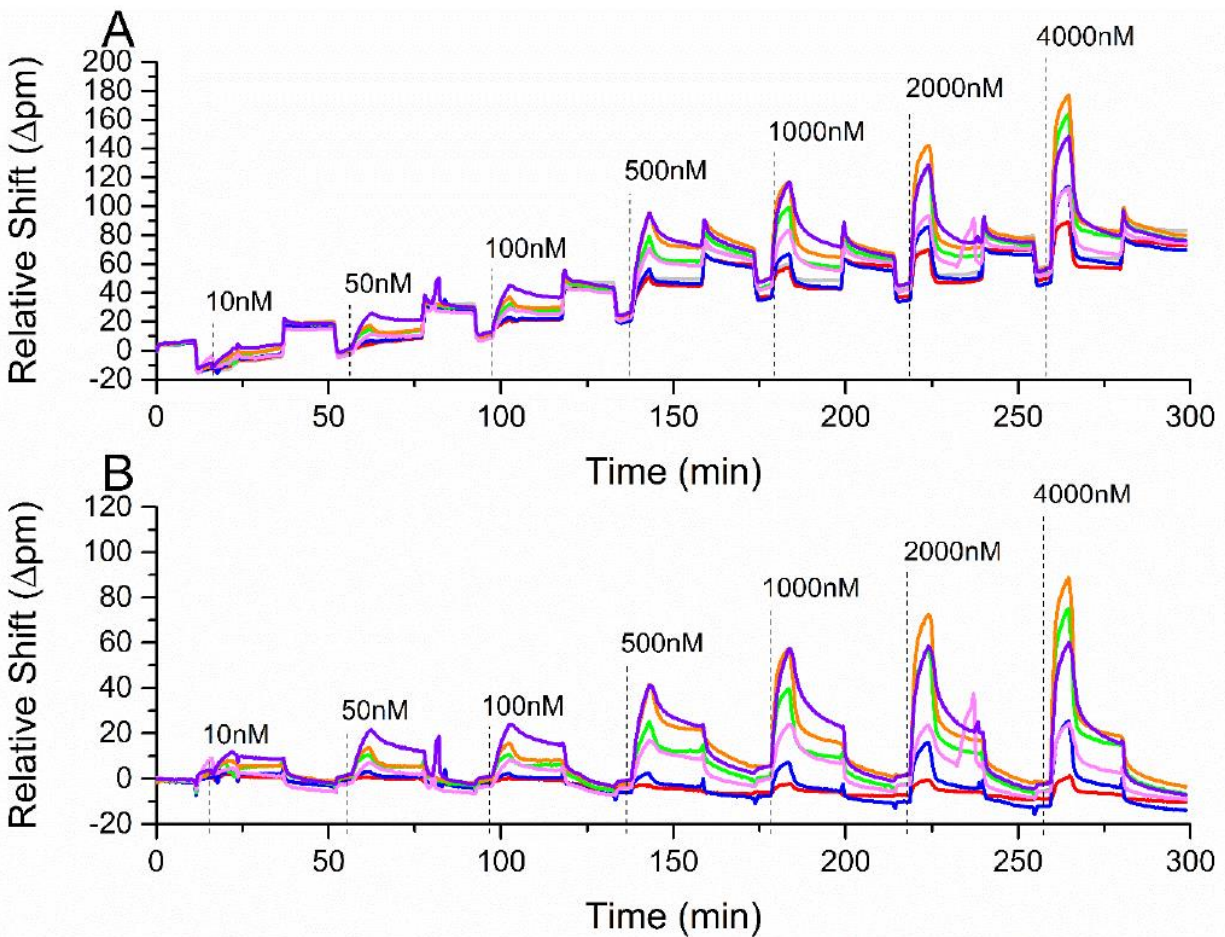
Figure III.15. Association and dissociation responses for aPC as a function of lipid proportions. (A) aPC binding and falloff titration, flowed at 5 μL/min. Each dashed line indicated when aPC was flowed across the surface. After a 5 min binding step, the HEPES buffer was flowed across the chip surface for 15 min and was then followed by a 5 min HEPES(-) rinse to remove any excess protein bound. The grey line represents aPC binding to 100% PC Nanodisc, orange is aPC binding to 70% PS Nanodiscs, green is aPC binding to 50% PS Nanodiscs, blue is aPC binding to 30% PS Nanodiscs, red is aPC binding to 10% PS Nanodiscs, pink is aPC binding to 30% PA Nanodiscs, and violet is aPC binding to 50% PA Nanodiscs. (B) aPC binding and falloff titration controlled for non-specific binding by subtraction of 100% PC Nanodisc binding curves.

112
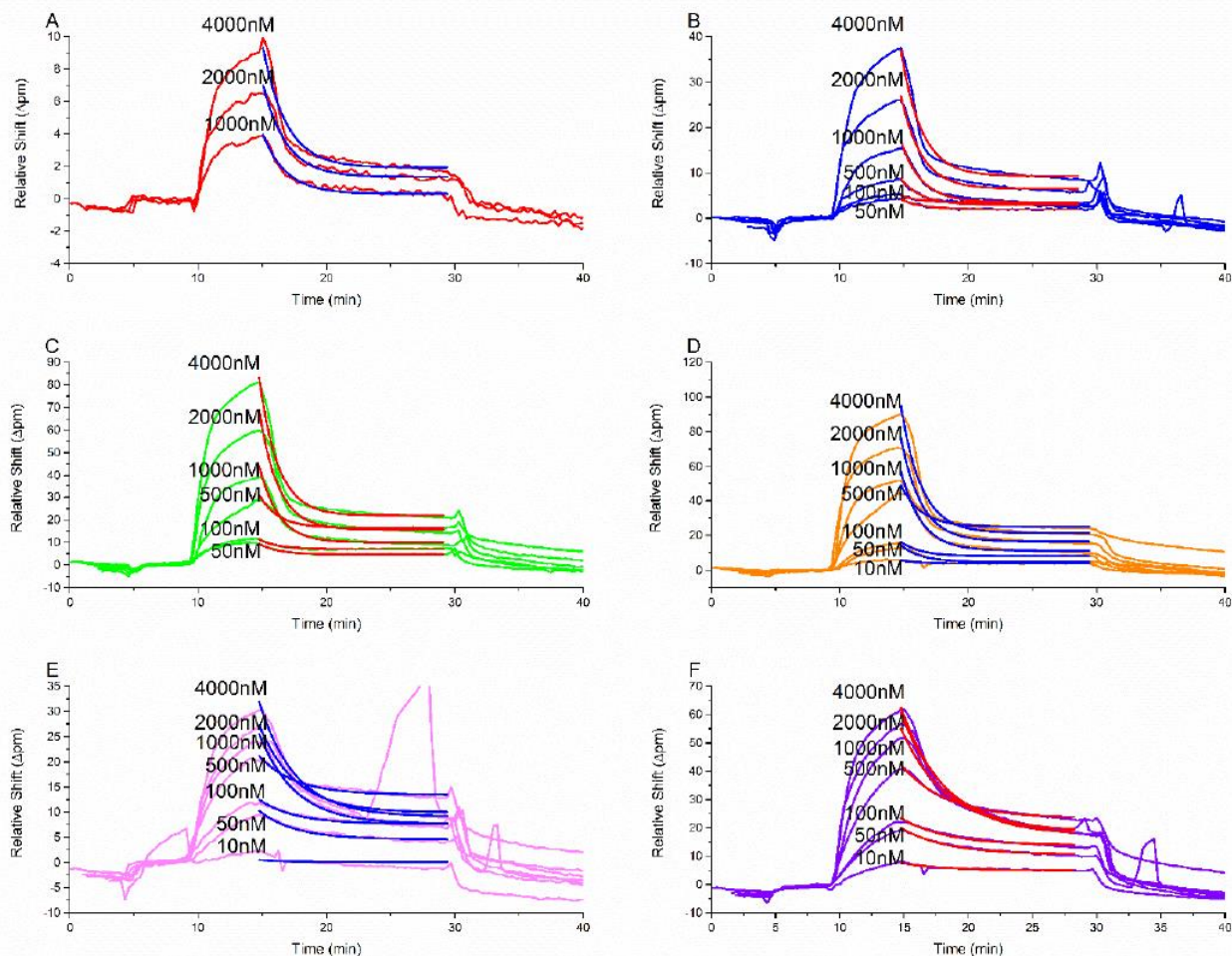
Figure III.16. k_{off} determination for aPC. After collecting the results from the binding and falloff titrations, the binding and falloff curves for each type of Nanodisc were stacked. The falloff curves were then globally fit using **Equation III.2**, the red curves are the fits (except for aPC-10% PS binding where the fit is shown in blue) (**A**) aPC-10% PS Nanodisc binding and falloff (**B**) aPC-30% PS Nanodisc binding and falloff (**C**) aPC-50% PS Nanodisc binding and falloff (**D**) aPC-70% PS Nanodisc binding and falloff (**E**) aPC-30% PA Nanodisc binding and falloff (**F**) aPC-50% PA Nanodisc binding and falloff.
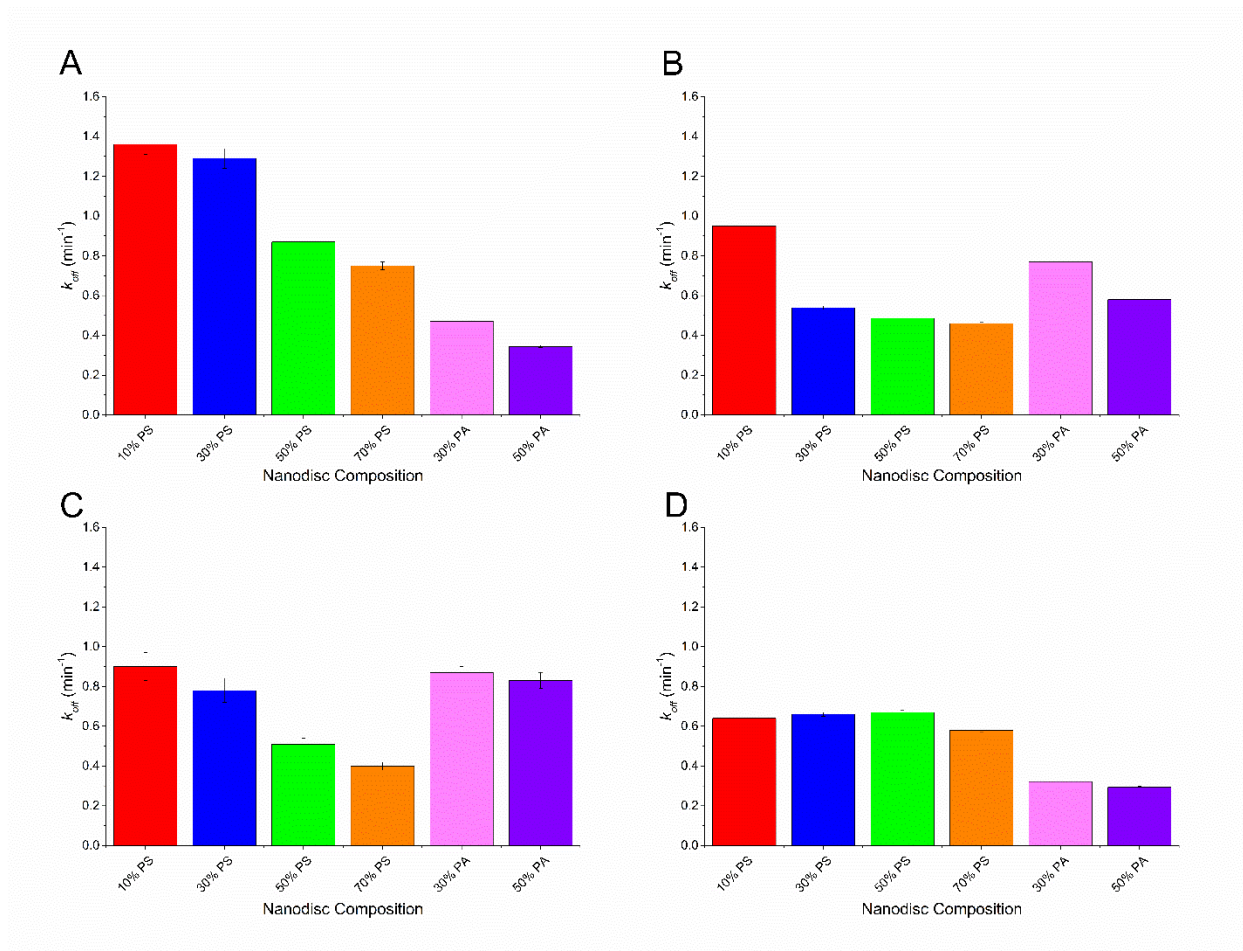
Figure III.17. The k_{off} values in min^{-1} of (**A**) PT (**B**) fX (**C**) fVIIa (**D**) aPC binding to variable lipid content Nanodiscs, as indicated. The k_{off} each protein-Nanodiscs was determined by stacking the association and dissociation curves of different protein concentrations to a single lipid composition and fitting protein dissociation curves to **Equation III.2**. Error bars represent the standard deviation from at least n = 8 microrings in a single detection experiment.

TABLES

Table III.1. *K_d values for 50% PS and 50% PA Nanodiscs* under different conditions.*

	Individual K_d values (nM)	*Trial #*	*[Ca²⁺] (mM) during spotting*	*Average K_d values*
50% PS	61 ± 7	1	0	55 ± 4
	53 ± 7	2	0	
	51 ± 7	3	0	
	98 ± 2	1	2.5	82.3 ± 1.2
	76 ± 2	2	2.5	
	73 ± 2	3	2.5	
50% PA	90 ± 40	1	0	90 ± 20
	80 ± 30	2	0	
	100 ± 30	3	0	
	130 ± 20	1	2.5	111 ± 9
	95 ± 13	2	2.5	
	109 ± 13	3	2.5	

Error represents standard deviation from at least n = 12 microrings in a single detection experiment.

*Nanodiscs were made with the MSP1E3D1 construct, which yields Nanodiscs that are roughly twice as large as the MSP1D1 Nanodiscs used in the full array-based measurements. Measurements were also performed using completely different lots of all reagents, which may account for variance with values in **Table III.2**. Interestingly, the ratio of K_d values from **Table III.2** (with MSP1D1 Nanodiscs) and **Table III.1** for identical disc composition and without Ca²⁺ in the spotting buffer is nearly identical (3.27 for 50% PS and 3.22 for 50% PA), which suggests a systematic offset.

Table III.2. K_d **values (in nM) of PT, fX, fVIIa, and aPC.**

	10% PS	30% PS	50% PS	70% PS	30% PA	50% PA
PT	2100 ± 100	337 ± 9	180 ± 10	140 ± 20	1020 ±40	290 ±13
fX	1060 ± 20	322 ± 3	193 ± 3	182 ± 3	1280 ± 80	1020 ±40
fVIIa	6000 ± 3000	3000 ±400	600 ± 80	200 ± 30	210 ± 20	125 ± 4
APC	5000 ± 900	4800 ± 500	1200 ± 100	440 ± 80	107 ± 7	90 ± 4

Error represents standard deviation from at least n = 8 microrings in a single detection experiment.

Table III.3. k_{off} values of PT, fX, fVIIa, and aPC.

	10% PS	30% PS	50% PS	70% PS	30% PA	50% PA
PT	1.36 ± 0.05	1.29 ± 0.05	0.87 ± 0.02	0.75 ± 0.02	0.47 ± 0.01	0.344 ± 0.005
fX	0.95 ± 0.02	0.539 ± 0.009	0.486 ± 0.008	0.459 ± 0.007	0.77 ± 0.02	0.58 ± 0.01
fVIIa	0.90 ± 0.07	0.78 ± 0.06	0.51 ± 0.03	0.40 ± 0.02	0.87 ± 0.03	0.83 ± 0.04
aPC	0.64 ± 0.02	0.66 ± 0.01	0.67 ± 0.01	0.58 ± 0.01	0.321 ± 0.007	0.293 ± 0.005

Error represents standard deviation from at least n = 8 microrings in a single detection experiment.

REFERENCES

(1)   Fahy, E.; Subramaniam, S.; Murphy, R. C.; Nishijima, M.; Raetz, C. R. H.; Shimizu, T.; Spener, F.; Van Meer, G.; Wakelam, M. J. O.; Dennis, E. A. Update of the LIPID MAPS Comprehensive Classification System for Lipids. *J. Lipid Res.* **2009**, *50* (SUPPL.), 9–14.

(2)   Seddon, A. M.; Curnow, P.; Booth, P. J. Membrane Proteins, Lipids and Detergents: Not Just a Soap Opera. *Biochim. Biophys. Acta - Biomembr.* **2004**, *1666* (1–2), 105–117.

(3)   Bayburt, T. H.; Grinkova, Y. V.; Sligar, S. G. Self-Assembly of Discoidal Phospholipid Bilayer Nanoparticles with Membrane Scaffold Proteins. *Nano Lett.* **2002**, *2* (8), 853–856.

(4)   Bayburt, T. H.; Sligar, S. G. Membrane Protein Assembly into Nanodiscs. *FEBS Lett.* **2010**, *584* (9), 1721–1727.

(5)   Denisov, I. G.; Grinkova, Y. V.; Lazarides, A. A.; Sligar, S. G. Directed Self-Assembly of Monodisperse Phospholipid Bilayer Nanodiscs with Controlled Size Directed Self-Assembly of Monodisperse Phospholipid Bilayer Nanodiscs with Controlled Size. *Nano Lett.* **2004**, *126* (11), 3477–3487.

(6)   Bayburt, T. H.; Leitz, A. J.; Xie, G.; Oprian, D. D.; Sligar, S. G. Transducin Activation by Nanoscale Lipid Bilayers Containing One and Two Rhodopsins. *J. Biol. Chem.* **2007**, *282* (20), 14875–14881.

(7)   Marty, M. T.; Zhang, H.; Cui, W.; Blankenship, R. E.; Gross, M. L.; Sligar, S. G. Native Mass Spectrometry Characterization of Intact Nanodisc Lipoprotein Complexes. *Anal. Chem.* **2012**, *84* (21), 8957–8960.

(8)   Schuler, M. A.; Denisov, I. G.; Sligar, S. G. Nanodiscs as a New Tool to Examine Lipid-Protein Interactions. In *Methods in Molecular Biology*; Kleinschmidt, J., Ed.; Springer Science: New York, 2013; Vol. 974, pp 415–433.

(9)   Shaw, A. W.; Pureza, V. S.; Sligar, S. G.; Morrissey, J. H. The Local Phospholipid Environment Modulates the Activation of Blood Clotting. *J. Biol. Chem.* **2007**, *282* (9), 6556–6563.

(10)   Baylon, J. L.; Lenov, I. L.; Sligar, S. G.; Tajkhorshid, E. Characterizing the Membrane-Bound State of Cytochrome P450 3A4: Structure, Depth of Insertion, and Orientation. *J. Am. Chem. Soc.* **2013**, *135* (23), 8542–8551.

(11)   Boettcher, J. M.; Davis-harrison, R. L.; Clay, M. C.; Nieuwkoop, A. J.; Ohkubo, Y. Z.;

Tajkhorshid, E.; Morrissey, J. H.; Rienstra, C. M. Atomic View of Calcium-Induced Clustering of Phoosphatidylserine in Mixed Lipid Bilayers. *Biochemistry* **2011**, *50*, 2264–2273.

(12)   Denisov, I. G.; Sligar, S. G. Nanodiscs in Membrane Biochemistry and Biophysics. *Chem. Rev.* **2017**, *117* (6), 4669–4713.

(13)   Washburn, A.; Gunn, L.; Bailey, R. Label-Free Quantitation of a Cancer Biomarker in Complex Media Using Silicon Photonic Microring Resonators. *Anal. Chem.* **2009**, *81* (22), 9499–9506.

(14)   Qavi, A. J.; Washburn, A. L.; Byeon, J. Y.; Bailey, R. C. Label-Free Technologies for Quantitative Multiparameter Biological Analysis. *Anal. Bioanal. Chem.* **2009**, *394* (1), 121–135.

(15)   Kindt, J. T.; Luchansky, M. S.; Qavi, A. J.; Lee, S. H.; Bailey, R. C. Subpicogram per Milliliter Detection of Interleukins Using Silicon Photonic Microring Resonators and an Enzymatic Signal Enhancement Strategy. *Anal. Chem.* **2013**, *85* (22), 10653–10657.

(16)   Wade, J. H.; Alsop, A. T.; Vertin, N. R.; Yang, H.; Johnson, M. D.; Bailey, R. C. Rapid, Multiplexed Phosphoprotein Profiling Using Silicon Photonic Sensor Arrays. *ACS Cent. Sci.* **2015**, *1* (7), 374–382.

(17)   Kindt, J. T.; Bailey, R. C. Chaperone Probes and Bead-Based Enhancement to Improve the Direct Detection of MRNA Using Silicon Photonic Sensor Arrays. *Anal. Chem.* **2012**, *84* (18), 8067–8074.

(18)   Qavi, A. J.; Kindt, J. T.; Gleeson, M. A.; Bailey, R. C. Anti-DNA_RNA Antibodies and Silicon Photonic Microring Resonators_increased Sensitivity for Multiplexed MicroRNA Detection.Pdf. *Anal. Biochem.* **2011**, *83* (15), 5949–5956.

(19)   Byeon, J.-Y.; Bailey, R. C. Multiplexed Evaluation of Capture Agent Binding Kinetics Using Arrays of Silicon Photonic Microring Resonators. *Analyst* **2011**, *136* (17), 3430–3433.

(20)   Marty, M. T.; Sloan, C. D. K.; Bailey, R. C.; Sligar, S. G. Nonlinear Analyte Concentration Gradients for One-Step Kinetic Analysis Employing Optical Microring Resonators. *Anal. Chem.* **2012**, *84* (13), 5556–5564.

(21)   Washburn, A. L.; Gomez, J.; Bailey, R. C. DNA-Encoding to Improve Performance and

Allow Parallel Evaluation of the Binding Characteristics of Multiple Antibodies in a Surface-Bound Immunoassay Format. *Anal. Chem.* **2011**, *83* (9), 3572–3580.

(22) Iqbal, M.; Gleeson, M. A.; Spaugh, B.; Tybor, F.; Gunn, W. G.; Hochberg, M.; Baehr-Jones, T.; Bailey, R. C.; Gunn, L. C. Label-Free Biosensor Arrays Based on Silicon Ring Resonators and High-Speed Optical Scanning Instrumentation. *IEEE J. Sel. Top. Quantum Electron.* **2010**, *16* (3), 654–661.

(23) Sloan, C. D. K.; Marty, M. T.; Sligar, S. G.; Bailey, R. C. Interfacing Lipid Bilayer Nanodiscs and Silicon Photonic Sensor Arrays for Multiplexed Protein − Lipid and Protein − Membrane Protein Interaction Screening. *Anal. Chem.* **2013**, *85* (5), 2970–2976.

(24) Tavoosi, N.; Davis-Harrison, R. L.; Pogorelov, T. V.; Ohkubo, Y. Z.; Arcario, M. J.; Clay, M. C.; Rienstra, C. M.; Tajkhorshid, E.; Morrissey, J. H. Molecular Determinants of Phospholipid Synergy in Blood Clotting. *J. Biol. Chem.* **2011**, *286* (26), 23247–23253.

(25) Zwaal, R. F. A.; Comfurius, P.; Bevers, E. M. Lipid–Protein Interactions in Blood Coagulation. *Biochim. Biophys. Acta (BBA)-Reviews Biomembr.* **1998**, *1376* (3), 433–453.

(26) Ohkubo, Y. Z.; Tajkhorshid, E. Distinct Structural and Adhesive Roles of Ca2+ in Membrane Binding of Blood Coagulation Factors. *Structure* **2008**, *16* (1), 72–81.

(27) Sunnerhagen, M.; Forsén, S.; Hoffrén, A. M.; Drakenberg, T.; Teleman, O.; Stenflo, J. Structure of the Ca2+-Free GLA Domain Sheds Light on Membrane Binding of Blood Coagulation Proteins. *Nat. Struct. Biol.* **1995**, *2* (6), 504–509.

(28) Stenflo, J.; Suttie, J. W. Vitamin K-Dependent Formation of Gamma-Carboxyglutamic Acid. *Annu. Rev. Biochem.* **1977**, *46*, 157-72.

(29) Furie, B.; Furie, B. C. The Molecular Basis of Blood Coagulation. *Cell* **1988**, *53* (4), 505–518.

(30) Banner, D. W.; D'Arcy, A.; Chene, C.; Winkler, F. K.; Guha, A.; Konigsberg, W. H.; Nemerson, Y.; Kirchhofer, D. The Crystal Structure of the Complex of Blood Coagulation Factor VIIa with Soluble Tissue Factor. *Nature*. 1996, pp 41–46.

(31) McDonald, J. F.; Shah, A. M.; Schwalbe, R. A.; Kisiel, W.; Dahlbäck, B.; Nelsestuen, G. L. Comparison of Naturally Occurring Vitamin K-Dependent Proteins: Correlation of Amino Acid Sequences and Membrane Binding Properties Suggests a Membrane Contact Site. *Biochemistry* **1997**, *36* (17), 5120–5127.

(32)   Nelsestuen, G. L.; Kisiel, W.; Scipio, R. G. D. Interaction of Vitamin K Dependent Proteins with Membranes. *Biochemistry* **1978**, *17* (11), 2134–2138.

(33)   Tavoosi, N.; Smith, S. A.; Davis-Harrison, R. L.; Morrissey, J. H. Factor VII and Protein C Are Phosphatidic Acid-Binding Proteins. *Biochemistry* **2013**, *52* (33), 5545–5552.

CHAPTER IV

Phosphatidylethanolamine-Phosphatidylserine Binding Synergy of Seven Coagulation Factors Revealed Using Nanodisc Arrays on Silicon Photonic Sensors

Abstract

Blood coagulation is regulated through protein-protein and protein-lipid interactions that occur at the sub-endothelium following vascular damage. Soluble clotting proteins bind to membrane components in a phosphatidylserine (PS) dependent manner to assemble multi-protein complexes that regulate clot formation; however, PS is of limited abundance physiologically. In this manuscript, we investigate synergy between PS and phosphatidylethanolamine (PE)—a lipid of much higher abundance naturally. Using a label-free, silicon photonic technology, we constructed arrays of Nanodiscs having variable lipid composition and probed the binding interactions of seven different clotting factors with GLA domains that have never been studied in tandem experiments before. The factors studied were prothrombin, activated factor VII, factor IX, factor X, activated protein C, protein S, and protein Z. Equilibrium dissociation constants (K_d) for each coagulation factor binding to Nanodiscs with unique compositions of PE and PS were determined. While all factors showed greater binding affinities in the presence of PS and PE, the most dramatic improvements in binding were observed when PS quantities were lowest. This demonstrates that synergy is effective in promoting coagulation factor binding under physiological lipid compositions, as opposed to the artificially high PS content probed in most *in vitro* activity studies.

1. Introduction

The phospholipid content of the cell membrane is a key regulator of the blood coagulation cascade.[1,2] Exposure of tissue factor and the negatively charged lipid, phosphatidylserine (PS), via cell membrane damage is one of the initiating factors of the cascade.[3,4] The majority of steps in the clotting cascade occur at the membrane surface and involve multiple PS lipid-binding proteins.[4] The most common PS-binding domain found in both pro- and anti-coagulant factors is the γ-carboxyglutamic acid-rich GLA domain located at the N-terminus of these proteins [Procoagulants: factor VII (fVII); factor IX (fIX); factor X (fX); and prothrombin (PT). Anticoagulants: activated protein C (aPC); protein S (PrS); and protein Z (PrZ).] The GLA domain reversibly binds to PS lipids in a calcium dependent manner.[4] While the structures of the GLA domains are highly conserved, they display membrane binding affinities that vary by more than two orders of magnitude,[2,4] which suggests differences in the lipid binding preferences of each.

Even though PS lipids are necessary for optimal activity of many clotting factors, they only constitute ~12% of the phospholipid content of the cell membrane,[5] which is much lower than what is required for optimal procoagulant activity of activated fVII (fVIIa) in vitro (~30% PS in liposomes).[1] Previous studies have shown that lipid composition influences the binding and activity of GLA domain-containing clotting proteins. For example, even though GLA domains of clotting proteins are structurally and compositionally homologous, aPC and fVIIa bind phosphatidic acid (PA) lipids much more tightly than PS lipid.[2] Maximal rates of activation of fX by fVIIa bound to tissue factor,[6–8] of activation of prothrombin by fXa bound to factor Va,[9] and of inactivation of factor Va by aPC[10], have been reported to require much less PS when membranes also contain phosphatidylethanolamine (PE). This phenomenon has been termed PE-PS synergy. The "Anything But Choline" (ABC) hypothesis explains PE-PS synergy by stating that almost any phospholipid, other than those with choline head groups, can work cooperatively with PS lipids to greatly reduce the amount of PS required for binding and activation of clotting proteins.[8] PE comprises ~25% of the phospholipid content of the plasma membrane and is normally sequestered, along with PS, in the inner leaflet of the bilayer.[5] Cell membrane damage exposes both PE and PS to support of blood coagulation reactions, showing physiological relevance for PE-PS synergy.

Since most of the previous work on PE-PS synergy focused on enzyme activity assays using membrane-bound enzyme, cofactors, and substrates, it is not clear which of the proteins within these multi-protein complexes actually exhibited enhanced membrane binding in the presence of PE. This is especially important since some of the proteins in these complexes (e.g., factors Va and VIIIa), bind to PS in membrane surfaces via discoidin-type C2 domains, not GLA domains.[4] In fact, to date, the only GLA domain-containing protein whose binding to membrane surfaces has been directly shown to be enhanced by PE is fX, raising the question of how generally PE-PS synergy promotes the binding of GLA domain-containing proteins.

The aim of this study was to comprehensively and quantitatively evaluate the degree to which PE-PS lipid synergy enhances membrane binding of all seven GLA domain-containing proteins of the clotting cascade in tandem experiments. As a model membrane system, Nanodiscs were constructed to present well-defined, variable lipid compositions. Nanodiscs are small lipid bilayer discs held together by two membrane scaffold proteins (MSPs) that offer a high degree of control over lipid composition.[11,12] Nanodiscs have proven to be a useful tool in the study of membrane-lipid interactions of the blood coagulation cascade.[1,2,8] Various Nanodisc were spatially arrayed onto a label-free and highly multiplexable silicon photonic detection platform to allow in series determination of binding constants (**Figure IV.1**). Recently, we demonstrated the ability to utilize this combination of Nanodiscs and microring resonator sensors for high-throughput interrogation of protein binding to model membrane surfaces,[13,14] including coagulation factors, PT, fX, fVIIa, and aPC. This work demonstrated that binding interactions can be rapidly probed simultaneously with reduced time and reagent consumption compared to conventional methods. Herein, we further extend this technology to probe the binding interactions of all seven GLA domain-containing coagulation factors to Nanodiscs presenting defined ratios of PS and PE. These experiments were performed in series on a single array of Nanodiscs to eliminate environmental changes day-to-day that can result in variation in array formation. Thus, providing an optimal surface for direct comparison of binding improvements due to lipid composition.

More specifically, we determined K_d values for fVIIa, fIX, fX, PT, aPC, PrS, and PrZ binding to Nanodiscs at eight distinct lipid compositions. We directly compared K_d values of binding to Nanodiscs of 10, 25, 40 and 50% PS to Nanodiscs containing 10% PS/40% PE, 25% PS/25% PE, and 40% PS/10% PE, or 50% PE. The balance in all Nanodiscs was made up with non-interacting

phosphatidylcholine (PC) lipids. Utilizing silicon photonic microring resonators as our sensing platform, we have shown that sequential titrations can be performed on a Nanodisc array surface.[14] Thus, experiments with each clotting factor were performed sequentially on the same Nanodisc array surface to eliminate day-to-day variation observed with other experimental setups.

We found that PE had a significant effect on K_d, driving much tighter binding of all factors to the model membrane surface. Using these calculated K_d values, we quantitated the fold-change in binding due to the addition of PE to PS. Interestingly, the magnitude of binding improvement was greatest at the lowest PS contents, consistent with physiological lipid abundances. This synergistic improvement in binding was more striking for the clotting proteins that showed poorest binding to PS alone which have not been shown to observe this synergy—fVIIa, PrZ, and aPC. These proteins yield very high (or unmeasurable) K_d values (poor binding) at near physiological PS content and therefore PE-PS synergy appears essential for regulation of coagulation. This work offers a comprehensive and quantitative view of the synergistic influence of PE on binding of clotting cascade proteins across all seven GLA domain-containing clotting proteins and is a high-throughput complement to activity-based studies of their pro- and anticoagulant activities modulated by protein-lipid interactions.

2. Materials and Methods

Chemicals and reagents

Lipids presenting phosphocholine (POPC; 1-palmitoyl-2-oleoyl-sn-glycero-3-phosphocholine), phosphoserine (POPS; 1-palmitoyl-2-oleoyl-sn-glycero-2-phosphoserine), and phosphoethanolamine (DOPE; 1,2-dioleoyl-sn-glycero-3-phosphoethanolamine) head groups were purchased from Avanti Polar Lipids (Alabaster, AL). MSP1E3D1 was expressed in *E. coli* and purified as described previously.[12] Human fVIIa, fX, PT, aPC, and PrZ were purchased from Enzyme Research Laboratories Inc. (South Bend, IN). Human fIX and PrS were purchased from Haematologic Technologies (Essex Junction, VT). Amberlite XAD-2 hydro-phobic beads and all other chemicals were purchased from Sigma Aldrich (St. Louis, MO) and used as received unless otherwise noted. Buffers were prepared with 18.2 MΩ water and sterile filtered prior to use.

Solution preparation

Nanodisc solutions were prepared in a TBS buffer (20 mM Tris-HCl, 100 mM NaCl, and 0.01% (w/v) NaN$_3$; pH 7.4). PT, fIX, and fX solutions were prepared in a HEPES buffer (10 mM HEPES, 150 mM NaCl, 50 µM EDTA, 2.5 mM CaCl$_2$, 0.1% (w/v) PEG 8000; pH 7.4). Solutions of fVIIa, aPC, PrS, and PrZ were prepared in HEPES buffer with 0.2% (w/v) BSA. The HEPES rinse buffer (HEPES(-)) for surface regeneration was made without CaCl$_2$.

Nanodisc preparation and purification

Nanodisc preparation and purification has been described in detail previously.[11,12,15] Briefly, lipids solubilized in chloroform were measured into test tubes and dried under nitrogen. For Nanodiscs containing mixtures of POPS, DOPE, and/or POPC, the lipids were mixed at defined ratios prior to drying. After drying, lipids were placed in a desiccator, under vacuum overnight. Once completely dry, lipids were dissolved in TBS buffer with 100 mM deoxycholate to give a final molar ratio of 2:1 dexoycholate:phospholipids. Dissolved lipids were then combined with MSP1E3D1 in TBS to give a final molar ratio of 135:1 phospholipid:MSP. The solution of MSP and lipids was actively mixed at 4˚C for approximately 1 hr. Amberlite XAD-2 hydrophobic beads were then added to the MSP/lipid solution with the amount of bead solution being half the total of the MSP/lipid solution volume. This combined solution was then mixed for approximately 1.5 hour at 4˚C. Amberlite XAD-2 hydrophobic beads were then removed by filtering through a 0.22 µm syringe filter. Nanodiscs were then purified using size exclusion chromatography using a Superdex 200 column (GE).

Silicon photonic microring resonators

The Maverick M1 optical scanning instrumentation and microring resonator sensor chips were purchased from Genalyte, Inc. (San Diego, CA). The operation of the instrument has been previously described.[16–20] The sensor chips were each 4 mm x 6 mm and contained 128, 30-µm diameter active sensor microrings arranged in clusters of four, plus four temperature control microrings and two dedicated to detecting leaks from the microfluidic gasket positioned atop the sensor chip during microring detection experiments.

Sensor chip array functionalization

Prior to use, sensor chips were placed in a vial of acetone for 2 min with gentle agitation. Sensor chips were then transferred to a vial of isopropanol for 2 min. After the sensor chips had been dried with N_2, between 0.1 and 0.2 µL of each type of Nanodisc were spotted at 0.5 µM. A spotting map showing the arrangement of the Nanodisc solutions on the sensor substrate is shown in **Figure 4.1**. After spotting, chips were stored in a humidity chamber at 4°C for at least 1 hour before use.

Protein binding titrations

Laser-cut Mylar gaskets to direct fluid flow across the chip were aligned onto the functionalized sensor chips, assembled into a Teflon cartridge, and loaded into the sensor scanner instrument. A 2% solution of BSA in HEPES(-) buffer was first flowed across the chip surface at 10 µL/min to prevent the non-specific binding of proteins. For K_d determination titrations, the proteins were flowed across the chip in increasing concentrations at 10 µL/min and the response allowed to approach steady state before the next solution injection. Following each titration, all of the coagulation factors were released from the surface by flowing HEPES(-) buffer solution. The titration was then performed for the next protein.

Data analysis

Data analysis was performed using custom R scripts in RStudio. Sensor traces were corrected for temperature fluctuations and any residual non-specific binding by subtraction of response of 100% PC Nanodiscs. The maximum shift for each protein concentration was calculated by subtracting the relative shift (Δpm) at the equilibration point for HEPES buffer (at 10 minutes) from the relative shift (Δpm) at equilibration for each protein concentration (the curve plateau). This maximum shift is plotted versus the protein concentration for fitting to the single-site ligand binding equation in order to determine K_d values:

$$\Delta\text{pm} = B_{max}\left(\frac{X}{K_d+X}\right) \tag{IV.1}$$

where X is the concentration of protein, B_{max} is the maximum binding shift, and K_d is the equilibrium dissociation constant. Fold-changes were calculated as ratios of K_d values without PE to those with PE, at each identical PS content. Standard errors in the ratios were determined based on Fieller's Theorem with independent values.[21]

3. Results and Discussion

Sensor array layout

PS lipids are necessary for binding of GLA domain-containing clotting proteins to membranes, yet PS constitutes only ~12% of the phospholipid content of the plasma membrane.[5] Due to the fact that PE is one of the most abundant phospholipids in the membrane (~25%), it has the potential to play a significant supporting role to PS lipids in clotting protein binding and activation, especially for those proteins with low PS binding affinity. In order to assess the influence of PE lipids on binding, the equilibrium dissociation constants, K_d values, of fVIIa, fIX, fX, PT, aPC, PrS, and PrZ, were determined for eight different lipid compositions using the same Nanodisc microarray to prevent experiment to experiment variation. The lipid compositions included four binary mixtures of PS and PC (10, 25, 40, and 50% PS with the balance PC), one binary mixture of PE and PC (50% PE and 50% PC), three ternary mixtures of PS, PE, and PC (10%/40%/50%, 25%/25%/50%, and 40%/10%/50% PS/PE/PC, respectively), and 100% PC as an off-target control. **Figure IV.1B** shows the layout of the spotted Nanodisc array sensor chip.

Effect of lipid composition on K_d values for membrane binding of all 7 Gla-domain containing clotting proteins

Binding titrations for each protein were sequentially performed to determine the K_d values across each of the eight different lipid compositions. As an example, the binding titration of fVIIa, monitored in real time via a shift in the resonant wavelength of the microring sensors on the Nanodisc-arrayed sensor chip is presented in **Figure IV.2A**. The concentration of fVIIa was increased in a stepwise fashion from 50 to 4000 nM. The titration shows preferential binding of fVIIa to PS-containing bilayers when PE lipids were also present in the Nanodiscs. At the end of the titration, HEPES(-) was flowed across the surface to regenerate a clean Nanodisc array for the next protein titration in the sequence. The 100% PC lipid Nanodiscs were used as a control due to the lack of specific binding of GLA domains to PC-Nanodiscs. For data analysis, the minimal binding of fVIIa to the PC-Nanodisc functionalized rings was subtracted to correct for any nonspecific binding. The maximum shift at each step of the titration versus concentration were then fit with a single-site binding model (**Figure IV.2B**). The titration experiments that were used in K_d determination for the other six clotting factors are shown in **Figures IV.3-8**.

The dissociation constant, K_d, for a binding event is defined as the concentration at which half of the binding sights in an interaction are occupied. Therefore, the lower K_d value for an interaction, the less analyte is needed to occupy these sites and the higher affinity the analyte has for the binding interaction. Here, K_d is measured directly using single-site ligand binding equation, but this value can also be calculated from the on- and off-rates (k_{on} and k_{off}) for a binding and dissociation event. Using this method, the ratio of the k_{off}/k_{on} is used to determine K_d. The rate constant definition still shows increased binding affinity with decreasing K_d since this would mathematically translate to a slower off-rate or a faster on-rate which correlate to a favored binding state. Conversely, an increase in K_d between interactions show that the binding even is less favorable due to the adjusted conditions. Thus, observing interactions between different lipid environments and proteins, a low K_d can be used to determine the lipids that the protein has a higher affinity for binding. **Figure IV.9** shows a comparison of the K_d values obtained for each clotting protein interacting with all tested lipid environments. Note that the *x*-axis in the figure indicates the percentage of PS in each Nanodisc. The blue lines indicate trends in K_d for Nanodiscs containing PE and red lines are for Nanodiscs without PE. **Table IV.1** contains the numerical values for K_d values at each Nanodisc composition. For all seven clotting proteins, the K_d values for binding to Nanodiscs containing PE and PS are lower (stronger binding) compared to those with PS but without PE—even at identical total amounts of PS—which is indicative of PE-PS synergy.

Quantifying the effect of lipid synergy membrane binding

The significance of PE lipids' influence on the binding of the clotting factors to the lipid bilayer can be most clearly seen in the cases of fVIIa and aPC, both of which bind relatively poorly to PS/PC bilayers. aPC and fVIIa have an even greater binding affinity towards PA lipids,[2] but PA lipids only constitute 1-2% of the plasma membrane.[22] **Figure IV.9D** and **E** show the K_d values for fVIIa and aPC respectively. aPC binding to Nanodiscs with 10% PS/90% PC was unmeasurably weak (**Figure IV.6B**), but upon addition of 40% PE lipids, binding was clearly observed. In fact, the addition of PE resulted in stronger fVIIa binding than for the 25% PS/75% PC Nanodiscs. K_d values obtained for fVIIa binding to any ratio of PS to PE lipids were lower than

that for 50% PS Nanodiscs. PrS (**Figure IV.9F**) showed extremely tight PS lipid binding affinity for all PS content, with the most dramatic synergy observed at low PS content (10% PS with 40% PE). Taken together, it is clear that PS is required for the binding of clotting factors to membrane surfaces; however, the addition of PE, which is in much higher natural abundance compared with PS and PA, can dramatically increase the binding affinities through synergistic effects. Further measurements that examine higher order lipid mixtures using this high-density sensor array technology could give additional insights into more complex synergistic binding interactions that help regulate coagulation in vitro.

Overall, the data collected from the binding titrations of the seven GLA domain-containing clotting proteins demonstrated that inclusion of PE lipids reduced the concentration of PS lipids needed for the strongest binding affinities. This work complements previous studies[6–10] that examined the synergistic effect of PE lipids to support activity of clotting proteins. The correlation of K_d values with the activity suggests that PE synergizes with PS to improve the binding and potentially enhance the activity of all GLA domain-containing clotting proteins under conditions of low PS content. While PE affected the binding of all the proteins within this study, the magnitude of PE-PS synergy varied. To more clearly show these differences, **Figure IV.10** shows the relative enhancement of binding affinity via the inclusion of PE for each given PS concentration. This also nicely highlights that the synergy is most effective at low PS compositions, which is important as these are the most physiologically relevant lipid compositions in the array.

4. Conclusion

Here, we utilized a high-throughput approach to rapidly screen the binding of all seven GLA domain-containing coagulation factors (fVIIa, fIX, fX, PT, aPC, PrS, and PrZ) interacting with Nanodiscs with nine different combinations of PS, PE, and PC lipids. This comprehensive study affirms previous observations of PE-PS synergy for some of these proteins from activity-based assays, but also reveals new protein-lipid synergies. Importantly, this platform allows for internally controlled measurements since the same sensor array can be regenerated and the measurements are performed under identical conditions in a single day. Furthermore, different magnitudes of synergy were observed for different clotting proteins which have never been compared before. The

enhancements in binding affinity were more pronounced at lower PS contents, which are most similar to true *in vivo* lipid compositions. This is in contrast to most *in vitro* experiments that use extremely high amounts of PS in both binding and activity assays. These observations of PE-PS synergy with all GLA domain-containing blood coagulation factors have been performed on model membrane mimetics *in vitro*; thus, the application shows the ability to characterize biological interactions but is not able to accurately depict what is occurring in the endothelium. However, this quantitative look at lipid synergy with PS and PE provides biological understanding to the lipid binding affinity of the GLA domain and different the binding affinity differences between GLA domain-containing proteins. In the future, more complex, multi-component mixtures can be explored to reveal more nuanced binding synergies. Furthermore, other PS-binding proteins such as Matrix GLA protein, Growth-Arrest-specific protein 6, factor VII and factor VIII could be investigated to see if these non-clotting factor proteins exhibit similar PE-PS binding synergies.

5. Acknowledgements

Figure IV.1. Nanodisc array setup. (**A**) Schematic of Nanodisc physisorption to a microring resonator. The MSP (purple) stabilizes the lipids (PC: yellow; PS: red; and PE: blue) to form the Nanodisc bilayer mimetic. Note: the schematic is not to scale. The microring resonator is 30 µm in diameter while the Nanodiscs are about 13 nm in diameter and 5 nm in thickness. (**B**) Spotting layout of the sensor chip for protein titrations. The flow path for experiments is shown in light blue.
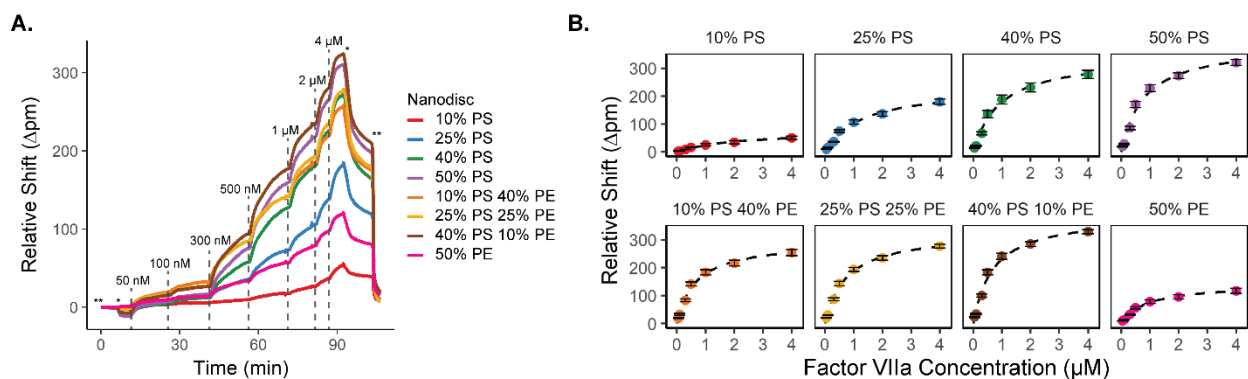
Figure IV.2. Titration and binding curves for factor VIIa. (**A**) Binding titration of activated factor VII (fVIIa) to Nanodiscs of the eight different lipid compositions 10% PS (red), 25% PS (blue), 40% PS (green), 50% PS (purple), 10% PS/40% PE (orange), 25% PS/25% PE (yellow), 40% PS/10% PS (brown), and 50% PE (pink), with the lipid balance of PC lipids. In all cases, background binding to 100% PC Nanodiscs was subtracted to correct for non-specific interactions. *Dashed lines* indicate time points where a new concentration of fVIIa was added (ranging from 50 to 4000 nM). The * marks the transition to HEPES buffer, and ** marks the transition to HEPES(-) to initiate surface regeneration. (**B**) Relative resonance wavelength shift as a function of fVIIa concentration for each Nanodisc type. **Equation IV.1** was used for fitting. Error bars represent standard deviation of at least n = 4 microrings.
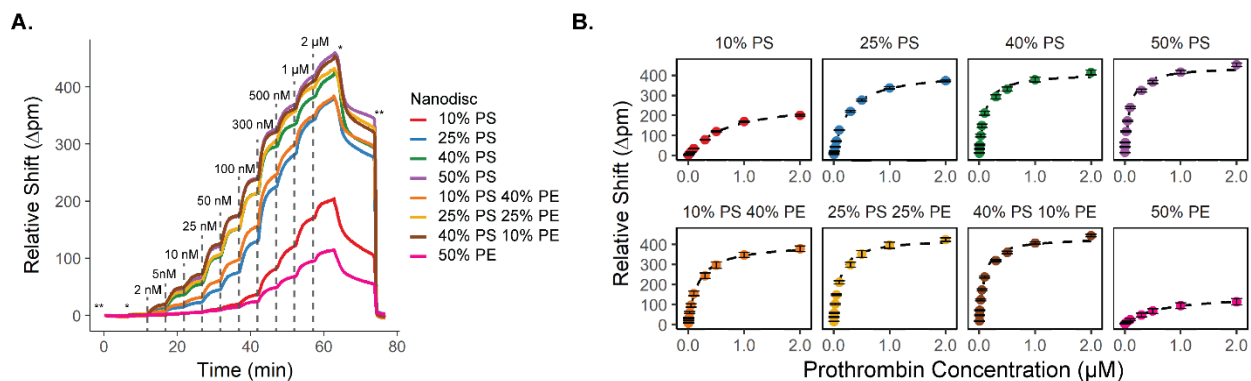
Figure IV.3. Prothrombin (PT) binding titration and K_d determination. For K_d determination, PT was flowed across a sensor chip, (**Figure IV.1**). The concentrations of PT used were 2 nM, 5 nM, 10 nM, 25 nM, 50 nM, 100 nM, 300 nM, 500 nM, 1000 nM, and 2000 nM. (**A**) The PT binding response during a titration, flowed at 10 µL/min. Subtraction of binding to 100% PC Nanodiscs was used to correct for nonspecific binding. Each trace depicts the average binding response to a different Nanodisc: 10% PS (red), 10% PS 40% PE (orange), 25% PS (blue), 25% PS 25% PE (yellow), 40% PS (green), 40% PS 10% PS (brown), 50% PE (pink), and 50% PS (purple) all made with PC as the balance. The dashed lines indicate the addition of a new concentration of PT, the *marks the transition to HEPES buffer, and ** marks the transition to HEPES(-). (**B**) The maximal shift of PT binding vs PT concentration fit to **Equation IV.1** for each type of Nanodisc used.
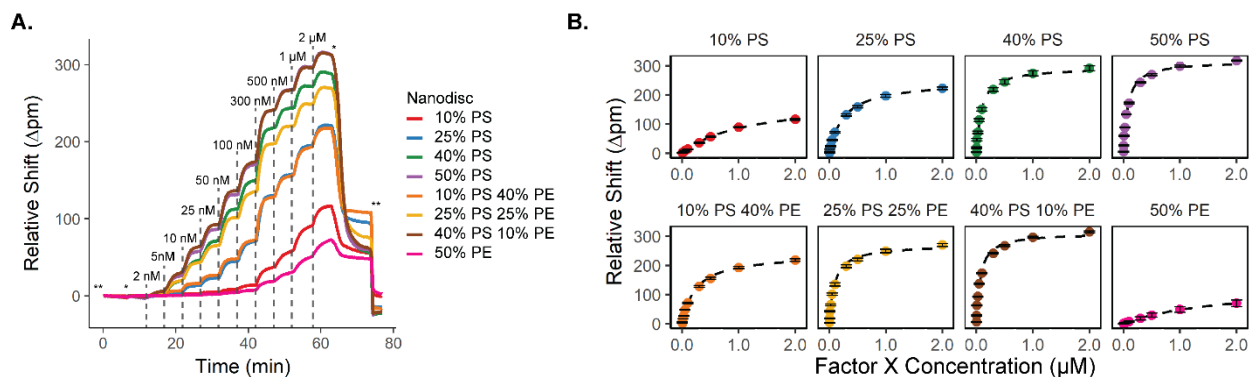
Figure IV.4. Factor X (fX) binding titration and K_d determination. For K_d determination, fX was flowed across a sensor chip, (**Figure IV.1**). The concentrations of fX used were 2 nM, 5 nM, 10 nM, 25 nM, 50 nM, 100 nM, 300 nM, 500 nM, 1000 nM, and 2000 nM. (**A**) The fX binding response during a titration, flowed at 10 μL/min. Subtraction of binding to 100% PC Nanodiscs was used to correct for nonspecific binding. Each trace depicts the average binding response to a different Nanodisc: 10% PS (red), 10% PS 40% PE (orange), 25% PS (blue), 25% PS 25% PE (yellow), 40% PS (green), 40% PS 10% PS (brown), 50% PE (pink), and 50% PS (purple) all made with PC as the balance. The dashed lines indicate the addition of a new concentration of fX, the *marks the transition to HEPES buffer, and ** marks the transition to HEPES(-). (**B**) The maximal shift of fX binding vs fX concentration fit to **Equation IV.1** for each type of Nanodisc used.
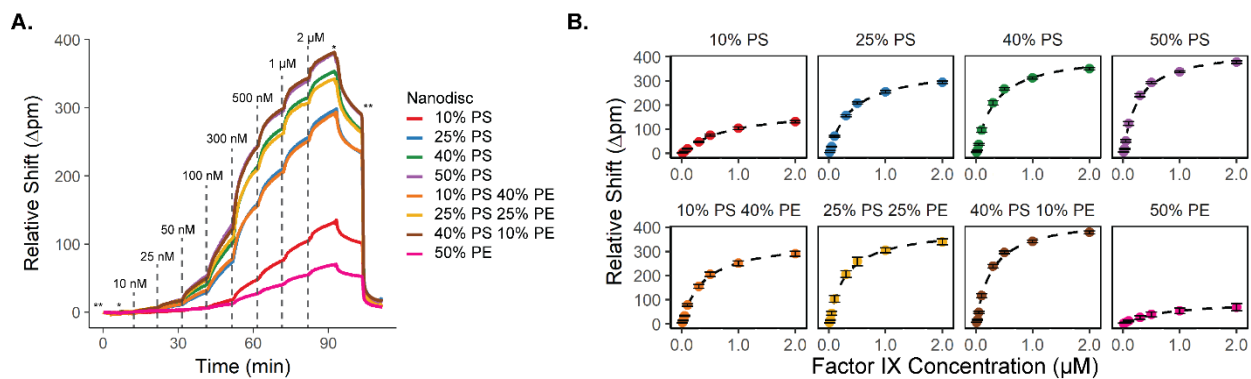
Figure IV.5. Factor IX (fIX) binding titration and K_d determination. For K_d determination, fIX was flowed across a sensor chip, (**Figure IV.1**). The concentrations of fIX used were 10 nM, 25 nM, 50 nM, 100 nM, 300 nM, 500 nM, 1000 nM, and 2000 nM. (**A**) The fIX binding response during a titration, flowed at 10 µL/min. Subtraction of binding to 100% PC Nanodiscs was used to correct for nonspecific binding. Each trace depicts the average binding response to a different Nanodisc: 10% PS (red), 10% PS 40% PE (orange), 25% PS (blue), 25% PS 25% PE (yellow), 40% PS (green), 40% PS 10% PS (brown), 50% PE (pink), and 50% PS (purple) all made with PC as the balance. The dashed lines indicate the addition of a new concentration of fIX, the *marks the transition to HEPES buffer, and ** marks the transition to HEPES(-). (**B**) The maximal shift of fIX binding vs fIX concentration fit to **Equation IV.1** for each type of Nanodisc used.
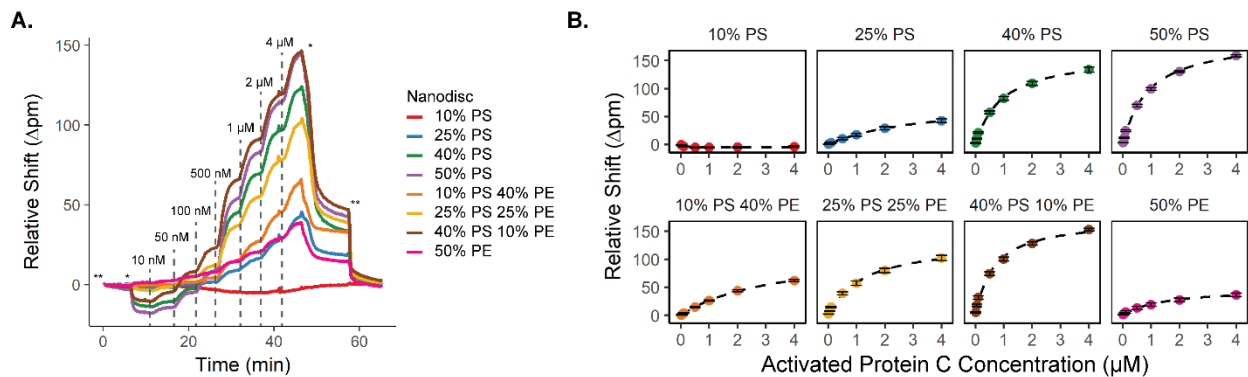
Figure IV.6. Activated protein C (aPC) binding titration and K_d determination. For K_d determination, aPC was flowed across a sensor chip, (**Figure IV.1**). The concentrations of aPC used were 10nM, 50 nM, 100 nM, 500 nM, 1000 nM, 2000 nM, and 4000 nM. (**A**) The aPC binding response during a titration, flowed at 10 µL/min. Subtraction of binding to 100% PC Nanodiscs was used to correct for nonspecific binding. Each trace depicts the average binding response to a different Nanodisc: 10% PS (red), 10% PS 40% PE (orange), 25% PS (blue), 25% PS 25% PE (yellow), 40% PS (green), 40% PS 10% PS (brown), 50% PE (pink), and 50% PS (purple) all made with PC as the balance. The dashed lines indicate the addition of a new concentration of aPC, the *marks the transition to HEPES buffer, and ** marks the transition to HEPES(-). (**B**) The maximal shift of aPC binding vs aPC concentration fit to **Equation IV.1** for each type of Nanodisc used.

137
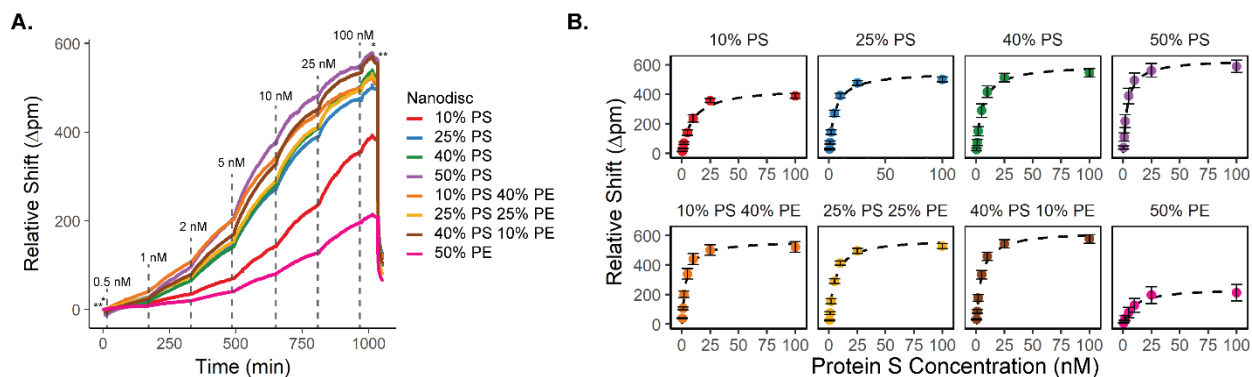
Figure IV.7. Protein S (PrS) binding titration and K_d determination. For K_d determination, PrS was flowed across a sensor chip, (**Figure IV.1**). The concentrations of PrS used were 10 nM, 25 nM, 50 nM, 100 nM, 300 nM, 500 nM, 1000 nM, 2000 nM, and 4000 nM. (**A**) The PrS binding response during a titration, flowed at 10 μL/min. Subtraction of binding to 100% PC Nanodiscs was used to correct for nonspecific binding. Each trace depicts the average binding response to a different Nanodisc: 10% PS (red), 10% PS 40% PE (orange), 25% PS (blue), 25% PS 25% PE (yellow), 40% PS (green), 40% PS 10% PS (brown), 50% PE (pink), and 50% PS (purple) all made with PC as the balance. The dashed lines indicate the addition of a new concentration of PrS, the *marks the transition to HEPES buffer, and ** marks the transition to HEPES(-). (**B**) The maximal shift of PrS binding vs PrS concentration fit to **Equation IV.1** for each type of Nanodisc used.
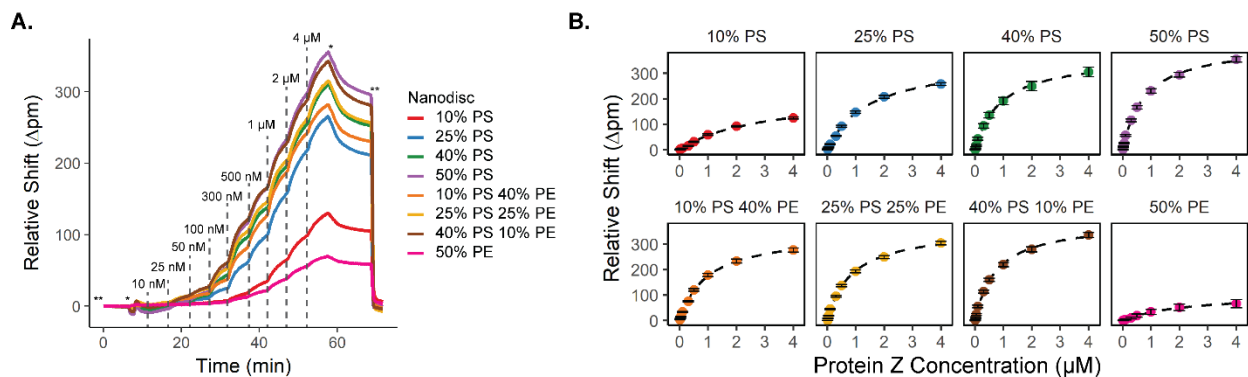
Figure IV.8. Protein Z (PrZ) binding titration and K_d determination. For K_d determination, PrZ was flowed across a sensor chip, (**Figure IV.1**). The concentrations of PrZ used were 10 nM, 25 nM, 50 nM, 100 nM, 300 nM, 500 nM, 1000 nM, 2000 nM, and 4000 nM. (**A**) The PrZ binding response during a titration, flowed at 10 µL/min. Subtraction of binding to 100% PC Nanodiscs was used to correct for nonspecific binding. Each trace depicts the average binding response to a different Nanodisc: 10% PS (red), 10% PS 40% PE (orange), 25% PS (blue), 25% PS 25% PE (yellow), 40% PS (green), 40% PS 10% PS (brown), 50% PE (pink), and 50% PS (purple) all made with PC as the balance. The dashed lines indicate the addition of a new concentration of PrZ, the *marks the transition to HEPES buffer, and ** marks the transition to HEPES(-). (**B**) The maximal shift of PrZ binding vs PrZ concentration fit to **Equation IV.1** for each type of Nanodisc used.
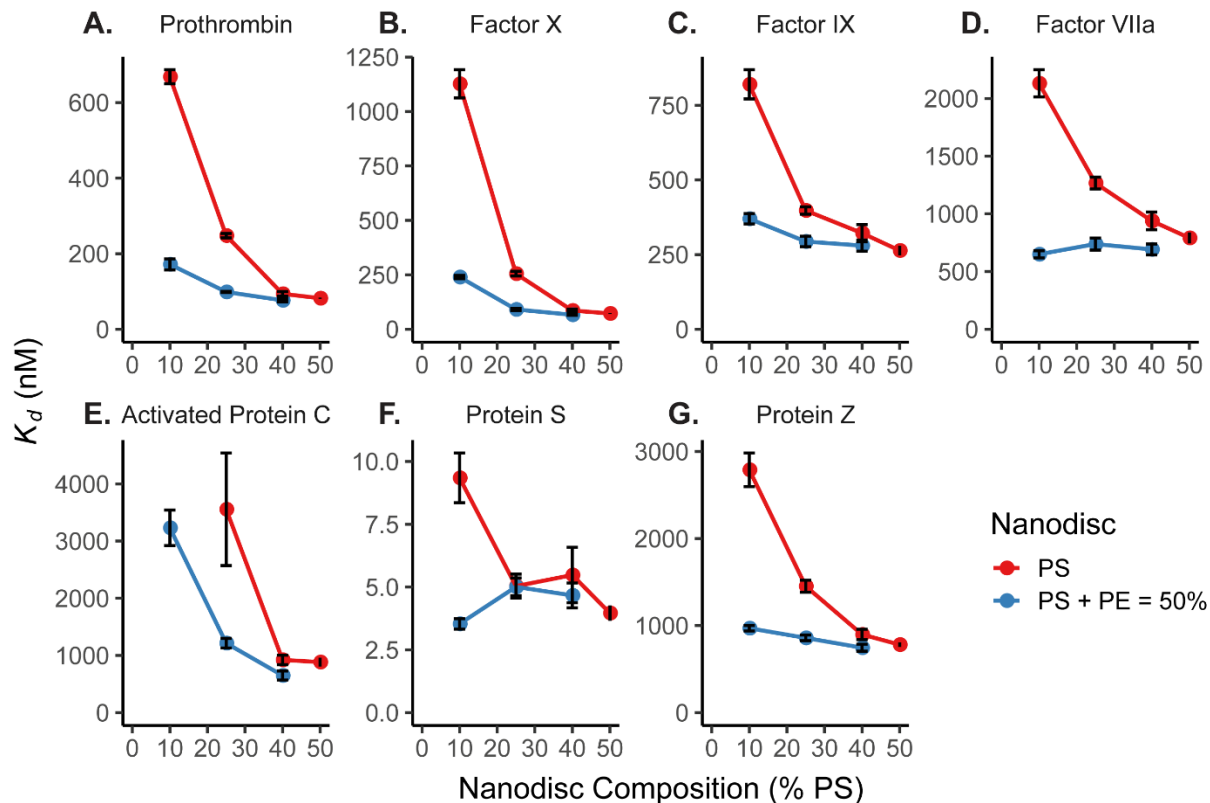
Figure IV.9. Comparison of K_d values from binding. (**A**) PT, (**B**) fX, (**C**) fIX, (**D**) fVIIa, (**E**) aPC, (**F**) PrS, and (**G**) PrZ to Nanodiscs with (blue) and without (red) PE lipids. K_d values are plotted as a function of percent PS where the PS + PE lipid composition is equal to 50% for the PE lipid containing Nanodiscs. Each was determined by plotting relative shift of binding vs. concentration of protein and fitting to **Equation IV.1**. Error bars represent the standard deviation from at least n = 4 microrings. K_d values for 50% PE/50% PC are not shown in the graphs due to the large error from the poor binding to this lipid environment by each clotting factor. # aPC binding to 10% PS without PE was too weak to calculate K_d.
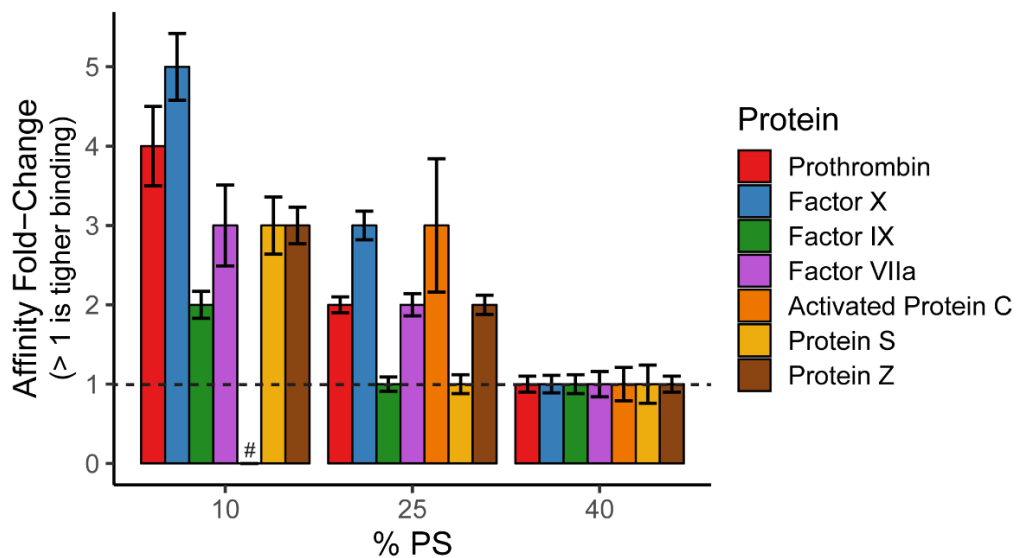
Figure IV.10. Affinity increase (K_d decrease) due to PE-PS synergy. These values were calculated by taking the ratio of K_d values without PE to those with PE. The dashed line represents no change in K_d with the addition of PE. Error bars represent standard error in calculating the ratio of these two values.[21] # Fold-change unable to be calculated since aPC binding to 10% PS without PE was too weak to measure.

TABLES

Table IV.1. K_d values in nM of PT, fX, fIX, fVIIa, aPC, PrZ, and PrS.

	10% PS	25% PS	40% PS	50% PS	10% PS 40% PE	25% PS 25% PE	40% PS 10% PE	50% PE
PT	670 ± 30	244 ± 8	93 ± 6	82 ± 1	190 ± 30	98 ± 2	76 ± 4	600 ± 200
fX	1130 ± 60	260 ± 10	87 ± 7	73 ± 2	250 ± 20	92 ± 5	67 ± 3	2000 ± 700
fIX	810 ± 30	390 ± 10	310 ± 30	260 ± 20	390 ± 30	290 ± 20	280 ± 20	800 ± 100
fVIIa	1800 ± 300	1260 ± 50	900 ± 90	790 ± 50	690 ± 50	740 ± 50	690 ± 50	860 ± 60
aPC	NA	3600 ± 1000	920 ± 80	880 ± 80	3200 ± 300	1210 ± 80	650 ± 80	1500 ± 600
PrS	9.7 ± 0.8	5.0 ± 0.5	5.3 ± 1.0	4.0 ± 0.3	3.8 ± 0.4	5.0 ± 0.4	4.7 ± 0.5	11 ± 2
PrZ	2800 ± 200	1430 ± 90	900 ± 60	780 ± 30	1010 ± 60	860 ± 30	750 ± 40	2500 ± 700

Error represents standard deviation from at least n = 4 microrings in a single detection experiment. NA values were unable to be calculated.

REFERENCES

(1)   Shaw, A. W.; Pureza, V. S.; Sligar, S. G.; Morrissey, J. H. The Local Phospholipid Environment Modulates the Activation of Blood Clotting. *J. Biol. Chem.* **2007**, *282* (9), 6556–6563.

(2)   Tavoosi, N.; Smith, S. A.; Davis-Harrison, R. L.; Morrissey, J. H. Factor VII and Protein C Are Phosphatidic Acid-Binding Proteins. *Biochemistry* **2013**, *52* (33), 5545–5552.

(3)   Davie, E. W.; Fujikawa, K.; Kisiel, W. The Coagulation Cascade: Initiation, Maintenance, and Regulation. *Perspect. Biochem.* **1991**, *30* (42), 10363–10370.

(4)   Zwaal, R. F. A.; Comfurius, P.; Bevers, E. M. Lipid–Protein Interactions in Blood Coagulation. *Biochim. Biophys. Acta (BBA)-Reviews Biomembr.* **1998**, *1376* (3), 433–453.

(5)   Leventis, P. A.; Grinstein, S. The Distribution and Function of Phosphatidylserine in Cellular Membranes. *Annu. Rev. Biophys.* **2010**, *39*, 407–427.

(6)   Neuenschwander, P. F.; Morrissey, J. H. Roles of the Membrane-Interactive Regions of Factor VIIa and Tissue Factor: The Factor VIIa Gla Domain Is Dispensable for Binding to Tissue Factor but Important for Activation of Factor X. *J. Biol. Chem.* **1994**, *269* (11), 8007–8013.

(7)   Neuenschwander, P. F.; Bianco-fisher, E.; Rezaie, A. R.; Morrissey, J. H. Phosphatidylethanolamine Augments Factor Vila — Tissue Factor Activity : Enhancement of Sensitivity to Phosphatidylserine. *Biochemistry* **1995**, *34* (43), 13988–13993.

(8)   Tavoosi, N.; Davis-Harrison, R. L.; Pogorelov, T. V.; Ohkubo, Y. Z.; Arcario, M. J.; Clay, M. C.; Rienstra, C. M.; Tajkhorshid, E.; Morrissey, J. H. Molecular Determinants of Phospholipid Synergy in Blood Clotting. *J. Biol. Chem.* **2011**, *286* (26), 23247–23253.

(9)   Smeets, E. F.; Comfurius, P.; Bevers, E. M.; Zwaal, R. F. A. Contribution of Different Phospholipid Classes to the Prothrombin Converting Capacity of Sonicated Lipid Vesicles. *Thromb. Res.* **1996**, *81* (4), 419–426.

(10)   Smirnov, M. D.; Esmon, C. T. Phosphatidylethanolamine Incorporation into Vesicles Selectively Enhances Factor Va Inactivation by Activated Protein C. *J. Biol. Chem.* **1994**, *269* (2), 816–819.

(11)   Denisov, I. G.; Grinkova, Y. V.; Lazarides, A. A.; Sligar, S. G. Directed Self-Assembly of Monodisperse Phospholipid Bilayer Nanodiscs with Controlled Size Directed Self-

143

Assembly of Monodisperse Phospholipid Bilayer Nanodiscs with Controlled Size. *Nano Lett.* **2004**, *126* (11), 3477–3487.

(12)   Bayburt, T. H.; Sligar, S. G. Membrane Protein Assembly into Nanodiscs. *FEBS Lett.* **2010**, *584* (9), 1721–1727.

(13)   Sloan, C. D. K.; Marty, M. T.; Sligar, S. G.; Bailey, R. C. Interfacing Lipid Bilayer Nanodiscs and Silicon Photonic Sensor Arrays for Multiplexed Protein − Lipid and Protein − Membrane Protein Interaction Screening. *Anal. Chem.* **2013**, *85* (5), 2970–2976.

(14)   Muehl, E. M.; Gajsiewicz, J. M.; Medfisch, S. M.; Wiersma, Z. S. B.; Morrissey, J. H.; Bailey, R. C. Multiplexed Silicon Photonic Sensor Arrays Enable Facile Characterization of Coagulation Protein Binding to Nanodiscs with Variable Lipid Content. *J. Biol. Chem.* **2017**, *292* (39), 16249–16256.

(15)   Bayburt, T. H.; Grinkova, Y. V.; Sligar, S. G. Self-Assembly of Discoidal Phospholipid Bilayer Nanoparticles with Membrane Scaffold Proteins. *Nano Lett.* **2002**, *2* (8), 853–856.

(16)   Iqbal, M.; Gleeson, M. a; Spaugh, B.; Tybor, F.; Gunn, W. G.; Hochberg, M.; Baehr-jones, T.; Bailey, R. C.; Gunn, L. C.; Resonators, R.; Optical, H.; Iqbal, M.; Gleeson, M. a; Spaugh, B.; Tybor, F.; Gunn, W. G.; Hochberg, M.; Baehr-jones, T.; Bailey, R. C.; Gunn, L. C. Label-Free Biosensor Arrays Based on Silicon Scanning Instrumentation. *IEEE J. Sel. Top. Quantum Electron.* **2010**, *16* (3), 654–661.

(17)   Byeon, J.-Y.; Limpoco, F. T.; Bailey, R. C. Efficient Bioconjugation of Protein Capture Agents to Biosensor Surfaces Using Aniline-Catalyzed Hydrazone Ligation. *Langmuir* **2010**, *26* (19), 15430–15435.

(18)   Luchansky, M. S.; Washburn, A. L.; Qavi, A. J.; Kindt, J. T.; McClellan, M. S.; Bailey, R. C. Silicon Photonic Microring Resonator Arrays for Scalable and Multiplexable Bioanalysis. *Proc. SPIE* **2011**, *7888*, 1–4.

(19)   Wade, J. H.; Alsop, A. T.; Vertin, N. R.; Yang, H.; Johnson, M. D.; Bailey, R. C. Rapid, Multiplexed Phosphoprotein Profiling Using Silicon Photonic Sensor Arrays. *ACS Cent. Sci.* **2015**, *1* (7), 374–382.

(20)   Washburn, A. L.; Shia, W. W.; Lenkeit, K. A.; Lee, S.-H.; Bailey, R. C. Multiplexed Cancer Biomarker Detection Using Chip-Integrated Silicon Photonic Sensor Arrays. *Analyst* **2016**, *141* (18), 5358–5365.

(21)   Dunlap, W. P.; Silver, N. C. Confidence Intervals and Standard Errors for Ratios of Normal Variables. *Behav. Res. Methods, Instruments, Comput.* **1986**, *18* (5), 469–471.

(22)   Vance, J. E.; Steenbergen, R. Metabolism and Functions of Phosphatidylserine. *Prog. Lipid Res.* **2005**, *44* (4), 207–234.

CHAPTER V

DNA-Tethered Nanodisc Arrays for Quantitative Characterization of Blood Coagulation Factor Lipid-Protein and Membrane Protein-Protein Interactions on Silicon Photonic Microring Resonators

Abstract

Initiation, propagation, and amplification of the blood coagulation cascade is reliant on lipid-protein interactions. These interactions are governed by soluble blood coagulation factors containing regions rich in γ-carboxyglutamate termed GLA domains. We have previously characterized GLA domain interactions with Nanodiscs on silicon photonic microring resonators by generating electrostatic Nanodisc arrays. This technique provides a simple, label-free method for comparison between environments in a single experiment but lacks control over Nanodisc orientation on the sensor surface. This lack of orientation control shows differences in surface functionalization when the Nanodisc environment varies in charge. To control the loading of Nanodiscs, we have covalently labeled MSP with DNA tags for assembly of labeled Nanodiscs. This DNA tethered Nanodisc anchoring to the surface provides unhindered access to incorporated membrane proteins; thus, allowing for characterization of up to 30 different membrane protein environments in a single experiment. DNA-tagged Nanodiscs loading on the sensor surface is observable for quantitation of lipid environment coverage to calculate protein binding per leaflet. Herein, we compare binding of the GLA domain-containing blood coagulation factor prothrombin to Nanodiscs arrayed on silicon photonic microring resonators using DNA-tagging and physisorption to show the optimization to lipid environment array generation that DNA-tagging provides. The lipid binding differences between GLA domains of prothrombin and factor X (fX)

146

are then compared to the discoidin C2 domain of factor Va through calculation of dissociation constants and protein binding per Nanodisc leaflet. To demonstrate the environment variation potential using DNA-tagged Nanodiscs, wildtype tissue factor (TF) binding was characterized with fX and factor IX (fIX) in various lipid environments. Here, we observed that lipids play a key role in selective association between fX and fIX to the membrane for interactions with TF without fVIIa.

1. Introduction

Membranes play essential roles in cellular processes such as cell signaling, trafficking, and compartmentalization. Even though membrane proteins make up 23% of the proteome,[1] over 60% of drugs are designed to target these proteins.[2] Therefore, characterization of the membrane environment and membrane proteins is crucial to understanding physiological processes and designing therapeutics. Interactions between proteins and lipids rely on electrostatic attraction and binding domains with almost exclusively involving acidic phospholipids as targets.[3,4] The driving forces are due to either high chemical or stereo-specificity, physical properties like charge or membrane curvature, or second messengers such as calcium ions. This complex environment of lipid-protein and membrane protein-protein interactions shows the need for a highly multiplexable technique to efficiently screen variables such as membrane environment and protein mutations for adequate characterization.

There are many characterization techniques for membrane protein interactions,[5] but not all of these techniques accurately portray the physiological membrane environment. Use of a bilayer membrane mimic is necessary to accurately portray physiological interactions at the membrane interface *in vitro*. One option for a bilayer environment is to use a supported bilayer which are easily assembled for surface-sensitive technique characterization.[6,7] The disadvantage to this technique is the surface restrained nature of the bilayer. This has been overcome by utilizing surface tethering,[8] but the bilayer surface is still susceptible to defects. Another option is bicelles which are lipid aggregates stabilized by short chain phospholipids or detergents.[9,10] The main limitations to bicelle use for studies is the limited list of lipids and detergents that can be used to form the bilayer.[11] Liposomes overcome these surface defects and limited reagent use by forming spherical bilayer vesicles by mechanical and chemical means.[12,13] However, strategic filtration

methods need to be employed to ensure an even distribution of liposome size, and they are prone to aggregation overtime.

High-density lipoprotein (HDL) mimetics overcome these limitations by utilizing a stabilizing agent such as peptides, polymers, DNA, or proteins to for disc-like bilayers termed "nanodiscs." These stabilizing agents are designed to be chemically similar to apolipoprotein A-I (apoA-I) which is found in biology for cholesterol transport.[14–16] Peptide nanodiscs were originally designed to characterize apoA-I HDL formation.[17–19] Their continued optimization has led to the development of treatments for various diseases such as coronary heart [20,21] and cancer.[22–26] The major limitation to peptide nanodiscs is the inability to control the number of peptides in disc formation which prevents control over functional groups for other applications. Polymer nanodiscs utilize amphipathic copolymers for HDL formation without the need for detergent.[27–31] The use of polymer to form nanodiscs does not eliminate the control over functional groups problem with peptide nanodiscs. Protein Nanodiscs utilize a membrane scaffold protein (MSP)[32] and have been extensively characterized to show that each disc contains two MSPs surrounding the lipids.[33–35] This feature makes Nanodiscs an ideal candidate for studying lipid-protein and membrane protein-protein interactions using a multitude of techniques.[36–39] A few noteworthy characterization techniques are activity assays,[40,41] NMR,[42–47] mass spectrometry,[48–51] fluorescence resonance energy transfer (FRET),[34,52–54] fluorescence polarization,[55] single Nanodisc array,[56] and surface plasmon resonance (SPR).[57–63]

Nanodiscs have been used to study numerous biological systems, including the extrinsic pathway of the blood coagulation cascade. In the extrinsic pathway, tissue damage exposes phosphatidylserine (PS) and tissue factor (TF), an integral membrane protein, to the inner blood vessel.[64] These are key elements for the recruitment and activation of blood coagulation factors starting with activated factor VII (fVIIa) to ultimately lead to a blood clot.[65] The TF-fVIIa complex activates factor X (fX to fXa) and factor IX (fIX to fIXa). Amplification of fXa production occurs through the fIXa-fVIIIa (activated factor VIII) complex. The influx of fXa is used to generate the prothrombinase complex formed with fXa and activated factor V (fVa) for activation of prothrombin (PT) to thrombin.[66] Thrombin acts to promote blood clot formation and coagulation cascade negative feedback.[65] The majority of these complex formations are occurring at the membrane interface driven by γ-carboxyglutamate-rich (GLA) domains that selectively bind to PS

headgroups using Ca^{2+} as a second messenger[67] or with discoidin C2 domains that bind PS using tryptophan.[68,69] Nanodiscs have been used to probe the calcium influence on the GLA domains using solid-state NMR,[70] calculate activities of clotting factors using colormetric assays,[71,72] and calculate dissociation constants using SPR.[73] These binding characterizations have only been performed for GLA domain association to PS and for fVIIa to TF.[74–76] Interactions with TF and fX or fIX have been studied only using activity assays.[77,78]

In this space, the Bailey lab has collaborated to expand the multiplexity of the screened interactions by utilizing Nanodiscs on silicon photonic microring resonators. This allows for reliance on electrostatic interactions between lipid headgroups and the silicon oxide surface to generate label-free arrays.[79] Physisorbed Nanodisc arrays on silicon photonic microring resonators increases the multiplexity up to 9 different lipid environments to be observed in a single experiment.[80,81] Though physisorption is an easy array generating technique, electrostatic interactions are not stable over time and do not provide control over Nanodisc orientation which will be more problematic with various charged lipids and incorporation membrane proteins.

Herein, we have expanded the Nanodisc utility on silicon photonic microring resonators by tethering Nanodiscs to the surface using DNA. The conjugation of DNA to MSP is done prior to Nanodisc formation and does not negatively affect assembly. DNA arrays are beneficial for their stability overtime and quantitation of Nanodisc loading. This technique eliminates lipid charge and incorporated protein electrostatic obstacles by tethering the Nanodiscs above the surface for monitoring of lipid-protein or membrane protein-protein interactions. To show the benefits of this technique, we have compared the loading differences of various lipid composition Nanodiscs using physisorption to the control with DNA-tagged Nanodiscs. To show that the technique is not biasing the normalization, different loading amounts of the same Nanodisc environment with various DNA tags are loaded. These arrays can be used to characterize different binding domains present such as the GLA domain of PT or fX and the discoidin C2 domain of Va from the blood coagulation cascade. Finally, an array of DNA-tagged Nanodiscs with various lipid environments with and without TF were used to characterize fX and fIX binding.

2. Materials and Methods

Chemicals and reagents

Phosphatidylcholine (PC; 1-palmitoyl-2-oleoyl-sn-glycero-3-phosphochiline), phosphatidylserine (PS; 1-palmitoyl-2-oleoyl-sn-glycero-3-phospho-L-serine), phosphatidic acid (PA; 1-palmitoyl-2-oleoyl-sn-glycero-3-phosphate), phosphatidylethanolamine (PE; 1,2-dipalmitoleoyl-sn-glycero-3-phosphoethanolamine), phosphatidylinositol-3,4,5-triphosphate (PI(3,4,5)P$_3$; 1,2-dioleoyl-sn-glycero-3-phospho-(1'-myo-inositol-3',4',5'-triphosphate), and total ganglioside extract (GM) were purchases from Avanti Polar Lipids (Alabaster, AL, USA). Chemicals were purchased from Sigma Aldrich (St. Louis, MO, USA) unless otherwise indicated. HisPur Ni-NTA (nitrilotriacetic acid) Resin, succinimidyl-[(N-maleimidopropionamido)-hexaethyleneglycol]ester (SM(PEG)$_6$), AminoLink^{TM} Plus Immobilization Kit, Pierce BCA protein assay kit, and StartingBlock^{TM} (PBS) Blocking Buffer were purchased from ThermoFisher Scientific (Waltham, MA, USA). DryCoat Assay Stabilizer was purchased from Virusys Corporation (Taneytown, MD, USA). Syringe filters (0.22 μm pore size) and Amberlite$^®$ XAD$^{®-}$2 beads were purchased from MilliporeSigma (Burlington, MA, USA). Custom DNA oligonucleotides were synthesized by Integrated DNA Technologies (IDT, San Jose, CA, USA) (See **Table V.1** for sequences). MSP1D1 D73C (aspartic acid 73 mutated to cysteine) sequence was synthesized and cloned into pET-28a(+) vector by GenScript (Piscataway, NJ, USA). Prothrombin and factor X were purchased from Enzyme Research Laboratories (South Bend, IN, USA). Factor Va was purchased from Haematologic Technologies, Inc. (Essex Junction, VA, USA). MSP1D1, Tissue factor (wildtype and mutants), and HPC4 columns were generously provided by the Morrissey Lab (University of Michigan, Department of Biological Chemistry, Ann Arbor, MI, USA).

MSP1D1 D73C expression and purification

MSP1D1 D73C was expression in BL21-Gold(DE3) competent cells (Agilent, Santa Clara, CA, USA) was modified from a previously described protocol.[82] Briefly, 50 mL of LB medium containing 30 μg/mL kanamycin was inoculated with a single colony and grown at 37°C while shaking at 250 rpm overnight. The starting culture was immediately used to inoculate 1 L of TB medium containing 10 μg/mL and 0.1-0.2 mL of Antifoam A. The culture was grown at 37°C while shaking at 250 rpm until the OD$_{600}$ reached 0.6-0.8 after about 2-3 hours. Induction with 1 M IPTG (isopropyl β-D-1-thiogalactopyranoside) was performed at 37°C while shaking at 250 rpm for 3 hours. Cells were collected by centrifugation at 8k xg for 15 minutes at 4°C. The cell

pellet was lysed by sonication in 10 mL of lysis buffer (200 mM sodium phosphate, 1% Triton X-100, pH 7.4) with the addition of a tablet of cOmplete, EDTA-free Protease Inhibitor Cocktail. Clarification was performed at 17k xg for 20 minutes at 4°C. The cleared lysate was loaded onto a 3 mL HisPur Ni-NTA column that was washed with 10 column volumes of equilibration buffer (40 mM Tris, 300 mM sodium chloride, 1% Triton X-100, pH 8) at 700 xg for 2 minutes at 4°C. Washes of the loaded cleared lysate were performed with 10 resin volumes of (1) equilibration buffer with 50 mM sodium cholate and 20 mM imidazole and (2) equilibration buffer with 50 mM imidazole with the same centrifuge conditions as the column equilibration. Elution was performed with equilibration buffer with 500 mM imidazole with pooled fractions of 3 resin volumes while monitoring absorbance at 280. Purification was confirmed using SDS-PAGE (4-20%). MSP1D1 D73C containing elution fractions were concentrated using 10K MWCO concentrators then buffer exchanged into standard disc buffer for long storage using desalting columns.

MSP1D1 D73C conjugation to DNA

SM(PEG)$_6$ was dissolved in dry DMSO. DNA capture probes (**Table V.1**) were dissolved in phosphate buffer saline (PBS; 10 mM sodium phosphate, 154 mM sodium chloride, pH 7.4) while DNA tags for conjugation were dissolved in PBS-8(+) (10 mM PBS, 3 mM EDTA, pH 8). Conjugation of DNA tags and SM(PEG)$_6$ was performed at a 10:1 mole ratio of SM(PEG)$_6$ to DNA in PBS-8(+) with 20% DMSO mixing at room temperature for 1 hour. Excess SM(PEG)$_6$ was removed by concentrating and buffer exchanging into PBS-6.5(+) (10 mM PBS, 3 mM EDTA, pH 6.5). MSP1D1 D73C in PBS-6.5(+) that was purged with argon for at least 30 minutes then incubated at a 10:5:1 mole ratio of sodium cholate to TCEP to MSP1D1 D73C for 15 minutes to ensure reduction of disulfide bonds. DNA was added to the reduced MSP1D1 D73C at a mole ratio of 8:1 for 2 hours at room temperature or overnight at 4°C. Removal of excess DNA was performed by purification of MSP1D1 D73C using Ni-NTA purification. Purified samples were buffer exchanged into SDB (20 mM Tris, 100 mM NaCl, 0.5 mM EDTA, 0.01% NaN$_3$, pH 7.4). To confirm conjugation, fluorescein-tagged DNA was coupled to MSP. Conjugation was confirmed using SDS-PAGE staining with either Coomassie Blue or Krypton^{TM} Fluorescent Protein Stain. DNA conjugated MSP was purified from unconjugated MSP using AminoLink^{TM} Plus Immobilization columns generated with capture DNA probes following the kit protocol. Purification using these columns were performed by first washing columns with SDB with

centrifugation at 1000 xg for 1 minutes at room temperature. MSP was incubated on the columns for 2 hours at room temperature or overnight at 4°C with end over end mixing. The columns were washed with 8 column volumes of SDB with 30% formamide before elution with 100% formamide at the same centrifugation conditions as equilibration. Purified DNA purified conjugated MSP was concentrated and buffer exchanged into SDB before determining concentration with BCA protein assay.

Empty Nanodisc preparation and purification

Nanodisc assembly was performed as previously described.[82,83] Briefly, phospholipids were dried at the desired mixed mole ratios of POPC, POPS, and/or POPA then vacuum incubated for a minimum of 4 hours prior to use. Lipids were reconstituted in 100 mM sodium cholate for a lipid concentration of 11.2 mM. The mole ratio of lipids to MSP1D1 or DNA-tagged MSP1D1 D73C used were 65:1 for 100% POPC, 50% POPS with 50% POPC, 50% POPA with 50% POPC and 60:1 for 50% PI(3,4,5)P$_3$ with 50% POPC and 50% GM with 50% POPC. The final concentration of MSP1D1 or DNA-tagged MSP1D1 D73C was brought to 2 μM with SDB. Nanodisc components were incubated at 4°C with end-over-end mixing for an hour before addition of half the assembly volume of Amberlite® XAD®-2 detergent removal beads with additional incubation at 4°C with end-over-end mixing for 3 hours. The detergent removal beads were removed using 0.22 μm filters. Assembled Nanodiscs were purified using a Superdex 200 Increase 3.2/30 (GE Healthcare, Pittsburgh, PA, USA) and a flow rate of 0.075 mL/min. Absorbance was observed at 280 nm and 260 nm to monitor fractions with Nanodiscs, MSP1D1 D73C, and DNA. Nanodisc concentration was determined using Qubit™ 3.0 Fluorometer (Invitrogen) Protein Assay Kit for untagged and ssDNA Assay Kit for DNA-tagged Nanodiscs.

Tissue factor containing nanodisc preparation and purification

Nanodisc assembly was performed similar to above, but with an addition of a 20:1 DNA-tagged MSP1D1 D73C to TF ratio. Lipid to MSP ratios of 65:1 and 55:1 were used for empty and TF containing Nanodiscs, respectively. Nanodiscs were prepared as discussed previously except that lipid mixtures containing PE were dissolved in 100 mM sodium deoxycholate to 11.2 mM. Assembled Nanodiscs were purified first with a calcium-dependent monoclonal antibody (HPC4) column against a synthetic peptide tag on TF to purify Nanodiscs containing TF from empty ones

as previously described.[71] Briefly, the HPC4 column was conditioned with wash buffer (20 mM Tris, 100 mM sodium chloride, 2 mM calcium chloride, 0.01% sodium azide, pH 7.4) using gravity flow. The Nanodisc sample was brought up to 2 mM calcium chloride before binding to the HPC4 column for 10 minutes mixing at room temperature. Gravity flow was used to collect unbound fractions and wash the resin with wash buffer for 20 column volumes. The Nanodiscs were eluted with elution buffer (20 mM Tris, 100 mM sodium chloride, 5 mM EDTA, 0.01% sodium azide, pH 7.4) before confirming collected fractions using SDS-PAGE. Nanodisc fractions containing TF were combined and purified using the same size exclusion chromatography mentioned earlier. Nanodisc concentration was determined using Qubit[TM] 3.0 Fluorometer ssDNA Assay Kit.

Silicon photonic microring resonators

The silicon photonic microring resonator system (Maverick M1) and sensor array chips were purchased from Genalyte, Inc. (San Diego, CA, USA). Detailed descriptions of instrumentation and sensor manufacturing are described elsewhere.[84–88] Briefly, microring resonators are silicon-on-insulator refractive index sensors with a diameter of 30 μm and an adjacent to a linear waveguide. A laser centered at 1550 cm utilizes total internal reflection to travel down the linear waveguide and couple into the microring resonator upon satisfaction of the resonant condition:

$$\lambda_r = \frac{2\pi r n_{eff}}{m} \tag{V.1}$$

where λ_r is the resonant wavelength, r is the radius of the ring, n_{eff} is the local effective refractive index, and m is an integer. The difference in resonant wavelength transmittance dip is observed as a relative shift in picometers (Δpm) which is directly related to the change in local refractive index overtime. The sensors are arrayed on a 4 mm x 6 mm chip with 128 individually addressable silicon-on-insulator rings and 4 thermal controls.

DNA array functionalization

Microring resonator chips were rinsed with acetone for 2 minutes followed by 4 minutes with 5% APTES in acetone and 2 minutes with acetone then isopropyl alcohol. There is continuous shaking during each of the rinses. The chips are then rinsed with water and dried under nitrogen before pipetting freshly prepared 2.85 mg/mL BS3 in 2 mM acetic acid onto the microring array to react for 3 minutes. Finally, chips were spotted with roughly 80 nL of 200 μM DNA Capture

sequences in discrete regions by micropipette. The chips were incubated in a humidity chamber for at least an hour prior to use. For long term storage, chips were incubated for an hour covered in StartingBlock[TM] before being dried under nitrogen and stored covered in DryCoat in a desiccator at 4°C.

DNA cross-reactivity testing

DNA functionalized chips were exposed to 200 µM ssDNA target sequences in SDB + 2.0% BSA with chip regeneration steps using formamide. The tests performed in SDB + 2.0 % BSA at 10 µL/min. The ssDNA of interest was flowed over the surface for 5 minutes, then rinsed with SDB + 2.0 % BSA for 5 minutes. The surface was regenerated with a formamide rinse 20 minutes at 10 µL/min. The DNA cross-reactivity studies are performed on the same chip until all targets have been checked and moving on to a different spotting layout.

DNA-tagged Nanodisc array loading

Chip layouts for DNA functionalized chips can be found in **Figures V.8**, **V.13A**, and **V.23**. Functionalized chips were loaded with DNA-tagged Nanodiscs by first performing an additional surface blocking step while on the instrument to ensure sufficient coating of the sensor surface with StartingBlock[TM] followed by rinsing with SDB + 2% BSA to maintain surface coverage. The surface was loaded with DNA-tagged Nanodiscs in SDB with 2.0% BSA. The loading can be performed sequentially or mixed.

Flow loaded physisorbed Nanodisc arrays

An example chip layout using flow loading is shown in **Figure V.13B**. Flow loaded arrays were generated as previously described.[79] Microring resonator chips were rinsed while shaking with acetone for 2 minutes followed by isopropyl alcohol for 2 minutes. The chips were rinsed with water and dried under nitrogen then used immediately. Nanodiscs were flowed over the surface using a 2-channel gasket at 0.5 µM or other specified concentration at 10 µL/min. The surface was then blocked with StartingBlock[TM] prior performing protein titrations.

Spotted physisorbed Nanodisc arrays

Spotted arrays were generated as previously described[80,81] with an example schematic shown in **Figure V.13C**. Briefly, Nanodiscs were diluted noted concentrations (0.25 µM to 4.00 µM). Microring resonator chips were rinsed with acetone for 2 minutes followed by isopropyl alcohol for 2 minutes before being dried under nitrogen. Nanodiscs were spotted on to the surface between 0.1 and 0.2 µL in volume under a microscope via pipette to generate spatially distinct environments. Spotted chips are incubated in a humidity chamber at 4ºC for 2 hours or overnight prior to use. Prior to performing protein binding, the chip is blocked with StartingBlock[TM].

Protein binding titrations

Titrations were performed at a flowrate of 10 µL/min in HEPES(+) buffer (10 mM HEPES, 150 mM sodium chloride, 50 µM EDTA, 0.5% BSA, 0.1% (w/v) PEG 8000, 2.5 mM $CaCl_2$, pH 7.4). Nanodisc arrays are rinsed with HEPES (no $CaCl_2$) before and after titrations.

Data analysis

Analysis of data was performed using a custom R script in RStudio. Changes in refractive index due to buffer mismatches between steps were corrected for by subtracting off-target ssDNA sequence response. Nanodisc loading was quantitated by subtracting the relative shift from the end of the first buffer step to the end of the last buffer step prior to ssDNA capping ($\Delta pm_{Nanodisc}$). This quantitation is used to calculate protein binding per Nanodisc leaflet by applying the following equation to the protein titration data:

$$Protein\ per\ leaflet = \left(\frac{\Delta pm_{Protein}}{M_{w,Protein}}\right)\left(\frac{M_{w,Nanodisc}}{\Delta pm_{Nanodisc}}\right)\left(\frac{1}{2}\right) \qquad (\textbf{V.2})$$

where $\Delta pm_{Protein}$ is the relative shift response during the protein titration, $M_{w,Protein}$ is the molecular weight of the titrated protein, $\Delta pm_{Nanodisc}$ is the quantified loading of Nanodisc, and $M_{w,Nanodisc}$ is the molecular weight of the Nanodisc. For experiments with physisorption normalization, this equation was used with and without the 0.5 multiplication factor due to inability to know the exact Nanodisc orientation on the surface. Binding curves are generated by plotting the relative shift in protein per leaflet at the equilibrium point of each titration step compared to the relative shift at

the end of the HEPES(+) step versus the concentration of protein. The curves are then fit to the following equation to characterize the binding:

$$Protein\ per\ leaflet = Protein\ per\ leaflet_{max}\ \left(\frac{X}{K_d + X}\right) \qquad \textbf{(V.3)}$$

where X is the concentration of the titrated protein and K_d is the dissociation constant. The hill coefficient gives information about the cooperativity of the binding while the K_d quantifies the binding affinity.

3. Results and Discussion

Nanodisc assembly with DNA-tagged MSP1D1 D73C

Nanodiscs made with MSP have been modified for applications such as FRET,[54] fluorescence polarization,[34,55] and MRI contrast reagent stabilization.[89] These modifications have not been used for multiplexed Nanodisc array generation. To date, Nanodisc immobilization technologies have generated single arrays using antibodies,[56] EDC chemistry,[63] or peptide nanodisc instability.[75] In order to increase the multiplexity of Nanodisc array generation, we covalently attached DNA to MSP using a single cysteine variant and amine-modified DNA. DNA was chosen as the covalent tether due to the ease of generating large, multiplexible DNA arrays. This is particularly useful because the silicon photonic microring resonator platform has the ability to functionalize 30 separate environments (with 1 off-target DNA and 1 off-target membrane control) with 4 technical replicates each.

Prior to conjugation, the DNA capture and analyte pairs (**Table V.1**) were tested to ensure there was no cross-reactivity. **Figure V.1** shows the cross-reactivity experiments in a grid. Each row represents a single experiment performed on the same array with formamide regeneration in between. No cross-reactivity was observed between the 14 DNA capture and analyte pairs.

Confirmation of conjugation was performed using fluorescein-labeled DNA. Fluorescently labeled conjugated MSP was purified using Ni-NTA columns for selectively purifying MSP to wash away excess DNA. **Figure V.2A-B** shows SDS-PAGEs for a Ni-NTA purification of Ni-NTA purification of fluorescein labeled DNA-tagged MSP. The ~7 kDa increase in size of MSP is indicative of a successful conjugation of one DNA per MSP. Further purification with

156

nonfluorescent DNA was performed using custom DNA columns (**Figure V.2C**) to ensure that Nanodiscs are assembled with only conjugated MSP.

Nanodiscs can be assembled as previously described using DNA-tagged MSP without hinderance. The hydrodynamic radius shift of Nanodiscs with DNA-tagged MSP is comparable to ssDNA (**Figure V.3**). The elution profile is unaffected by the addition of DNA to MSP. By collecting SEC data at 280 and 260 nm, the presence of DNA can be observed in the 260 to 280 ratio (**Figure V.4**) with a value around 1.6 indicating a protein and DNA mixture.

DNA-tagged Nanodisc loading on silicon photonic microring resonators

To compare the effects of Nanodisc loading on silicon photonic microring resonators using DNA-tags, Nanodiscs were assembled with high percentage of different lipids with and without DNA (**Figure V.5**). The environments chosen were 100% phosphatidylcholine (PC) to act as a control, 50% PS and 50% phosphatidic acid (PA) for highly negatively charged naturally abundant lipids, and 50% phosphatidylinositol-3,4,5-triphosphate (PIP$_3$) and 50% ganglioside (GM) for bulky lipid headgroups.

Physisorption experiments utilize an electrostatic interaction between lipid headgroups of the Nanodisc and the silicon oxide coated microring surface.[79–81] These experiments are all performed on new microring chips with 100% PC used as a control to correct for chip-to-chip variation (**Figure V.6A-D**). The loading in question for each of these experiments is calculated by the change in relative shift from the beginning to the end buffer rinse. These various lipid environments show a wide range of loading at the same concentration that is not comparable to 100% PC. Even when the concentration of 50% PIP$_3$ is increased to 15x 100% PC similar loading is not achieved (**Figure V.6D-I**). For further comparison, 100% PC and 50% PIP$_3$ were run at a lower concentration for a longer binding time but showed comparable difference in binding to before (**Figure V.7**). This maximum loading of Nanodiscs with various charges is due to the negatively charged silicon oxide surface that will functionalize easier with non-anionic lipids, especially PC. These results align with negative charge calculations for Nanodiscs containing PS, PA, and a similar PIP lipids.[90]

DNA-tagged Nanodisc loading was performed using the sensor layout in **Figure V.8** where DNA capture probes are spatially arrayed. **Figure V.9** shows sequential loading of each Nanodisc

with binding to their complementary DNA strand. This experiment is controlled to an off-target ssDNA strand to subtract out any bulk refractive index shifts that can occur from buffer mismatches between steps. The loading for each of these Nanodiscs is comparable between environments. The sensor surface can be regenerated with a formamide rinse for reproducible loading sequentially (**Figure V.10A**) or mixed (**Figure V.10B**). The maximum relative shift of Nanodisc loading using DNA tags is similar to that of DNA-tagged antibodies shown previously[91] and is higher than DNA alone at the same concentration (**Figure V.10C**). Compared to physisorption, the loading of DNA-tagged Nanodiscs is more dynamic when changing the concentrations of the Nanodiscs (**Figure V.10D-I**).

Calculated relative shifts can be found in **Figure V.11**. For comparison of physisorption to DNA-tagging, the relative shift to 100% PC was calculated for each experiment to control for the method and chip-chip difference (**Figure V.12**). Using physisorption, Nanodiscs of various charge and sterically hindered environments are not loaded onto the sensor surface equally (**Figure V.12A**). The use of DNA-tagged loading of Nanodiscs above the surface overcomes these charge and steric differences to achieve similar loading (**Figure V.12B**). The challenge of surface loading cannot be overcome by adjusting the concentration for physisorption (**Figure V.12C**); however, this can provide control over DNA-tagged Nanodisc loading (**Figure V.12D**). This shows that overall, DNA-tagged Nanodiscs can overcome lipid environment challenges and provide control over surface loading that physisorption cannot.

Performing per leaflet studies using DNA-tagged Nanodiscs

To further characterize the DNA-tagged Nanodisc loading method, arrays were compared using DNA-tags and physisorption with flow loading[79] and spotting[80,81] (**Figure V.13**). These arrays were generated with 50% PS Nanodiscs for subsequent titrations with prothrombin for binding characterization with and without loading corrections. Prior to generating DNA-tagged Nanodisc arrays, the surface is blocked then Nanodiscs are functionalized to their complement surface capture (**Figure V.14A-B**). The array was designed to load three different quantities of 50% PS Nanodiscs for surface loading correction. In comparison, sensor arrays with physisorbed Nanodiscs undergo flow loading or spotting prior to surface blocking (**Figure V.14C-D**). Arrays generated with DNA-tags and using flow loading are performed online for observation and

calculation of surface loading while spotted Nanodisc arrays cannot be quantified. Each of these different arrays was used to perform a PT titration.

Data workup for PT titrations on these arrays are shown side-by-side in **Figure V.15**. The data analysis for Nanodisc spotting has been shown previously by simply subtracting 100% PC Nanodiscs. This can prove to be a problem if there are more nonspecific interactions are happening due to there being more binding site available than for specific interactions simply due to the Nanodisc array orientation and availability. This is shown in the spotted physisorption workup for the low concentration spotted nanodisc. Using flow loading, the loading can be corrected for, but there is a limit to a 2-environment maximum based on the flow cell. DNA-tagged Nanodiscs overcome this limitation.

The data analysis for DNA-tagged Nanodiscs is shown in **Figure V.16**. The surface loading is quantitated from ssDNA-controlled data by subtracting the relative shift in the buffer step prior to loading from the equilibrated buffer after loading (**Figure V.16**). The ssDNA control accounts for any bulk refractive index shifts that can occur from buffer mismatches between steps. Next, a protein titration is run on the surface, **Figure V.16B**. The protein titration data shows little to no nonspecific binding to the dsDNA (green), ssDNA (orange and yellow), and 100% PC (black) controls. To account for bulk refractive index changes, the protein titration is corrected to one of the ssDNA controls, **Figure V.16C**. This correction ensures that any bulk changes are not amplified during the loading correction step. Loading correction or normalization was performed using **Equation V.2**. Every microring is corrected to account for the differences from the DNA capture array from microring to microring. This is shown in **Figure V.16D** where the data is now plotted as prothrombin per leaflet. This correction shows that titration with PT on the differential loaded 50% PS Nanodiscs are more similar than they originally appeared to be.

This data can then be worked up in the normal manner by subtracting 100% PC (**Figure V.16E**) then plotting the net shifts at each concentration against the concentration to characterize binding (**Figure V.16F**) using the **Equation V.3**. This data workup was performed on the same DNA-tagged Nanodisc array two times and once on newly reloaded chip that was rinsed with formamide prior to loading (**Figure V.17**). The values are reproducible between chip regenerations by removing calcium to make PT dissociate and on the newly loaded chip.

159

Binding curves for each of the data workup methods are shown in **Figure V.18** with values for the fits shown in **Table V.2**. The DNA-loading variations are within error of each other for K_d calculations but do vary in maximum loading due to potential biological differences in lipid packing. Regardless of normalization of the data or not, the dissociation constants are between 1.2-1.5 µM which is similar to literature reported values.[73] When looking at physisorption flow loading, calculating the maximum shift can be done by assuming access to one side of the Nanodisc with the Nanodisc laying flat on the microring or with assuming access to both sides with the Nanodisc oriented at an angle on the surface since there is no way to truly control this orientation using physisorption. This provides very different values for maximum total binding and subsequent lipid binding calculations. The dissociation constants for physisorption flow loading with and without normalization are different. They are also different from the dissociation constants calculated from Nanodisc spotting. In previous studies using physisorption, the actual calculated values were not the aim of the paper, the trends between environments were the focus that matched literature.[80,81] Using DNA-tagged Nanodiscs, we are able to observe values that more closely match literature for dissociation constant and maximum protein bound per leaflet.[73]

Further demonstration of DNA-tagged Nanodiscs was used to compare the GLA domains of PT and fX to the discoidin C2 domain of fVa (**Figure V.19**). Experiments were performed sequentially on the same Nanodisc loaded chip using the differential loaded Nanodiscs as biological replicates. The observed K_d values for PT and fX are drastically different while the total protein per leaflet is similar (**Figure V.20** and **Table V.3**). This trend matches previously published data[73] but has not been observed using silicon photonic microring resonators previously.[80,81] In contrast, the discoidin C2 binds the membrane more with a higher binding affinity (lower K_d) on the nM scale[68,69] but with a much lower maximum protein binding due to the need for many more PS headgroup interactions for binding. Thus, this demonstrates the ability of the DNA-tagged Nanodisc technique to distinguish proteins within and between a lipid binding domain families.

Characterization of TF binding to fX and fIX

The main limitation to physisorption other than the lipid charge constraints is the inability to array Nanodiscs with a membrane protein incorporated. Using DNA-tagged Nanodiscs, the Nanodisc sits above the sensor surface which allows a membrane protein of interest to be studied.

Coagulation factors in the extrinsic pathway are activated at the membrane surface by enzymatic complexes. The first enzymatic complex in the cascade, the extrinsic tenase, is formed with soluble fVIIa and integral membrane protein TF.[64] Association to the membrane for fX and fIX activation by the extrinsic tenase is driven through interactions with PS with their GLA domains.[65] The mechanism for activation of fX has been proposed to associate with the exosite of TF prior to docking for cleavage.[78] It has also been shown that PS and phosphatidylethanolamine (PE) can cooperate to enhance activity of the extrinsic tenase.[92]

The previously mentioned studies relied on activity assays to characterize the interactions in the activation of fX and/or fIX. Here, we utilized DNA-tagged Nanodiscs with and without TF incorporated to characterize the binding of fX and fIX to TF. Environments without TF act as a control to tease out interactions with TF compared to the phospholipids. Due to the weak binding of fVIIa,[73] the interactions were simplified by omitting fVIIa from the complex to observe TF interactions alone with fX or fIX.

TF can be easily incorporated into DNA-tagged Nanodiscs (**Figure V.21A**) with selective purification for Nanodiscs containing TF using HPC4 affinity column against TF (**Figure V.21B, full image Figure V.22A**). The panel of lipid environments was designed based on previous study observations of fVIIa binding with phosphatidic acid (PA)[73,93] and PS-PE synergy of GLA domains with[92] and without[72,81] TF. Using this knowledge, Nanodiscs were assembled with and without TF using 20% PS; 5% PA; 35% PE; 20% PS 5% PA; 20% PS 35% PE; 20% PS 5% PA 35% PE; and 100% PC as a control (**Figure V.22B-C**). Each environment was formed with a different DNA-tagged MSP for generating 14-plex array on the silicon photonic microring resonator surface (**Figure V.23**). Titrations with fX and fIX were performed on this array then normalized to loading using **Equation V.2**, controlled for by subtracting interactions to 100% PC with no TF to deconvolute binding to PC, and finally a binding curve was fit using **Equation V.3**. The titrations and binding curves are shown in **Figure V.24** with binding values in **Table V.4**. The dissociation constants for each lipid environment with and without TF are plotted in **Figure V.25**. fX (**Figure V.25A**) demonstrates less binding specificity due to the lipid environment than fIX (**Figure V.25B**) due to overall more observed binding; however, fIX displayed a higher binding affinity. No binding was observed in either case with TF in 100% PC which supports the "Anything

But Choline" (ABC) hypothesis that phospholipids other than PC are needed to support GLA domain interactions.[72]

In all cases with 20% PS, binding was observed with and without TF for fX (**Figure V.25A**). The binding affinity for these environments were tighter without TF except in the mixture of 20% PS 5% PA 35% PE where the binding is comparable. These observations make deconvolution of binding to just TF to conclude on due to the high affinity for these lipid environments with fX. There were no observable interactions with fX in 5% PA or 35% PE alone; however, the binding was revived in the presence of TF. fX activation and binding with PA alone have been shown previously,[73,93] but never before has binding with PA and TF in the membrane been shown at this low abundance of PA. For the 5% PA environment there are about 3 PA molecules per leaflet due to each leaflet containing about 67 phospholipid[82] and the integral membrane region of TF being small enough to have little effect on lipid incorporation.[71,94] Typically, 5-7 PS molecules are need for the GLA domain to associate to the membrane;[71,73] however, TF and ~3 PA molecules are able to provide enough support for binding for fX (**Figure V.25A**, blue). Similarly, PE alone is unable to support GLA domain binding,[72,81] but here PE and TF are showing binding affinity with fX (**Figure V.25B**, blue).

In comparison to fX, fIX shows similar binding with and without TF in 20% PS making this environment hard to conclude on interactions directly with TF (**Figure V.25B**, red). The binding with fIX is different from fX due to the lack of binding to most lipid environments. Exceptions are seen with the mixtures of 20% PS 5% PA and 20% PS 35% PE. These binary mixtures show binding to fIX in the presence of TF only (**Figure V.25B**, green and orange). This observation demonstrates a potential synergistic interaction with PS/PA and PS/PE in the presence of TF that has never been characterized for binding.

The binding between fX and fIX with TF without fVIIa has not been characterized. This provides a more simplistic system to understand the localization of fX and fIX for activation. There are very different binding affinities for fX and fIX observed with and without TF based on the lipid environment (**Figure V.25**). These stark differences based on lipids alone could be part of the mechanism for determining which substrate to activate by the extrinsic tenase. The binding trends may be different in the presence of fVIIa. Future experiments into this area using a wider

range of lipids, incorporation of fVIIa, and maybe mutants of any of these coagulation factors could shed light on what is species are driving the association of fX and fIX to the membrane for activation.

4. Conclusion

In summary, we have developed a new DNA-tagged Nanodisc platform for interfacing with silicon photonic microring resonators. This technique positions the Nanodisc above the sensor surface to eliminate environmental effects on Nanodisc array generation that can be the result of highly charged lipids or incorporation of a membrane protein of interest. These DNA-tethered Nanodisc arrays were used to characterize the binding of PT, fX, and fVa with per leaflet calculations that have not been feasible using physisorption of Nanodiscs to the microrings.

Using DNA arrays, the multiplexity of a membrane protein experiment was pushed to observe 14 total environments in a single experiment: 7 different lipid environments with and without TF incorporated. When characterizing fX binding to TF, the interaction was difficult to deconvolute in the presence of 20% PS due to similar binding with and without TF; however, binding was observed with 5% PA and 35% PE alone with TF only. In comparison, fIX binding in 20% PS was also difficult to determine the contributions of TF to the association, but binding was observed to 20% PS mixed with 5% PA or 35% PE only with TF present. These differences in binding due to the environment demonstrate that there may be a lipid dependence in associating fX or fIX for activation. Future work using more mixture of lipids, mutants of clotting factors, and incorporating fVIIa into the complex will be necessary to determine what factors are determining the substrate specificity between fX and fIX.

Overall, the DNA-tagged Nanodisc platform coupled with silicon photonic microring resonators allows for high multiplexity studies of lipid-protein and membrane protein-protein interactions. Further development on this platform will involve screening of more DNA complement pairs to increase the throughput even further.

5. Acknowledgements

Interactions at the Membrane Interface in the Blood Coagulation Cascade on Silicon Photonic Microring Resonators."
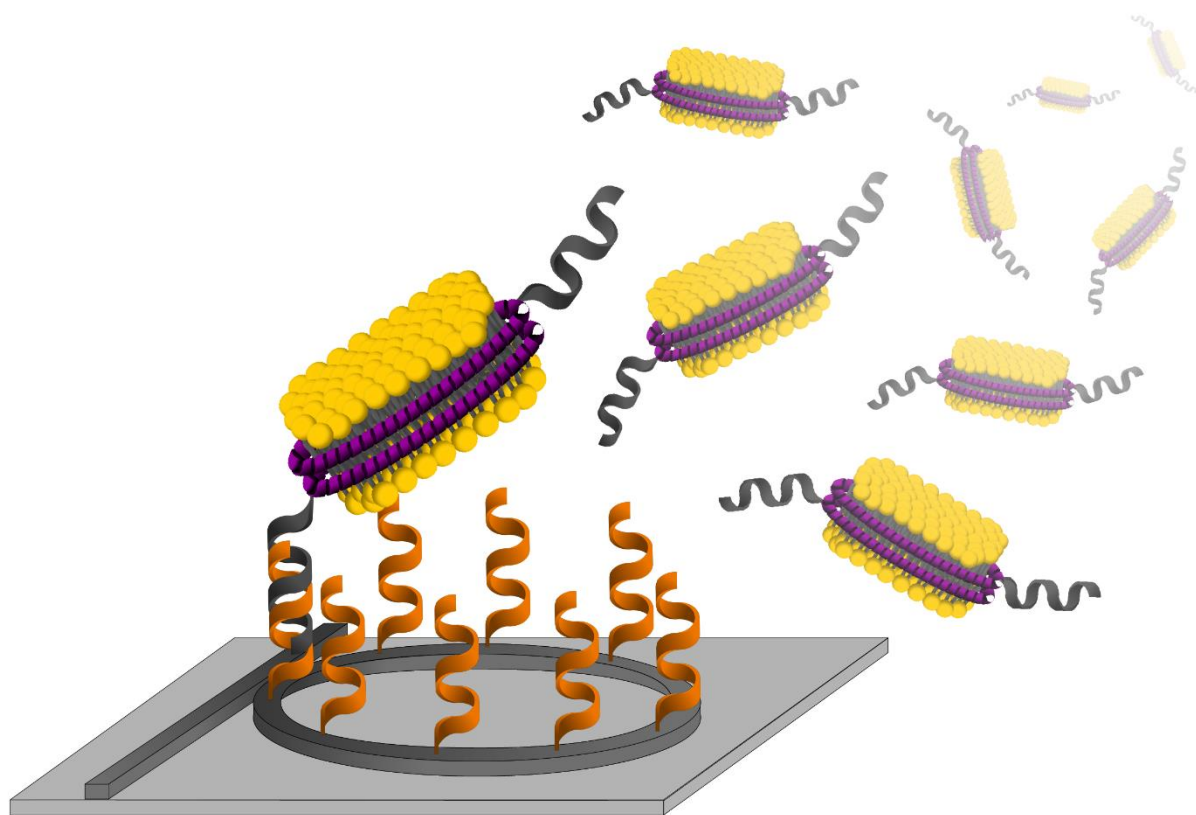
Figure V.0. Graphical Abstract.
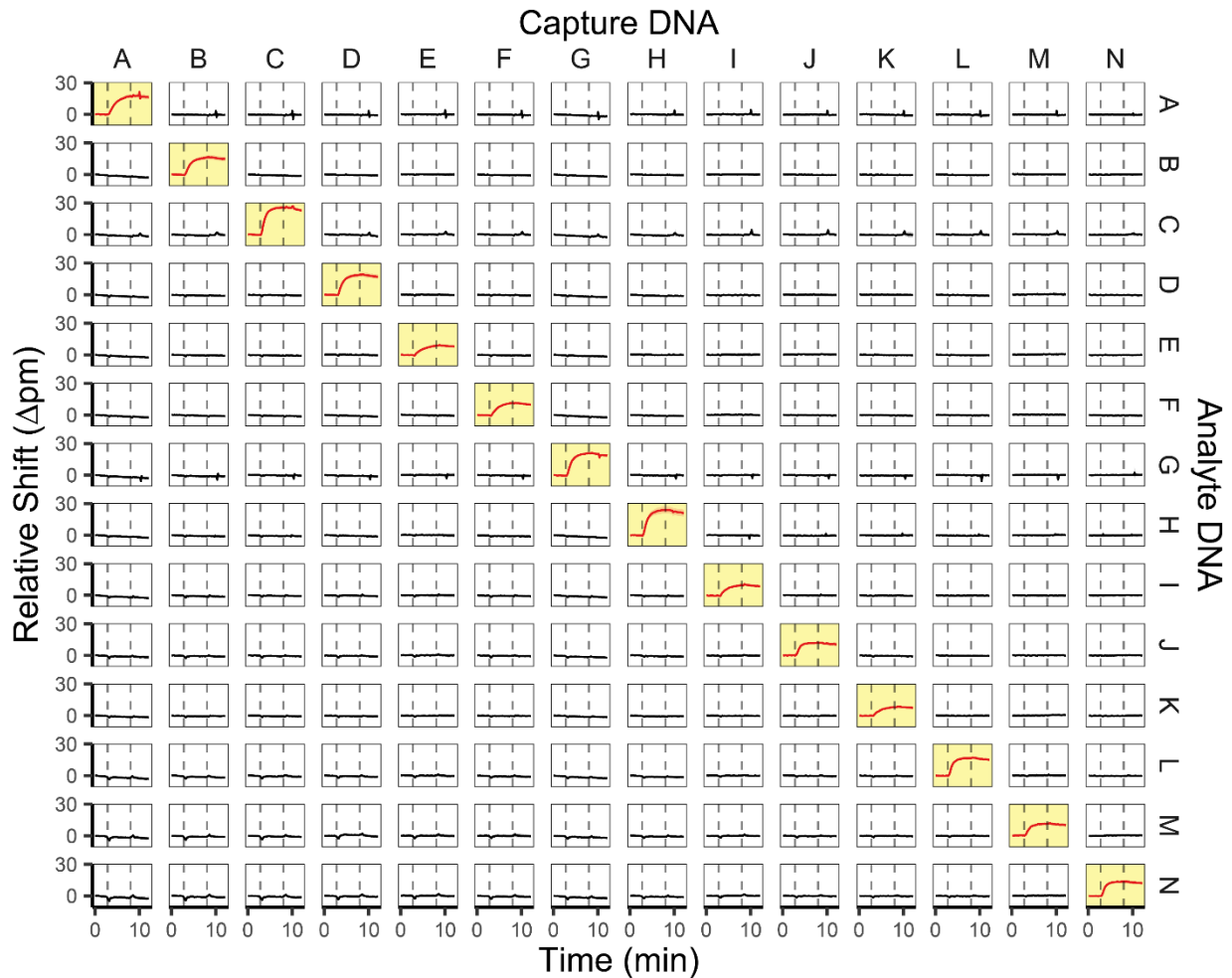
Figure V.1. DNA Cross-reactivity Testing. Each row represents a sensor chip arrayed with different capture probes and exposed to a single complement analyte probe. Columns represent the response for an individual capture probe to each analyte sequence. Sensors show response to complementary sequences (shown in red and yellow) with minimal to no interactions to off-targets. *Dashed lines* represent assay step switching from buffer (20 mM Tris, 100 mM NaCl, 0.01% NaN$_3$, and 2% BSA) to 200 µM analyte DNA then switching back to buffer.
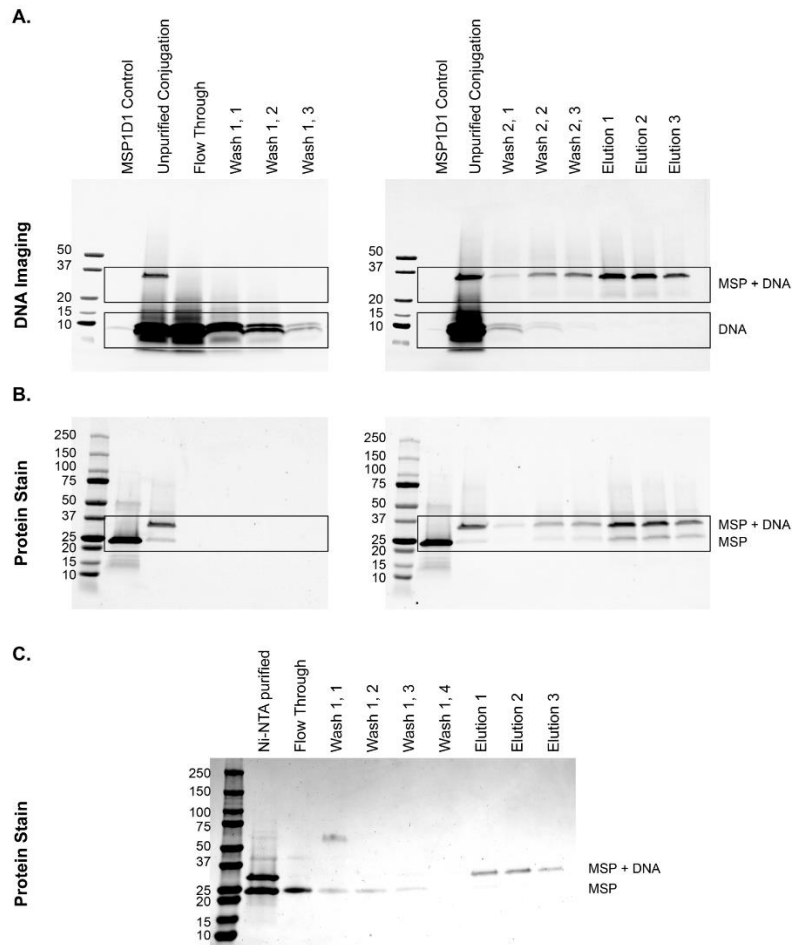
Figure V.2. SDS-PAGE of Purified Conjugated MSP1D1. (**A**) Fluorescein and IR imaging of Ni-NTA purification SDS-PAGE. Conjugation of MSP1D1 D73C was performed with fluorescein labelled DNA for imaging DNA. MSP1D1 was run as a control to show bromophenol blue imaging with IR. The unpurified conjugation shows a band around 32 kDa representing conjugated MSP and bands around 10 kDa representing free DNA as monomers or dimers due to side-product formation. The flow through shows excess DNA that did not bind the Ni-NTA column. Washes 1 and 2 contain low concentrations of sodium cholate and imidazole to rinse nonspecifically bound DNA off the resin. There is loss of conjugated MSP in the wash 2 steps potentially due to nonspecific binding of the DNA to the column. After the non-specific DNA is washed off, elution shows successful purification of conjugated MSP. (**B**) Krypton stain and IR imaging of the same gel. This stain shows the co-purification of conjugated (~25 kDa) and not conjugated MSP (~32 kDa). Comparing the intensities of the bands in the elution, the yield is about 70% conjugated MSP. (**C**) Coomassie stain of DNA purification SDS-PAGE. Ni-NTA purified MSP is concentrated for purification on DNA columns. The flow through that did not bind to the DNA column shows a band around 25 kDa for not conjugated MSP. Washes are performed with 30% formamide to eliminate non-specifically bound not conjugated MSP. Elutions show successful extraction of purified DNA-tagged MSP.
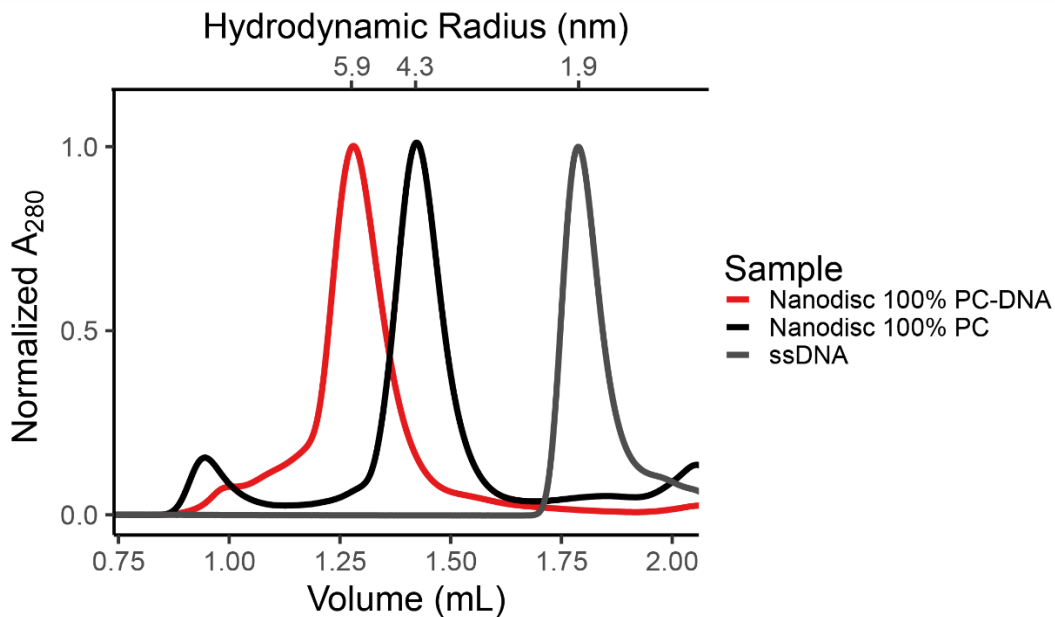
Figure V.3. SEC of Nanodiscs and ssDNA. HPLC separation on a Superdex Increase 2000 with hydrodynamic radius calculated from a standard curve of known hydrodynamic radii. Nanodiscs without DNA (black) are shown to elute at the volume corresponding to the expected hydrodynamic radius around 4.3 nm while ssDNA (grey) elutes around 1.9 nm. In *red*, DNA-tagged Nanodiscs display a shifted hydrodynamic radius due to the addition of DNA to the MSP. The shift is similar to the hydrodynamic radius of DNA.
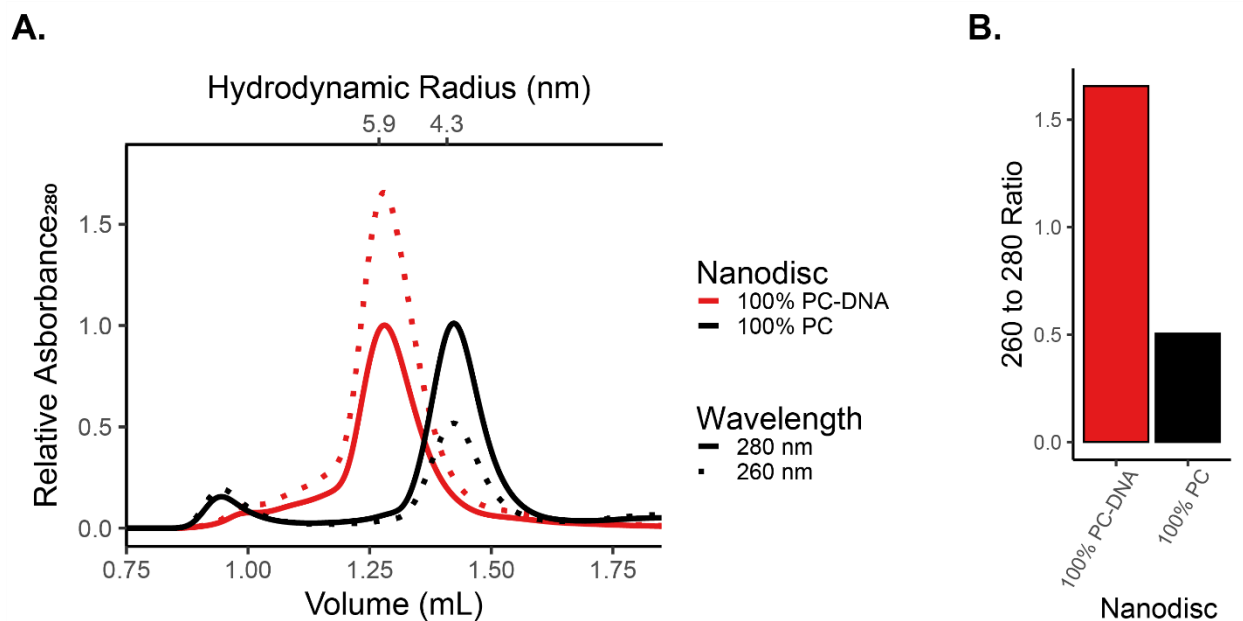
Figure V.4. SEC of Nanodiscs at 280 and 260 nm Absorbance. (**A**) HPLC separation on a Superdex Increase 2000 with hydrodynamic radius calculated from a standard curve of known hydrodynamic radii. Nanodiscs without DNA (black) are shown to elute at the volume corresponding to the expected hydrodynamic radius around 4.3 nm while DNA-tagged Nanodiscs (red) display a shifted hydrodynamic radius due to the addition of DNA to the MSP. DNA-tagged Nanodiscs show a higher absorbance at 260 nm due to the presence of DNA. (**B**) The ratios of 260 to 280 absorbance for Nanodiscs with (red) and without (black) DNA. The ratio of DNA-tagged Nanodiscs correlates to a protein contaminated DNA sample.
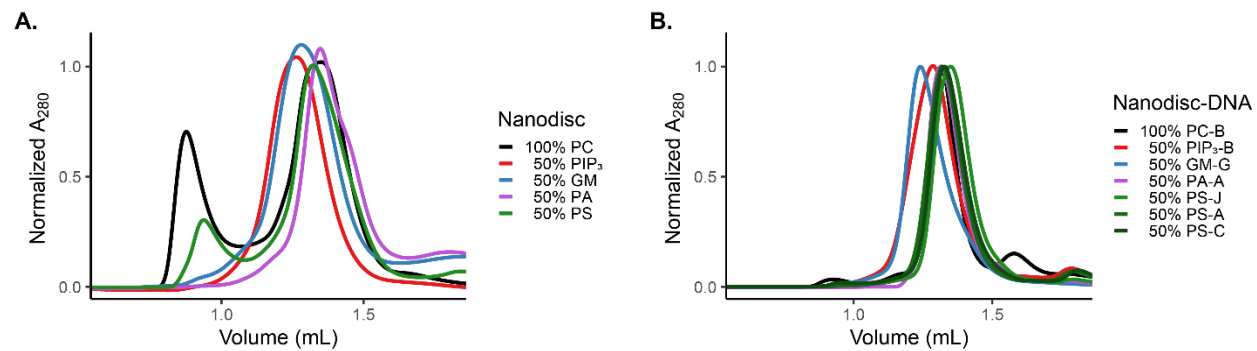
Figure V.5. SEC of Various Nanodiscs. (**A**) Elution profile of Nanodiscs without DNA. (**B**) Elution profile of DNA-tagged Nanodiscs 50% PIP$_3$ (red) and 50% GM (blue) elute earlier due to increased hydrodynamic size due to the larger lipid headgroups. Peaks eluting before 1.0 mL are lipid aggregates.
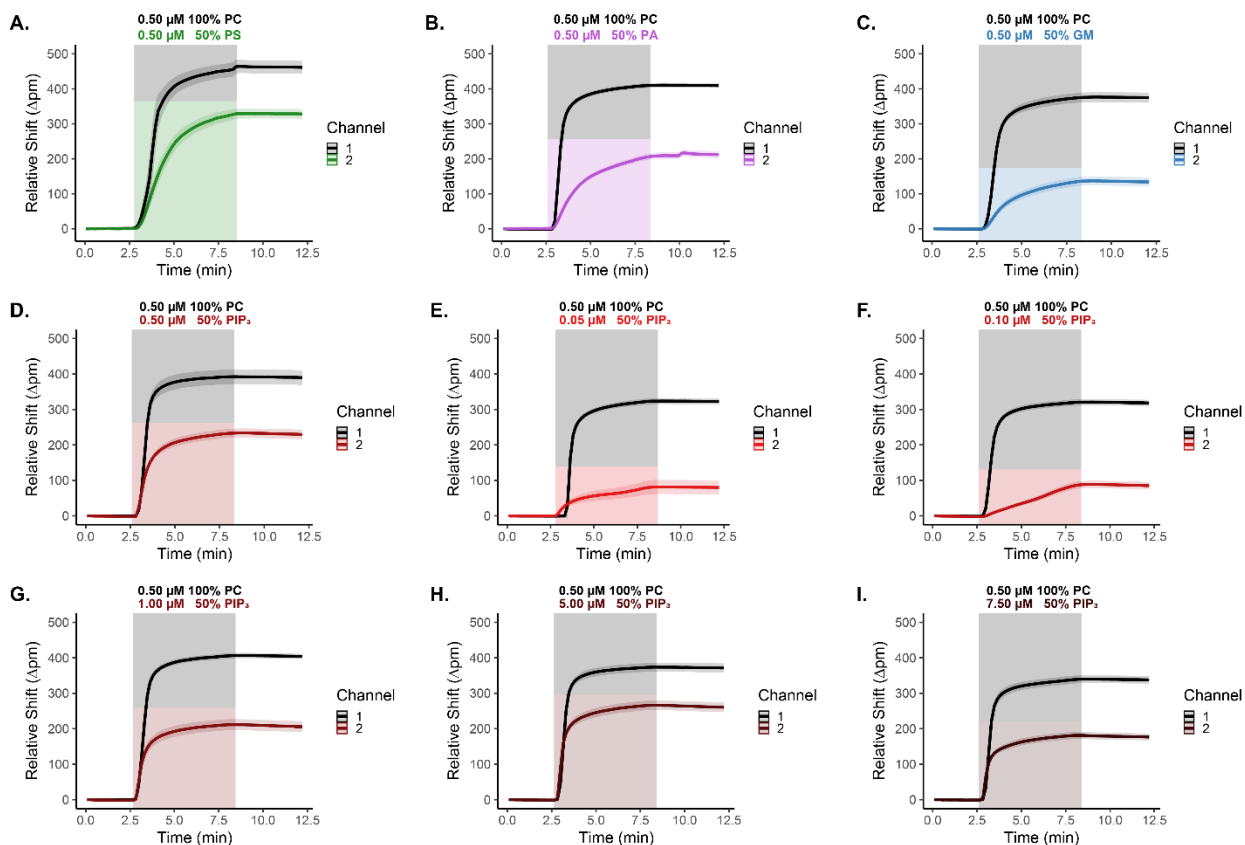
Figure V.6. Physisorption Flow Loading of Nanodiscs. Loading of Nanodiscs using physisorption onto silicon photonic microring resonators using a two-channel setup to allow for use of 100% PC as a control to account for chip-to-chip variation. The assay is thermally controlled and starts with buffer (SDB; 20 mM Tris, 100 mM NaCl, and 0.01% NaN_3) then switches to Nanodisc loading in the boxed region before switching back to buffer. Channel 1 is always showing the loading for 0.5 µM 100% PC (black) with the comparison for (**A**) 0.5 µM 50% PS (green), (**B**) 0.5 µM 50% PA (purple), (**C**) 0.5 µM 50% GM (blue), and (**D-I**) 0.05 µM to 7.50 µM 50% PIP_3 (red). The shaded ribbon shows the standard deviation of microrings (n = 64).
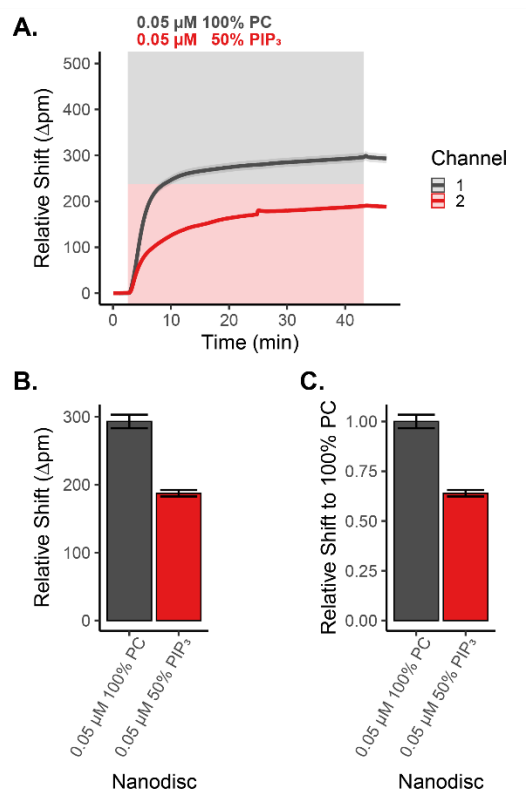
Figure V.7. Extended Physisorption Loading. (**A**) Loading of Nanodiscs using physisorption onto silicon photonic microring resonators using a two-channel setup to allow for use of 100% PC as a control to account for chip-to-chip variation. The assay is thermally controlled and starts with buffer (SDB) then switches to Nanodisc loading at a low concentration in the boxed region before switching back to buffer. The loading step here is 40 minutes compared to 5 minutes showed previously. The shaded ribbon shows the standard deviation of microrings (n = 64). (**B**) Comparison of the total relative shift loading based on the shift right before loading and at the end of the final buffer step. (**C**) Comparison of the relative shift of 100% PC.
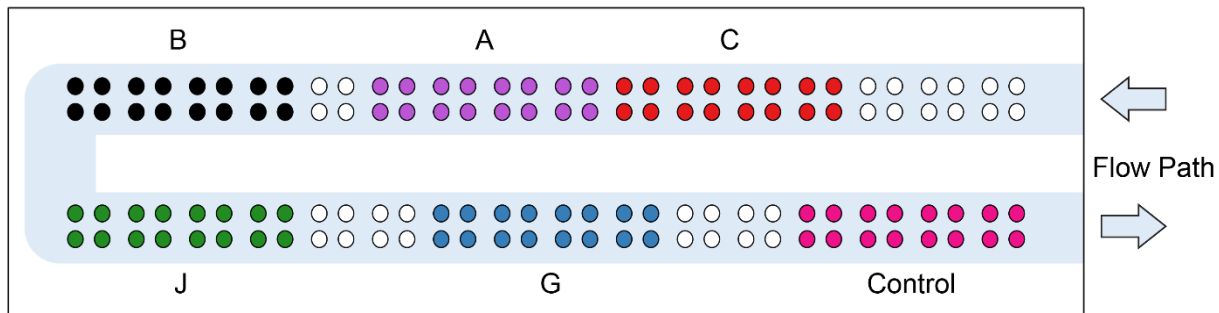
Figure V.8. Schematic of Sensor Array for Loading Test. The flow path for loading and assays is shown by the *light blue box* and *arrows*. Hand-spotting was used to generate the array of C (red), A (purple), B (black), J (green), G (blue), and control (pink) while white represents unfunctionalized microrings.
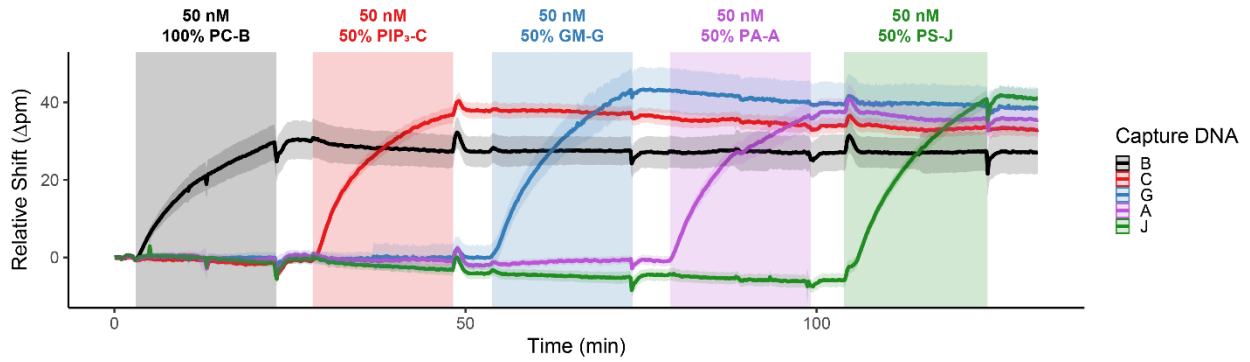
Figure V.9. DNA-Tagged Loading of Nanodiscs. Loading of Nanodiscs onto silicon photonic microring resonators is ssDNA controlled using a U-channel setup. The assay starts with buffer (SDB + 2% BSA) then switches to Nanodisc loading in the boxed region before switching back to buffer for the duration of the assay. Boxed regions are colored coded to show the matched complementary Nanodisc and capture DNA pairs 100% PC (black), 50% PIP_3 (red), 50% GM (blue), 50% PA (purple), and 50% PS (green). The shaded ribbon shows the standard deviation of microrings (n = 16).
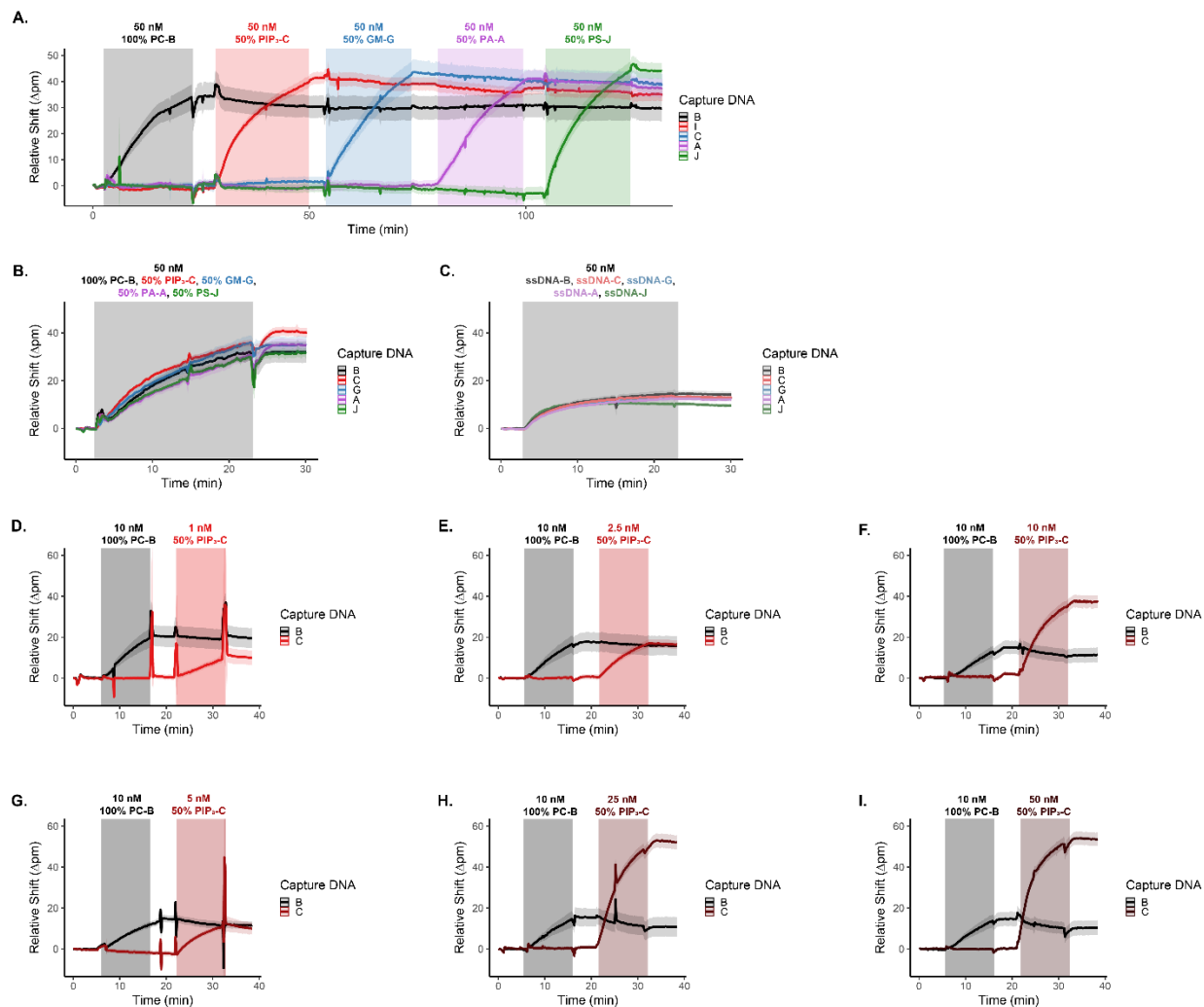
Figure V.10. DNA-Tagged Loading of Nanodiscs and DNA Loading. (**A**) Loading of Nanodiscs onto silicon photonic microring resonators is ssDNA controlled using a U-channel setup. The assay starts with buffer (SDB + 2% BSA) then switches to Nanodisc loading in the boxed region before switching back to buffer for the duration of the assay. Boxed regions are colored coded to show the matched complementary Nanodisc and capture DNA pairs 100% PC (black), 50% PIP$_3$ (red), 50% GM (blue), 50% PA (purple), and 50% PS (green).The shaded ribbon shows the standard deviation of microrings (n = 16). (**B**) Mixed loading of DNA-tagged Nanodiscs with ssDNA control. The assay starts with buffer then switches to mixed Nanodiscs in the boxed region before switching back to buffer. The shaded ribbon shows the standard deviation of microrings (n = 16). (**C**) Representative loading of complementary DNA at the same concentration with the same assay setup. The shaded ribbon shows the standard deviation of microrings (n = 16). (**D-I**) Observation of DNA-tagged loading with 50% PIP$_3$ at various concentrations. Sharp changes in the baseline are from air bubbles. The shaded ribbon shows the standard deviation of microrings (n = 16).
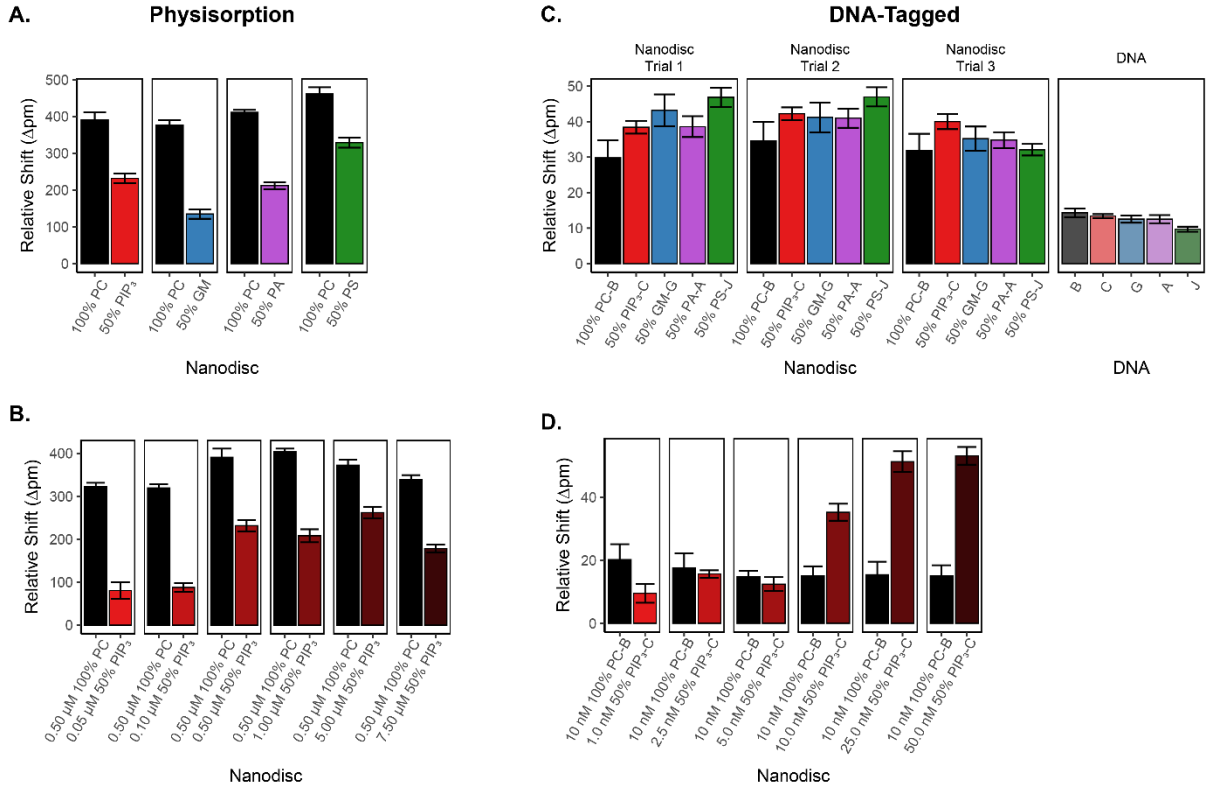
Figure V.11. Comparison of Loading for Physisorption and DNA-Tagged Nanodiscs. (**A**) Comparison of the total relative shift based on the shift right before loading and at the end of the final buffer step for physisorption of various Nanodisc environments at the same concentration from **Figures V.6A-D**. (**B**) Relative shift comparison of 50% PIP₃ Nanodiscs loaded at different concentrations compared to the same concentration of 100% PC Nanodisc from **Figures V.6D-I**. (**C**) Comparison of the total relative shift based on the shift right before the loading and at the end a particular loading step for DNA-tagged Nanodiscs and DNA performed on the same chip sequentially with formamide rinses. Trial 1 and 2 are shown in **Figure V.9** and **Figure V.10A**, respectively while Trial 3 and DNA are from **Figure V.10B-C**. (**D**) Relative shift comparison of 50% PIP₃ DNA-tagged Nanodiscs at different concentrations from **Figures V.10D-I**.
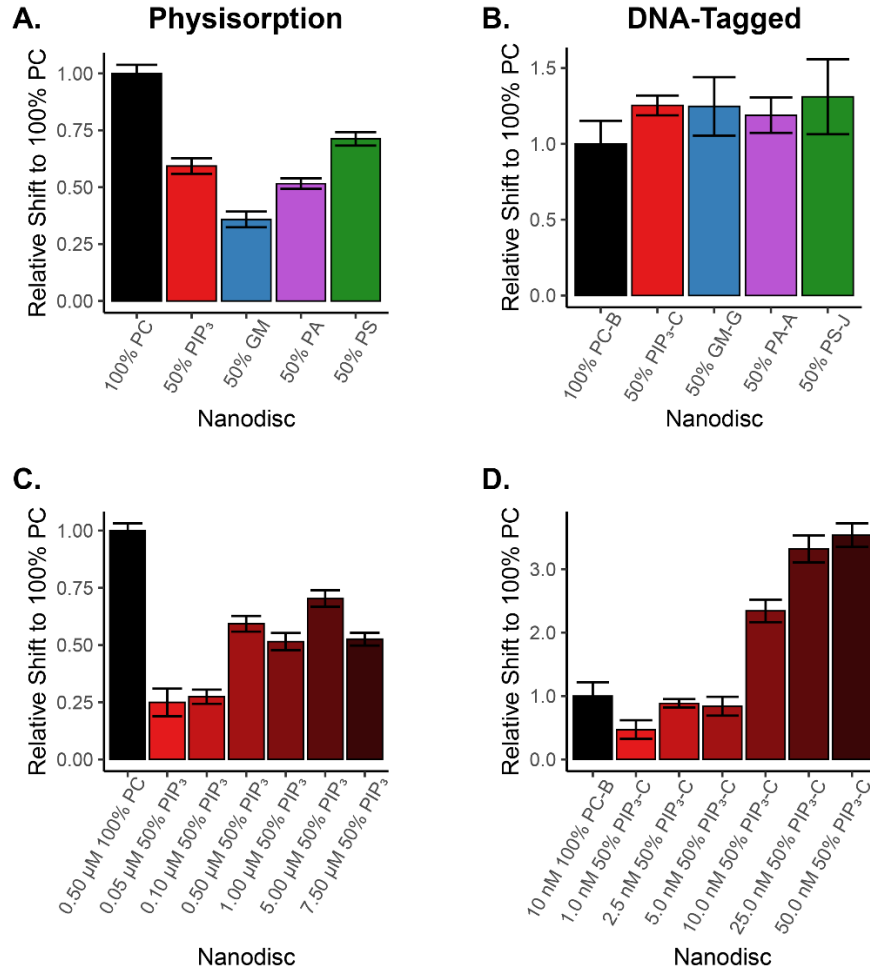
Figure V.12. Comparison of Loading for Physisorption and DNA-Tagged Nanodiscs. (**A**) Comparison of the total relative shift relative to 100% PC based on the shift right before loading and at the end of the final buffer step for physisorption of various Nanodisc environments at the same concentration from **Figures V.6A-D**. (**B**) Relative shift to 100% PC comparison of 50% PIP_3 Nanodiscs loaded at different concentrations compared to the same concentration of 100% PC Nanodisc from **Figures V.6D-I**. (**C**) Comparison of the relative shift to 100% PC based on the shift right before the loading and at the end a particular loading step for DNA-tagged Nanodiscs and DNA performed on the same chip sequentially with formamide rinses. Trial 1 and 2 are shown in **Figure V.9** and **Figure V.10A**, respectively while Trial 3 and DNA are from **Figure V.10B-C**, respectively. (**D**) Relative shift to 100% PC comparison of 50% PIP_3 DNA-tagged Nanodiscs at different concentrations from **Figures V.10D-I**.
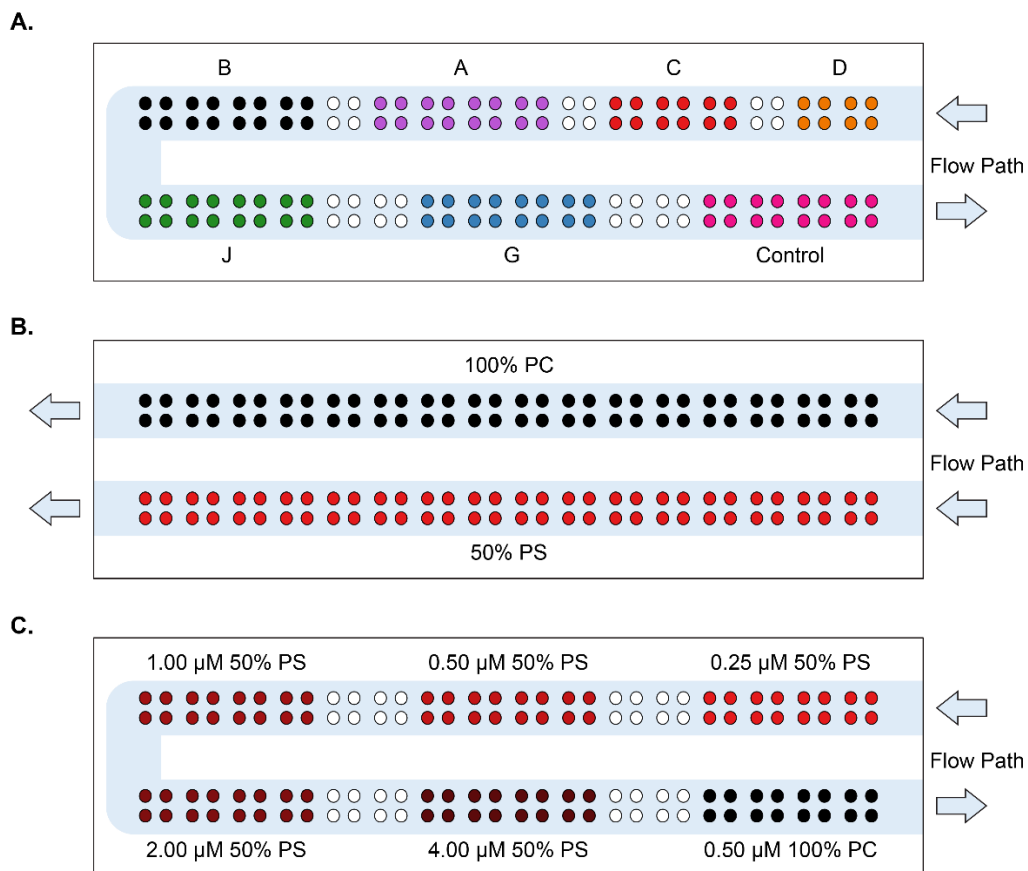
Figure V.13. Schematic of Sensor Array for Titrations. The flow path for loading and assays is shown by the *light blue box* and *arrows*. (**A**) Hand-spotting was used to generate the array of D (orange, control), C (red), A (purple), B (black), J (green), G (blue), and control (pink) while white represents unfunctionalized microrings. (**B**) Flow loading of 100% PC (black) and 50% PS (red) Nanodiscs. (**C**) Hand-spotting of 100% PC (black) and various concentrations of 50 % PS (red).

178
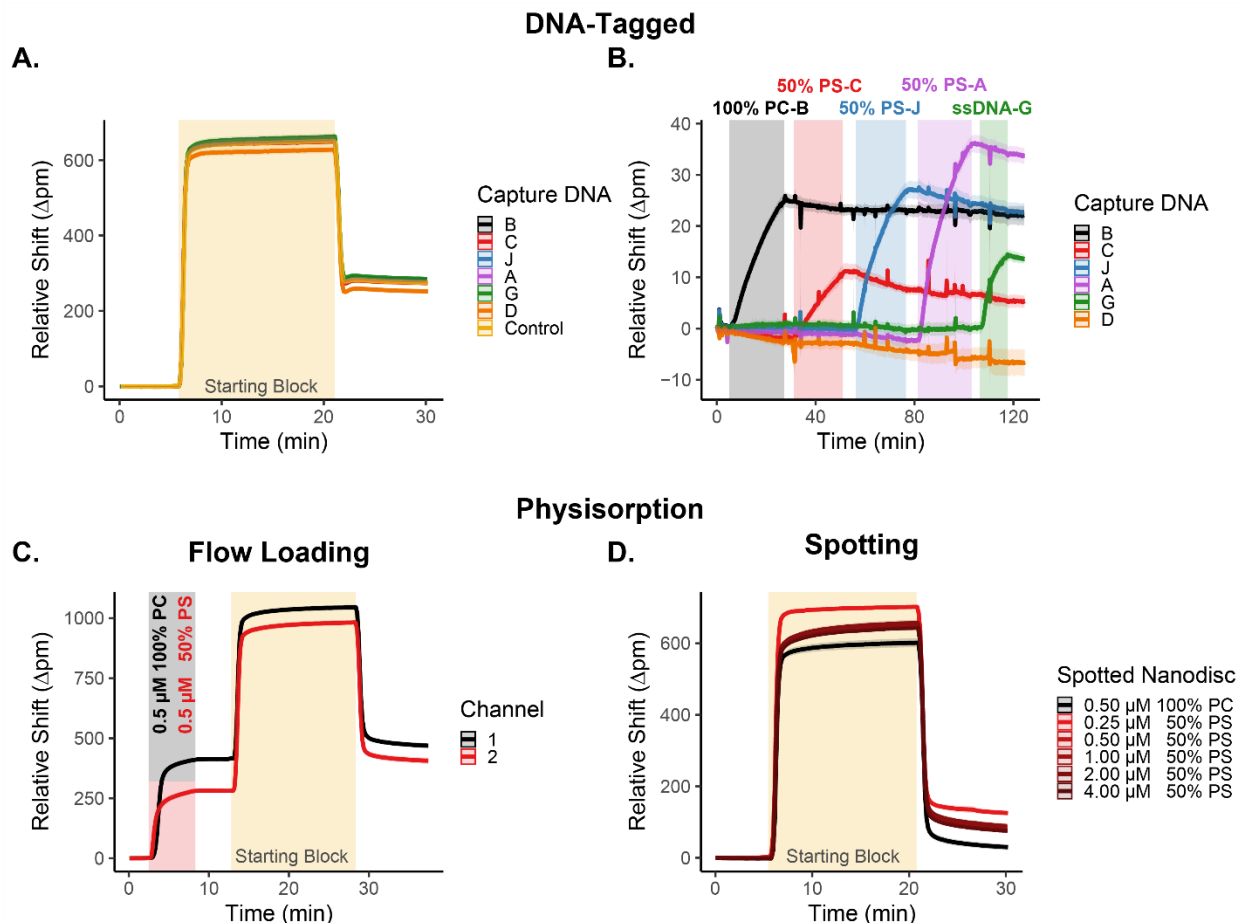
Figure V.14. Method of Nanodisc Array Generation Comparison for Titrations. (**A**) Blocking of the sensor surface with Starting Block prior to DNA-tagged Nanodisc loading. The assay starts in water before switching to starting block in the boxed region (yellow) then switches to buffer (SDB + 2% BSA). The shaded ribbon shows the standard deviation of microrings (n = 8-16). (**B**) Loading of DNA-tagged Nanodiscs on the blocked surface. The assay alternates between buffer and Nanodiscs or DNA in the boxed regions (various colors based on complementary DNA). The shaded ribbon shows the standard deviation of microrings (n = 8-16). (**C**) Physisorption flow loading of Nanodiscs followed by Starting Block surface blocking. The assay starts in SDB then switches to Nanodiscs in the boxed region (various colors based on channel) before switching back to SDB and blocking in the second boxed region (yellow) then returned to SDB. The shaded ribbon shows the standard deviation of microrings (n = 64). (**D**) Blocking of the sensor surface after hand-spotting of Nanodiscs. The assay starts in SDB before switching to starting block in the boxed region (yellow) then switches to SDB.

179
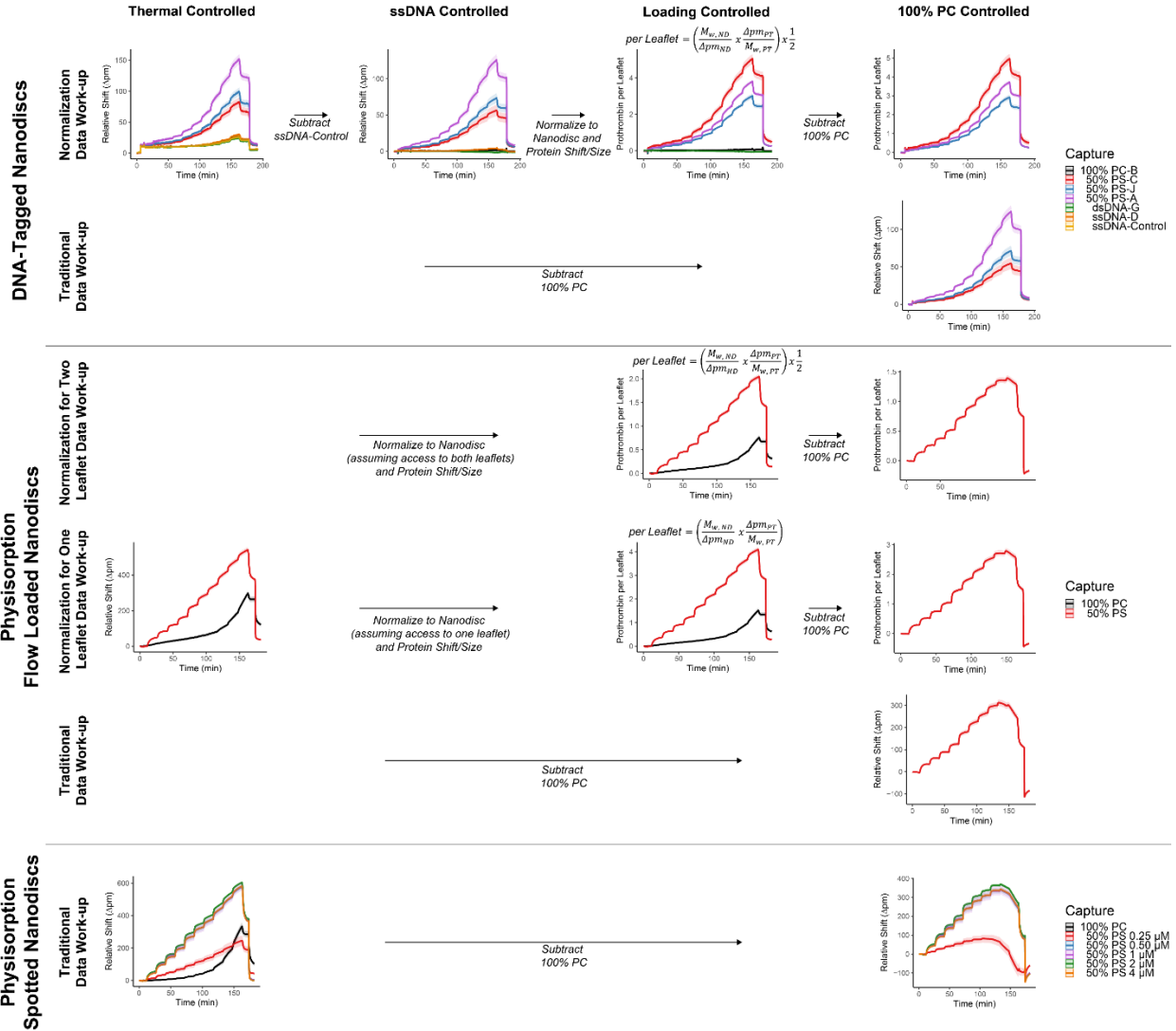
Figure V.15. Schematic Comparing Data Workup Based on the Loading Method.
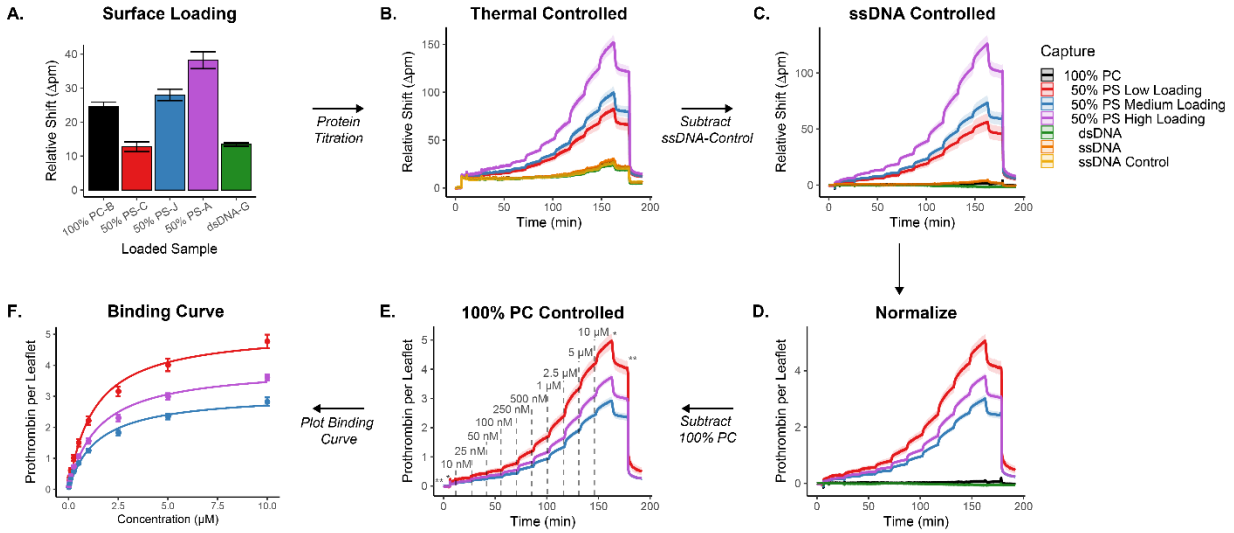
Figure V.16. Process for Titrations on DNA-tagged Nanodisc Arrays Using Prothrombin.
(**A**) Nanodiscs are loaded on to the surface then (**B**) prothrombin (or other protein) titration is performed from 10 nM to 10 µM. The shaded ribbon shows the standard deviation of microrings (n = 12-16). (**C**) The titration is corrected using a ssDNA control. (**D**) The data is normalized using **Equation V.2** to correct for surface loading of Nanodiscs and plot for prothrombin per leaflet. (**E**) Nonspecific interactions with 100% PC are subtracted. The maximum prothrombin per leaflet per titration step is calculated by subtracting the equilibrated shift during the HEPES(+) buffer step (*) from the equilibrated concentration step. This is plotted versus concentration (**F**) for binding characterization with **Equation V.3**. *Note*: ** = HEPES buffer and * = HEPES(+) buffer.
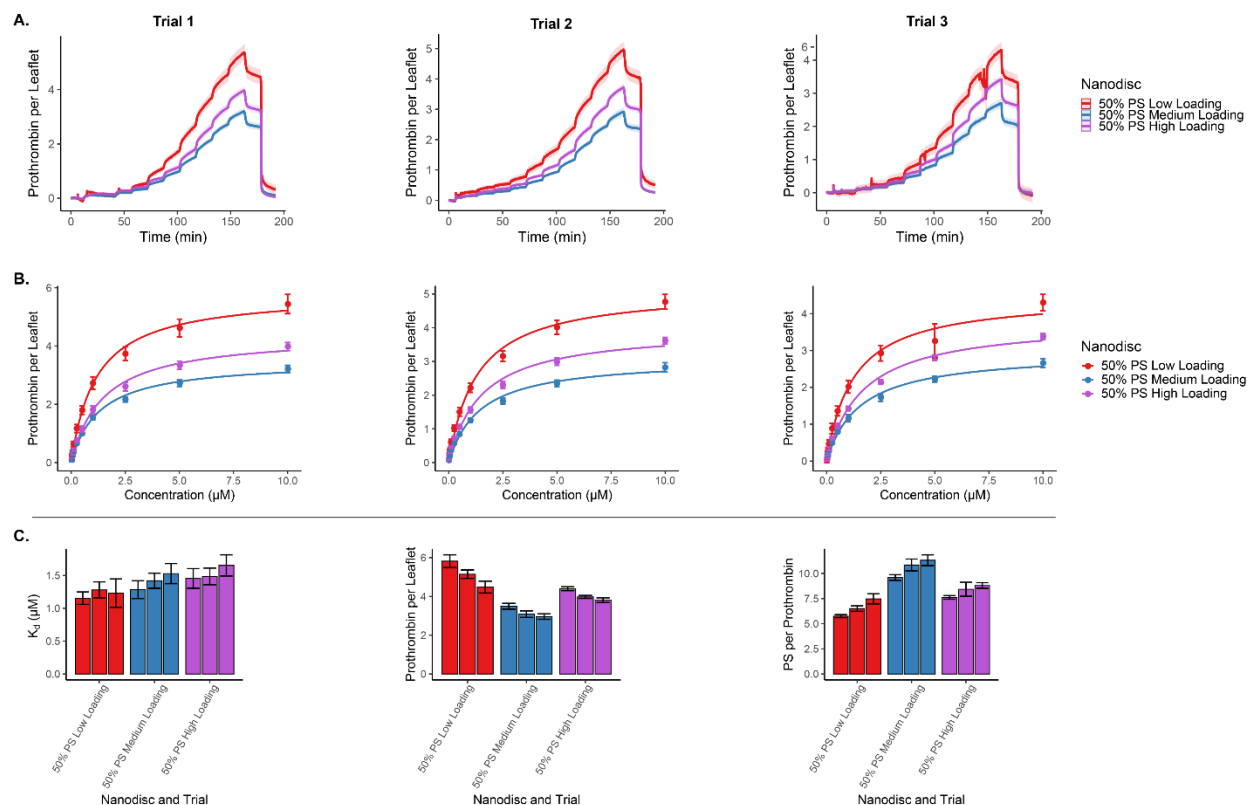
Figure V.17. Prothrombin Titration Replication. (**A**) Prothrombin titrations from 10 nM to 10 µM with buffer steps of HEPES (**) and HEPES(+) (*). Trials 1 and 2 were performed in sequence on the same array with surface regeneration with a non-calcium containing buffer while Trial 3 was performed on a newly loaded surface. Colors correspond to surface loading: low surface loading (red), medium surface loading (blue), and high surface loading (purple). The shaded ribbon shows the standard deviation of microrings (n = 12-16). (**B**) Binding curves and (**C**) values for each trial. Slight differences are observed between Nanodiscs due to variation in lipid packing between biological replicates.
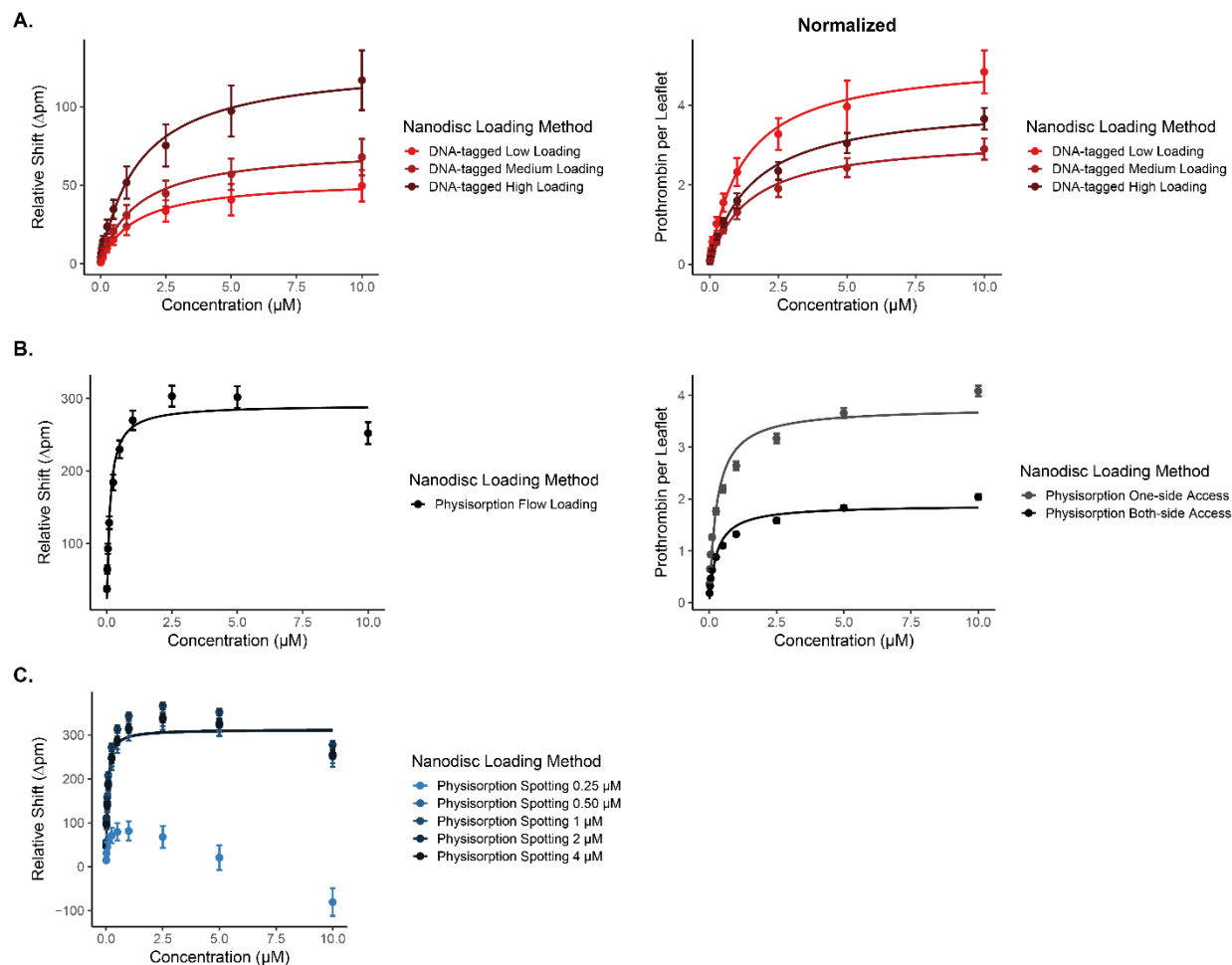
Figure V.18. Various Nanodisc Loading Method Prothrombin Binding Curves. All binding curves were fit with **Equation V.3**. Methods of Nanodisc loading (**A**) DNA-tagged, (**B**) physisorption flow loading, and (**C**) physisorption spotting. For (**A**) and (**B**), normalization was performed using **Equation V.2** for the graphs on the right. Physisorption flow loading for one-side access (**B**, grey) **Equation V.2** was modified by not multiplying by a half to assume that there is only access to one side of the Nanodisc.
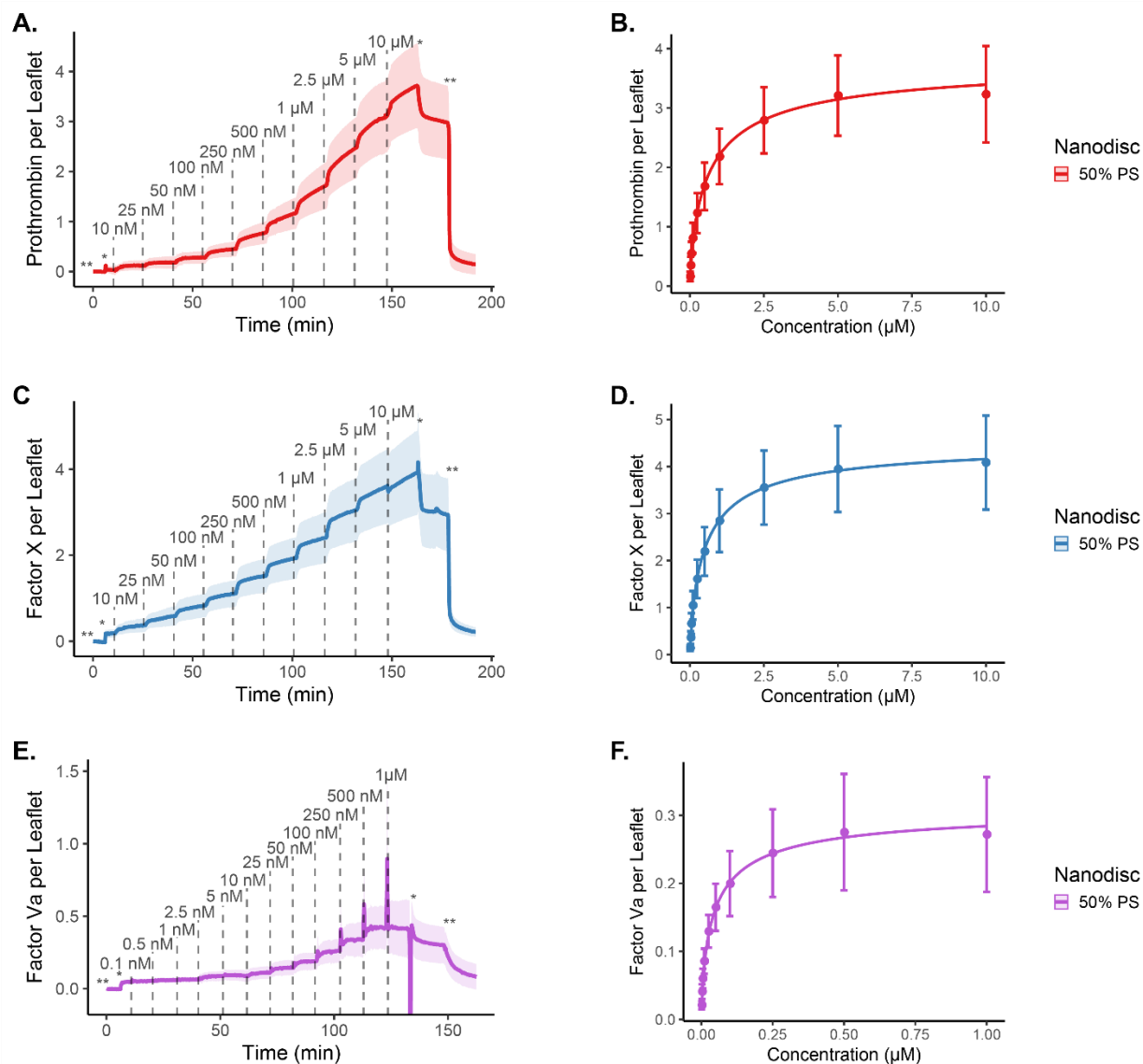
Figure V.19. Protein Titrations and Binding Curves. (**A**) Normalized and 100% PC controlled prothrombin titration from 10 nM to 10 µM with buffer steps of HEPES (**) and HEPES(+) (*). The shaded ribbon shows the standard deviation of microrings (n = 44). (**B**) Prothrombin binding curve with prothrombin per leaflet values calculated from equilibrated steps in the titration using the first calcium buffer step as a zero point. (**C**) Normalized and 100% PC factor X titration from 10 nM to 10 µM with buffer steps of HEPES (**) and HEPES(+) (*). The shaded ribbon shows the standard deviation of microrings (n = 44). (**D**) Factor X binding curve with factor X per leaflet values calculated from equilibrated steps in the titration using the first calcium buffer step as a zero point. (**E**) Normalized and 100% PC factor Va titration from 1 nM to 1 µM with buffer steps of HEPES (**) and HEPES(+) (*). The shaded ribbon shows the standard deviation of microrings (n = 32). (**B**) Factor Va binding curve with factor Va per leaflet values calculated from equilibrated steps in the titration using the first calcium buffer step as a zero point.
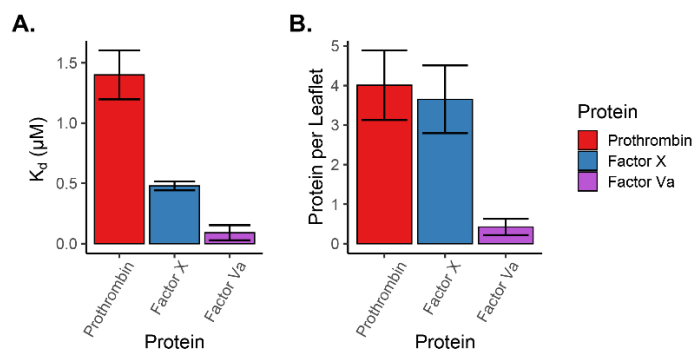
Figure V.20. Binding Values for Prothrombin, Factor X, and Factor Va with 50% PS Nanodiscs. Binding values, (**A**) dissociation constant and (**B**) protein per leaflet, calculated from the protein binding curves of prothrombin (red), factor X (blue), and factor Va (purple). Bars represent an average of microrings (n = 32 or 44) with standard deviation shown as error.
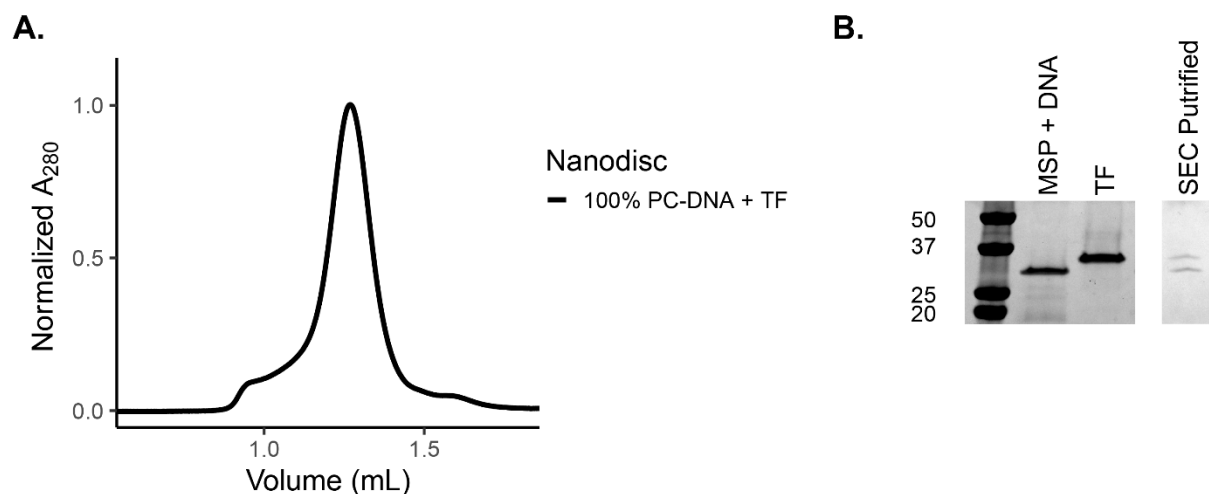
Figure V.21. Tissue Factor Incorporation. (**A**) Representative elution profile of 100% PC DNA-tagged Nanodiscs with TF incorporated. (**B**) Coomassie stained SDS-PAGE for determination of TF to MSP ratio. Conjugated MSP and TF are run as standards at 0.75 µg and SEC purified before running on the gel. Comparing the intensities to the controls to normalize membrane protein staining, the ratio of TF to MSP is 1 to 2 which corresponds to 1 TF per Nanodisc. All TF Nanodisc profiles and the full gel can be seen in **Figure V.22**.
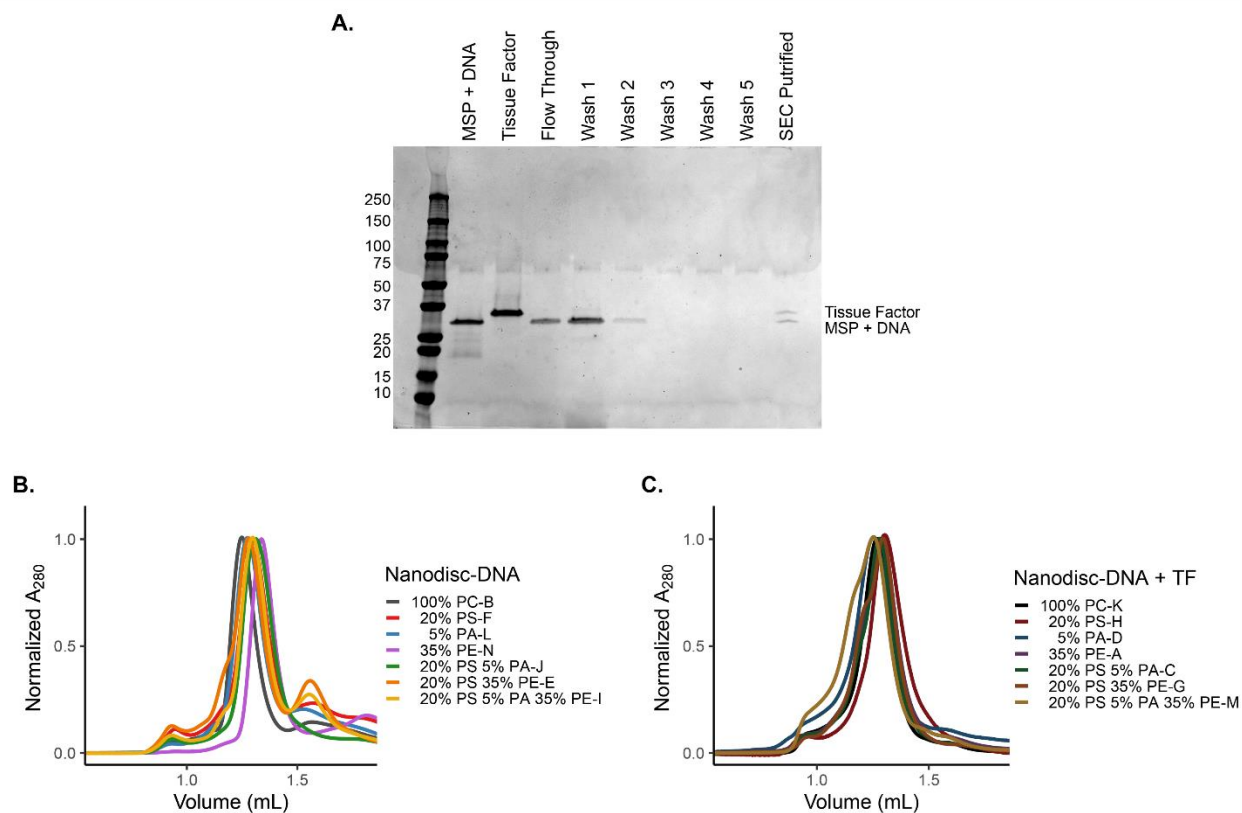
Figure V.22. Tissue Factor Nanodisc Formation. (**A**) Full Coomassie stained SDS-PAGE for determination of TF to MSP ratio. Conjugated MSP and TF are run as standards at 0.75 µg followed by the flow through that did not bind to the HPC4 column that is specific for TF. Washes are performed with a calcium containing buffer to maintain the HPC4 interaction before the elution with 5 mM EDTA to break the interaction. The elution was concentrated, and SEC purified before running on the gel. Comparing the intensities to the controls to normalize membrane protein staining, the ratio of TF to MSP is 1 to 2 which corresponds to 1 TF per Nanodisc. (**B**) Elution profile of empty DNA-tagged Nanodiscs. (**C**) Elution profile of all DNA-tagged Nanodiscs with TF incorporated. Note: 100% PC-K is shown in **Figure V.21** as "100% PC-DNA + TF," it is shown again here for comparison.
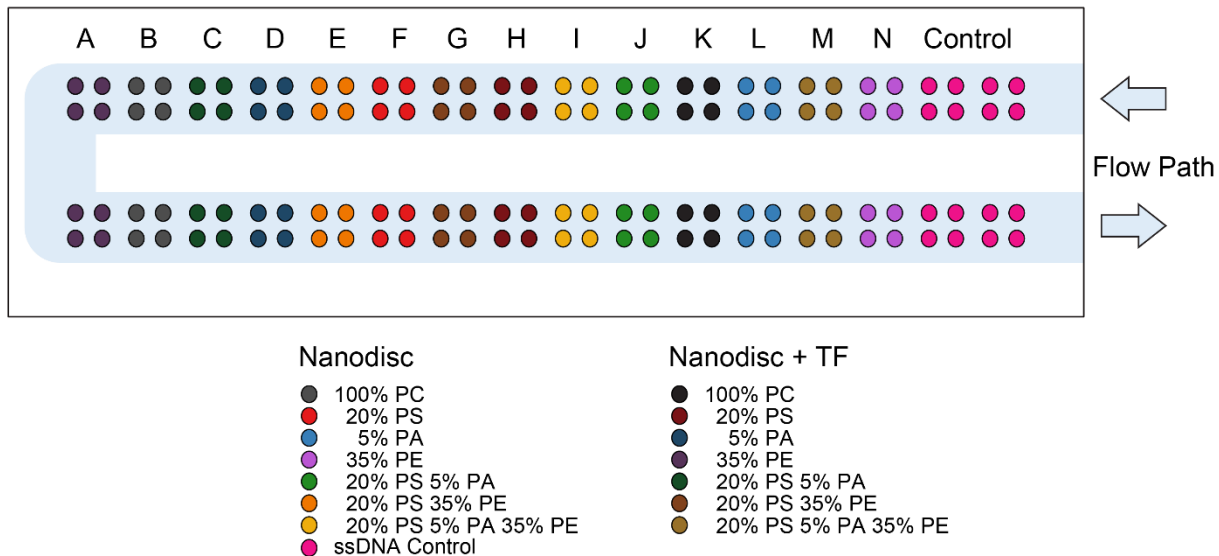
Figure V.23. Schematic of High-multiplexity Sensor Array. The flow path for loading and assays is shown by the *light blue box* and *arrows*. The array was generated by Genalyte for functionalization of control (pink), N (purple), M (gold), L (blue), K (black), J (green), I (yellow), H (dark red), G (brown), F (red), E (orange), D (dark blue), C (dark green), B (grey), and A (dark purple). The key denotes the DNA-tagged Nanodisc that is complementary to the capture DNA.

Figure V.24. Factor X and Factor IX Titrations. (**A**) Normalized and 100% PC controlled fX titration from 50 nM to 10 µM with buffer steps of HEPES (**) and HEPES(+) (*). The shaded ribbon shows the standard deviation of microrings (n = 8). (**B**) fX binding curve with fX per leaflet values calculated from equilibrated steps in the titration using the first calcium buffer step as a zero point. (**C**) Normalized and 100% PC fIX titration from 50 nM to 10 µM with buffer steps of HEPES (**) and HEPES(+) (*). The shaded ribbon shows the standard deviation of microrings (n = 8). (**D**) fIX binding curve with fIX per leaflet values calculated from equilibrated steps in the titration using the first calcium buffer step as a zero point.

Figure V.25. Tissue Factor Binding to Factor X and Factor IX. Binding values for fX and fIX binding to membranes with and without TF shown with light and dark color pairings, respectively. Graphs show comparisons of dissociation constants calculated for (**A**) fX and (**B**) fIX. Bars represent an average of microrings (n = 8) with standard deviation shown as error. Note: # represents no observed binding.

Table V.1. Complementary DNA Strands for Capture and Conjugation.

Name	Capture	Analyte
A	ATAGAGAGAGTCCACACACGC	GCGTGTGTGGACTCTCTCTAT[a]
B	ATAGATACTGCCACTTCACAT	ATGTGAAGTGGCAGTATCTAT
C	ATCCGACGCAACAATAGGG	CCCTATTGTTGCGTCGGAT
D	AGCCGAAGCAGACTTAATCAC	GTGATTAAGTCTGCTTCGGCT
E	AACAGGTTCAGAATCCTCGAC	GTCGAGGATTCTGAACCTGTT
F	ATCTTCTAGTTGTCGAGCAGG	CCTGCTCGACAACTAGAAGAT
G	TGACCCAGACCAGTTAGTGC	GCACTAACTGGTCTGGGTCA
H	AGCCTCATTGAATCATGCCTA	TAGGCATGATTCAATGAGGCT
I	TGCCCTATTGTTGCGTCG	CGACGCAACAATAGGGCA
J	ATCAGGTAAGGTTCACGGTA	TACCGTGAACCTTACCTGAT
K	GAGTAGCCTTCCCGAGCATT	AATGCTCGGGAAGGCTACTC
L	TACCAGTGACCATACATCG	CGATGTATGGTCACTGGTA
M	TACAGACTTAGCTCGAATG	CATTCGAGCTAAGTCTGTA
N	ATTGACTAAACTGCTTCCG	CGGAAGCAGTTTAGTCAAT
Control	AGCCCTCCCGTATCGTAGTT	

DNA listed from 5' to 3'. All capture and analyte DNA were modified with a 12-hydrocarbon chain and accessible amino group on the 5' end (code: /5AmMC12/). Capture strands were used for surface and column functionalization. Target strands were used for conjugation to MSP.

[a]Fluorescently labeled on 3' with 6-FAM (Fluorescein) for confirmation studies only (code: /36-FAM/)

Table V.2. Prothrombin Binding Loading Method Comparison.

Nanodisc Loading Method	Amount Loaded	Loading Normalized	K_d (µM)	Max Value	Max Unit
DNA-tagged	12 ± 1	✓	1.2 ± 0.2	5.1 ± 0.6	PT per leaflet
		X	1.3 ± 0.2	50 ± 10	Relative Δpm
	28 ± 2	✓	1.4 ± 0.2	3.2 ± 0.3	PT per leaflet
		X	1.4 ± 0.2	70 ± 10	Relative Δpm
	38 ± 2	✓	1.5 ± 0.2	4.1 ± 0.3	PT per leaflet
		X	1.5 ± 0.2	130 ± 20	Relative Δpm
Physisorption	281 ± 9	✓	0.27 ± 0.02	3.77 ± 0.09	PT per leaflet[a]
				1.89 ± 0.05	PT per leaflet[b]
		X	0.116 ± 0.005	290 ± 10	Relative Δpm
Spotted	0.25 µM	X	NA[c]	NA[c]	Relative Δpm
	0.5 µM	X	0.056 ± 0.007	310 ± 20	
	1 µM	X	0.058 ± 0.008	310 ± 30	
	2 µM	X	0.056 ± 0.003	341 ± 8	
	4 µM	X	0.062 ± 0.004	316 ± 9	

[a]Surface normalized to assume access to both sides of the Nanodisc.

[b]Surface normalized to assume access to one side of the Nanodisc.

[c]Unable to fit binding curve.

Table V.3. Prothrombin, Factor X, and Factor Va Binding to 50% PS Nanodiscs.

Value	Prothrombin	Factor X	Factor Va
K_d	1.4 ± 0.2	0.48 ± 0.04	0.09 ± 0.06
Protein per Leaflet	4.0 ± 0.9	3.7 ± 0.9	0.4 ± 0.2

Table V.4. Factor X and Factor IX Fit Values with and without TF or TF mutants.

Nanodisc	Factor X		Factor IX	
	Maximum Protein per Leaflet	K_d (µM)	Maximum Protein per Leaflet	K_d (µM)
100% PC + TF	NA[a]	NA[a]	NA[a]	NA[a]
20% PS	7.3 ± 0.3	0.47 ± 0.04	1.0 ± 0.2	0.13 ± 0.04
20% PS + TF	11 ± 1	0.7 ± 0.1	10 ± 1	0.19 ± 0.01
5% PA	NA[a]	NA[a]	NA[a]	NA[a]
5% PA + TF	3.6 ± 0.4	0.4 ± 0.1	NA[a]	NA[a]
35% PE	NA[a]	NA[a]	NA[a]	NA[a]
35% PE + TF	1.3 ± 0.1	0.66 ± 0.07	NA[a]	NA[a]
20% PS 5% PA	5.3 ± 0.3	0.27 ± 0.01	NA[a]	NA[a]
20% PS 5% PA + TF	3.8 ± 0.3	0.43 ± 0.04	2.1 ± 0.2	0.17 ± 0.02
20% PS 35% PE	4.7 ± 0.2	0.29 ± 0.02	NA[a]	NA[a]
20% PS 35% PE + TF	8.2 ± 0.6	0.49 ± 0.04	4.4 ± 0.6	0.23 ± 0.03
20% PS 35% PE 5% PA	3.2 ± 0.3	0.22 ± 0.2	NA[a]	NA[a]
20% PS 35% PE 5% PA + TF	3.7 ± 0.2	0.17 ± 0.03	NA[a]	NA[a]

[a]Unable to fit binding curve.

REFERENCES

(1)   Uhlén, M.; Fagerberg, L.; Hallström, B. M.; Lindskog, C.; Oksvold, P.; Mardinoglu, A.; Sivertsson, Å.; Kampf, C.; Sjöstedt, E.; Asplund, A.; Olsson, I. M.; Edlund, K.; Lundberg, E.; Navani, S.; Szigyarto, C. A. K.; Odeberg, J.; Djureinovic, D.; Takanen, J. O.; Hober, S.; Alm, T.; Edqvist, P. H.; Berling, H.; Tegel, H.; Mulder, J.; Rockberg, J.; Nilsson, P.; Schwenk, J. M.; Hamsten, M.; Von Feilitzen, K.; Forsberg, M.; Persson, L.; Johansson, F.; Zwahlen, M.; Von Heijne, G.; Nielsen, J.; Pontén, F. Tissue-Based Map of the Human Proteome. *Science (80-.).* **2015**, *347* (6220), 1–9.

(2)   Overington, J. P.; Al-Lazikani, B.; Hopkins, A. L. How Many Drug Targets Are There? PubMed Commons. *Nat. Rev. Drug Discov.* **2006**, *5* (12), 993–996.

(3)   McLaughlin, S.; Murray, D. Plasma Membrane Phosphoinositide Organization by Protein Electrostatics. *Nature* **2005**, *438* (7068), 605–611.

(4)   Lemmon, M. A. Membrane Recognition by Phospholipid-Binding Domains. *Nat. Rev. Mol. Cell Biol.* **2008**, *9* (2), 99–111.

(5)   Saliba, A.-E.; Vonkova, I.; Gavin, A.-C. The Systematic Analysis of Protein–Lipid Interactions Comes of Age. *Nat. Rev. Mol. Cell Biol.* **2015**, *16* (12), 753–761.

(6)   Loose, M.; Schwille, P. Biomimetic Membrane Systems to Study Cellular Organization. *J. Struct. Biol.* **2009**, *168* (1), 143–151.

(7)   Mingeot-Leclercq, M.-P.; Deleu, M.; Brasseur, R.; Dufrêne, Y. F. Atomic Force Microscopy of Supported Lipid Bilayers. *Nat. Protoc.* **2008**, *3* (10), 1654–1659.

(8)   Rossi, C.; Briand, E.; Parot, P.; Odorico, M.; Chopineau, J. Surface Response Methodology for the Study of Supported Membrane Formation. *J. Phys. Chem. B* **2007**, *111* (26), 7567–7576.

(9)   Whiles, J. A.; Deems, R.; Vold, R. R.; Dennis, E. A. Bicelles in Structure-Function Studies of Membrane-Associated Proteins. *Bioorg. Chem.* **2002**, *30* (6), 431–442.

(10)   Dürr, U. H. N.; Gildenberg, M.; Ramamoorthy, A. The Magic of Bicelles Lights up Membrane Protein Structure. *Chem. Rev.* **2012**, *112* (11), 6054–6074.

(11) Mäler, L.; Gräslund, A. Artificial Membrane Models for the Study of Macromolecular Delivery. In *Macromolecular Drug Delivery: Methods and Protocols*; Belting, M., Ed.; Humana Press: New York, 2009; Vol. 480, pp 129–138.

(12) Wagner, A.; Vorauer-Uhl, K. Liposome Technology for Industrial Purposes. *J. Drug Deliv.* **2011**, *2011*, 1–9.

(13) Akbarzadeh, A.; Rezaei-sadabady, R.; Davaran, S.; Joo, S. W.; Zarghami, N.; Hanifehpour, Y.; Samiei, M.; Kouhi, M.; Nejati-Koshki, K. Liposome: Classification, Preparation, and Applications. *Nanoscale Res. Lett.* **2013**, *8* (1), 102–110.

(14) Brouillette, C. G.; Jones, J. L.; Ng, T. C.; Kercret, H.; Chung, B. H.; Segrest, J. P. Structural Studies of Apolipoprotein A-I/Phosphatidylcholine Recombinants by High-Field Proton NMR, Nondenaturing Gradient Gel Electrophoresis, and Electron Microscopy. *Biochemistry* **1984**, *23* (2), 359–367.

(15) Koppaka, V.; Silvestro, L.; Engler, J. A.; Brouillette, C. G.; Axelsen, P. H. The Structure of Human Lipoprotein A-I: Evidence for the "Belt" Model. *J. Biol. Chem.* **1999**, *274* (21), 14541–14544.

(16) Gordon, T.; Castelli, W. P.; Hjortland, M. C.; Kannel, W. B.; Dawber, T. R. High Density Lipoprotein as a Protective Factor against Coronary Heart Disease. The Framingham Study. *Am. J. Med.* **1977**, *62* (5), 707–714.

(17) Kanellis, P.; Romans, A. Y.; Johnson, B. J.; Kercretg, H.; Chiovetti, R.; Allen, T. M.; Segrest, J. P. Studies of Synthetic Peptide Analogs of the Amphiphatic Helix: Effect of Charged Amino Acid Residue Topography on Lipid Affinity. *J. Biol. Chem.* **1980**, *255* (23), 11464–11472.

(18) Anantharamaiah, G. M.; Jones, J. L.; Brouillette, C. G.; Schmidt, C. F.; Chung, B. H.; Hughes, T. A.; Bhown, A. S.; Segrest, J. P. Studies of Synthetic Peptide Analogs of the Amphiphatic Helix: Structure of Complexes with Dimyrstoyl Phosphatidylcholine. *J. Biol. Chem.* **1985**, *260* (18), 10256–10262.

(19) Chung, B. H.; Anantharamaiah, G. M.; Brouillette, C. G.; Nishida, T.; Segrest, J. P. Studies of Synthetic Peptide Analogs of the Amphiphatic Helix. Correlation of Structure with

Function. *J. Biol. Chem.* **1985**, *260* (18), 10256–10262.

(20) *Apolipoprotein Mimetic Peptides for Stimulating Cholesterol Efflux*; Anantharamaiah, G. M., Goldberg, D., Eds.; Adis: Switzerland, 2015.

(21) Anantharamaiah, G. M.; Mishra, V. K.; Garber, D. W.; Datta, G.; Handattu, S. P.; Palgunachari, M. N.; Chaddha, M.; Navab, M.; Reddy, S. T.; Segrest, J. P.; Fogelman, A. M. Structural Requirements for Antioxidative and Anti-Inflammatory Properties of Apolipoprotein A-I Mimetic Peptides. *J. Lipid Res.* **2007**, *48* (9), 1915–1923.

(22) Kuai, R.; Sun, X.; Yuan, W.; Xu, Y.; Schwendeman, A.; Moon, J. J. Subcutaneous Nanodisc Vaccination with Neoantigens for Combination Cancer Immunotherapy. *Bioconjug. Chem.* **2018**, *29* (3), 771–775.

(23) Scheetz, L.; Park, K. S.; Li, Q.; Lowenstein, P. R.; Castro, M. G.; Schwendeman, A.; Moon, J. J. Engineering Patient-Specific Cancer Immunotherapies. *Nat. Biomed. Eng.* **2019**, *3* (10), 768–782.

(24) Kadiyala, P.; Li, D.; Nunez, F. M.; Altshuler, D.; Doherty, R.; Kuai, R.; Yu, M.; Kamran, N.; Edwards, M.; Moon, J. J.; Lowenstein, P. R.; Castro, M. G.; Schwendeman, A. High-Density Lipoprotein-Mimicking Nanodiscs for Chemo-Immunotherapy against Glioblastoma Multiforme. *ACS Nano* **2019**, *13* (2), 1365–1384.

(25) Kuai, R.; Yuan, W.; Son, S.; Nam, J.; Xu, Y.; Fan, Y.; Schwendeman, A.; Moon, J. J. Elimination of Established Tumors with Nanodisc-Based Combination Chemoimmunotherapy. *Sci. Adv.* **2018**, *4* (4), 1–14.

(26) Kuai, R.; Ochyl, L. J.; Bahjat, K. S.; Schwendeman, A.; Moon, J. J. Designer Vaccine Nanodiscs for Personalized Cancer Immunotherapy. *Nat. Mater.* **2017**, *16* (4), 489–498.

(27) Dörr, J. M.; Scheidelaar, S.; Koorengevel, M. C.; Dominguez, J. J.; Schäfer, M.; van Walree, C. A.; Killian, J. A. The Styrene–Maleic Acid Copolymer: A Versatile Tool in Membrane Research. *Eur. Biophys. J.* **2016**, *45* (1), 3–21.

(28) Lee, S. C.; Knowles, T. J.; Postis, V. L. G.; Jamshad, M.; Parslow, R. A.; Lin, Y. P.; Goldman, A.; Sridhar, P.; Overduin, M.; Muench, S. P.; Dafforn, T. R. A Method for

Detergent-Free Isolation of Membrane Proteins in Their Local Lipid Environment. *Nat. Protoc.* **2016**, *11* (7), 1149–1162.

(29)   Stroud, Z.; Hall, S. C. L.; Dafforn, T. R. Purification of Membrane Proteins Free from Conventional Detergents: SMA, New Polymers, New Opportunities and New Insights. *Methods* **2018**, *147*, 106–117.

(30)   Ravula, T.; Hardin, N. Z.; Ramamoorthy, A. Polymer Nanodiscs: Advantages and Limitations. *Chem. Phys. Lipids* **2019**, *219*, 45–49.

(31)   Overduin, M.; Klumperman, B. Advancing Membrane Biology with Poly(Styrene-Co-Maleic Acid)-Based Native Nanodiscs. *Eur. Polym. J.* **2019**, *110*, 63–68.

(32)   Bayburt, T. H.; Grinkova, Y. V.; Sligar, S. G. Self-Assembly of Discoidal Phospholipid Bilayer Nanoparticles with Membrane Scaffold Proteins. *Nano Lett.* **2002**, *2* (8), 853–856.

(33)   Skar-Gislinge, N.; Johansen, N. T.; Høiberg-Nielsen, R.; Arleth, L. Comprehensive Study of the Self-Assembly of Phospholipid Nanodiscs: What Determines Their Shape and Stoichiometry? *Langmuir* **2018**, *34* (42), 12569–12582.

(34)   Camp, T.; McLean, M.; Kato, M.; Cheruzel, L.; Sligar, S. The Hydrodynamic Motion of Nanodiscs. *Chem. Phys. Lipids* **2019**, *220*, 28–35.

(35)   Camp, T.; Mehta, K.; Sligar, S. G.; Zhang, K. Molecular Orientation Determination in Nanodiscs at the Single-Molecule Level. *Anal. Chem.* **2020**, *92* (2), 2229–2236.

(36)   Ritchie, T. K.; Grinkova, Y. V.; Bayburt, T. H.; Denisov, I. G.; Zolnerciks, J.; Atkins, W. M.; Sligar, S. G. Reconstitution of Membrane Proteins in Phospholipid Bilayer Nanodiscs. In *Methods in Enzymology*; Duzgunes, N., Ed.; Elsevier Masson SAS: San Diego, CA, 2009; Vol. 464, pp 211–231.

(37)   Schuler, M. A.; Denisov, I. G.; Sligar, S. G. Nanodiscs as a New Tool to Examine Lipid-Protein Interactions. In *Methods in Molecular Biology*; Kleinschmidt, J., Ed.; Springer Science: New York, 2013; Vol. 974, pp 415–433.

(38)   Denisov, I. G.; Sligar, S. G. Nanodiscs in Membrane Biochemistry and Biophysics. *Chem. Rev.* **2017**, *117* (6), 4669–4713.

(39)   McLean, M. A.; Gregory, M. C.; Sligar, S. G. Nanodiscs: A Controlled Bilayer Surface for the Study of Membrane Proteins. *Annu. Rev. Biophys.* **2018**, *47* (1), 107–124.

(40)   Finkenwirth, F.; Sippach, M.; Landmesser, H.; Kirsch, F.; Ogienko, A.; Grunzel, M.; Kiesler, C.; Steinhoff, H. J.; Schneider, E.; Eitinger, T. ATP-Dependent Conformational Changes Trigger Substrate Capture and Release by an ECF-Type Biotin Transporter. *J. Biol. Chem.* **2015**, *290* (27), 16929–16942.

(41)   Heuveling, J.; Frochaux, V.; Ziomkowska, J.; Wawrzinek, R.; Wessig, P.; Herrmann, A.; Schneider, E. Conformational Changes of the Bacterial Type i ATP-Binding Cassette Importer HisQMP2 at Distinct Steps of the Catalytic Cycle. *Biochim. Biophys. Acta - Biomembr.* **2014**, *1838* (1 Pt B), 106–116.

(42)   Viegas, A.; Viennet, T.; Etzkorn, M. The Power, Pitfalls and Potential of the Nanodisc System for NMR-Based Studies. *Biol. Chem.* **2016**, *397* (12), 1335–1354.

(43)   Kobashigawa, Y.; Harada, K.; Yoshida, N.; Ogura, K.; Inagaki, F. Phosphoinositide-Incorporated Lipid-Protein Nanodiscs: A Tool for Studying Protein-Lipid Interactions. *Anal. Biochem.* **2011**, *410* (1), 77–83.

(44)   Zhang, Z.; Dai, C.; Bai, J.; Xu, G.; Liu, M.; Li, C. Ca(2+) Modulating α-Synuclein Membrane Transient Interactions Revealed by Solution NMR Spectroscopy. *Biochim. Biophys. Acta - Biomembr.* **2014**, *1838* (3), 853–858.

(45)   Wan, C.; Wu, B.; Song, Z.; Zhang, J.; Chu, H.; Wang, A.; Liu, Q.; Shi, Y.; Li, G.; Wang, J. Insights into the Molecular Recognition of the Granuphilin C2A Domain with PI(4,5)P2. *Chem. Phys. Lipids* **2015**, *186*, 61–67.

(46)   Yokogawa, M.; Kobashigawa, Y.; Yoshida, N.; Ogura, K.; Harada, K.; Inagaki, F. NMR Analyses of the Interaction between the FYVE Domain of Early Endosome Antigen 1 (EEA1) and Phosphoinositide Embedded in a Lipid Bilayer. *J. Biol. Chem.* **2012**, *287* (42), 34936–34945.

(47)   Inagaki, S.; Ghirlando, R.; White, J. F.; Gvozdenovic-Jeremic, J.; Northup, J. K.; Grisshammer, R. Modulation of the Interaction between Neurotensin Receptor NTS1 and Gq Protein by Lipid. *J. Mol. Biol.* **2012**, *417* (1–2), 95–111.

(48)   Redhair, M.; Clouser, A. F.; Atkins, W. M. Hydrogen-Deuterium Exchange Mass Spectrometry of Membrane Proteins in Lipid Nanodiscs. *Chem. Phys. Lipids* **2019**, *220*, 14–22.

(49)   Marin, V. L.; Bayburt, T. H.; Sligar, S. G.; Mrksich, M. Functional Assays of Membrane-Bound Proteins with SAMDI-TOF Mass Spectrometry. *Angew. Chemie - Int. Ed.* **2007**, *46* (46), 8796–8798.

(50)   Marty, M. T.; Hoi, K. K.; Gault, J.; Robinson, C. V. Probing the Lipid Annular Belt by Gas-Phase Dissociation of Membrane Proteins in Nanodiscs. *Angew. Chemie - Int. Ed.* **2016**, *55* (2), 550–554.

(51)   Keener, J. E.; Zambrano, D. E.; Zhang, G.; Zak, C. K.; Reid, D. J.; Deodhar, B. S.; Pemberton, J. E.; Prell, J. S.; Marty, M. T. Chemical Additives Enable Native Mass Spectrometry Measurement of Membrane Protein Oligomeric State within Intact Nanodiscs. *J. Am. Chem. Soc.* **2019**, *141* (2), 1054–1061.

(52)   Nath, A.; Trexler, A. J.; Koo, P.; Miranker, A. D.; Atkins, W. M.; Rhoades, E. Single-Molecule Fluorescence Spectroscopy Using Phospholipid Bilayer Nanodiscs. In *Methods in Enzymology*; Abelson, J. N., Simon, M. I., Colowick, S. P., Kaplan, N. O., Eds.; Elsevier Inc.: San Diego, CA, 2010; Vol. 472, pp 89–117.

(53)   Ye, X.; McLean, M. A.; Sligar, S. G. Conformational Equilibrium of Talin Is Regulated by Anionic Lipids. *Biochim. Biophys. Acta - Biomembr.* **2016**, *1858* (8), 1833–1840.

(54)   Gregory, M. C.; McLean, M. A.; Sligar, S. G. Interaction of KRas4b with Anionic Membranes: A Special Role for PIP 2. *Biochem. Biophys. Res. Commun.* **2017**, *487* (2), 351–355.

(55)   Lee, C. M.; He, C. H.; Nour, A. M.; Zhou, Y.; Ma, B.; Park, J. W.; Kim, K. H.; Cruz, C. Dela; Sharma, L.; Nasr, M. L.; Modis, Y.; Lee, C. G.; Elias, J. A. IL-13Rα2 Uses TMEM219 in Chitinase 3-like-1-Induced Signalling and Effector Responses. *Nat. Commun.* **2016**, *7*, 1–12.

(56)   Lee, M.; Yang, H.; Kim, D.; Yang, M.; Park, T. H.; Hong, S. Human-like Smelling of a Rose Scent Using an Olfactory Receptor Nanodisc-Based Bioelectronic Nose. *Sci. Rep.*

2018, *8* (1), 1–12.

(57)   Trahey, M.; Li, M. J.; Kwon, H.; Woodahl, E. L.; McClary, W. D.; Atkins, W. M. Applications of Lipid Nanodiscs for the Study of Membrane Proteins by Surface Plasmon Resonance. *Curr. Protoc. Protein Sci.* **2015**, *81*, 29.13.1-29.13.16.

(58)   Goluch, E. D.; Shaw, A. W.; Sligar, S. G.; Liu, C. Microfluidic Patterning of Nanodisc Lipid Bilayers and Multiplexed Analysis of Protein Interaction. *Lab Chip* **2008**, *8* (10), 1723–1728.

(59)   Borch, J.; Torta, F.; Sligar, S. G.; Roepstorff, P. Nanodiscs for Immobilization of Lipid Bilayers and Membrane Receptors: Kinetic Analysis of Cholera Toxin Binding to a Glycolipid Receptor. *Anal. Chem.* **2008**, *80* (16), 6245–6252.

(60)   Das, A.; Zhao, J.; Schatz, G. C.; Sligar, S. G.; Van Duyne, R. P. Screening of Type I and II Drug Binding to Human Cytochrome P450-3A4 in Nanodiscs by Localized Surface Plasmon Resonance Spectroscopy. *Anal. Chem.* **2009**, *81* (10), 3754–3759.

(61)   Bocquet, N.; Kohler, J.; Hug, M. N.; Kusznir, E. A.; Rufer, A. C.; Dawson, R. J.; Hennig, M.; Ruf, A.; Huber, W.; Huber, S. Real-Time Monitoring of Binding Events on a Thermostabilized Human A2A Receptor Embedded in a Lipid Bilayer by Surface Plasmon Resonance. *Biochim. Biophys. Acta - Biomembr.* **2015**, *1848* (5), 1224–1233.

(62)   Borch, J.; Roepstorff, P.; Møller-Jensen, J. Nanodisc-Based Co-Immunoprecipitation for Mass Spectrometric Identification of Membrane-Interacting Proteins. *Mol. Cell. Proteomics* **2011**, *10* (7), 1–9.

(63)   Jang, H.; Abraham, S. J.; Chavan, T. S.; Hitchinson, B.; Khavrutskii, L.; Tarasova, N. I.; Nussinov, R.; Gaponenko, V. Mechanisms of Membrane Binding of Small GTPase K-Ras4B Farnesylated Hypervariable Region. *J. Biol. Chem.* **2015**, *290* (15), 9465–9477.

(64)   Davie, E. W.; Fujikawa, K.; Kisiel, W. The Coagulation Cascade: Initiation, Maintenance, and Regulation. *Perspect. Biochem.* **1991**, *30* (42), 10363–10370.

(65)   Zwaal, R. F. A.; Comfurius, P.; Bevers, E. M. Lipid–Protein Interactions in Blood Coagulation. *Biochim. Biophys. Acta (BBA)-Reviews Biomembr.* **1998**, *1376* (3), 433–453.

(66) Zelaya, H.; Rothmeier, A. S.; Ruf, W. Tissue Factor at the Crossroad of Coagulation and Cell Signaling. *J. Thromb. Haemost.* **2018**, *16* (10), 1941–1952.

(67) Huang, M.; Rigby, A. C.; Morelli, X.; Grant, M. A.; Huang, G.; Furie, B.; Seaton, B.; Furie, B. C. Structural Basis of Membrane Binding by Gla Domains of Vitamin K-Dependent Proteins. *Nat. Struct. Biol.* **2003**, *10* (9), 751–756.

(68) Majumder, R.; Quinn-Allen, M. A.; Kane, W. H.; Lentz, B. R. The Phosphatidylserine Binding Site of the Factor Va C2 Domain Accounts for Membrane Binding but Does Not Contribute to the Assembly or Activity of a Human Factor Xa-Factor Va Complex. *Biochemistry* **2005**, *44* (2), 711–718.

(69) Majumder, R.; Quinn-Allen, M. A.; Kane, W. H.; Lentz, B. R. A Phosphatidylserine Binding Site in Factor Va C1 Domain Regulates Both Assembly and Activity of the Prothrombinase Complex. *Blood* **2008**, *112* (7), 2795–2802.

(70) Boettcher, J. M.; Davis-harrison, R. L.; Clay, M. C.; Nieuwkoop, A. J.; Ohkubo, Y. Z.; Tajkhorshid, E.; Morrissey, J. H.; Rienstra, C. M. Atomic View of Calcium-Induced Clustering of Phoosphatidylserine in Mixed Lipid Bilayers. *Biochemistry* **2011**, *50*, 2264–2273.

(71) Shaw, A. W.; Pureza, V. S.; Sligar, S. G.; Morrissey, J. H. The Local Phospholipid Environment Modulates the Activation of Blood Clotting. *J. Biol. Chem.* **2007**, *282* (9), 6556–6563.

(72) Tavoosi, N.; Davis-Harrison, R. L.; Pogorelov, T. V.; Ohkubo, Y. Z.; Arcario, M. J.; Clay, M. C.; Rienstra, C. M.; Tajkhorshid, E.; Morrissey, J. H. Molecular Determinants of Phospholipid Synergy in Blood Clotting. *J. Biol. Chem.* **2011**, *286* (26), 23247–23253.

(73) Tavoosi, N.; Smith, S. A.; Davis-Harrison, R. L.; Morrissey, J. H. Factor VII and Protein C Are Phosphatidic Acid-Binding Proteins. *Biochemistry* **2013**, *52* (33), 5545–5552.

(74) Ohkubo, Y. Z.; Morrissey, J. H.; Tajkhorshid, E. Dynamical View of Membrane Binding and Complex Formation of Human Factor VIIa and Tissue Factor. *J. Thromb. Haemost.* **2010**, *8* (5), 1044–1053.

(75) Luchini, A.; Tidemand, F. G.; Johansen, N. T.; Campana, M.; Sotres, J.; Ploug, M.; Cárdenas, M.; Arleth, L. Peptide Disc Mediated Control of Membrane Protein Orientation in Supported Lipid Bilayers for Surface-Sensitive Investigations. *Anal. Chem.* **2020**, *92* (1), 1081–1088.

(76) Tidemand, F. G.; Østergaard, H.; Ploug, M.; Kragelund, B. B.; Arleth, L. Efficient Refolding and Reconstitution of Tissue Factor into Nanodiscs Facilitates Structural Investigation of a Multicomponent System on a Lipid Bilayer. *Biochim. Biophys. Acta - Biomembr.* **2020**, *1862* (6), 1–10.

(77) Kirchhofer, D.; Lipari, M. T.; Moran, P.; Eigenbrot, C.; Kelley, R. F. The Tissue Factor Region That Interacts with Substrates Factor IX and Factor X. *Biochemistry* **2000**, *39* (25), 7380–7387.

(78) Baugh, R. J.; Dickinson, C. D.; Ruf, W.; Krishnaswamy, S. Exosite Interactions Determine the Affinity of Factor X for the Extrinsic Xase Complex. *J. Biol. Chem.* **2000**, *275* (37), 28826–28833.

(79) Sloan, C. D. K.; Marty, M. T.; Sligar, S. G.; Bailey, R. C. Interfacing Lipid Bilayer Nanodiscs and Silicon Photonic Sensor Arrays for Multiplexed Protein − Lipid and Protein − Membrane Protein Interaction Screening. *Anal. Chem.* **2013**, *85* (5), 2970–2976.

(80) Muehl, E. M.; Gajsiewicz, J. M.; Medfisch, S. M.; Wiersma, Z. S. B.; Morrissey, J. H.; Bailey, R. C. Multiplexed Silicon Photonic Sensor Arrays Enable Facile Characterization of Coagulation Protein Binding to Nanodiscs with Variable Lipid Content. *J. Biol. Chem.* **2017**, jbc.M117.800938.

(81) Medfisch, S. M.; Muehl, E. M.; Morrissey, J. H.; Bailey, R. C. Phosphatidylethanolamine-Phosphatidylserine Binding Synergy of Seven Coagulation Factors Revealed Using Nanodisc Arrays on Silicon Photonic Sensors. *Sci. Rep.* **2020**, *10* (17407), 1–7.

(82) Denisov, I. G.; Grinkova, Y. V.; Lazarides, A. A.; Sligar, S. G. Directed Self-Assembly of Monodisperse Phospholipid Bilayer Nanodiscs with Controlled Size Directed Self-Assembly of Monodisperse Phospholipid Bilayer Nanodiscs with Controlled Size. *Nano Lett.* **2004**, *126* (11), 3477–3487.

(83) Bayburt, T. H.; Sligar, S. G. Single-Molecule Height Measurements on Microsomal Cytochrome P450 in Nanometer-Scale Phospholipid Bilayer Disks. *Proc. Natl. Acad. Sci.* **2002**, *99* (10), 6725–6730.

(84) Iqbal, M.; Gleeson, M. a; Spaugh, B.; Tybor, F.; Gunn, W. G.; Hochberg, M.; Baehr-jones, T.; Bailey, R. C.; Gunn, L. C.; Resonators, R.; Optical, H.; Iqbal, M.; Gleeson, M. a; Spaugh, B.; Tybor, F.; Gunn, W. G.; Hochberg, M.; Baehr-jones, T.; Bailey, R. C.; Gunn, L. C. Label-Free Biosensor Arrays Based on Silicon Scanning Instrumentation. *IEEE J. Sel. Top. Quantum Electron.* **2010**, *16* (3), 654–661.

(85) Byeon, J.-Y.; Limpoco, F. T.; Bailey, R. C. Efficient Bioconjugation of Protein Capture Agents to Biosensor Surfaces Using Aniline-Catalyzed Hydrazone Ligation. *Langmuir* **2010**, *26* (19), 15430–15435.

(86) Luchansky, M. S.; Washburn, A. L.; Qavi, A. J.; Kindt, J. T.; McClellan, M. S.; Bailey, R. C. Silicon Photonic Microring Resonator Arrays for Scalable and Multiplexable Bioanalysis. *Proc. SPIE* **2011**, *7888*, 1–4.

(87) Wade, J. H.; Alsop, A. T.; Vertin, N. R.; Yang, H.; Johnson, M. D.; Bailey, R. C. Rapid, Multiplexed Phosphoprotein Profiling Using Silicon Photonic Sensor Arrays. *ACS Cent. Sci.* **2015**, *1* (7), 374–382.

(88) Washburn, A. L.; Shia, W. W.; Lenkeit, K. A.; Lee, S.-H.; Bailey, R. C. Multiplexed Cancer Biomarker Detection Using Chip-Integrated Silicon Photonic Sensor Arrays. *Analyst* **2016**, *141* (18), 5358–5365.

(89) Carney, C. E.; Lenov, I. L.; Baker, C. J.; Macrenaris, K. W.; Eckermann, A. L.; Sligar, S. G.; Meade, T. J. Nanodiscs as a Modular Platform for Multimodal MR-Optical Imaging. *Bioconjug. Chem.* **2015**, *26* (5), 899–905.

(90) Her, C.; Filoti, D. I.; McLean, M. A.; Sligar, S. G.; Alexander Ross, J. B.; Steele, H.; Laue, T. M. The Charge Properties of Phospholipid Nanodiscs. *Biophys. J.* **2016**, *111* (5), 989–998.

(91) Washburn, A. L.; Gomez, J.; Bailey, R. C. DNA-Encoding to Improve Performance and Allow Parallel Evaluation of the Binding Characteristics of Multiple Antibodies in a

Surface-Bound Immunoassay Format. *Anal. Chem.* **2011**, *83* (9), 3572–3580.

(92) Neuenschwander, P. F.; Bianco-fisher, E.; Rezaie, A. R.; Morrissey, J. H. Phosphatidylethanolamine Augments Factor Vila — Tissue Factor Activity : Enhancement of Sensitivity to Phosphatidylserine. *Biochemistry* **1995**, *34* (43), 13988–13993.

(93) Muehl, E. M.; Gajsiewicz, J. M.; Medfisch, S. M.; Wiersma, Z. S. B.; Morrissey, J. H.; Bailey, R. C. Multiplexed Silicon Photonic Sensor Arrays Enable Facile Characterization of Coagulation Protein Binding to Nanodiscs with Variable Lipid Content. *J. Biol. Chem.* **2017**, *292* (39), 16249–16256.

(94) Banner, D. W.; D'Arcy, A.; Chene, C.; Winkler, F. K.; Guha, A.; Konigsberg, W. H.; Nemerson, Y.; Kirchhofer, D. The Crystal Structure of the Complex of Blood Coagulation Factor VIIa with Soluble Tissue Factor. *Nature*. 1996, pp 41–46.

CHAPTER VI

Characterization of the Factor X GLA Domain Using DNA-Tagged Nanodisc Arrays

Abstract

Factor X (fX) is a crucial protein that gets activated at the intersection of the intrinsic and extrinsic blood coagulation cascade pathways. The active form of fX forms the prothrombinase complex with activated factor V to proteolytically cleave prothrombin to thrombin. Thrombin is the key blood coagulation enzyme for creating blood clots and commencing negative feedback on the whole cascade. Without activation of fX, prothrombin will not be activated to achieve the necessary cascade propagation and regulation. Activation of fX occurs through the extrinsic tenase and intrinsic tenase complex interactions at the plasma membrane surface. Membrane interactions with fX are facilitated by its GLA domain that is rich in γ-carboxyglutamate for chelation of Ca^{2+} ions. These metal ions facilitate interactions with phosphatidylserine (PS) headgroups on the membrane. Previous molecular dynamic simulations have identified key residues interactions between chemical environments on PS and the GLA domain of bovine fX. Based on the predicted interactions, 12 fX-GLA domain residues with maximum contacts to PS were chosen for site-directed mutagenesis to characterize their molecular interactions with the membrane. Herein, we utilize DNA-tagged Nanodiscs to generate 26 different Nanodisc array for the first time on silicon photonic microring resonators. This array encompassed 2-3 biological replicates of 10 lipid environments, containing either PS and/or phosphatidylethanolamine (PE), with 4 technical replicates each. The surface was used to characterize the binding of wildtype human fX (wtfX) and 12 GLA domain mutants. This binding study is part of a bigger project to characterize the role

of fX-GLA domain in the initiation of the blood coagulation cascade currently ongoing in the Morrissey lab.

1. Introduction

Factor X (fX) activation is the pivotal point in the blood coagulation cascade. Proteolytic cleavage of fX occurs where the extrinsic and intrinsic pathways converge to generate the activated factor X (fXa) protease.[1] This protease propagates the cascade forward through formation of the prothrombinase complex on the plasma membrane with soluble activated factor V (fVa) by proteolytic cleavage of soluble prothrombin to its active form—thrombin.[2] Activation of thrombin is the turning point of the cascade. Thrombin is responsible for activation of key factors to produce a blood clot and act as negative feedback on the pathway.[3] The key role of thrombin would not be fulfilled without the activation of fX.

The complexes that activate fX are the extrinsic tenase and intrinsic tenase which are complexes made of two soluble protein localized to the plasma membrane in regions enriched with phosphatidylserine (PS).[4] For this activation to occur, fX associates to the membrane interface using its GLA domain.[5,6] This lipid binding domain is 44 amino acids long with 11 γ-carboxyglutamate (Gla) residues. The GLA domain forms a bundle of three α-helices stabilizes by as core of hydrophobic residues.[7] Gla residues are responsible for chelating Ca^{2+} to form an electrostatic interaction with PS[8] and induce conformational changes that result in tryptophan insertion into the membrane.[9] GLA domain interactions with the membrane are pertinent to the positioning of fX for activation by the extrinsic tenase[10,11] and intrinsic tenase[12] as well as formation of prothrombinase with fXa and fVa.[13]

Interactions with fX GLA domain are stereospecific for naturally occurring L-phosphatidylserine.[14] Recent molecular dynamics simulations have been used to identify chemical region interactions on PS with amino acids of bovine fX.[15] This study determined that Gla19 and Gla29 are two potential PS specific binding sides, and Gla32 preferential binding for the amine on PS could contribute to fX specific binding affinity due the absence of this Gla residue in factor VII and protein C which bind weakly to PS in comparison. Other interesting GLA domain observations have been made for the enhancement in activity[14] and binding[16] in low percentages of PS when phosphatidylethanolamine (PE) is present. This phenomenon has been termed the

"Anything But Choline" (ABC) hypothesis which justifies that phospholipids other than phosphatidylcholine (PC) can enhance GLA domain binding to the membrane.[17]

To further understand these previously made observations, the Morrissey lab generated a panel of human fX single GLA domain mutants (**Table VI.1**). The mutated residues have been selected based on the molecular dynamics simulations previously mentioned.[15] There is only one amino acid residue mismatch in this panel of mutants due to sequence differences from bovine to human at residue 10 which is a Gln or Lys, respectively. The Morrissey lab has performed fXa generation assays in solution (using soluble tissue factor) and on 20% PS 80% PC liposomes (membrane bound tissue factor) for each these mutants.[18] All mutants generate fXa in solution to some degree which shows that the mutations are not completely misfolding fX. Of particular interest was the observed change in activity for E19D, E25D, E32A, K9Q, R15Q, and R28Q in the presence of membranes. These mutations all show similar or more fX generation to the wtfX in solution but show less to no activity on liposomes. Thus, demonstrating the membrane binding properties of these residues.

Herein, we use DNA-tagged Nanodiscs on silicon photonic microring resonators[19] to characterize the binding interactions between these fX mutants and various lipid environments. DNA-tagged Nanodiscs were assembled with 50% PS for comparison in trends to the activity assays with 100% PC as a control. Additional environments of 10% PS, 20% PS, 35% PS, 10% PS 50% PE, 20% PS 40% PE, 35% PS 25% PE, 50% PS 10% PE, and 50% PE were used to study GLA domain mutation effects to PS-PE synergy. We found that all mutated residues do affect membrane binding. The data presented here is a snapshot of the fX mutant study with a focus on binding data and with minor comparisons to the activity assay data. Further studies are ongoing in the Morrissey lab to complete the story for understanding the key residues in the fX GLA domain.[18]

2. Materials and Methods

Chemicals and reagents

Phosphatidylcholine (POPC; 1-palmitoyl-2-oleoyl-sn-glycero-3-phosphocholine), phosphatidylserine (POPS; 1-palmitoyl-2-oleoyl-sn-glycero-2-phosphoserine), and phosphatidylethanolamine (POPE; 1,2-dipalmitoleoyl-sn-glycero-3-phosphoethanolamine) were purchased from Avanti Polar Lipids (Alabaster, AL). MSP1D1 D73C was expressed in *E. coli* and

purified as described previously.[20]. Custom DNA oligonucleotides were synthesized by Integrated DNA Technologies (IDT, San Jose, CA, USA) based on previous work.[19] Syringe filters (0.22 μm pore size) and Amberlite® XAD®-2 beads were purchased from MilliporeSigma (Burlington, MA, USA). HisPur Ni-NTA (nitrilotriacetic acid) Resin, succinimidyl-[(N-maleimidopropionamido)-hexaethyleneglycol]ester (SM(PEG)$_6$), AminoLink^{TM} Plus Immobilization Kit, Pierce BCA protein assay kit, and StartingBlock^{TM} (PBS) Blocking Buffer were purchased from ThermoFisher Scientific (Waltham, MA, USA). Human wtfX and mutants were generously provided by the Morrissey Lab (University of Michigan, Department of Biological Chemistry, Ann Arbor, MI, USA).

DNA-Tagged Nanodisc preparation and purification

DNA-tagged Nanodiscs were preparation and purification has been described in detail previously.[19] DNA oligoes are covalently attached to MSP1D1 D73C using SM(PEG)$_6$. First, DNA is conjugated to SM(PEG)$_6$ (dissolved in DMSO) at a 10:1 mole ratio of SM(PEG)$_6$ to DNA in PBS-8(+) (10 mM PBS, 3 mM EDTA, pH 8) and 20% DMSO for 1 hour at room temperature with mixing. Excess SM(PEG)$_6$ is removed by spin concentrating and DNA is buffer exchanged into PBS-6.5(+) (10 mM PBS, 3 mM EDTA, pH 6.5). MSP1D1 D73C in PBS-6.5(+) that was purged with argon for at least 30 minutes is incubated at a 10:5:1 mole ratio of sodium cholate to TCEP to MSP1D1 D73C for 15 minutes at room temperature. DNA is then added to the MSP1D1 D73C mixture to incubate at room temperature for 2 hours or overnight at 4°C. Excess DNA is removed by Ni-NTA purification. Conjugated MSP is purified by using DNA columns generated by the AminoLink^{TM} Plus Immobilization Kit with a modified purification protocol that used SDB (20 mM Tris, 100 mM NaCl, 0.5 mM EDTA, 0.01% NaN$_3$, pH 7.4) for column equilibration, a 30% formamide in SDB for wash steps, and 100% formamide for elution. Elutions are concentrated and buffer exchanged into SDB. Final concentrations of DNA-tagged MSP were determined using BCA assays.

Nanodiscs were assembled with DNA-tagged MSP as previously described.[19,21,22] Briefly, mixtures of PS, PE, and/or PC were generated at defined ratios prior to drying. All dried lipid mixtures contained PC as a balance. After drying, lipids were placed in a desiccator, under vacuum for at least 4 hours. Lipids were reconstituted in 100 mM sodium cholate for a final lipid concentration of 11.2 mM except for mixtures containing PE were reconstituted in 100 mM sodium

deoxycholate. DNA-tagged MSP and lipids were mixed at a ratio of 65:1 lipid to MSP in SDB with a final concentration of 20 mM sodium cholate for all mixtures for 1 hour at 4°C. Half the sample volume of Amberlite® XAD®-2 detergent removal beads were added to mix overnight at 4°C. Detergent removal beads were filtered off using 0.22 µm filters. Assembled Nanodiscs were purified using a Superdex 200 Increase 3.2/30 (GE Healthcare, Pittsburgh, PA, USA). Nanodisc concentration was determined using Qubit™ 3.0 Fluorometer (Invitrogen) ssDNA Assay Kit.

Silicon photonic microring resonators

The Maverick M1 optical scanning instrumentation and microring resonator sensor chips were purchased from Genalyte, Inc. (San Diego, CA). The operation of the instrument has been previously described.[23–27] Briefly, silicon photonic microring resonators are refractive index-based sensors with a diameter of 30 µm. The microring has an adjacent linear waveguide that directs a 1550 nm centered laser using total internal reflection next to the optical cavity. When the resonance condition is met, light couples into the microring allowing the detector to read a dip in transmittance at that resonant wavelength. The change in resonant wavelength is observed overtime.

Sensor chip array functionalization

Sensor chips were spotted by Genalyte (**Figure VI.1A**) and stored with DryCoat in a desiccator at 4°C. A laser-cut 2-channel Mylar gasket was used to generate 2-3 biological replicates for each lipid environment in clusters of 4 technical replicates (n = 8-12). DNA-tagged Nanodiscs were loaded on to the surface as previously described.[19] Briefly, functionalized chips were blocked with StartingBlock™ at a flow rate of 10 µL/min then rinsed with SDB + 2% BSA to maintain surface coverage. DNA-tagged Nanodiscs were loaded in SDB + 2% BSA as mixtures at 10 µL/min to ensure surface loading above 10 Δpm relative shift. Rinses of SDB + 2% BSA are performed between each loading step. Loading of each DNA-tagged Nanodisc is calculated per microring by taking the difference in Δpm relative shift of the trailing rinse step compared to the preceding rinse after controlling data to a ssDNA control. The final DNA-tagged Nanodisc array is shown in **Figure VI.1B** with a U-channel gasket for subsequent protein titrations.

Protein binding titrations

Titrations were performed in HEPES(+) (10 mM HEPES, 150 mM sodium chloride, 50 µM EDTA, 0.2% BSA, 0.1% (w/v) PEG 8000, 2.5 mM CaCl$_2$, pH 7.4) at 10 µL/min flow rate. Regeneration of the chip surface between titrations was performed in HEPES without CaCl$_2$. Most fX mutant titrations were performed at 100 nM, 250 nM, 750 nM, 2.5 µM, and 5 µM steps except for K9Q and K10Q which used 100 nM, 250 nM, 750 nM, 2 µM, and 4 µM due to protein availability.

Data analysis

Analysis was performed using a custom R script in RStudio. Sensor traces were corrected for temperature fluctuations and bulk non-specific binding by subtraction of response to the ssDNA control. Protein titrations use calculated DNA-tagged Nanodisc loading to correct for array surface coverage using the equation:

$$Protein \ per \ leaflet = \left(\frac{\Delta pm_{Protein}}{M_{w,Protein}}\right)\left(\frac{M_{w,Nanodisc}}{\Delta pm_{Nanodisc}}\right)\left(\frac{1}{2}\right) \qquad \textbf{(VI.1)}$$

where $\Delta pm_{Protein}$ is the relative shift response during the protein titration, $M_{w,Protein}$ is the molecular weight of the titrated protein, $\Delta pm_{Nanodisc}$ is the quantified loading of Nanodisc, and $M_{w,Nanodisc}$ is the molecular weight of the Nanodisc. This calculation is performed on each microring individually to account for surface coverage differences. Binding curves are generated by plotting the relative shift in protein per leaflet at the equilibrium point of each titration step compared to the relative shift at the end of the HEPES(+) step versus the concentration of protein. The curves are then fit to the following equation to characterize the binding:

$$Protein \ per \ leaflet = Protein \ per \ leaflet_{max} \ \left(\frac{X}{K_d + X}\right) \qquad (VI.2)$$

where X is the concentration of the titrated protein and K_d is the dissociation constant. The hill coefficient gives information about the cooperativity of the binding while the K_d quantifies the binding affinity. Standard errors in the ratios for values relative to wtfX were determined based on Fieller's Theorem with independent values.[28]

3. Results and Discussion

DNA-tagged Nanodiscs were loaded on to the sensor surface to generate the array shown in **Figure 6.1B**. In total, 26 different Nanodisc preparations were arrayed for the first time on silicon photonic microring resonators. This array is comprised of 2-3 biological replicate of 10 lipid environments with 4 technical replicates each. The array consisted of 10% PS, 20% PS, 35% PS, 50% PS, 10% PS 50% PE, 20% PS 40% PE, 35% PS 25% PE, 50% PS 10% PE, 50% PE, and 100% PC as a control.

Factor X mutant membrane association comparison to activity

For simplicity, biological and technical replicates are plotted as an average with standard deviations for error between individual microrings (**Figure VI.2**, left). All calculates for normalization and binding are performed on each microring individually (**Figure VI.2**, right) with final values reported as averages with standard deviations for error (**Table VI.2**).

For comparison to the mentioned unpublished data from the Morrissey lab, the binding values relative to wtfX for 50% PS Nanodiscs have been plotted in **Figure VI.3**. Dissociation constants characterize binding with an inverse relationship to activity. For activity, higher activity means that the enzymatic turnover occurs at a higher rate. Higher binding affinity is, however, shown by a lower K_d due to the value representing the concentration at which half the binding sites are occupied, and a lower concentration that does this more efficiently has a higher affinity. To make an argument showing the same trends, we have plotted the K_a relative to wtfX (**Figure VI.3A**).

The mutants E19D, E25D, E32A, K9Q, R15Q, and R28Q showed the most interesting trends in activity due to their similarities to wtfX in solution compared to the diminished activity on liposomes. The Gla residues in particular showed almost no activity whereas, the adjacent residues showed close to 50% reduction.[18] The association constants for these mutants show similar trends in terms of diminished binding affinity (**Figure VI.3A**).

Starting with the Gla mutants, no binding was observed to 50% PS Nanodiscs by E7D, E20D, E25D, and E29D. These residues are clearly essential for GLA domain interactions with the membrane. Two mutants were generated of Gla32 that showed differential binding. The E32A mutant showed no binding while E32D (**Figure VI.3A**, yellow) was able to interact with the

membrane. Though the E32D binding affinity looks stronger, there is a very diminished maximum binding per leaflet (**Figure VI.3B**, yellow). The similar environment generated by substituting an aspartate in place of the γ-carboxyglutamate can stabilize interactions on the surface, but not as efficiently as the native state. A similar interaction that was observed at E32D was also observed at E14D (**Figure VI.3**, red). E19D (**Figure VI.3**, orange) shows weak binding with around 50% maximum binding compared to wtfX which trends similarly to the decrease in activity with membranes present.

The lysine and arginine mutants are adjacent to Gla residues. K10Q, and R28Q show similar binding to wtfX (**Figure VI.3**, blue and green), but also exhibit a lower efficiency due to displaying less loading per leaflet. In contrast, K9Q and R15Q have lower binding affinities compared to wtfX (**Figure VI.3**, indigo and teal) with slightly higher maximum binding compared to K10Q, and R28Q. The lysine and arginine residues are necessary for membrane interactions but are not necessarily destroying the membrane interactions compared to the mutation of γ-carboxyglutamate.

These observations track well with the predicted contact points observed between γ-carboxyglutamate residues to calcium and the amine on PS compared to the phosphate or carboxyl PS interactions seen with lysine and arginine.[15] GLA domains require calcium to bind to the membrane; thus, mutating the docking points abolishes the interaction. In particular, there are two predicted PS binding sites with bovine fX involving 1) Gla19 with two calcium ions and 2) Gla29 with Gln10 and one calcium.[15] For human fX, mutation of Gla19 and Lys10 did not eliminate the membrane association while the Gla29 did prohibit binding completely due to the high affinity at this site for calcium. For the second PS interaction, the mutations demonstrate that Gla29 is more important for the interaction with PS than Lys10.

Factor X lipid synergy characterization

The ABC hypothesis states that any phospholipid but PC can cooperate with PS to achieve comparable or tighter binding affinity in environments with low PS.[17] This trend has been shown

in the literature[14,16] and **Figure VI.4A** for the GLA domain with PS and PE for wtfX. No binding is observed with 50% PE alone which demonstrates that both PS and PE are needed to achieve this interaction with the fX-GLA domain.

The fX mutants were screened for this synergistic behavior to potentially observe a change in this synergistic trend, but this was not the case. For all mutants with observable binding, there PS-PE cooperation is present (**Figure VI.4B**). Mutants, in most cases, show a similar trend to wtfX due to increased binding affinity with increasing PS or with the addition of PE. In contrast to this trend, R28Q shows no difference in binding affinity when increasing PS or PE content except in the case of low PS. Arg28 shows preference for carboxyl interactions with PS in simulations.[15] Changes to this interaction may have adjusted the lipid binding preferences for this surface of fX which would be interesting for future experiments potentially with synthetic analogs to PS.

The maximum binding efficiency per leaflet for wtfX did not vary between PS and PE environments (**Figure VI.5A**) with the exception of no observable binding with 50% PE. Mutants of fX show diminished maximum binding in comparison to wtfX but do not show a difference in maximal binding for environments where affinity was observed (**Figure VI.5B**). This could be due to a potential cooperativity in binding with fX near the membrane interface.

4. Conclusion

We screened a panel of fX-GLA mutants using highly multiplexed DNA-tagged Nanodisc technology on silicon photonic microring resonators. This study is part of a larger ongoing study in the Morrissey lab in the Department of Biological Chemistry at the University of Michigan.[18] The Morrissey lab has collected activity data for each of these mutants which were the main motivation for collection of complementary binding data. The conclusions complement each other to show that Gla residues in the fX are essential for membrane association while adjacent residues contribute minorly.

Amino acids of interest for these interactions are Gla19 and Lys10. Molecular modeling simulations show that Gla19 bind with two calcium ions which contribute to GLA domain association to PS.[15] Mutation of this residue to aspartate minimized binding, but did not abolish it. More studies are needed to understand the potential calcium interactions with amino acids adjacent to Gla19 that may also be present in chelating calcium. The same simulation study predicted

214

interactions between calcium, Gln10, and Gla29 for bovine fX. Mutation of Gla29 resulted in no binding in most lipid environments but mutation of Lys10 to glutamine simply diminished the interactions. This could be potentially due to a difference in homology between bovine and human fX.

Overall, this portion of the overarching project has provided binding data that complements activity data for the panel of fX-GLA domain mutants. This was the highest multiplexed study run on the silicon photonic microring resonators with Nanodiscs. This technique has promise to open the door for screening of interactions at a higher multiplexity than currently available for lipid-protein or membrane protein-protein interactions.

5. Acknowledgements

Divyani Paul from the Morrissey lab conceived the project, generated/provided the factor X mutant panel, collected preliminary activity assay data, and assisted in proofreading this chapter. These assays are not shown here but are referenced. My contribution in the research corresponds to assisting in design of a lipid environment panel and performing the binding characterization experiments outlined in this chapter.

Figure VI.1. Sensor Chip Layout. (**A**) The flow path for loading is shown by the *light blue box* and *arrows* using a 2-channel setup. The array was generated by Genalyte for functionalization of control (pink), N (black), M (gold), L (dark blue), K (dark purple), J (dark green), I (yellow), H (dark red), G (brown), F (red), E (orange), D (blue), C (green), B (grey), and A (purple). (**B**) The flow path for Nanodisc array titration is shown by the *light blue box* and *arrows* using a U-channel setup. Flow loading in *(A)* was used to generate the array of 100 % PC (black), 10% PS (red), 20% PS (orange), 35% PS (yellow), 50% PS (pink), 50% PE (purple), 10% PS 50% PE (indigo), 20% PS 40% PE (blue), 35% PS 20% PE (teal), and 50% PS 10% PE (green) while white represents unfunctionalized microrings that act as ssDNA controls. This allows 2-3 biological replicates with 4 technical replicates each for every Nanodisc (n = 8-12).
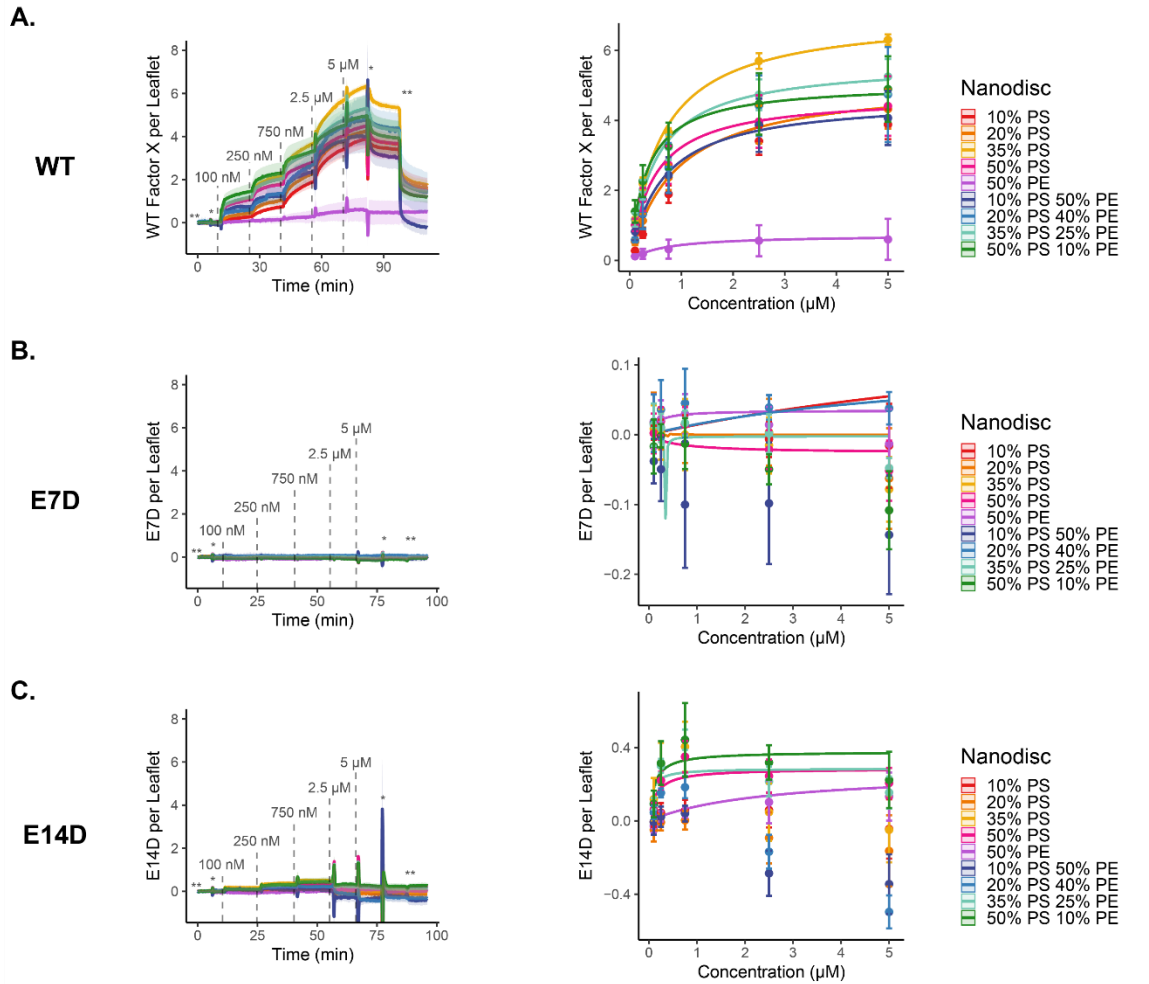
Figure VI.2. Factor X Wildtype and Mutant Titrations. (**A-C**) *Right:* Normalized and 100% PC controlled fX titration from 100 nM to 5 µM with buffer steps of HEPES (**) and HEPES(+) (*). The shaded ribbon shows the standard deviation of microrings (n = 8-12). *Left:* fX binding curve with fX per leaflet values calculated from equilibrated steps in the titration using the first calcium buffer step as a zero point. The plotted binding fit is generated with the average values from the fit for each microring (n = 8-12).
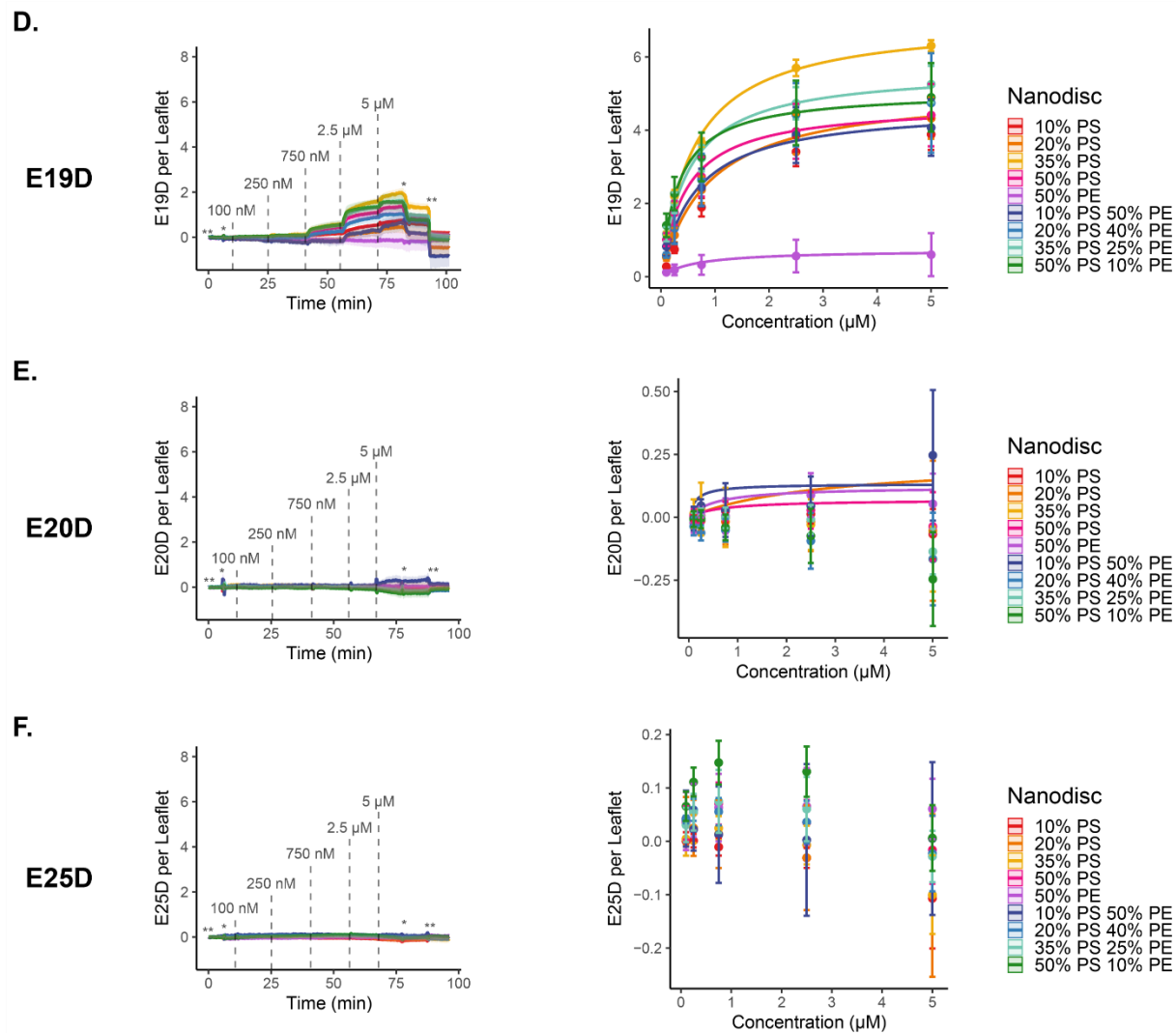
Figure VI.2. Factor X Wildtype and Mutant Titrations. (**D-F**) *Right:* Normalized and 100% PC controlled fX titration from 100 nM to 5 µM with buffer steps of HEPES (**) and HEPES(+) (*). The shaded ribbon shows the standard deviation of microrings (n = 8-12). *Left:* fX binding curve with fX per leaflet values calculated from equilibrated steps in the titration using the first calcium buffer step as a zero point. The plotted binding fit is generated with the average values from the fit for each microring (n = 8-12).
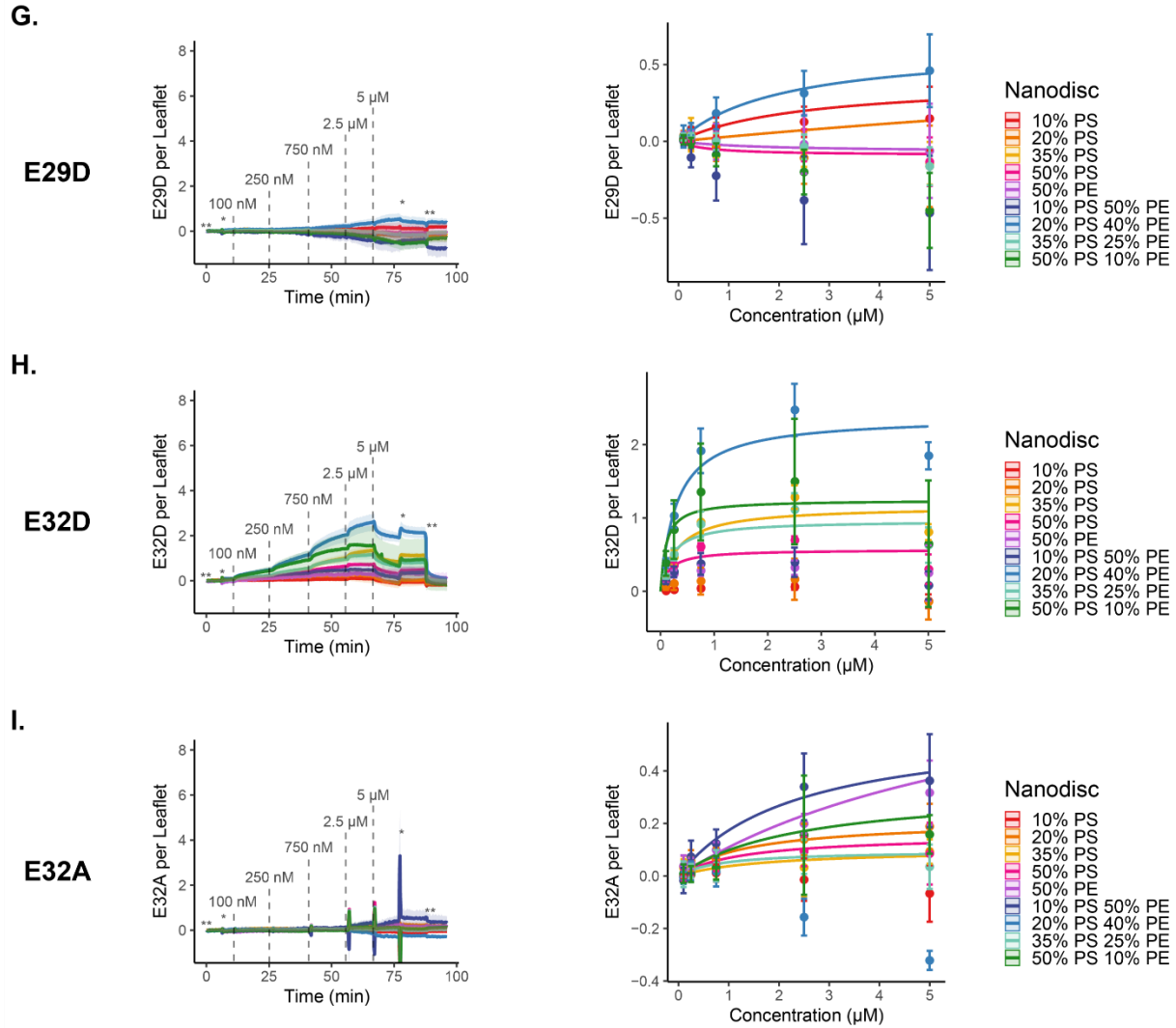
Figure VI.2. Factor X Wildtype and Mutant Titrations. (**G-I**) *Right:* Normalized and 100% PC controlled fX titration from 100 nM to 5 µM with buffer steps of HEPES (**) and HEPES(+) (*). The shaded ribbon shows the standard deviation of microrings (n = 8-12). *Left:* fX binding curve with fX per leaflet values calculated from equilibrated steps in the titration using the first calcium buffer step as a zero point. The plotted binding fit is generated with the average values from the fit for each microring (n = 8-12).
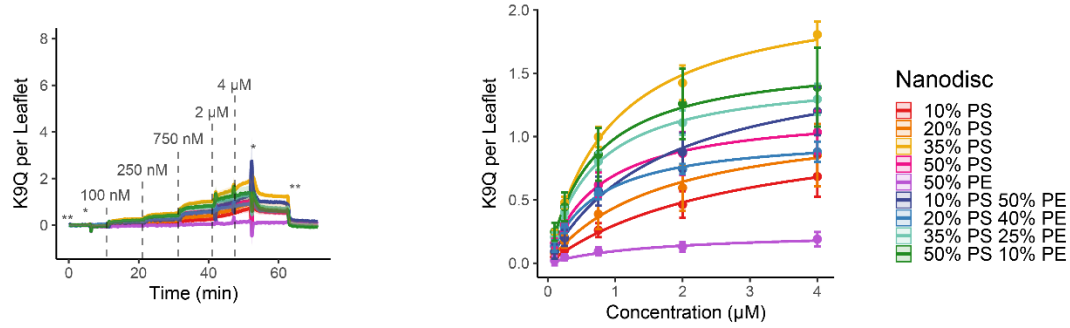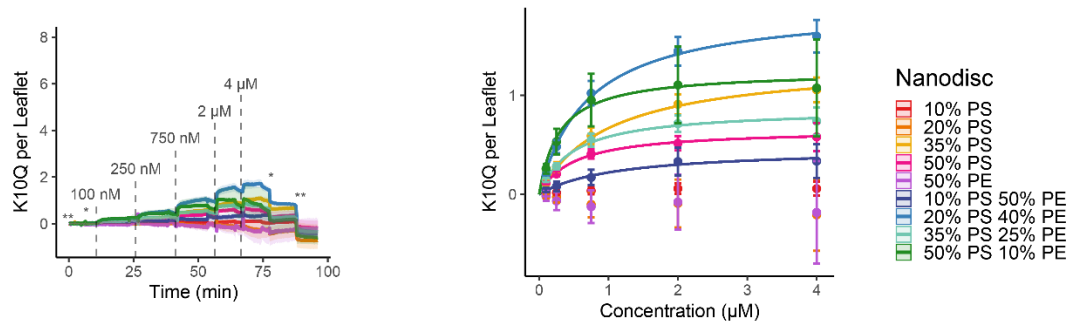
Figure VI.2. Factor X Wildtype and Mutant Titrations. (**J-K**) *Right:* Normalized and 100% PC controlled fX titration from 100 nM to 4 µM with buffer steps of HEPES (******) and HEPES(+) (*****). The shaded ribbon shows the standard deviation of microrings (n = 8-12). *Left:* fX binding curve with fX per leaflet values calculated from equilibrated steps in the titration using the first calcium buffer step as a zero point. The plotted binding fit is generated with the average values from the fit for each microring (n = 8-12).
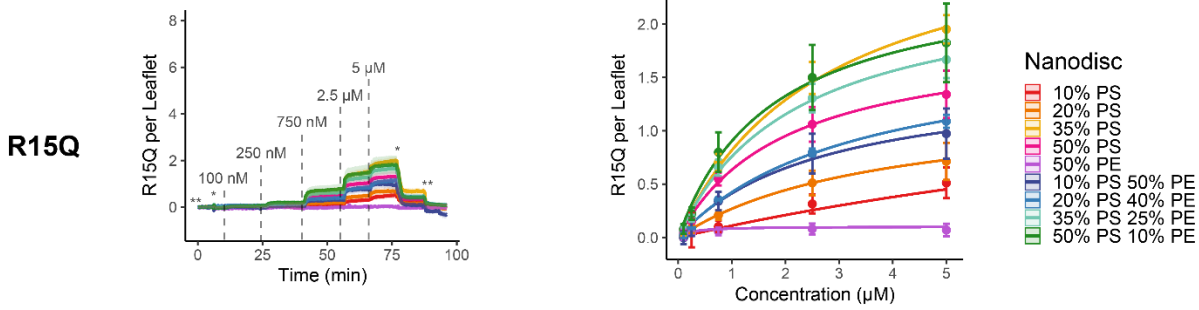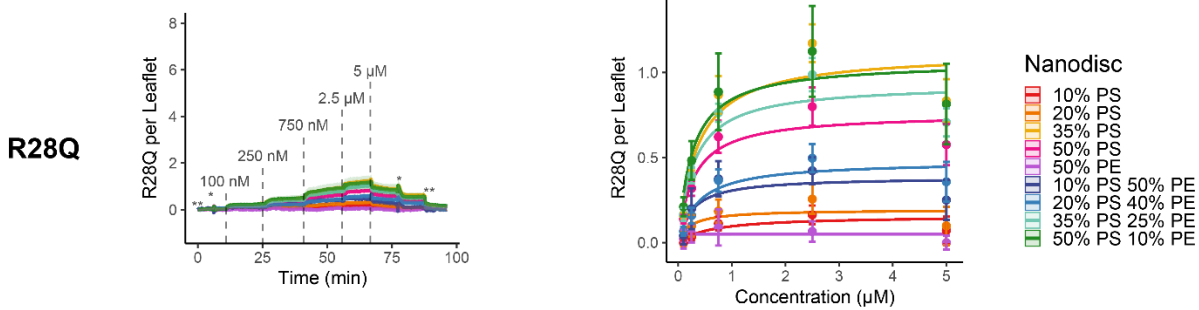
Figure VI.2. Factor X Wildtype and Mutant Titrations. (**L-M**) *Right:* Normalized and 100% PC controlled fX titration from 100 nM to 5 µM with buffer steps of HEPES (**) and HEPES(+) (*). The shaded ribbon shows the standard deviation of microrings (n = 8-12). *Left:* fX binding curve with fX per leaflet values calculated from equilibrated steps in the titration using the first calcium buffer step as a zero point. The plotted binding fit is generated with the average values from the fit for each microring (n = 8-12).
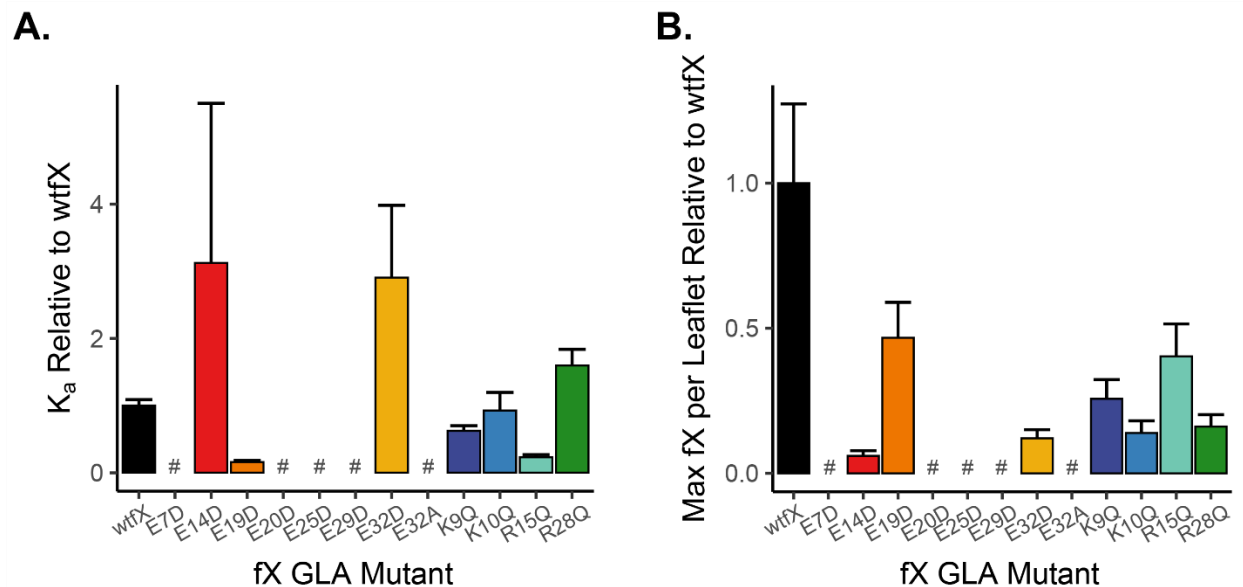
Figure VI.3. Values for Factor X Binding to 50% PS Nanodiscs. (**A**) The inverse dissociation constant relative to wtfX is plotted to mirror activity data. Values above 1 have a higher affinity than wtfX while values less than 1 have a lower affinity. (**B**) Maximum binding per leaflet of fX and fX mutants relative to fX. *Note:* Error bars represent standard error in calculating ratios of these values[28] (n = 12) and values denoted with # were unable to be calculated due to no observed binding.
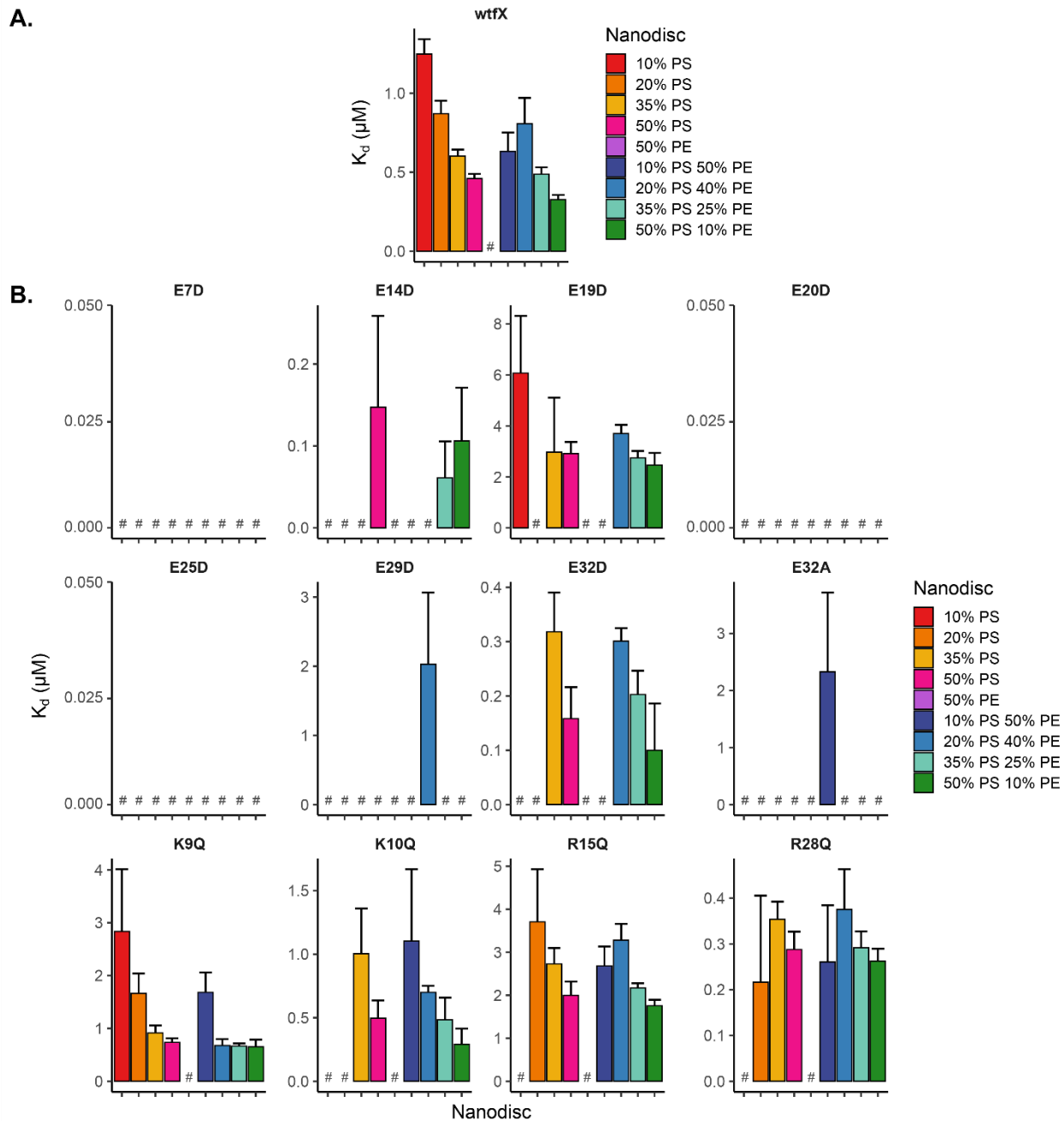
Figure VI.4. Factor X Dissociation Constants with Various Lipid Environments. Dissociation constants plotted with different y-axes to observe lipid synergy between PS and PE for (**A**) wtfX and (**B**) fX mutants. *Note:* n = 8-12 and values denoted with *#* were unable to be calculated due to no observed binding.

Figure VI.5. Maximum Factor X Binding per Leaflet on Various Lipid Environments. Maximum binding per leaflet for (**A**) wtfX and (**B**) fX mutants with the same y-axes for comparison to wtfX. *Note:* n = 8-12 and values denoted with # were unable to be calculated due to no observed binding.
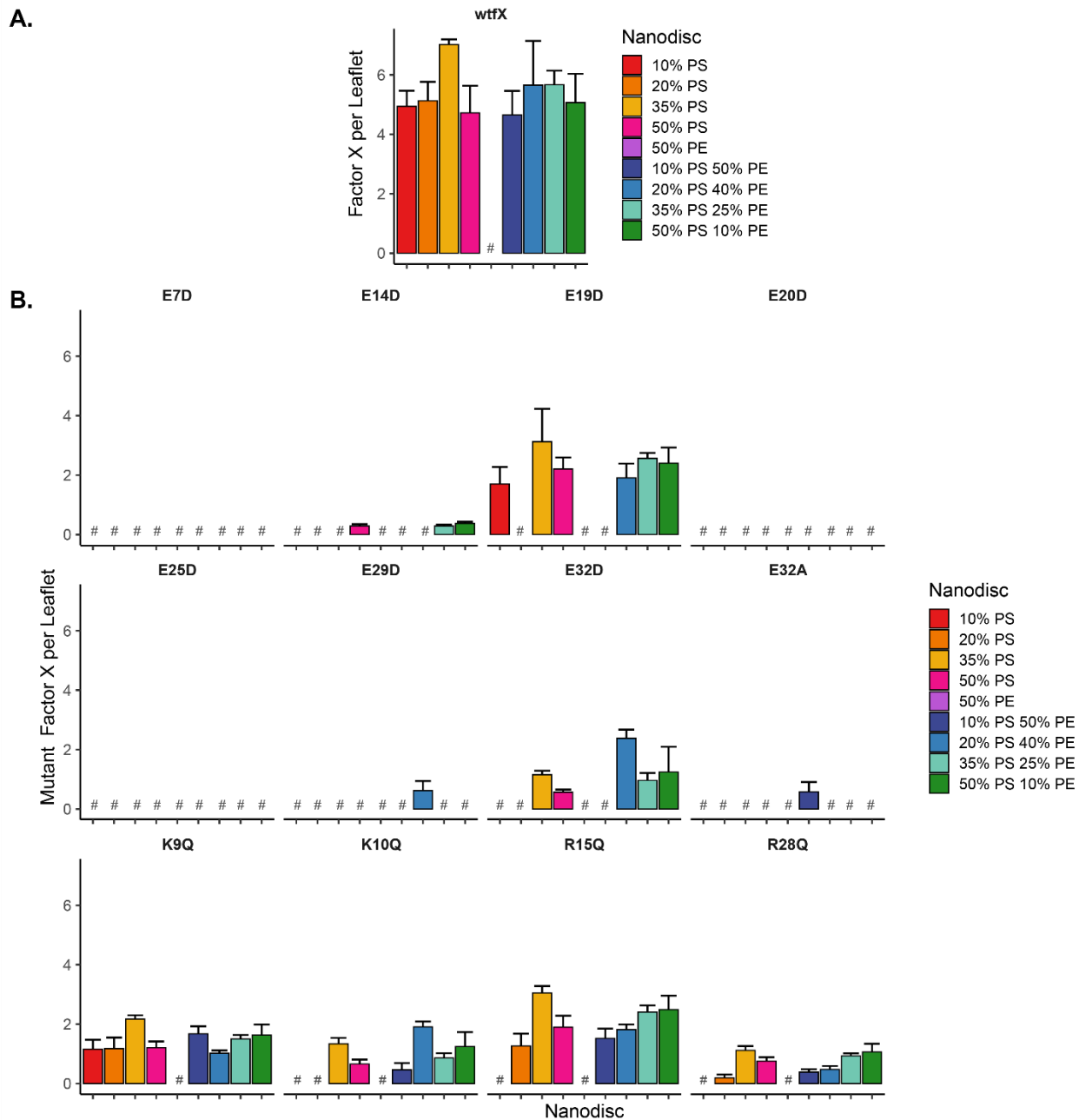
TABLES

Table VI.1. List of Factor X Mutants.

Mutations[a]
E7D
E14D
E19D
E20D
E25D
E29D
E32D
E32A
K9Q
K10Q
R15Q
R28Q

[a]Mutations designed and provided by Divyani Paul in the Morrissey lab[18]

Table VI.2. Factor X Binding Data.

Protein	10 % PS K_d (µM)	10 % PS Max. fX per Leaflet	20 % PS K_d (µM)	20 % PS Max. fX per Leaflet	35% PS K_d (µM)	35% PS Max. fX per Leaflet	50% PS K_d (µM)	50% PS Max. fX per Leaflet	50% PE K_d (µM)	50% PE Max. fX per Leaflet	10% PS 50% PE K_d (µM)	10% PS 50% PE Max. fX per Leaflet	20% PS 40% PE K_d (µM)	20% PS 40% PE Max. fX per Leaflet	35% PS 25% PE K_d (µM)	35% PS 25% PE Max. fX per Leaflet	50% PS 10% PE K_d (µM)	50% PS 10% PE Max. fX per Leaflet
wtfX	1.2 ± 0.1	4.9 ± 0.5	0.87 ± 0.08	5.1 ± 0.6	0.60 ± 0.04	7.0 ± 0.2	0.46 ± 0.03	4.7 ± 0.9	NA[a]	NA[a]	0.6 ± 0.1	4.7 ± 0.8	0.8 ± 0.2	6 ± 1	0.49 ± 0.04	5.7 ± 0.5	0.33 ± 0.03	5 ± 1
E7D	NA[a]	NA[a]	NA[a]	NA[a]	NA[a]	NA[a]	NA[a]	NA[a]	NA[a]	NA[a]	NA[a]	NA[a]	NA[a]	NA[a]	NA[a]	NA[a]	NA[a]	NA[a]
E14D	NA[a]	NA[a]	NA[a]	NA[a]	NA[a]	NA[a]	0.2 ± 0.1	0.28 ± 0.06	NA[a]	NA[a]	NA[a]	NA[a]	NA[a]	NA[a]	0.06 ± 0.04	0.29 ± 0.06	0.11 ± 0.06	0.38 ± 0.05
E19D	6 ± 2	1.7 ± 0.6	NA[a]	NA[a]	3 ± 2	3 ± 1	2.9 ± 0.5	2.2 ± 0.4	NA[a]	NA[a]	NA[a]	NA[a]	3.7 ± 0.3	1.9 ± 0.5	2.7 ± 0.3	2.6 ± 0.2	2.5 ± 0.5	2.4 ± 0.5
E20D	NA[a]	NA[a]	NA[a]	NA[a]	NA[a]	NA[a]	NA[a]	NA[a]	NA[a]	NA[a]	NA[a]	NA[a]	NA[a]	NA[a]	NA[a]	NA[a]	NA[a]	NA[a]
E25D	NA[a]	NA[a]	NA[a]	NA[a]	NA[a]	NA[a]	NA[a]	NA[a]	NA[a]	NA[a]	NA[a]	NA[a]	NA[a]	NA[a]	NA[a]	NA[a]	NA[a]	NA[a]
E29D	NA[a]	NA[a]	NA[a]	NA[a]	NA[a]	NA[a]	NA[a]	NA[a]	NA[a]	NA[a]	NA[a]	NA[a]	2 ± 1	0.6 ± 0.3	NA[a]	NA[a]	NA[a]	NA[a]
E32D	NA[a]	NA[a]	NA[a]	NA[a]	0.32 ± 0.07	1.2 ± 0.1	0.15 ± 0.06	0.57 ± 0.09	NA[a]	NA[a]	NA[a]	NA[a]	0.30 ± 0.02	2.4 ± 0.3	0.20 ± 0.04	1.0 ± 0.3	0.10 ± 0.09	1.2 ± 0.9
E32A	NA[a]	NA[a]	NA[a]	NA[a]	NA[a]	NA[a]	NA[a]	NA[a]	NA[a]	NA[a]	2 ± 1	0.6 ± 0.3	NA[a]	NA[a]	NA[a]	NA[a]	NA[a]	NA[a]
K9Q	3 ± 1	1.2 ± 0.3	1.7 ± 0.4	1.2 ± 0.4	0.9 ± 0.1	2.1 ± 0.1	0.74 ± 0.08	1.2 ± 0.2	NA[a]	NA[a]	1.7 ± 0.4	1.7 ± 0.3	0.7 ± 0.1	1.0 ± 0.1	0.66 ± 0.05	1.5 ± 0.1	0.7 ± 0.1	1.6 ± 0.4
K10Q	NA[a]	NA[a]	NA[a]	NA[a]	1.0 ± 0.4	1.3 ± 0.2	0.5 ± 0.1	0.7 ± 0.2	NA[a]	NA[a]	1.1 ± 0.6	0.5 ± 0.2	0.70 ± 0.05	1.9 ± 0.2	0.5 ± 0.2	0.9 ± 0.2	0.3 ± 0.1	1.2 ± 0.5
R15Q	NA[a]	NA[a]	4 ± 1	1.3 ± 0.4	2.7 ± 0.4	3.0 ± 0.2	2.0 ± 0.3	1.9 ± 0.4	NA[a]	NA[a]	2.7 ± 0.5	1.5 ± 0.3	3.3 ± 0.4	1.8 ± 0.2	2.2 ± 0.1	2.4 ± 0.2	1.8 ± 0.1	2.5 ± 0.5
R28Q	NA[a]	NA[a]	0.2 ± 0.1	0.2 ± 0.1	0.35 ± 0.04	1.1 ± 0.1	0.28 ± 0.04	0.8 ± 0.1	NA[a]	NA[a]	0.3 ± 0.1	0.4 ± 0.1	0.38 ± 0.09	0.5 ± 0.1	0.29 ± 0.04	0.93 ± 0.09	0.26 ± 0.03	1.1 ± 0.3

[a]Unable to fit data

Table VI.3. Factor X Mutant Binding Data Relative to Wildtype for 50% PS.

Protein	K_a Relative to WT	Maximum fX per Leaflet Relative to WT
WT	1.00 ± 0.09	1 ± 0.2
E7D	NA[a]	NA[a]
E14D	3 ± 2	0.06 ± 0.02
E19D	0.16 ± 0.03	0.5 ± 0.1
E20D	NA[a]	NA[a]
E25D	NA[a]	NA[a]
E29D	NA[a]	NA[a]
E32D	3 ± 1	0.12 ± 0.03
E32A	NA[a]	NA[a]
K9Q	0.62 ± 0.08	0.26 ± 0.07
K10Q	0.9 ± 0.3	0.14 ± 0.04
R15Q	0.2 ± 0.04	0.4 ± 0.1
R28Q	1.6 ± 0.2	0.16 ± 0.04

[a]Unable to fit data

REFERENCES

(1)   Furie, B.; Furie, B. C. The Molecular Basis of Blood Coagulation. *Cell* **1988**, *53* (4), 505–518.

(2)   Hertzberg, M. Biochemistry of Factor X. *Blood Rev.* **1994**, *8* (1), 56–62.

(3)   Davie, E. W.; Fujikawa, K.; Kisiel, W. The Coagulation Cascade: Initiation, Maintenance, and Regulation. *Perspect. Biochem.* **1991**, *30* (42), 10363–10370.

(4)   Zwaal, R. F. A.; Comfurius, P.; Bevers, E. M. Lipid–Protein Interactions in Blood Coagulation. *Biochim. Biophys. Acta (BBA)-Reviews Biomembr.* **1998**, *1376* (3), 433–453.

(5)   Mizuno, H.; Fujimoto, Z.; Atoda, H.; Morita, T. Crystal Structure of an Anticoagulant Protein in Complex with the Gla Domain of Factor X. *Proc Natl Acad Sci U S A* **2001**, *98* (13), 7230–7234.

(6)   Maignan, S.; Guilloteau, J. P.; Pouzieux, S.; Choi-Sledeski, Y. M.; Becker, M. R.; Klein, S. I.; Ewing, W. R.; Pauls, H. W.; Spada, A. P.; Mikol, V. Crystal Structures of Human Factor Xa Complexed with Potent Inhibitors. *J. Med. Chem.* **2000**, *43* (17), 3226–3232.

(7)   Wang, S. X.; Hur, E.; Sousa, C. A.; Brinen, L.; Slivka, E. J.; Fletterick, R. J. The Extended Interactions and Gla Domain of Blood Coagulation Factor Xa. *Biochemistry* **2003**, *42* (26), 7959–7966.

(8)   Häfner, A.; Merola, F.; Duportail, G.; Hutterer, R.; Schneider, F. W.; Hof, M. Calcium-Induced Conformational Change in Fragment 1-86 of Factor X. *Biopolym. - Biospectroscopy Sect.* **2000**, *57* (4), 226–234.

(9)   Sunnerhagen, M.; Olah, G. A.; Stenflo, J.; Forsén, S.; Drakenberg, T.; Trewhella, J. The Relative Orientation of Gla and EGF Domains in Coagulation Factor X Is Altered by Ca2+ Binding to the First EGF Domain. A Combined NMR-Small Angle X-Ray Scattering Study. *Biochemistry* **1996**, *35* (36), 11547–11559.

(10)   Ndonwi, M.; Broze, G. J.; Agah, S.; Schmidt, A. E.; Bajaj, S. P. Substitution of the Gla Domain in Factor X with That of Protein C Impairs Its Interaction with Factor VIIa/Tissue Factor: Lack of Comparable Effect by Similar Substitution in Factor IX. *J. Biol. Chem.* **2007**, *282* (21), 15632–15644.

(11)   Valcarce, C.; Selander-Sunnerhagen, M.; Tamlitz, A. M.; Drakenberg, T.; Bjork, I.; Stenflo, J. Calcium Affinity of the NH2-Terminal Epidermal Growth Factor-like Module of Factor

X. Effect of the γ-Carboxyglutamic Acid-Containing Module. *J. Biol. Chem.* **1993**, *268* (35), 26673–26678.

(12)   Basavaraj, M. G.; Krishnaswamy, S. Exosite Binding Drives Substrate Affinity for the Activation of Coagulation Factor X by the Intrinsic Xase Complex. *J. Biol. Chem.* **2020**, *295* (45), 15198–15207.

(13)   Rosing, J.; Tans, G.; Govers-Riemslag, J. W. P.; Zwaal, R. F.; Hemker, H. C. The Role of Phospholipids and Factor Va in the Prothrombinase Complex. *J. Biol. Chem.* **1980**, *255* (1), 274–283.

(14)   Tavoosi, N.; Smith, S. A.; Davis-Harrison, R. L.; Morrissey, J. H. Factor VII and Protein C Are Phosphatidic Acid-Binding Proteins. *Biochemistry* **2013**, *52* (33), 5545–5552.

(15)   Muller, M. P.; Wang, Y.; Morrissey, J. H.; Tajkhorshid, E. Lipid Specificity of the Membrane Binding Domain of Coagulation Factor X. *J. Thromb. Haemost.* **2017**, *15* (10), 2005–2016.

(16)   Medfisch, S. M.; Muehl, E. M.; Morrissey, J. H.; Bailey, R. C. Phosphatidylethanolamine-Phosphatidylserine Binding Synergy of Seven Coagulation Factors Revealed Using Nanodisc Arrays on Silicon Photonic Sensors. *Sci. Rep.* **2020**, *10* (17407), 1–7.

(17)   Tavoosi, N.; Davis-Harrison, R. L.; Pogorelov, T. V.; Ohkubo, Y. Z.; Arcario, M. J.; Clay, M. C.; Rienstra, C. M.; Tajkhorshid, E.; Morrissey, J. H. Molecular Determinants of Phospholipid Synergy in Blood Clotting. *J. Biol. Chem.* **2011**, *286* (26), 23247–23253.

(18)   Paul, D.; Morrissey, J. H. No Title. *Unpubl. results*.

(19)   Medfisch, S. M.; Morrissey, J. H.; Bailey, R. C. Development of DNA Tethered Nanodisc Arrays for Quantitative Characterization of Lipid-Protein and Membrane Protein-Protein Interactions on Silicon Photonic Microring Resonators in the Blood Coagulation Cascade. *Prep.*

(20)   Bayburt, T. H.; Sligar, S. G. Membrane Protein Assembly into Nanodiscs. *FEBS Lett.* **2010**, *584* (9), 1721–1727.

(21)   Bayburt, T. H.; Sligar, S. G. Self-Assembly of Single Integral Membrane Proteins into Soluble Nanoscale Phospholipid Bilayers. *Protein Sci.* **2003**, *12* (11), 2476–2481.

(22)   Denisov, I. G.; Grinkova, Y. V.; Lazarides, A. A.; Sligar, S. G. Directed Self-Assembly of Monodisperse Phospholipid Bilayer Nanodiscs with Controlled Size Directed Self-Assembly of Monodisperse Phospholipid Bilayer Nanodiscs with Controlled Size. *Nano*

Lett. **2004**, *126* (11), 3477–3487.

(23) Iqbal, M.; Gleeson, M. a; Spaugh, B.; Tybor, F.; Gunn, W. G.; Hochberg, M.; Baehr-jones, T.; Bailey, R. C.; Gunn, L. C.; Resonators, R.; Optical, H.; Iqbal, M.; Gleeson, M. a; Spaugh, B.; Tybor, F.; Gunn, W. G.; Hochberg, M.; Baehr-jones, T.; Bailey, R. C.; Gunn, L. C. Label-Free Biosensor Arrays Based on Silicon Scanning Instrumentation. *IEEE J. Sel. Top. Quantum Electron.* **2010**, *16* (3), 654–661.

(24) Byeon, J.-Y.; Limpoco, F. T.; Bailey, R. C. Efficient Bioconjugation of Protein Capture Agents to Biosensor Surfaces Using Aniline-Catalyzed Hydrazone Ligation. *Langmuir* **2010**, *26* (19), 15430–15435.

(25) Luchansky, M. S.; Washburn, A. L.; Qavi, A. J.; Kindt, J. T.; McClellan, M. S.; Bailey, R. C. Silicon Photonic Microring Resonator Arrays for Scalable and Multiplexable Bioanalysis. *Proc. SPIE* **2011**, *7888*, 1–4.

(26) Wade, J. H.; Alsop, A. T.; Vertin, N. R.; Yang, H.; Johnson, M. D.; Bailey, R. C. Rapid, Multiplexed Phosphoprotein Profiling Using Silicon Photonic Sensor Arrays. *ACS Cent. Sci.* **2015**, *1* (7), 374–382.

(27) Washburn, A. L.; Shia, W. W.; Lenkeit, K. A.; Lee, S.-H.; Bailey, R. C. Multiplexed Cancer Biomarker Detection Using Chip-Integrated Silicon Photonic Sensor Arrays. *Analyst* **2016**, *141* (18), 5358–5365.

(28) Dunlap, W. P.; Silver, N. C. Confidence Intervals and Standard Errors for Ratios of Normal Variables. *Behav. Res. Methods, Instruments, Comput.* **1986**, *18* (5), 469–471.

CHAPTER VII

Conclusions and Future Directions

1. Introduction

This work summarized four years of effort toward development of a high throughput system for lipid-protein and membrane protein-protein interaction characterization. Chapter I began with an overview of the importance of biological membranes in physiology. Membrane mimetics and their use in a myriad of techniques was discussed before giving an introduction into the biological process of interest for this thesis—blood coagulation. The main lipid interaction of interest is that of the GLA domain which is a lipid binding domain rich in γ-carboxyglutamate that chelates calcium ions to form electrostatic interactions with phosphatidylserine (PS). Next, Chapter II told the story of high-density lipoprotein mimetic development. The narrative provided an unbiased comparison of peptide, protein, DNA, and polymer for stabilization of lipids into disc-like mimetics termed *nanodiscs*. Each of these scaffolding reagents have their advantages and disadvantages but many can be used interchangeably to achieve the same studies.

2. Nanodiscs on Silicon Photonic Microring Resonators

This work utilized Nanodiscs formed with membrane scaffold protein (MSP) due to the stoichiometric control over MSP incorporation around the mimetic.[1–4] The following chapters worked toward optimization of the interface between Nanodiscs and silicon photonic microring resonators for multiplexed lipid-protein and membrane protein-protein characterization of blood coagulation cascade interactions.

Chapter III and IV focused on spotting Nanodiscs in spatially different clusters on silicon photonic microring resonator chips. These arrays are formed with physisorption interactions between the silicon oxide coated microring surface and lipid headgroup electrostatic interactions. First, this technique was used as a proof of concept study to show increased binding affinity for GLA domain-containing blood coagulation factors with increasing amounts of phosphatidylserine (PS) and phosphatidic (PA).[5] Factor VIIa and activated protein C were also shown to preferentially bind PA as previously seen in the literature. Secondly, an array of PS. Secondly, an array of PS and phosphatidylethanolamine (PE) environments were used to quantify lipid synergy.[6]

There are two major drawbacks to physisorption Nanodisc arrays: membrane environment limitations and inability to quantitate surface coverage. Due to relying on electrostatic interactions with silicon oxide, lipid environments that are anionic will cover the surface differently than those with a more neutral or cationic charge. This charge can change with modifications to the lipids or by incorporation of membrane proteins. In addition to environment limitations, the reliance on electrostatic interactions compared to covalent interactions on the surface results in arrays that need to be used within a few days of generating. The resulting arrays exhibit difference in surface coverage that cannot be quantitated which can result in subtracting off more nonspecific interactions than specific interactions. To quantitate the surface coverage, Nanodiscs need to be loaded onto the surface in the instrument setup; however, only two Nanodisc environments can be loaded on to the surface at a due to the flow cell setup.

To overcome these challenges, we developed a DNA-tagged Nanodisc protocol for sequential loading onto the microring resonator surface that can be observed overtime and quantitated.[7] The DNA-tags allow for the generation of DNA encoded Nanodisc environment libraries that are oriented above the surface. In Chapter V, we showed analytical optimization of this technique and use for characterizing mutated Nanodisc incorporated tissue factor (TF) interactions with factor X (fX) and factor IX. Further implication of this technique to generate a 26-plex panel of 10 different Nanodiscs with biological replicates was used in Chapter VI. Using this panel, binding of fX-GLA domain mutants was characterized to complement an ongoing experimentation in the Morrissey lab.[8]

Each of these projects relied on the multiplexable capabilities of the silicon photonic microring resonator platform. No other current technology has the sensitivity and multiplexable capacity for lipid-protein or membrane protein-protein interaction characterization than this system.

In the next section, we show preliminary results that utilized physisorption to characterize the stereochemical and chemical interactions of the GLA domain of prothrombin (PT). We utilized PS analogs to tease out the interactions that are driving PT to the membrane surface with different binding affinity than other GLA domain-containing proteins. Future work will use these PS analogs and DNA-tagged Nanodiscs to understand the different affinities of all GLA domain-containing factors on a chemical level.

3. Phosphatidylserine Analogs for Chemical and Stereochemical Binding Characterization

Abstract

The main lipid binding domain present in the blood coagulation cascade is the GLA domain. This domain is rich in γ-glutamate and utilizes interactions with calcium ions to specifically bind to phosphatidylserine (PS) headgroups. There are seven blood coagulation factors that contain this binding domain, and each display differential binding affinities with PS. To understand the differential binding, we utilized PS analogs that display various stereochemical and chemical headgroup characteristics. These PS analogs were incorporated into Nanodiscs for array generation on silicon photonic microring resonators. Prothrombin binding to these PS analogs showed little to no change in binding affinity when changing the stereochemical PS environment or in the presence of phosphatidic acid; however, the binding affinity was lower when the amine and/or phosphate are removed. These PS analogs demonstrate the potential to characterize the binding preferences for chemical environments on PS that differentiate GLA domain-containing blood coagulation factors or other PS binding domains.

3.1. Introduction

Phospholipid binding domains are in the top 15 most modular domains that are most often connected to signal transduction and membrane trafficking.[9] Many phospholipid binding domains contain cationic surfaces that bind to anionic membranes while others have surface topography

association.[10–16] Both of these interactions can also involve second messengers such as calcium or be affected by pH.

Phosphatidylserine (PS) is enriched on the cytoplasmic side of the plasma membrane; thus, the exposure of PS to the extracellular domain can be used to initiate processes such as cell death which is common with annexin core lipid binding domains.[17] The first PS binding domain studied was the C2 domain of protein kinase C.[18] Here, the lipid binding interaction was discovered to occur in a calcium dependent manner.

The extrinsic blood coagulation cascade involves PS specific binding interactions from blood coagulation factors containing GLA or discoidin C2 domains. GLA domains are N-terminal regions rich in γ-carboxyglutamate which bind PS in a calcium dependent manner.[19] There are seven GLA domain-containing blood coagulation factors that are involved in coagulation propagation and negative feedback mechanisms.[20] Each of these GLA domains contain 47 amino acids with 9 to 12 glutamate residues (all of which are converted to γ-carboxyglutamate prior to secretion), three of which are conserved in all factors. There are currently crystal structures available for several GLA domains.[21–23] Compared to GLA domains, the discoidin-type C2 domain is less common in blood coagulation. This domain utilizes tryptophan to bind with PS in the membrane.[24,25] There have been numerous molecular dynamics[26,27] and NMR[19] studies designed to understand how these clotting factors bind to PS. There has been one study to date that has identified stereospecificity of fVIIa-TF complex formation using various forms of PS using activity assays and molecular dynamics simulations.[28]

To understand differential PS binding specificities within a binding domain family, we have selected a PS analog panel (**Figure VII.1**) to test for stereochemical and chemical binding preferences. Herein, we utilize Nanodiscs as a membrane mimetic to generate a membrane environment array. Nanodiscs are disc-like membrane bilayers that are stabilized by membrane scaffold proteins (MSP).[29,30] Previously, we have utilized Nanodiscs to generate arrays on silicon photonic microring resonators[31] and characterize GLA domain interactions with PS.[5,6] This work is preliminary but shows promising results for later studies comparing PS containing proteins within and between lipid binding domain families.

3.2. Materials and methods

Materials

Phosphatidyl-L-serine (P$_L$S, POPS, 1-palmitoyl-2-oleoyl-sn-glycero-3-phospho-L-serine), phosphatidic acid (PA, 1-palmitoyl-2-oleoyl-sn-glycero-3-phosphate), phosphatidylethanolamine-N-methyl (PM, 1-palmitoyl-2-oleoyl-sn-glycero-3-phosphoethanolamine-N-methyl), phosphatidylglycerol (PG, 1-palmitoyl-2-oleoyl-sn-glycero-3-phospho-(1'-rac-glycerol)), and dioleoylsuccinylglycerol (GS, 1,2-dioleoyl-sn-glycero-3-succinate) were purchased from Avanti Polar Lipids (Alabaster, AL). MSP1E3D1 was expressed in *E. coli* and purified as described previously.[32] PT was purchased from Enzyme Research Laboratories Inc. (South Bend, IN). Amberlite® XAD®-2 beads and all other chemicals were purchased from Sigma Aldrich (St. Louis, MO) and used as received unless otherwise noted.

Nanodisc preparation

Nanodiscs were prepared as described previously.[29,30,32] Briefly, lipids were dried under nitrogen and stored under vacuum for at least 4 hours. Nanodiscs were formed in TBS buffer (20 mM Tris-HCl, 100 mM NaCl, and 0.01% (w/v) NaN$_3$; pH 7.4) by mixing MSP, lipids, and cholate up to 20 mM in solution. The lipid to MSP ratio used for all Nanodiscs were 135:1 except for 50% PA Nanodiscs which were formed using a ratio of 130:1. The components were incubated with mixing at 4°C for 1 hour before adding half the sample volume of Amberlite® XAD®-2 beads for an additional 2 hours. Beads were removed with 0.22 µm syringe filters. Nanodiscs were purified using size exclusion chromatography on a Superdex 200 Increase 3.2/30 column (GE, Pittsburgh, PA). Nanodisc concentrations were determined using Qubit™ Protein Assay.

Silicon photonic microring resonators

The silicon photonic microring resonator system (Maverick M1) and sensor array chips were purchased from Genalyte, Inc. (San Diego, CA). The operation of the instrument has been previously described.[33–37] Sensor chips are 4 x 6 mm with 128 individually functionalize silicon-on-insulator rings and 4 thermal control. The microrings function as a refractive index-based sensing platform.

Sensor chip array functionalization

Nanodisc arrays were generated using hand spotting via pipette onto the silicon photonic microring chips.[6,38] Prior to functionalization, the chips are washed with acetone and isopropanol. Nanodiscs are spotted on to the surface at a concentration of 0.5 µM in spatially different regions (**Figure VII.2**). The chip is then incubated in a humidity chamber for at least 1 hour at 4°C.

Prothrombin binding titration

The Nanodisc array surface was blocked with a solution of 2% BSA prior performing titrations. The titration was performed in HEPES(+) buffer (10 mM HEPES, 150 mM NaCl, 50 µM EDTA, 2.5 mM CaCl$_2$, 0.1% (w/v) PEG 8000; pH 7.4) with chip regenerations performed in a HEPES buffer without CaCl$_2$. The concentration range for the PT titration was from 2 nM to 2 µM.

Data analysis

Data was analyzed using custom R scripts in RStudio. The titrations are controlled by subtracting interactions to 100% PC Nanodiscs as described previously.[6,38] The relative Δpm shift for each titration step is calculated by subtracting the shift at for the initial HEPES buffer from the equilibrated titration step. This shift is then plotted against concentration to fit to the equation:

$$\Delta\text{pm} = \Delta\text{pm}_{max}\left(\frac{X}{K_d+X}\right) \quad\quad \textbf{(VII.1)}$$

where *X* is the concentration of prothrombin, *Δpm$_{max}$* is the maximum shift, and *K$_d$* is the dissociation constant.

3.3. Results and discussion

Nanodisc array generation

The Nanodiscs used to generate the arrays are shown in **Figure VII.3**. When this study was run, Pβ-Lac was not synthesized. This remains a future aim to really understand the chemical and stereochemical interactions of PS binding domains due to its structural similarities to PS without the amine. After spotting the Nanodiscs at 0.5 µM, the chip is stored in a humidity chamber for at least 1 hour at 4°C. The chip is then ready undergo a surface block on the instrument. This is done to ensure that the surface is completely covered and minimize nonspecific interactions. The surface here was blocked with BSA (**Figure VII.4**). During this blocking step, extra calcium containing buffers have been added to the end which are not normally used. When adding calcium, 50% PA

(green) and 50% P$_D$S (blue) exhibit some dissociation from the surface. In particular high percentages of PA in Nanodiscs have been shown to form aggregates in the presence of calcium.[4] This aggregation could be the reason for Nanodiscs dissociating off the surface.

Prothrombin titration

The 100% PC controlled PT titration and binding curve are shown in **Figure VII.5** with using **Equation VII.1** as the fit parameter. First impressions looking at the binding curve in **Figure VII.5B** show similar binding to P$_L$S, P$_D$S, PhS, and PA with differential binding to GS, PG, and PM. The main differences here are the lack of phosphate group for GS and the lack of anionic character for PG and PM.

The calculated binding values follow these immediate assumptions (**Figure VII.6** and **Table VII.1**). PT shows mild preference for binding with GS and PG over PM which is interesting due to the lack of phosphate for GS. This binding trend displays a PT binding potential for the carboxylic acid of GS and glycerol shielded phosphate of PG; thus, demonstrating a binding pocket for the carboxylic acid or hydroxide group in the GLA domain of PT. The weakness of these binding interactions are similar to results shown that fX favors binding with the amine and phosphate over the carboxyl.[26]

Due to the similar binding observed with P$_L$S and P$_D$S, PT does not appear to have a stereochemical preference with regards to the amine group on PS. However, there is a slightly better affinity observed with PA and PhS. This could be due to the ease of access to the phosphate region due to PA being unhindered and PhS having a more flexible headgroup. The Tajkhoshid model predicts that calcium ions are held in close proximity to the phosphate of PS.[19,27,39] Therefore, the ease of access to the phosphate group may explain the tighter binding affinity displayed by PA and PhS compared to P$_L$S and P$_D$S.

3.4. Conclusion

This panel of PS analogs was used as a preliminary study into the stereo- and chemical-selectivity of PT. The findings show that the GLA domain interaction of PT with PS preferentially bind with phosphate groups that are easily accessible and show no stereoselectivity based on the amine positioning. The future of this panel of PS analogs is to compare binding selectivity within

and between PS binding domains. Within blood coagulation, there is a wide range of binding affinity displayed by the GLA domains (nM to µM); therefore, these PS analogs could be used to understand why there is such a difference. This does not have to be limited to just GLA domain-containing proteins. Other domains such as annexin core, C2 domain, and discoidin C2 domains can be characterized with this panel to understand the differences within and between each family.

3.5. Acknowledgements

4. Future Directions

The DNA-tagged Nanodisc technology interfaced on silicon photonic microring resonators is a promising method for future work for characterizing interactions at the membrane surface. First, DNA-tagged Nanodiscs with the methods in this dissertation utilized MSP1D1 D73C only. There are many other MSP variations that can be used to generate Nanodiscs.[40,41] If the variation chosen has a single cysteine mutation, then this technique will work for generating DNA-tagged Nanodiscs. Currently, there are 14 DNA complement pairs that are usable for generating these arrays. For an easier user interface that does not involve taking the flow cell apart to achieve 28-plex, the addition of more complement pairs is needed. There is potential to add 16 more complements to achieve this ideal user setup. There are no limitations on needing to use DNA-tagged Nanodiscs on just silicon photonic microring resonators. Any surface sensitive detection method can be used with these chemically modified arrays such as SPR.

The reaction to generate the DNA-tagged MSP, currently, is rigorous in terms of conjugation reaction clean up. The process of running the reaction then undergoing multiple rounds of Ni-NTA purification due to adenosine stacking with NTA that can generate a lot of nonspecific binding then undergoing multiple rounds of DNA purifications due to the current small size of the columns is a long process. The process can be cleaned up in multiple ways: packing larger columns (which

is obvious) and further optimizing the conjugation reaction. The current conjugation efficiency for the reaction variable from 50-90%. Work on optimization of the reaction could help with some of the workup to maybe not even need to do the DNA purification column.

Another future direction for DNA-tagged Nanodiscs is stability studies. MSP Nanodiscs are typically stable for a month or so without aggregation or breakdown, but does the addition of DNA change this? This would also be interesting to study when changing the types of lipids in the Nanodiscs based on potential interactions with the DNA.

Aside from optimization needed for DNA-tagged Nanodiscs, the uses of the technology are limitless. Currently the technology has only been used for blood coagulation to characterize PS-GLA domain and TF interactions. The preliminary study on PS analogs shows promise for implications in understanding the binding affinity variation displayed by GLA domain-containing proteins; however, there are other PS binding domains with physiological importance.[42] Discoidin C2 domains are another blood coagulation cascade PS binding domain displayed by factor V and factor VIII.[24,25] This binding interaction does not require calcium but instead utilizes tryptophan intercalation into the membrane.[43,44] Another binding domain is C2 domain. Protein kinase C and synaptotagmins utilize this binding domain for calcium dependent interactions with PS and sometimes other lipids.[45–48] Annexin cores are the final and largest major PS binding domain. These domains employ interactions with PS and high concentrations of calcium for signaling of processes such as cell death.[49,50]

TF is simply an integral membrane protein with activity only on one side of the membrane. It would be interesting to study a more complicated system such as G-protein coupled receptors (GPCR). GPCRs are governed by agonists and phospholipids for interactions on both sides of the membrane.[51] This system, and many others, is attractive to highlight characterization of interactions to both sides of the membrane.

5. Limitations

When using DNA-tagged Nanodiscs on silicon photonic microring resonators the type of interactions being studied need to be carefully considered. Since the interactions can be corrected to calculate interactions per leaflet, the total surface binding needs to scale. If only one of a protein is making it to the surface, this can be calculated, but it may be difficult to see the whole range of

interactions needed to characterize the binding. Binding curves require at least 5 data points, so more than one interaction is needed. In these cases, larger Nanodiscs could be used to generate more than one binding event per Nanodisc.

Another limitation is the potential need for membrane curvature. Smaller Nanodiscs are more constrained, thus do not sure appreciable curvature in comparison to physiological membranes. The use of larger Nanodiscs may be able to overcome this limitation, but this would need to be tested.

There are a few key limitations to consider when using Nanodiscs in general. Free lipids are separated away from assembled Nanodiscs using size exclusion chromatography (SEC), but this does not give information about what lipids did not incorporate. Studies have shown that incorporation is easily controlled and mimics the lipid mixture that was dried,[52] but this may vary depending on the types of lipids used.

6. Concluding Remarks

In closing, this work has contributed to the fields of membrane characterization and blood coagulation. The developed and optimized interface with Nanodiscs and silicon photonic microring resonators required of innovation from analytical assay development to chemical biology. Further implementations of this platform will continue to push the limits of high throughput screening of lipid-protein and membrane protein-protein interactions. Characterization of interactions at the membrane interface will lead to better understanding of physiological process which will enable more informative design of future therapeutics.
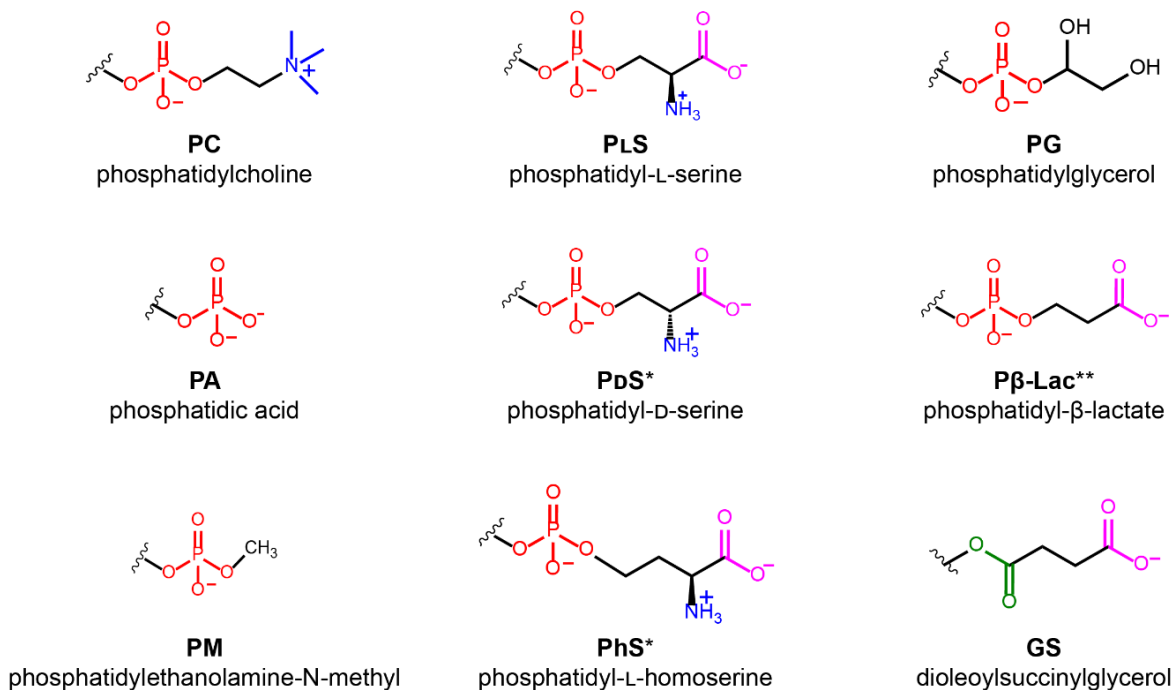
Figure VII.1. Phosphatidylserine Analog Structures. Headgroup structures for phospholipid analogs to test stereochemical and chemical selectivity of PS binding domains. Note: * = synthetic lipids provided by the Morrissey lab; ** = synthetic lipid synthesized by the Morrissey lab that is proposed for the continuation of this work.
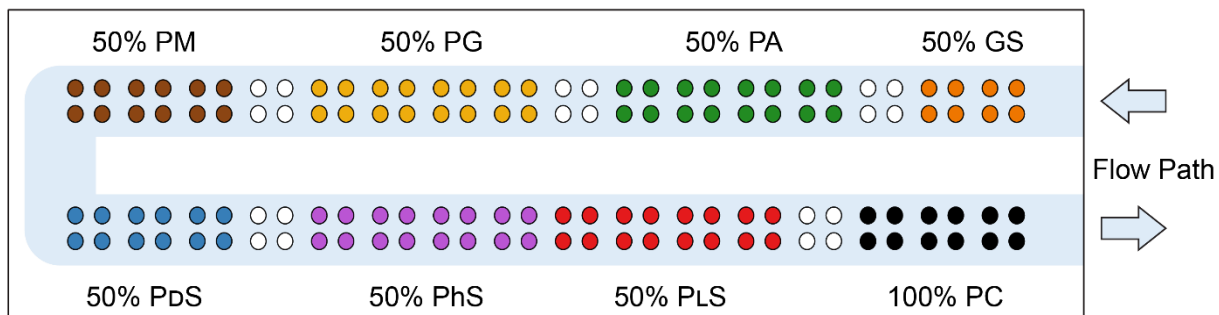
Figure VII.2. Sensor Chip Layout. The flow path for loading and assays is shown by the *light blue box* and *arrows*. Hand-spotting was used to generate the array of 50% GS (orange), 50% PA (green), 50% PG (yellow), 50% PM (brown), 50% P_DS (blue), 50% PhS (purple), P_LS (red), and 100% PC (black) while white represents unfunctionalized microrings.
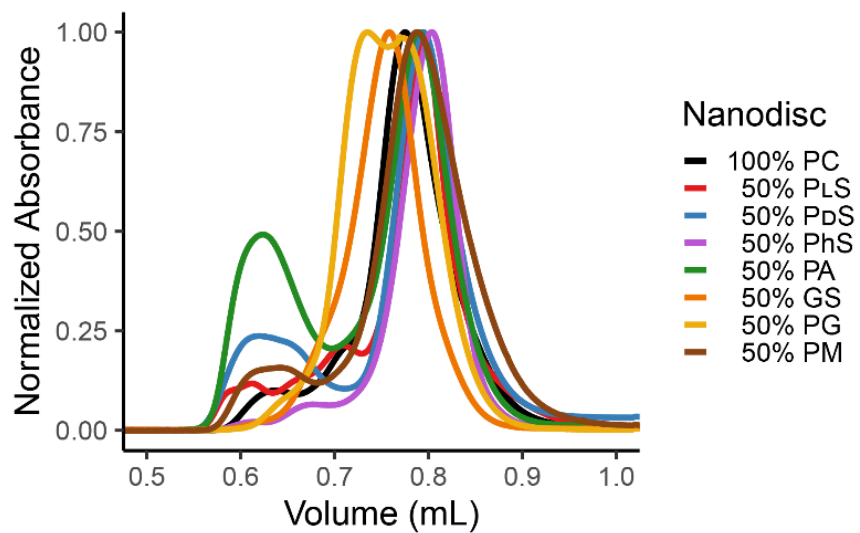
Figure VII.3. SEC of PS Analog Nanodiscs. Elution profile of Nanodiscs made with either 100% PC or 50% PS analog with 50% PC as a balance.
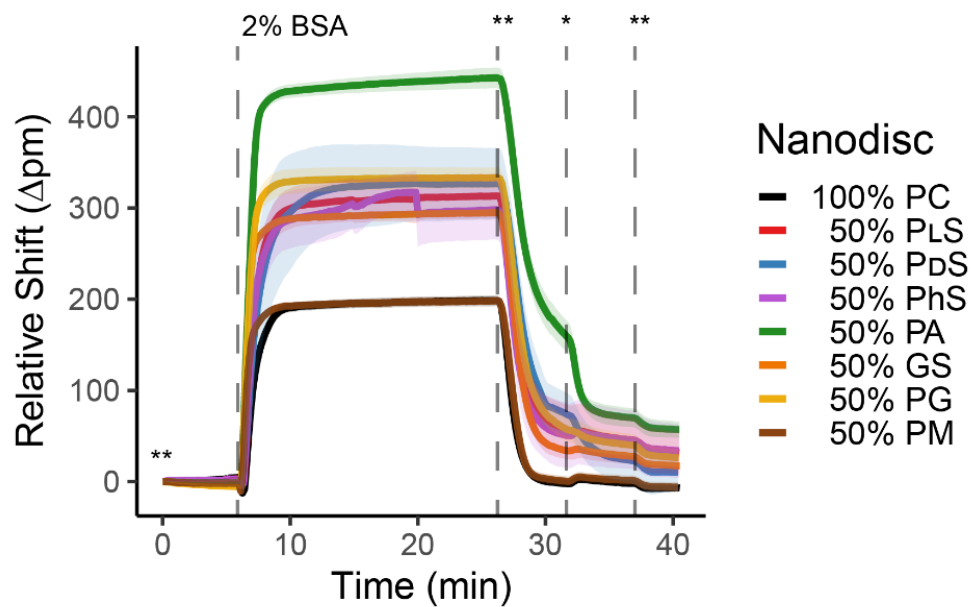
Figure VII.4. BSA Blocking of Nanodisc Array. Blocking of the sensor surface after Nanodisc spotting. The assay starts in HEPES(**) before blocking with 2% BSA in HEPES. Afterwards, the surface is rinsed with alternating HEPES(+)(*). and HEPES (**). The shaded ribbon shows the standard deviation of microrings (n = 8-16).
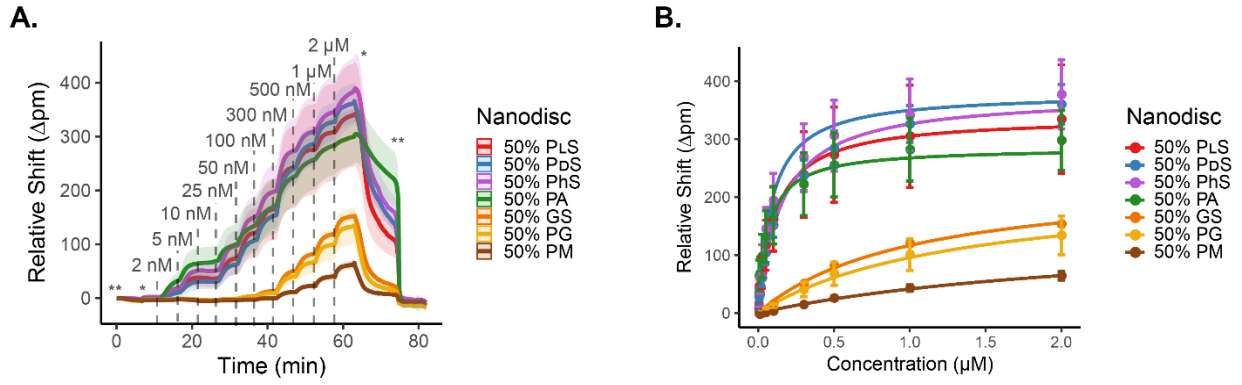
Figure VII.5. Prothrombin Titration. (**A**) 100% PC controlled prothrombin titration from 2 nM to 2 µM with buffer steps of HEPES (**) and HEPES(+) (*). The shaded ribbon shows the standard deviation of microrings (n = 8-16).
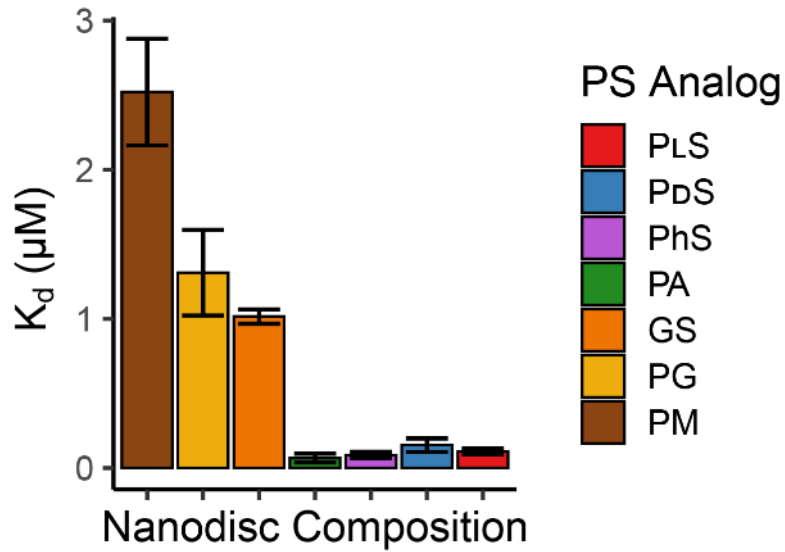
Figure VII.6. Prothrombin Dissociation Constants. Plotted values are from the binding curve in **Figure VII.5**. The binding curve is fit for every microring functionalized with a given Nanodisc, then plotted as an average. Error is the standard deviation between the microrings.

TABLES

Table VII.1. Prothrombin Dissociation Constants for PS Analogs.

Nanodisc	K_d (µM)
50% P_LS	0.11 ± 0.02
50% P_DS	0.15 ± 0.05
50% PhS	0.09 ± 0.02
50% PA	0.06 ± 0.03
50% GS	1.02 ± 0.05
50% PG	1.3 ± 0.3
50% PM	2.5 ± 0.4

REFERENCES

(1)   Skar-Gislinge, N.; Johansen, N. T.; Høiberg-Nielsen, R.; Arleth, L. Comprehensive Study of the Self-Assembly of Phospholipid Nanodiscs: What Determines Their Shape and Stoichiometry? *Langmuir* **2018**, *34* (42), 12569–12582.

(2)   Camp, T.; McLean, M.; Kato, M.; Cheruzel, L.; Sligar, S. The Hydrodynamic Motion of Nanodiscs. *Chem. Phys. Lipids* **2019**, *220*, 28–35.

(3)   Camp, T.; Mehta, K.; Sligar, S. G.; Zhang, K. Molecular Orientation Determination in Nanodiscs at the Single-Molecule Level. *Anal. Chem.* **2020**, *92* (2), 2229–2236.

(4)   Her, C.; Filoti, D. I.; McLean, M. A.; Sligar, S. G.; Alexander Ross, J. B.; Steele, H.; Laue, T. M. The Charge Properties of Phospholipid Nanodiscs. *Biophys. J.* **2016**, *111* (5), 989–998.

(5)   Muehl, E. M.; Gajsiewicz, J. M.; Medfisch, S. M.; Wiersma, Z. S. B.; Morrissey, J. H.; Bailey, R. C. Multiplexed Silicon Photonic Sensor Arrays Enable Facile Characterization of Coagulation Protein Binding to Nanodiscs with Variable Lipid Content. *J. Biol. Chem.* **2017**, *292* (39), 16249–16256.

(6)   Medfisch, S. M.; Muehl, E. M.; Morrissey, J. H.; Bailey, R. C. Phosphatidylethanolamine-Phosphatidylserine Binding Synergy of Seven Coagulation Factors Revealed Using Nanodisc Arrays on Silicon Photonic Sensors. *Sci. Rep.* **2020**, *10* (17407), 1–7.

(7)   Medfisch, S. M.; Morrissey, J. H.; Bailey, R. C. Development of DNA Tethered Nanodisc Arrays for Quantitative Characterization of Lipid-Protein and Membrane Protein-Protein Interactions on Silicon Photonic Microring Resonators in the Blood Coagulation Cascade. *Prep.*

(8)   Paul, D.; Morrissey, J. H. No Title. *Unpubl. results*.

(9)   Cho, W.; Stahelin, R. V. Membrane-Protein Interactions in Cell Signaling and Membrane Trafficking. *Annu. Rev. Biophys. Biomol. Struct.* **2005**, *34*, 119–151.

(10)   Leventis, P. A.; Grinstein, S. The Distribution and Function of Phosphatidylserine in Cellular Membranes. *Annu. Rev. Biophys.* **2010**, *39*, 407–427.

(11)   Narayan, K.; Lemmon, M. A. Determining Selectivity of Phosphoinositide-Binding Domains. *Methods* **2006**, *39* (2), 122–133.

(12)   Lemmon, M. A. Membrane Recognition by Phospholipid-Binding Domains. *Nat. Rev. Mol.*

Cell Biol. **2008**, *9* (2), 99–111.

(13) McLaughlin, S.; Murray, D. Plasma Membrane Phosphoinositide Organization by Protein Electrostatics. *Nature* **2005**, *438* (7068), 605–611.

(14) Stace, C. L.; Ktistakis, N. T. Phosphatidic Acid- and Phosphatidylserine-Binding Proteins. *Biochim. Biophys. Acta - Mol. Cell Biol. Lipids* **2006**, *1761* (8), 913–926.

(15) Stahelin, R. V. Lipid Binding Domains: More than Simple Lipid Effectors. *J. Lipid Res.* **2009**, *50* (Suppl), 299–304.

(16) DiNitto, J. P.; Cronin, T. C.; Lambright, D. G. Membrane Recognition and Targeting by Lipid-Binding Domains. *Sci. STKE* **2003**, *2003* (213), 1–16.

(17) Fadok, V. A.; Bratton, D. L.; Frasch, S. C.; Warner, M. L.; Henson, P. M. The Role of Phosphatidylserine in Recognition of Apoptotic Cells by Phagocytes. *Cell Death Differ.* **1998**, *5* (7), 551–562.

(18) Takai, Y.; Kishimoto, A.; Iwasa, Y.; Kawahara, Y.; Mori, T.; Nishizuka, Y. Calcium-Dependent Activation of a Multifunctional Protein Kinase by Membrane Phospholipids. *J. Biol. Chem.* **1979**, *254* (10), 3692–3695.

(19) Ohkubo, Y. Z.; Tajkhorshid, E. Distinct Structural and Adhesive Roles of Ca2+ in Membrane Binding of Blood Coagulation Factors. *Structure* **2008**, *16* (1), 72–81.

(20) Davie, E. W.; Fujikawa, K.; Kisiel, W. The Coagulation Cascade: Initiation, Maintenance, and Regulation. *Perspect. Biochem.* **1991**, *30* (42), 10363–10370.

(21) Huang, M.; Rigby, A. C.; Morelli, X.; Grant, M. A.; Huang, G.; Furie, B.; Seaton, B.; Furie, B. C. Structural Basis of Membrane Binding by Gla Domains of Vitamin K-Dependent Proteins. *Nat. Struct. Biol.* **2003**, *10* (9), 751–756.

(22) Mizuno, H.; Fujimoto, Z.; Atoda, H.; Morita, T. Crystal Structure of an Anticoagulant Protein in Complex with the Gla Domain of Factor X. *Proc Natl Acad Sci U S A* **2001**, *98* (13), 7230–7234.

(23) Huang, M.; Furie, B. C.; Furie, B. Crystal Structure of the Calcium-Stabilized Human Factor IX Gla Domain Bound to A Conformation-Specific Anti-Factor IX Antibody. *J. Biol. Chem.* **2004**, *279* (14), 14338–14346.

(24) Majumder, R.; Quinn-Allen, M. A.; Kane, W. H.; Lentz, B. R. The Phosphatidylserine Binding Site of the Factor Va C2 Domain Accounts for Membrane Binding but Does Not Contribute to the Assembly or Activity of a Human Factor Xa-Factor Va Complex.

Biochemistry **2005**, *44* (2), 711–718.

(25) Majumder, R.; Quinn-Allen, M. A.; Kane, W. H.; Lentz, B. R. A Phosphatidylserine Binding Site in Factor Va C1 Domain Regulates Both Assembly and Activity of the Prothrombinase Complex. *Blood* **2008**, *112* (7), 2795–2802.

(26) Muller, M. P.; Wang, Y.; Morrissey, J. H.; Tajkhorshid, E. Lipid Specificity of the Membrane Binding Domain of Coagulation Factor X. *J. Thromb. Haemost.* **2017**, *15* (10), 2005–2016.

(27) Morrissey, J. H.; Tajkhorshid, E.; Rienstra, C. M. Nanoscale Studies of Protein-Membrane Interactions in Blood Clotting. *J. Thromb. Haemost.* **2011**, *9* (Suppl 1), 162–167.

(28) Mallik, S.; Prasad, R.; Bhattacharya, A.; Sen, P. Synthesis of Phosphatidylserine and Its Stereoisomers: Their Role in Activation of Blood Coagulation. *ACS Med. Chem. Lett.* **2018**, *9* (5), 434–439.

(29) Bayburt, T. H.; Grinkova, Y. V.; Sligar, S. G. Self-Assembly of Discoidal Phospholipid Bilayer Nanoparticles with Membrane Scaffold Proteins. *Nano Lett.* **2002**, *2* (8), 853–856.

(30) Denisov, I. G.; Grinkova, Y. V.; Lazarides, A. A.; Sligar, S. G. Directed Self-Assembly of Monodisperse Phospholipid Bilayer Nanodiscs with Controlled Size Directed Self-Assembly of Monodisperse Phospholipid Bilayer Nanodiscs with Controlled Size. *Nano Lett.* **2004**, *126* (11), 3477–3487.

(31) Sloan, C. D. K.; Marty, M. T.; Sligar, S. G.; Bailey, R. C. Interfacing Lipid Bilayer Nanodiscs and Silicon Photonic Sensor Arrays for Multiplexed Protein − Lipid and Protein − Membrane Protein Interaction Screening. *Anal. Chem.* **2013**, *85* (5), 2970–2976.

(32) Bayburt, T. H.; Sligar, S. G. Membrane Protein Assembly into Nanodiscs. *FEBS Lett.* **2010**, *584* (9), 1721–1727.

(33) Iqbal, M.; Gleeson, M. a; Spaugh, B.; Tybor, F.; Gunn, W. G.; Hochberg, M.; Baehr-jones, T.; Bailey, R. C.; Gunn, L. C.; Resonators, R.; Optical, H.; Iqbal, M.; Gleeson, M. a; Spaugh, B.; Tybor, F.; Gunn, W. G.; Hochberg, M.; Baehr-jones, T.; Bailey, R. C.; Gunn, L. C. Label-Free Biosensor Arrays Based on Silicon Scanning Instrumentation. *IEEE J. Sel. Top. Quantum Electron.* **2010**, *16* (3), 654–661.

(34) Byeon, J.-Y.; Limpoco, F. T.; Bailey, R. C. Efficient Bioconjugation of Protein Capture Agents to Biosensor Surfaces Using Aniline-Catalyzed Hydrazone Ligation. *Langmuir* **2010**, *26* (19), 15430–15435.

(35) Luchansky, M. S.; Washburn, A. L.; Qavi, A. J.; Kindt, J. T.; McClellan, M. S.; Bailey, R. C. Silicon Photonic Microring Resonator Arrays for Scalable and Multiplexable Bioanalysis. *Proc. SPIE* **2011**, *7888*, 1–4.

(36) Wade, J. H.; Alsop, A. T.; Vertin, N. R.; Yang, H.; Johnson, M. D.; Bailey, R. C. Rapid, Multiplexed Phosphoprotein Profiling Using Silicon Photonic Sensor Arrays. *ACS Cent. Sci.* **2015**, *1* (7), 374–382.

(37) Washburn, A. L.; Shia, W. W.; Lenkeit, K. A.; Lee, S.-H.; Bailey, R. C. Multiplexed Cancer Biomarker Detection Using Chip-Integrated Silicon Photonic Sensor Arrays. *Analyst* **2016**, *141* (18), 5358–5365.

(38) Muehl, E. M.; Gajsiewicz, J. M.; Medfisch, S. M.; Wiersma, Z. S. B.; Morrissey, J. H.; Bailey, R. C. Multiplexed Silicon Photonic Sensor Arrays Enable Facile Characterization of Coagulation Protein Binding to Nanodiscs with Variable Lipid Content. *J. Biol. Chem.* **2017**, jbc.M117.800938.

(39) Morrissey, J. H.; Pureza, V.; Davis-Harrison, R. L.; Sligar, S. G.; Ohkubo, Y. Z.; Tajkhorshid, E. Blood Clotting Reactions on Nanoscale Phospholipid Bilayers. *Thromb. Res.* **2008**, *122* (Sipple 1), S23-6.

(40) Grinkova, Y. V.; Denisov, I. G.; Sligar, S. G. Engineering Extended Membrane Scaffold Proteins for Self-Assembly of Soluble Nanoscale Lipid Bilayers. *Protein Eng. Des. Sel.* **2010**, *23* (11), 843–848.

(41) Hagn, F.; Etzkorn, M.; Raschle, T.; Wagner, G. Optimized Phospholipid Bilayer Nanodiscs Facilitate High-Resolution Structure Determination of Membrane Proteins. *J. Am. Chem. Soc.* **2013**, *135* (5), 1919–1925.

(42) Ferguson, K. M.; Lemmon, M. A.; Schlessinger, J.; Sigler, P. B. Structure of the High Affinity Complex of Inositol Trisphosphate with a Phospholipase C Pleckstrin Homology Domain. *Cell* **1995**, *83* (6), 1037–1046.

(43) Shi, J.; Heegaard, C. W.; Rasmussen, J. T.; Gilbert, G. E. Lactadherin Binds Selectively to Membranes Containing Phosphatidyl-L-Serine and Increased Curvature. *Biochim. Biophys. Acta - Biomembr.* **2004**, *1667* (1), 82–90.

(44) Shi, J.; Gilbert, G. E. Lactadherin Inhibits Enzyme Complexes of Blood Coagulation by Competing for Phospholipid-Binding Sites. *Blood* **2003**, *101* (7), 2628–2636.

(45) Hinderliter, A.; Almeida, P. F. F.; Creutz, C. E.; Biltonen, R. L. Domain Formation in a

Fluid Mixed Lipid Bilayer Modulated through Binding of the C2 Protein Motif. *Biochemistry* **2001**, *40* (13), 4181–4191.

(46)   Kertz, J. A.; Almeida, P. F. F.; Frazier, A. A.; Berg, A. K.; Hinderliter, A. The Cooperative Response of Synaptotagmin I C2A. A Hypothesis for a Ca 2+-Driven Molecular Hammer. *Biophys. J.* **2007**, *92* (4), 1409–1418.

(47)   Krishnakumar, S. S.; Kümmel, D.; Jones, S. J.; Radoff, D. T.; Reinisch, K. M.; Rothman, J. E. Conformational Dynamics of Calcium-Triggered Activation of Fusion by Synaptotagmin. *Biophys. J.* **2013**, *105* (11), 2507–2516.

(48)   Fernandez, I.; Araç, D.; Ubach, J.; Gerber, S. H.; Shin, O. H.; Gao, Y.; Anderson, R. G. W.; Südhof, T. C.; Rizo, J. Three-Dimensional Structure of the Synaptotagmin 1 C2B-Domain: Synaptotagmin 1 as a Phospholipid Binding Machine. *Neuron* **2001**, *32* (6), 1057–1069.

(49)   Tait, J. F.; Gibson, D. Phospholipid Binding of Annexin V: Effects of Calcium and Membrane Phosphatidylserine Content. *Arch. Biochem. Biophys.* **1992**, *298* (1), 187–191.

(50)   Gerke, V.; Moss, S. E. Annexins : From Structure to Function. *Physiol. Rev.* **2002**, *82* (2), 331–371.

(51)   Komolov, K. E.; Du, Y.; Duc, N. M.; Betz, R. M.; Rodrigues, J. P. G. L. M.; Leib, R. D.; Patra, D.; Skiniotis, G.; Adams, C. M.; Dror, R. O.; Chung, K. Y.; Kobilka, B. K.; Benovic, J. L. Structural and Functional Analysis of a B2-Adrenergic Receptor Complex with GRK5. *Cell* **2017**, *169* (3), 407–421.

(52)   Shaw, A. W.; Pureza, V. S.; Sligar, S. G.; Morrissey, J. H. The Local Phospholipid Environment Modulates the Activation of Blood Clotting. *J. Biol. Chem.* **2007**, *282* (9), 6556–6563.